Photochemistry from Density-Functional Theory

Felipe Cordova Lozano

THÈSE

Soutenue le 30 Octobre 2007 devant

L'UNIVERSITÉ JOSEPH FOURIER - GRENOBLE 1

au Département de Chimie Moléculaire (DCM)

en vue de l'obtention du titre de

DOCTEUR DE L'UNIVERSITÉ JOSEPH FOURIER

Spécialité : Chimie Physique Moléculaire et Structurale

École Doctorale de Chimie et Sciences du Vivant

présentée par

Felipe CORDOVA LOZANO

Photochemistry from Density-Functional Theory

Jury

Rapporteurs	Alberto VELA AMIEVA	Professeur à CINVESTAV, México, México
	Ivano TAVERNELLI	Docteur à EPFL, Lausanne, Switzerland
Examinateurs	Henry CHERMETTE	Professeur à l'Université de Lyon, France
	Valerio OLEVANO	Docteur, CNRS, Grenoble, France
	Pascale MALDIVI	Docteur, CEA, Grenoble, France
Directeur de thèse	Mark E. CASIDA	Professeur à l'Université de Grenoble, France

Thèse préparée au sein du Département de Chimie Moléculaire (DCM)

Grenoble, France

Acknowledgements

I am deeply indebted to France, this beautiful country in which my family and I passed an important part of our life. Thanks for allowing us to learn from your culture and making us feel at home during this time.

Many people have made the last four years of my stay in Grenoble an exciting time, both professionally and otherwise. I feel fortunate for the stimulating and supportive environment in which I carried out my thesis work.

First, I would like to express my gratitude to my thesis director Professor Mark E. CASIDA for introducing me to the field of theoretical chemistry. His advice, support, and encouragement throughout my life as a doctoral student have helped me to establish my career in this interesting field. His exhortation to work hard always will be an incentive to better myself. The time that I have spent in his group (Laboratoire d'Études Dynamiques et Structurales de la Sélectivité, LEDSS, Équipe de Chimie Théorique, of the Département de Chimie Moléculaire, Université Joseph-Fourier, Grenoble) has been a remarkable learning experience for which I am sincerely thankful.

Second, I would like to thank both Professor Alberto VELA and Professor Ivano TAVERNELLI who kindly accepted to be Reviewers and Examiners of my thesis. Both deserve special recognition for their professional and constructive criticism of my work. Their valuable criticism pushed me to reach a higher level than would otherwise have been possible. I especially thank Professor VELA, because his suggestions and advice throughout my research as a PhD student have been invaluable. I also want to address my acknowledgements to the members of the jury to have accepted to assess my work. To Docteur Pascale MALDIVI who is Head of the Laboratory of Inorganic and Biological Chemistry in the CEA, the French Atomic Energy Commission in Grenoble. To Henry CHERMETTE who is Professor at the Université Claude Bernard in Lyon, France and to Docteur Valerio OLEVANO who is researcher at the Laboratoire d'Etudes de Propriétés Electroniques des Solides, CNRS, Grenoble, France. To all of them I would like to express my gratitude for taking time to read the thesis.

Third, I could not have survived the past 4 years without the love, support, optimism, and presence of my wife Paty and my children Ana, Luis, and Carlos. To all them my admiration and my love forever. To Paty for her love, courage, and daily support every day that we have passed in Grenoble. No matter what the situation (easy or difficult) you have stayed aside of me. I recognize and acknowledge the effort you make every day. To Ana, Luis and Carlos this thesis also represents your work. I have learned a lot from you. For example, a large part of my knowledge of the French language comes from helping you with your homework. You gave me the faith to go on. To my extended family in Mexico (parents, brothers, and sister and my all "querida" family in law) thanks for your prayers, support, and love during the time we were "in exile" in France. Truly, though we were far in distance we were close in heart. Particularly I would like to dedicate this thesis to my "sobrinos." I hope that one day you will read the thesis and that it encourages you to pursue your studies and to travel to foreign countries. It is an excellent experience!

Fourth, an especial "Merci" to the Université Joseph Fourier in Grenoble where I realized my doctoral studies and I particularly want to express my gratitude to Anne MILET (directeur de recherche at the LEDSS), Helène JAMET (Maître de conférences), Carlos PEREZ del VALLE (Maître de conférences), Pierre VATTON, Denis CHARAPOFF, Régis GRAS, Sébastien MORIN, and Marie-Louise DHEU-ANDRIES all them of informatics service, for academic and technical support and for the facilities proportioned for the use of computers employed for the calculations reported in this thesis.

J'aimerais remercier tout le personnel de l'École Doctorale Chimie et Science du Vivant pour leur aide dans les différents démarches administratives pendant la durée de la thèse.

I enormously acknowledge financial support from the Mexican Ministry of Education via a CONACYT scholarship (Program SFERE 2004, scholarship number 66559) and from the Universidad de las Américas Puebla (UDLAP) to give me this opportunity to do my Ph.D. degree, and so be able to contribute to the educational superior system in Mexico. Both CONACYT and UDLAP always proportioned all the facilities in all time for my thesis and support me so rapidly anytime. Thanks to contribute to formation of human resources to develop our Mexico.

Je remercie également tout le soutien de la Societé Française d'Exportation des Ressources Éducatives (SFERE) pour leur monitorat et leur tutorat académique tout au long de ma thèse. Particulièrement Mme Anna MANETA pour toute l'information et les services proportionnés par rapport à la bourse d'études.

I would like to express my sincere gratefulness to my Mexican friends in Grenoble.

In fact the Mexican community replaced our Mexican family in Grenoble. I will never forget all the good moments at the meetings, celebrations, discussions and party's we have passed together. An especial thank to Dr. Moises BAUTISTA who helped me at the beginning of my thesis in Grenoble.

Finally, I also thank to my beloved "French family" in Saint Laurent du Pont and Grenoble, who we coexisted and shared the spiritual and material food. I will always remember all you. I am also grateful to my friends in anywhere in France sincerely many thanks for receiving us in your homes.

Felipe CORDOVA LOZANO
Automne 2007

Résumé

Les méthodes de la chimie quantique sont aujourd'hui des outils importants pour étudier la structure électronique des molécules et pour calculer les énergies totales associées. Les méthodes de la chimie quantique sont souvent utilisées pour interpréter toutes sortes d'expériences spectroscopiques. Ces méthodes servent également pour étudier les mécanismes chimiques des réactions chimiques. Un cas particulier est celui de la photochimie. Actuellement grâce à l'élaboration des méthodologies théoriques, l'analyse théorique de l'état fondamental et des états excités a évolué jusqu'au point qu'il fournit des solutions aidant à mieux comprendre ou même prédire les processus photochimiques.

Parmi tous les méthodes de la chimie quantique, la théorie de la fonctionnelle de la densité (DFT, pour l'anglais *density functional theory*) a émergé comme une méthode de choix pour le calcul de l'état fondamental des grandes molécules. En particulier, grâce à son applicabilité et son exactitude, la DFT a pu servir dans l'étude de problèmes d'intérêt pratique.

Pour les états excités, la DFT dépendante du temps (TDDFT, pour l'anglais *time-dependent density functional theory*) est actuellement une des approches les plus populaires. La TDDFT permet le calcul des propriétés de l'état excité des systèmes moléculaires telles que, par exemple, les énergies d'excitation, les forces oscillatrices et les géométries des états excités. Cependant les méthodes informatiques standards ont des inconvénients inhérents qui parfois limitent sérieusement leur utilité.

C'est ça le sujet de cette thèse : *évaluer l'implémentation, l'applicabilité et la validité de la TDDFT en utilisant différentes approximations et dans différentes situations.*

Dans ce contexte différentes étapes ont été effectuées. Premièrement, une nouvelle implémentation de la TDDFT a été fait dans le programme de deMon2k et a été validé dans le cas des calculs des énergies et des forces oscillatrices contre les résultats du programme Gaussian pour les cas du dimère de sodium, du tétramère de sodium et pour *para*-aminobenzonitrile.

Deuxièmenent, bienque la TDDFT dans sa formation de réponse linéaire a été ini-

tielement utilisée pour le calcul des excitations des molécules à couche fermée, à son origine la formulation de Casida permettait son application dans le cas des molécules à couches ouvertes avec différentes-orbitales-pour-différentes-spins (DODS) et même pour le cas d'occupation fractionnelle. Dans ce travail les équations pour calculer la contamination de spin des états excités en utilisant la TDDFT sont présentés.

Troisièment (et finalement) le but principal de cette thèse est la validation de la TDDFT pour la réaction d'ouverture de la molécule d'oxirane en cassant la liaison C-C. Il s'agît d'une réaction de chimie organique d'importance classique. Selon les règles de Woodward et de Hoffmann (WH), l'ouverture d'oxirane en cassant la liaison de C-C sera conrotatoire (c'est-à-dire que la rotation des groupes terminaux méthylèniques suivent le même sens) dans l'état fondamental et disrotatoire (c'est-à-dire que la rotation des groupes terminaux méthylèniques est dans le sens opposée) dans le premier état excité singulet. Nous présentons pour les processus conrotatoire et distrotatoire les surfaces d'énergie potentielle pour la rupture de la liaison C-C en utilisant la TDDFT et avec les fonctionnelles LDA (pour l'anglais *local density approximation*) et B3LYP, avec et sans l'approximation de Tamm et de Dancoff (TDA pour l'anglais *Tamm-Dancoff approximation*). Les résultats déterminés ainsi, ensemble avec la méthode de Hartree-Fock dépendante du temps (TDHF, pour l'anglais *time-dependent Hartree-Fock*) et avec la méthode de l'interaction de configurations monoexcités (CIS, pour l'anglais *configuration interaction singles*) sont présentés. Il est bien connu que la TDDFT est une méthode formellement exacte, mais qu'il y a des problèmes pratiques dûs à l'utilisation des fonctionnelles approximatives tel que le problème d'instabilité triplet. Nous constatons que les problèmes d'instabilité triplet augmentent dans l'ordre TDLDA $<$ TDB3LYP $<$ TDHF. Dans ce sens, l'approximation le plus simple (LDA) a le comportement le plus proche à celui attendu de la théorie exacte. Les problèmes dûs aux instabilités triplet peuvent être encore réduits au minimum en utilisant l'approximation TDA, faisant la TDA TDLDA une méthode de choix pour notre étude. On montre que le premier état singulet excité est du type ^{1}(n,3s), donc un état de type Rydberg. Finalement à cause de la prépondérance du simple mécanisme photochimique WH dans la littérature, nous présentons également des surfaces pour l'excitation de WH ^{1}(n, σ^*) (de type valence) calculé par la méthode TDDFT.

Mots-clé. Chimie Quantique, Théorie de la Fonctionnelle de la Densité, Théorie de la Fonctionnelle de la Densité Dépendent du Temps, Molécules à Couche Fermé et Ouvert, Spectre d'Excitation Électronique, Photochimie, État Excités, Instabilité Triplet, Oxirane.

Abstract

Quantum chemical methods are today important tools for predictions of electronic structure and energetics of molecules, for providing the interpretation of all kinds of spectroscopic experiments, and as a conceptual model of fundamental importance for the understanding of chemical reaction mechanisms in certain processes. In the same sense, photochemistry has been considered an important subject in chemistry. At the present time thanks to the development of theoretical methodologies for analyzing both ground and excited states would seem possible to have inexpensive alternatives to better understand or modelling photochemical process.

In this manner Density-Functional Theory (DFT) has emerged as the method of choice for the ground state for the solution of many chemical problems due to principally to its applicability and accuracy.

For excited states, time-dependent DFT (TDDFT), which is an extension of DFT has become one of the most prominent and most widely used approaches for the calculation of excited-state properties of molecular systems, for example, excitation energies, oscillator strengths, and excited-state geometries. However, the widespread standard computational methods have inherent drawbacks that seriously limit their usefulness.

This is the subject of this thesis, *to evaluate the implementation, applicability and validity of TDDFT using different approximations and in different situations.*

In this context different steps have been carried out. First the new implementation of TDDFT in deMon2k program to calculate the excitation energies of the sodium dimer and tetramer as well as to *para*-aminobenzonitrile with a comparison against Gaussian program has been evaluated.

Second, knowing that TDDFT in its linear formulation was initially introduced to the quantum chemistry community for calculating excitation spectra of molecules in its closed-shell form, the Casida's formulation allowed both different-orbitals-for-different-spin (DODS) and fractional occupation numbers, thus permitting to apply the method to molecules with open-shell ground states. Basically this work presents equations for calculating the spin contamination of TDDFT excited states,

thus presenting an analytic tool which can help to better interpret the results from TDDFT calculations for open-shell molecules.

Third and the principal goal in this thesis was the application of the TDDFT for the description of the C-C ring-opening reaction of oxirane molecule, a textbook example of photochemical reaction. In this process, according to the Woodward-Hoffmann (WH) rules, the ring opening of C-C bond will be conrotatory (rotation of the end methylene groups in the same direction) in the ground state and disrotatory (rotation of the end methylene groups in opposite direction) in the singlet excited state. We present both ground and excited state potential energy surfaces for conrotatory and disrotatory movements on the C-C opening ring reaction using TDDFT and LDA and B3LYP functional, with and without the Tamm-Dancoff approximation (TDA). The results with the time-dependent Hartree-Fock (TDHF) and configuration interaction singles (CIS) methods were also obtained. It is well-known that (TD)DFT is a formally exact singlet-reference method, but in practice the use of approximate functionals leads to the breakdown of the single-reference method in the form of triplet instabilities. We find that the problems with triplet instabilities increases in the order TDLDA $<$ TDB3LYP $<$ TDHF. In this sense, the simple TDLDA behaves closest to the exact theory. Problems due to triplet instabilities may be further minimized using the TDA, so making the TDA TDLDA a method of choice for our investigation. It is shown that the first excited singlet is the expected $^1(n, 3s)$ Rydberg excited state. Since the simple WH photochemical mechanism is deeply entrenched in the chemical literature, we also present surfaces for the WH (valence) $^1(n, \sigma^*)$ excited state calculated using (TD)DFT.

Key-words. Quantum Chemistry, Density Functional Theory, Time-Dependent Density Functional Theory, Open and Closed-shell molecules, Excitation Spectra, Photochemistry, Excited States, Triplet Instability, Oxirane.

Contents

Chapter 1

Introduction

Photochemistry in a narrow sense is the study of chemical reactions induced by or producing light, more often ultraviolet (UV 200-400 nm) or visible (400-800 nm) light. Photochemistry may be used to induce any number of chemical processes, from initiating a chemical reaction or in the case of chemiluminescence, as a product. By extension, photochemistry is concerned with any chemical reaction passing through electronic excited states. Examples of photochemistry abound in inorganic chemistry, in synthetic organic chemistry, in biology, and in material science. Silver-based photography (now being rapidly replaced by digital photography) is a familiar example of inorganic photochemistry. Photochemical reactions extend the repertory of synthetic tools beyond that available from only thermal reactions. Moreover the initiation of photoreactions by specific absorptions means that photochemistry can be more site specific than are the heat-induced reactions. (The image on photographic film is a good example of site specificity.) For example in biology the photosynthesis process (of green plants for instance) uses solar energy to ultimately combine water and carbon dioxide to form saccharides, or polysaccharides. These products are the most important components of the living matter of plants, e.g. cellulose. In simple terms the photosynthesis involves the absorption of light by a photoactivated catalyst, the chlorophyll molecule, which oxidizes water and reduces carbon dioxide. Another interesting example in daily life concerns commercial organic sunscreens which are designed to offer photoprotection to the skin. They contain a wide variety of ingredients with differing function (e.g. UV absorbers, moisturizers, antioxidants, perfumes, etc). Amongst those ingredients are organic UV filters, which are carefully design by chemists to efficiently absorb UV radiation of the appropriate wavelengths and to dissipate the absorbed energy harmless as heat. Yet another important of photochemistry is the vision process (considered as the most important of all our senses) where 11-*cis* rhodopsin is transformed to the all-*trans* photoproduct. Finally, the firefly's living light, is a form of chemiluminescence known as bioluminescence,

which can be cited as an illustrative relevant example of a photochemical process. Here the chemical reaction involves the oxidation of: luciferin, the light-emitting molecule; adenosine triphosphate (ATP), the energy-rich molecule that is the immediate source of energy for the numerous functions involved in movements and growth in all organisms; luciferase, the enzyme that catalyzes the reaction; and a co-factor, magnesium or manganese, which works with luciferase to facilitate the reaction. In the materials science the UV-induced aging of plastics and solar cells exist as two representative examples of photochemistry in this field.

Although photochemistry, like all of science, is based on experiment, a well-known important goal is the construction and validation of hypothesis - that is, models. This model-building process has progressed to the point that, at the present time a great part of our understanding may be gained thanks to the modelling process. In this sense, the ultimate proof of understanding how a photochemical process works is to be able to simulate it theoretically. Along the way much may be learned to suggest new experiments and even to predict their outcome. Photochemically once a photon is absorbed, the molecule is an excited state with different interatomic forces than in the ground state. This excited state has higher energy than the ground state and has a shorter lifetime, making it difficult to analyze experimentally. Therefore we must learn to model how the molecule's geometry will change in this new electronic state and under what conditions it is subsequently possible to change from one electronic state to another by intersystem crossing or radiationless relaxation. Of course, sometimes emission of a photon during fluorescence or phosphorescence is also important for modeling an experiment. The job is complex but not impossible provided suitable simplifying approximations can be found.

In this context quantum chemical methods have emerged as efficient tools for the calculation of structural and other properties of solids and molecules. An important method used principally to determine the structure electronic of solids and molecules is density-functional theory (DFT) which is a formally rigorous yet computationally simple method. DFT is well established as a tool for modelling thermal reactions, and in comparison with *ab initio* methods DFT has the important advantage that it includes electron-correlation effects in a simple Hartree-Fock manner, thus allowing its application to larger molecules (e.g. biological molecules). At the same time, the time-dependent extension of DFT (TDDFT) also provides a formally rigorous method for treating excited states. At the beginning TDDFT was successfully applied to atoms, solids, and metal clusters with a jellium sphere model and the spherical average pseudopotential model. Further algorithms have had to be developed to treat excited states for molecules and TDDFT is at the moment

a good theoretical method for calculating excitation energies in molecules (principally electronic excitation spectra). However TDDFT is still relatively new and so requires testing and probably much further development will be needed for photochemical applications. In particular an important goal of this thesis is to shed light on the strengths and weaknesses of TDDFT to photochemical problems by assessing the ability of TDDFT for describing the excited-state potential energy surfaces of oxirane– a relatively simple, yet photochemically interesting molecule.

The remainder of this thesis is organized as follow. Chapter 2 first introduces important general concepts for photochemical modelling and then reviews the photochemistry of oxiranes. Chapter 3 is a review of the electronic structure methods used in this thesis. Chapters 4 to 6 are the manuscripts for four articles. Two are published (Refs. [1] and [2]) and of the two additional manuscripts one has been submitted [4] and the other one is in preparation [3]. Each of these chapters begins with a brief, somewhat informal, "insider" overview of each research project including who did what. The final chapter of this thesis summarizes what we have accomplished and provides perspectives for future work. So, in some details chapter 4 describes a new implementation of TDDFT in the deMon2k program to calculate the excitation energies of the sodium dimer and tetramer as well as to *para*-aminobenzonitrile with a comparison against Gaussian program. It is well-known that TDDFT in its linear formulation was initially introduced to the quantum chemistry community for calculating excitation spectra of molecules in its closed-shell form. However, Casida's formulation allowed both different-orbitals-for-different-spin (DODS) and fractional occupation numbers, thus opening the way to applying the method to molecules with open-shell ground states. This is the aim of chapter 5 which discusses difficulties encountered when applying TDDFT to molecules with an open-shell ground state. Basically this work presents equations for calculating the spin contamination of TDDFT excited states, thus presenting an analytic tool which can help to better interpret the results from TDDFT calculations for open-shell molecules. The work on the application of the TDDFT to modelling conrotatory and disrotatory opening ring reaction of oxirane is presented in the chapter 6, which essentially constitutes the heart of my thesis and collects together the results of my DFT, TDDFT and CASSCF (using the Molcas program) calculations as well as the HF, CIS and TDHF results from an undergraduate project that I co-directed. Comparisons are made with the high quality Quantum Monte Carlo (QMC) calculations realized by Claudia Filippi at the Instituut-Lorentz for Theoretical Physics, Universiteit Leiden in The Netherlands. This work formed the basis for photodynamics calculations carried out by our collaborators in Lausanne, Switzerland.

Major results of my thesis work are summarized and perspectives for future work are presented in the final chapter.

Bibliography

[1] Andrei Ipatov, Antony Fouqueau, Carlos Perez del Valle, Felipe Cordova, Mark E. Casida, Andreas M. Köster, Alberto Vela, and Christine Jödicke Jamorski, *J. Molec. Struct. (Theochem)* **762**, 179 (2006).
"Excitation Energies from an Auxiliary-Function Formulation of Time-Dependent Density-Functional Response Theory with Charge Conservation Constraint"

[2] M.E. Casida, A. Ipatov, and F. Cordova, in *Time-Dependent Density-Functional Theory*, edited by M.A.L. Marques, C. Ullrich, F. Nogueira, A. Rubio, and E.K.U. Gross, *Lecture Notes in Physics* (Springer: Berlin, 2006), pp. 243-257.
"Linear-Response Time-Dependent Density-Functional Theory for Open-Shell Molecules"

[3] A. Ipatov, F. Cordova, and M.E. Casida, *in preparation.*
"Excited-State Spin-Contamination in Time-Dependent Density-Functional Theory for Molecules with Open-Shell Ground States"

[4] F. Cordova, L. Joubert Doriol, A. Ipatov, M.E. Casida, C. Filippi and A. Vela, *accepted* 2007, in *J. Chem. Phys.*
"Troubleshooting Time-Dependent Density-Functional Theory for Photochemical Applications: Oxirane"

Chapter 2

Photochemistry

The previous chapter has presented the importance of photochemistry in different fields and the role of theoretical methods. In this chapter we set up the principal concepts or definitions to explore photochemical reactions. First the concept of potential energy surfaces (PES), central to our modern understanding of photochemical reactions [1] will be presented. This concept arises due to the Born-Oppenheimer approximation and surface hopping. Then a qualitative review in terms of PES is presented which gives rise to the notation of the range of photophysical and photochemical processes that happen when a molecule is excited from a singlet ground state to an excited electronic state. Finally the photochemistry of both oxirane and oxirane derivatives is discussed first from the point of view of the historically-important Woodward-Hoffmann rules and after in terms of the known experimental results as well as previous theoretical studies regarding the photochemistry of oxirane and substituted oxirane structures.

2.1 Potential Energy Surfaces

Electronic structure calculations are now widely used and very successful in applications to solving problems in many fields [3], such as spectroscopy, photochemistry and the design of optical materials where geometrical optimizations, calculations of excitation energies, and the reactions path on the surfaces are useful. Therefore, computational studies can help scientists to understand the experimental results, testing theories and making predictions of the reactions where for example the experimental conditions are too hard or too difficult to apply [4]. An important field in this subject is the photochemical process.

The way a theoretical chemist thinks about a chemical reactions is very different from just the "simple" valence-bond representation embodied in the Lewis structures present throughout the chemical literature. In addition to using this

important chemical representation of molecules, stable molecules, transition states, and photochemical intermediates are thought of as critical points (minima, saddle points, conical intersections....) on PESs. It is the goal of this section describe how the idea of a PES arises through the Born-Oppenheimer approximation to the full many-electron/many-nuclei Schrödinger equation.

Qualitatively electrons are the "glue" that holds the nuclei together in the chemical bonds of the molecules and ions. Of course, it is the nuclei's positive charges that bind the electrons to the nuclei. The competition among Coulomb repulsions and attractions, as well as the existence of non-zero electronic and nuclear kinetic energies, makes the treatment of the full Schrödinger equation an extremely difficult problem. Electronic structure theory deals with the quantum states of the electrons, usually within the Born-Oppenheimer approximation (i.e., with the nuclei held fixed) [2]. It also addresses the forces that the electrons' presence creates on the nuclei. It is these forces that determine the geometries and energies of the various stable structures of the molecule as well as transition states connecting these stable structures. Because there are ground and excited electronic states, there are different stable-structures and transition-state geometries for each different electronic state.

Let us now discuss how this qualitative picture arises out of a first-principles treatment of the Schrödinger equation.

2.1.1 Time-Independent Schrödinger equation

The term "*ab initio*" is Latin for "first principles", meaning that an *ab initio* calculation is to be performed without the use of experimentally-derived quantities except for the mass of the electron, m, the magnitude of the charge of the electron, e, and Planck's constant, h. The units we use throughout this thesis are called atomic units. These are Gaussian electromagnetic units rescaled so that

$$m = e = \frac{h}{2\pi} = 1 \text{ a.u.} \tag{2.1}$$

We are particularly interested in an *ab initio* solution of the Schrödinger equation.

In 1926, Erwin Schrödinger introduced the most fundamental equation in quantum mechanics, the time-dependent Schrödinger wave equation,

$$\hat{H}\Psi(t) = i\frac{\partial}{\partial t}\Psi(t) \tag{2.2}$$

where $\hat{H}$ is the Hamiltonian operator, $\Psi(t)$ is the wave function. Wave functions

with a well-defined energy, E, are called stationary states and have the form,

$$\Psi(t) = \Psi e^{-iEt}. \tag{2.3}$$

Inserting this equation in Eq. (2.2) leads easily to the time-independent Schrödinger equation,

$$\hat{H}\Psi = E\Psi, \tag{2.4}$$

which plays a central role in much of Quantum Chemistry. By finding a solution for the energy and wave function (eigenvalues and eigenvectors of the Hamiltonian operator), it is possible to determine theoretically important molecular properties, including optimized geometries, electric and magnetic moments, harmonic vibrational frequencies, etc. Considering all the terms in atomic units, the Hamiltonian looks like,

$$\begin{aligned} \hat{H} &= -\sum_{i=1,N} \tfrac{1}{2}\nabla_i^2 - \sum_{A=1,M} \tfrac{1}{2M_A}\nabla_A^2 - \sum_{i=1,N}\sum_{A=1,M} \frac{Z_A}{r_{iA}} \\ &+ \sum_{i=1,N}\sum_{j=1,N}^{i<j} \frac{1}{r_{ij}} + \sum_{A=1,M}\sum_{B=1,M}^{A<B} \frac{Z_A Z_B}{R_{AB}} \end{aligned} \tag{2.5}$$

The two first terms in Eq. (2.5) are the kinetic energy of the N electrons and the M nuclei, respectively. M_A is the ratio of the mass of the nucleus A to the mass of an electron (i.e., M_A is expressed in atomic units). The Coulomb attraction between the electrons and the nuclei is represented by term three, and the fourth and fifth terms describe respectively the interelectron and internuclear repulsion energies. Equation (2.2) or (2.4) with the Hamiltonian in Eq. (2.5) is a partial differential equation. To be able to solve these equations, it is necessary to approximate both the Hamiltonian and the wave function.

2.1.2 Born-Oppenheimer Approximation

The most important approximation is that of Born and Oppenheimer [2]. The Born-Oppenheimer approximation is based on the idea of a separation of time scales. Since the mass of even the lightest nuclei is much larger than the mass of an electron, one would expect classically that the electrons move faster. If they move fast enough we may consider them to move in the field of stationary nuclei (whose position is "clamped" in space.) The corresponding electronic Hamiltonian is,

$$\hat{H}_{el} = -\frac{1}{2}\sum_{i=1,N} \nabla_i^2 - \sum_{i=1,N}\sum_{A=1,M} \frac{Z_A}{r_{iA}} + \sum_{i,j=1,N}^{i<j} \frac{1}{r_{ij}}, \tag{2.6}$$

while the corresponding Schrödinger equation is,

$$\hat{H}_{el}\Psi_I^{el} = E_I^{el}\Psi_I^{el}, \tag{2.7}$$

with $\left\langle \Psi_I^{el} | \Psi_J^{el} \right\rangle = \delta_{IJ}$. Let us present a rigorous discussion of the Born-Oppenheimer approximation.

The total wave function $\Psi(\mathbf{x}, \mathbf{R}, t)$ is a function of the electron coordinates, $\mathbf{x} = (\vec{x}_1, \vec{x}_2, \cdots, \vec{x}_N)$, where $\vec{x}_i = (\vec{r}_i, \sigma_i)$ is a combined spatial, $\vec{r}_i$, and spin σ_i, coordinate and the nuclear coordinates, $\mathbf{R} = (\vec{R}_1, \vec{R}_1, \cdots, \vec{R}_N)$. Since the solutions of the electronic Schrödinger equation form a complete basis set at each geometry,

$$\Psi(\mathbf{x}, \mathbf{R}, t) = \sum_J \Psi_J^{el}(\mathbf{x}; \mathbf{R}) \chi_J(\mathbf{R}, t). \tag{2.8}$$

This is the Born-Oppenheimer expansion. Substituting into Eq. (2.2) gives,

$$\begin{aligned} &\sum_J \left(-\tfrac{1}{2} \sum_{A=1,M} \tfrac{1}{M_A} \nabla_A^2 + \sum_{A,B=1,M}^{A<B} \tfrac{Z_A Z_B}{R_{AB}} + \hat{H}_{el} \right) \Psi_J^{el}(\mathbf{x}; \mathbf{R}) \chi_J(\mathbf{R}, t) \\ &\qquad = \sum_J \Psi_J^{el}(\mathbf{x}; \mathbf{R}) \left(i \tfrac{\partial}{\partial t} \chi_J(\mathbf{R}, t) \right) \end{aligned} \tag{2.9}$$

Now,

$$\begin{aligned} &\nabla_A^2 \left(\Psi_J^{el}(\mathbf{x}, \mathbf{R}) \chi_J(\mathbf{R}, t) \right) \\ &= \vec{\nabla}_A \cdot \left[\left(\vec{\nabla}_A \Psi_J^{el}(\mathbf{x}, \mathbf{R}) \right) \chi_J(\mathbf{R}, t) + \Psi_J^{el}(\mathbf{x}, \mathbf{R}) \left(\vec{\nabla}_A \chi_J(\mathbf{R}, t) \right) \right] \\ &= \Psi_J^{el}(\mathbf{x}, \mathbf{R}) \nabla_A^2 \chi_J(\mathbf{R}, t) \\ &+ \left[\left(\nabla_A^2 \Psi_J^{el}(\mathbf{x}, \mathbf{R}) \right) + 2 \left(\vec{\nabla}_A \Psi_J^{el}(\mathbf{x}, \mathbf{R}) \right) \cdot \vec{\nabla}_A \right] \chi_J(\mathbf{R}, t), \end{aligned} \tag{2.10}$$

so left multiplying Eq. (2.9) by $\Psi_J^{el*}(\mathbf{x}; \mathbf{R})$ and integrating over $\mathbf{x}$ gives

$$\left(-\frac{1}{2} \sum_{A=1,M} \frac{1}{M_A} \nabla_A^2 + V_I(\mathbf{R}) \right) \chi_I(\mathbf{R}, t) - \sum_J \hat{\Lambda}_{IJ}(\mathbf{R}) \chi_J(\mathbf{R}, t) = i \frac{\partial}{\partial t} \chi_I(\mathbf{R}, t). \tag{2.11}$$

This is the equation of motion for the nuclear wave function $\chi_I(\mathbf{R}, t)$ on the Ith

PES,

$$V_I(\mathbf{R}) = \sum_{A,B=1,M}^{A<B} \frac{Z_A Z_B}{R_{AB}} + E_I^{el}(\mathbf{R}), \tag{2.12}$$

with nonadiabatic coupling (hopping) operator,

$$\begin{aligned} \hat{\Lambda}_{IJ}(\mathbf{R}) &= +\tfrac{1}{2}\textstyle\sum_{A=1,M} \frac{1}{M_A}\langle\Psi_I^{el}(\mathbf{R})|\nabla_A^2\Psi_J(\mathbf{R})\rangle \\ &\quad + \textstyle\sum_{A=1,M} \frac{1}{M_A}\langle\Psi_I^{el}(\mathbf{R})|\vec{\nabla}_A\Psi_J^{el}(\mathbf{R})\rangle \cdot \vec{\nabla}_A. \end{aligned} \tag{2.13}$$

The Born-Oppenheimer approximation consists of ignoring the hopping operator so that the nuclear motion is confined to a single PES.

2.1.3 Surface Hopping

The nonadiabatic operator is responsible for the fact that a time-dependent wave packet initially in a Born-Oppenheimer state,

$$\Psi(\mathbf{x}, \mathbf{R}, t) = \Psi_J^{el}(\mathbf{x}; \mathbf{R})\chi_J(\mathbf{R}, t), \tag{2.14}$$

will eventually involve into a superposition of Born-Oppenheimer states,

$$\Psi(\mathbf{x}, \mathbf{R}, t) = \sum_J \Psi_J^{el}(\mathbf{x}; \mathbf{R})\chi_J(\mathbf{R}, t). \tag{2.15}$$

The probability of observing the system in a given nuclear ($\mathbf{R}$) and electronic ($\mathbf{x}$) configuration at time t is given by

$$\begin{aligned} |\Psi(\mathbf{x}, \mathbf{R}, t)|^2 &= \sum_J |\Psi_J^{el}(\mathbf{x}, \mathbf{R})\chi_J(\mathbf{R}, t)|^2 \\ &\quad + \sum_{I,J}^{I\neq J} \Psi_I^{el}(\mathbf{x}, \mathbf{R})\chi_I(\mathbf{R}, t)\Psi_J^{el*}(\mathbf{x}, \mathbf{R})\chi_J^*(\mathbf{R}, t). \end{aligned} \tag{2.16}$$

The first term describes the probability of finding the system in electronic state J. It is called the decoherence term. The remaining coherence term describes the coherent superposition of wave functions corresponding to different electronic states.

Quantum-classical photochemical dynamics treats the electron quantum mechanically and the nuclei classically. Coherence is a quantum idea and so is normally ignored in the classical treatment of the nuclei. The nuclei are described by an ensemble of classical trajectories ("rolling balls") on the various PES and hops be-

tween the surfaces with a probability which must somehow be derived from the nonadiabatic coupling (hopping) operator.

We will now try to obtain a better understanding of the physical meaning of the hopping operator and when it can be neglected. That is, we want to study the term

$$\sum_J \hat{\Lambda}_{IJ}(\mathbf{R})\chi_J(\mathbf{R},t) = \sum_{A=1,M} \frac{1}{2M_A} \sum_J \left(G^A_{IJ}(\mathbf{R}) + 2\vec{F}^A_{IJ}(\mathbf{R}) \cdot \vec{\nabla}_A \right) \chi_J(\mathbf{R},t), \quad (2.17)$$

where

$$G^A_{IJ}(\mathbf{R}) = \left\langle \Psi^{el}_I(\mathbf{R}) | \nabla^2_A \Psi^{el}_J(\mathbf{R}) \right\rangle \quad (2.18)$$

is called the scalar coupling matrix and

$$\vec{F}^A_{IJ}(\mathbf{R}) = \langle \Psi^{el}_I(\mathbf{R}) | \vec{\nabla}_A \Psi^{el}_J(\mathbf{R}) \rangle \quad (2.19)$$

is called the derivative coupling matrix. At first sight both coupling matrices seem necessary but in fact only the derivative coupling matrix is really necessary. This is because

$$\begin{aligned} &\sum_J \left(G^A_{IJ}(\mathbf{R}) + 2\vec{F}^A_{IJ}(\mathbf{R}) \cdot \vec{\nabla}_A \right) \chi_J(\mathbf{R},t) \\ &= \sum \vec{F}^A_{IJ}(\mathbf{R}) \cdot \vec{\nabla}_A \chi_J(\mathbf{R}) + \sum \vec{\nabla}_A \cdot \vec{F}^A_{IJ}(\mathbf{R}) \chi_J(\mathbf{R}) \\ &+ \sum \vec{F}^A_{IJ} \cdot \vec{F}^A_{JK} \chi_K(\mathbf{R},t). \end{aligned} \quad (2.20)$$

The proof of the Eq. (2.20) involves a straightforward, if tedious, series of derivatives. It makes use of the relation

$$\begin{aligned} 0 &= \vec{\nabla}_A \left\langle \Psi^{el}_I(\mathbf{R}) | \Psi^{el}_J(\mathbf{R}) \right\rangle \\ &= \left\langle \vec{\nabla}_A \Psi^{el}_I(\mathbf{R}) | \Psi^{el}_J(\mathbf{R}) \right\rangle + \left\langle \Psi^{el}_I(\mathbf{R}) | \vec{\nabla}_I \Psi^{el}_J(\mathbf{R}) \right\rangle \end{aligned} \quad (2.21)$$

and the completeness relation

$$\hat{I} = \sum |\Psi^{el}_I(\mathbf{R})\rangle\langle\Psi^{el}_I(\mathbf{R})|. \quad (2.22)$$

Thus it suffices to ask when the derivative coupling Eq. (2.19) will be small. Since the scalar coupling matrix [Eq. (2.18)] will then necessarily also be small. To answer this question begin with

$$\hat{H}_{el}(R)\Psi^{el}_J(\mathbf{R}) = E_J(\mathbf{R})\Psi^{el}_J(\mathbf{R}) \quad (2.23)$$

Then

$$\langle\Psi_J^{el}(\mathbf{R})|\vec{\nabla}_A[\hat{H}_{el}(\mathbf{R})\Psi_J^{el}(\mathbf{R})]\rangle = \langle\Psi_I^{el}(\mathbf{R})|\vec{\nabla}_A[E_J(\mathbf{R})\Psi_J^{el}(\mathbf{R})]\rangle \tag{2.24}$$

or

$$\begin{aligned}&\langle\Psi_I^{el}(\mathbf{R})|\vec{\nabla}_A\hat{H}_{el}(\mathbf{R})|\Psi_J^{el}(\mathbf{R})\rangle + \langle\Psi_I^{el}(\mathbf{R})|\hat{H}_{el}(\mathbf{R})|\vec{\nabla}_A\Psi_J^{el}(\mathbf{R})\rangle \\ &= \left(\vec{\nabla}_A E_J(\mathbf{R})\right)\langle\Psi_I^{el}(\mathbf{R})|\Psi_J^{el}(\mathbf{R})\rangle + E_J(\mathbf{R})\langle\Psi_I^{el}(\mathbf{R})|\vec{\nabla}_A\Psi_J^{el}(\mathbf{R})\rangle.\end{aligned} \tag{2.25}$$

For $I \neq J$,

$$\langle\Psi_I^{el}(\mathbf{R})|\vec{\nabla}_A\hat{H}_{el}(\mathbf{R})|\Psi_J^{el}(\mathbf{R})\rangle + E_I(\mathbf{R})\vec{F}_{IJ}^A(\mathbf{R}) = E_J(\mathbf{R})\vec{F}_{IJ}^A(\mathbf{R}), \tag{2.26}$$

so

$$\vec{F}_{IJ}^A(\mathbf{R}) = \frac{\langle\Psi_I^{el}(\mathbf{R})|\vec{\nabla}\hat{H}_{el}(\mathbf{R})|\Psi_I^{el}(\mathbf{R})\rangle}{E_J(\mathbf{R}) - E_I(\mathbf{R})} \tag{2.27}$$

The numerator is the matrix element of the electronic force on the nuclei. It is small when the nuclei are moving slowly. The dominator is the energy difference between two surfaces. Thus the Born-Oppenheimer approximation is valid for slowly moving nuclei on widely separated surfaces. Otherwise surfaces hopping can occur.

These ideas can be directly seen in the Landau-Zener formula for the probability of the surfaces hopping,

$$P = e^{-2\pi\gamma}, \tag{2.28}$$

used in quantum-classical photodynamics calculations. Here [6],

$$\gamma = \frac{\min|\Delta E(t)|^2}{4\ \max|\frac{d\Delta E(t)}{dt}|}, \tag{2.29}$$

where $\Delta E(t)$ is the difference at time t of the energies of two nearly PESs and $\frac{d\Delta E(t)}{dt}$ is their rate of approach. In particular, the surface hopping probability,

$$P \cong 1 - \frac{2}{\pi}\frac{\min|\Delta E(t)|^2}{\max|\frac{d\Delta E(t)}{dt}|}, \tag{2.30}$$

increases as the surfaces come together and with the speed of passing through the surface-hopping region.

Although no quantum-classical photodynamics calculations were performed as part of this thesis, our calculations motivated successful Landau-Zener photodynamics calculations on oxirane in the Lausanne group, thus helping to validate our work. The physical picture presented here is also essential to understanding the qualitative picture of the photochemical process.

We close this section by mentioning the famous "non-crossing rule" for PESs. This states that two surfaces belonging to the same irreductible representation may cross in an F-2 dimensional "conical intersection" [4], where F is the number of the degrees of freedom in the molecule. For a diatomic, $F = 1$ and so all crossings are avoided. Nevertheless avoided intersections in diatomic can be small and resemble near crossing. Funnels, that is conical intersections and avoided crossing play a key role in photochemical modeling.

2.2 Qualitative Photochemistry

The notion of PESs and surface hopping defined in the previous subsection may now be exploited in a qualitative discussion of photochemical and photophysical phenomena. The goal here is to introduce some of the notions used by experimental photo-chemists to postulate mechanisms. These notions will be used in section 2.3 to discuss the specific case of the photochemistry of oxiranes.

2.2.1 Photochemical Landscape

Fig. 2.1 provides a schematic description of several processes that can occur when a molecule is excited from a singlet ground state (S_0). According to the usual spectroscopic selection rules, the initial photoexcitation may be to the first (S_1), second (S_2), or even higher excited state. Radiationless relaxation arises from the coupling with vibrational degrees of freedom or with other molecules in the environment. The rate of this relaxation is such that photochemistry is most likely to occur from one of the lower excited states (e.g., S_1 in Fig. 2.1). Let us suppose that the molecule is first excited to S_1. The Born-Oppenheimer approximation implies that the electronic excitation is too quick for the nuclei to move. Thus the point ("ball") is excited vertically in geometric configuration space from S_0 to the Franck-Condon (FC) point on S_1. Since the FC point is not normally a minimum on S_1, dynamics begins ("The ball begins to roll"). Now several things can happen. If the dynamics gets stuck in a minimum on S_1, and the process is not quenched by radiationless relaxation, then the $S_0 \rightarrow S_1$ transition may occur with emission of a photon. This is fluorescence. After fluorescence, the molecule may either return to its original S_0 PES minimum (no photoreaction) or go to a new S_0 PES corresponding to a chemically different composition adiabatic photoreaction because the essential change of geometry occurred on a single PES (i.e., the S_1 PES).

Changes involving more than one PES are called non-adiabatic (or diabatic). In

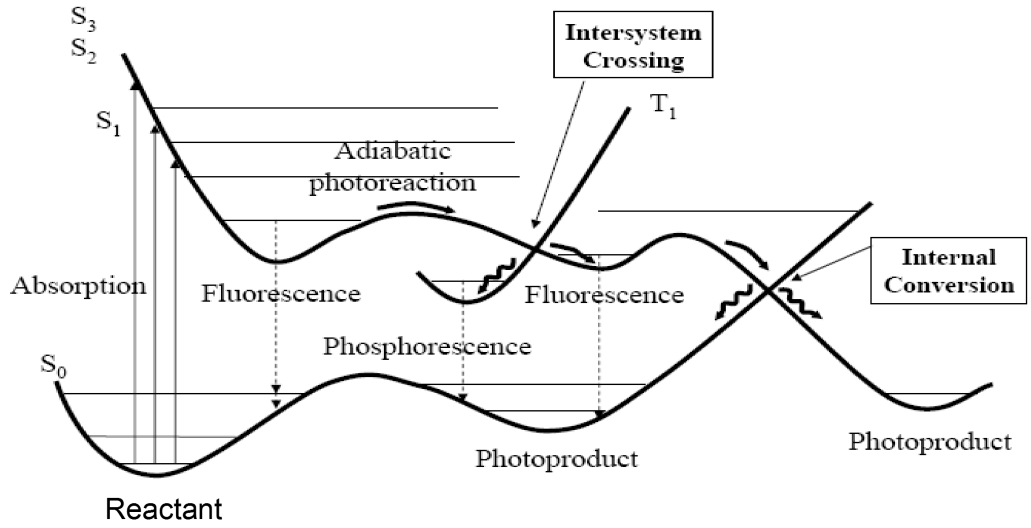

Figure 2.1: Principal photophysical and photochemical events. Picture taken from Ref. [5]

this case one has to deal with at least two electronic excited states, each one having different levels of electronic correlation and whose descriptions may require different one-electron basis functions. The determination of excited-state PES, is a much more difficult task than for the ground state.

If the transfer takes place between states of the same spin multiplicity (e.g. $S_0 \rightarrow S_1$), the system undergoes an internal conversion (IC), and the operator which drives the probability is just the nuclear kinetic energy operator (as described in the previous section in surface hopping). When the two states involved belong to different spin multiplicities (e.g. $S_0 \rightarrow T_1$) the process is called intersystem crossing (ISC) and the perturbation operator is the spin-orbit Hamiltonian [7].

Obviously, as discussed earlier the smaller is the gap between the states, the larger is the probability for transfer. Here it is clear that the most favorable topology for the transfer is the so-called "conical intersection points" where the crossing occurs between states of the same spatial and spin symmetry. The term "funnel" is sometimes used to include both conical intersections and avoided crossings where internal conversion may occur.

All these phenomena may also be described in a Jablonski diagram (Fig. 2.2). In this diagram, emission occurs either to as fluorescence (which results in a transition of the molecule from an excited state to the ground state without a change in multiplicity and occurs typically with a half-life of about 10^{-9} to 10^{-8} sec.) or phosphorescence (which implies the loss of energy from the lowest triplet state to

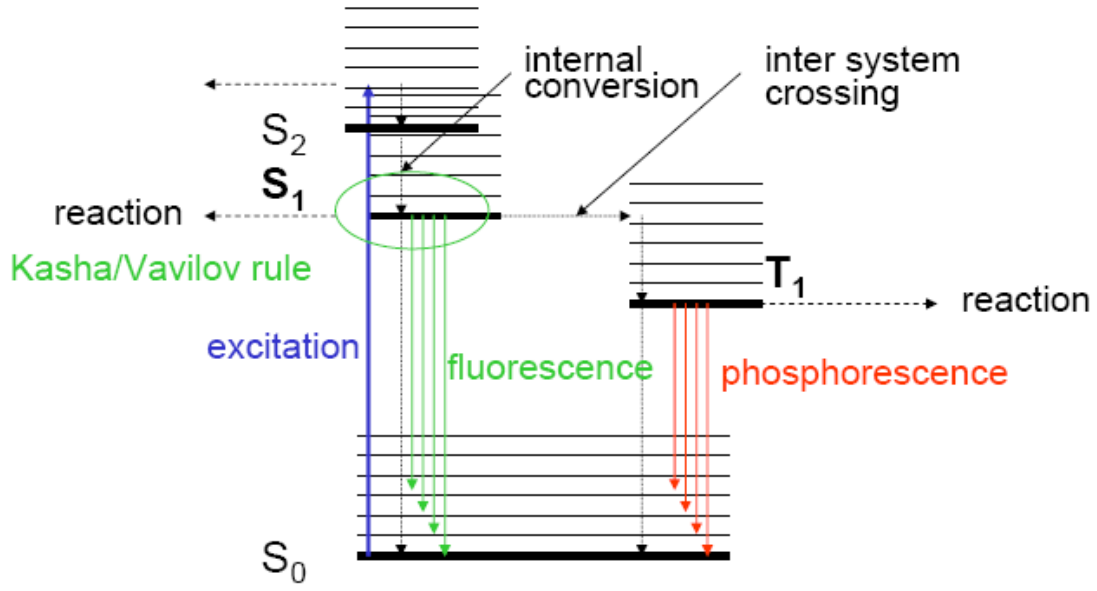

Figure 2.2: Jablonski diagram

the ground state with a half-life of about 10^{-4} seconds to minutes or even hours). Fluorescence usually occurs from the lowest vibrational state of S_1(Kasha's rule), and emission, like absorption, is always vertical. The molecule descends to an excited vibrational level of the ground state. In general both non-adiabatic transitions fluorescence and phosphorescence, like absorption, must obey the Franck-Condon principle which implies a preference for "vertical" jumps between surfaces for the representative point of the molecule.

2.2.2 Woodward-Hoffmann Rules

In 1965 Robert Burns Woodward and Roald Hoffmann published a set of rules known in organic chemistry as the Woodward-Hoffmann rules (WH), which predicted the stereochemistry of pericyclic reactions (which include electrocyclic reactions, cycloadditions, and sigmatropic reactions), based on ideas known variously as "the conservation of orbital symmetry" or "orbital symmetry control" [8]. Thanks to their work, on qualitative electronic structure theory, R. Hoffmann and Fukui were awarded the Nobel Prize in Chemistry in 1981. Principally in this work, they used a variety of theoretical approaches from simple frontier orbital (Highest Orbital Molecular Occupied, HOMO/Lowest Unoccupied Molecular Orbital, LUMO) arguments, through orbital correlation diagrams, interaction diagrams, and perturbation theory arguments.

The WH rules basically states that pericyclic reactions are allowed if the occupied orbitals in the reactants have the same symmetry as the occupied orbitals in the products. Here the properties of the primary π orbitals involved in the process are important. So, if the symmetries of the occupied/unoccupied orbitals of the reagents and the products match, then this implies that they can easily transform into one another and the reaction is said to be (orbital) symmetry allowed. On the other hand, symmetry correspondence between occupied and unoccupied orbitals results in an unfavorable situation with an associated high activation barrier; such reactions are classified as orbital symmetry forbidden reactions. An additional technique that helps to recognize if the reaction is allowed or forbidden is more pictorial, and relies on considering the frontier molecular orbitals (FMOs) of the interacting molecules. This interpretation is mathematically justified using perturbation theory. One analyzes the HOMO of one reactant and the LUMO of the other with respect to the nodal properties of the (FMOs) at the interaction centers to determine whether or not a bonding overlap will occur. This means that the lobes of the π orbitals of the interacting centers must have the same sign. An interesting example in the literature concerns the electrocyclic reaction of cyclobutenes [9]. The Fig. 2.3 shows the FMOs for the thermal electrocyclic ring-opening reaction of cyclobutene. In this case a conrotatory[1] process is allowed in the reaction. In this orbital correlation diagram we can see that the ground state of cyclobutene correlates with the ground state of butadiene ($\sigma^2\pi^2$ correlates with $\psi_1^2\psi_2^2$), therefore the thermal process is thus allowed in either direction.

When an electron is promoted, now the ψ_3 becomes or corresponds to the HOMO in the butadiene structure. The Fig. 2.4 shows the correlation diagram for this process. In this orbital correlation diagram we can see that the first excites state of cyclobutene correlates with the first excited state of butadiene ($\sigma^2\pi\pi^*$ correlates with $\psi_1^2\psi_2\psi_3$) which permits that the photochemical electrocyclic ring-opening reaction of cyclobutene be allowed by a disrotatory[2] process. It is worthwhile to note, that a symmetry plane σ is maintained along of the reaction. In chapter 6 we will present the correlation diagrams for the conrotatory and disrotatory processes for the oxirane molecule.

[1] In a conrotatory manner the orbitals lobes involved in the bond-breaking or bond-forming process will rotate in the same direction

[2] In a disrotatory motion the orbitals lobes implied in the bond-breaking or bond-forming process will rotate in the opposite direction

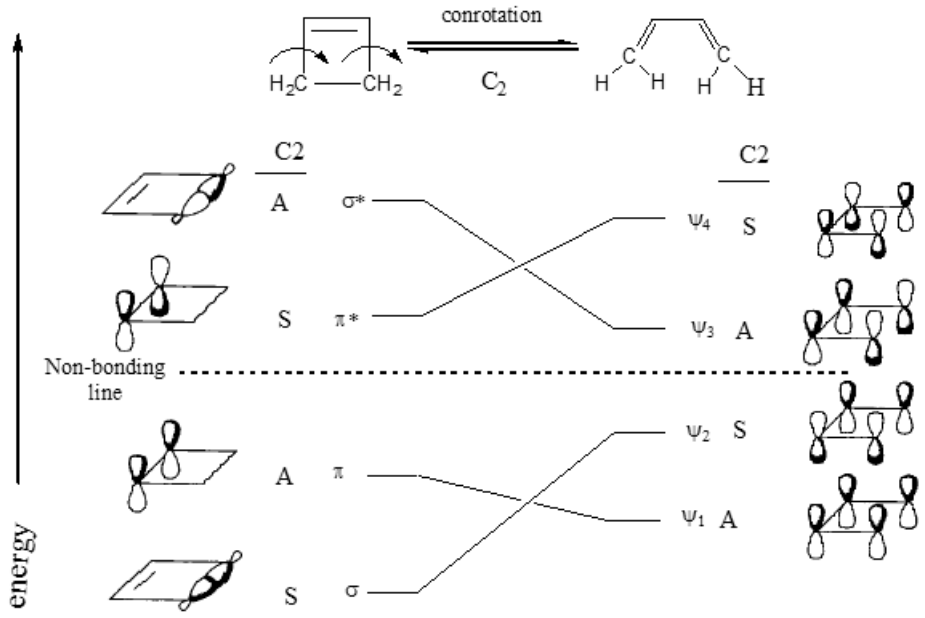

Figure 2.3: Woodward-Hoffmann correlation diagram for the conrotatory process in the electrocyclic reaction of cyclobutene. Diagram done considering Ref. [9].

2.3 Photochemistry and Thermal Reactions of Oxiranes

The photochemical and thermal reaction of ethylene oxide (EO commonly known as oxirane and whose structure is shown in the Fig. 2.5) have been extensively studied for a long time both in an experimentally and theoretically manner. Experimentally the first study reported is attributed to Phibbs et al., [10], who studied the mercury photosensitized reaction of oxirane and where the experimental conditions were in function of the pressure (between 10 and 600 mmHg) using temperatures of 200 and 300 °C. In this study, the following processes were detected:

1. The occurrence of an isomerization reaction by which acetaldehyde was formed as a major product,

2. The formation of the principal products in this reaction were H_2, CO, CH_3CHO, and,

3. A polymerization process was also found, which substances of the types $((CH_2)_2O)_n$ and $(CH_2)_n$ were implied.

The nature of the products was explained in function of a mechanism based principally on the previous formation of the activated oxirane molecule from which ac-

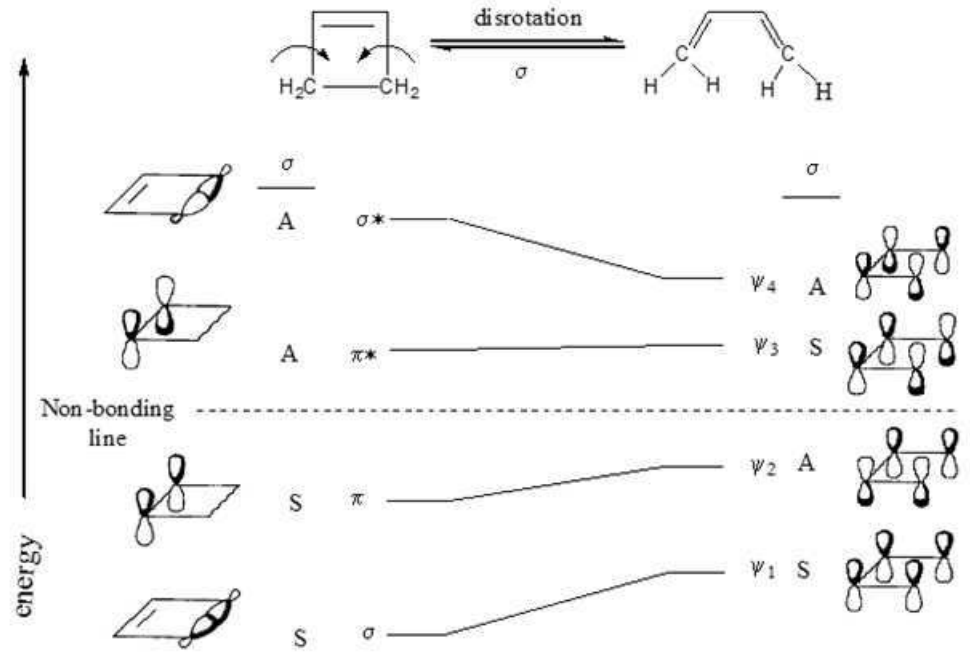

Figure 2.4: Woodward-Hoffmann correlation diagram for the disrotatory process in the electrocyclic reaction of cyclobutene. Diagram done considering Ref. [9].

etaldehyde is formed by either a first or second order process:

$$\begin{aligned} (CH_2OCH_2)^* &\xrightarrow{h\nu} CH_3CHO, \\ (CH_2OCH_2)^* + (CH_2)_2O &\xrightarrow{h\nu} CH_3CHO + (CH_2)_2O. \end{aligned} \tag{2.31}$$

The formation of others products was also explained on the basis of the decomposition of activated oxirane, or its interaction with saturated hydrocarbons leading to the formation of the corresponding alkyl radical and an H atom.

$$\begin{aligned} (CH_2OCH_2)^* &\xrightarrow{h\nu} H_2 + CO + CH_2, \\ (CH_2OCH_2)^* + (CH_2)_2O &\xrightarrow{h\nu} H_2 + CO + CH_2 + (CH_2)_2O. \end{aligned} \tag{2.32}$$

In 1950, Gomer and Noyes [11] confirmed the formation of the products found by Phibbs's work and additionally explained the formation of CH_4, CH_3CH_3, and small

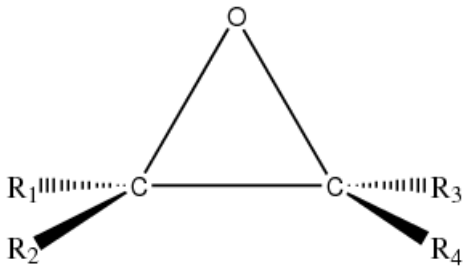

Figure 2.5: General structure of oxiranes. For oxirane molecule R_1, R_2, R_3, R_4=H.

quantities of formaldehyde and acetaldehyde. Here the vapor phase photochemistry of oxirane and of the mixtures of this compound with mercury dimethyl were analyzed in considerable detail in addition to the direct photochemical reaction of oxirane. The variables used were also pressure, temperature and the light intensity (in this case they used a hydrogen discharge as a light source which irradiated to oxirane molecules at wavelengths below 2000 Å)[3]. In the direct photodecomposition of oxirane, the products were carbon monoxide, hydrogen, methane, ethane, acetaldehyde, and possibly formaldehyde. In the mercury dimethyl sensitized decomposition, the products were much the same except hydrogen was absent and some evidence, was found for propionaldehyde. The photochemical reaction of the mixture could be expressed as,

$$\mathrm{CH_3} + (\mathrm{CH_2})_2\mathrm{O} \xrightarrow{h\nu} \mathrm{CH_4} + \mathrm{C_2H_3O}. \tag{2.33}$$

The C_2H_3O radical appeared to be stable and was thought to disappear in part in the formation of propionaldehyde. In the photolysis of pure oxirane, the primary step was assumed to be

$$(\mathrm{CH_2})_2\mathrm{O} \xrightarrow{h\nu} \mathrm{CH_3} + \mathrm{HCO}. \tag{2.34}$$

In this manner, we can observe that the Gomer-Noyer mechanism [11] for the oxirane molecule involves first C - O cleavage, followed by the hydrogen migration, and finally the C - C bond is broken. Figure 2.6 shows this mechanism.

In an attempt to elucidate the mechanism of the reaction between oxirane and CH_3 radicals, the pyrolisis of oxirane was studied in the temperatures range 400

[3]The laser was not invented until later 1964 (Noble prize in physics).

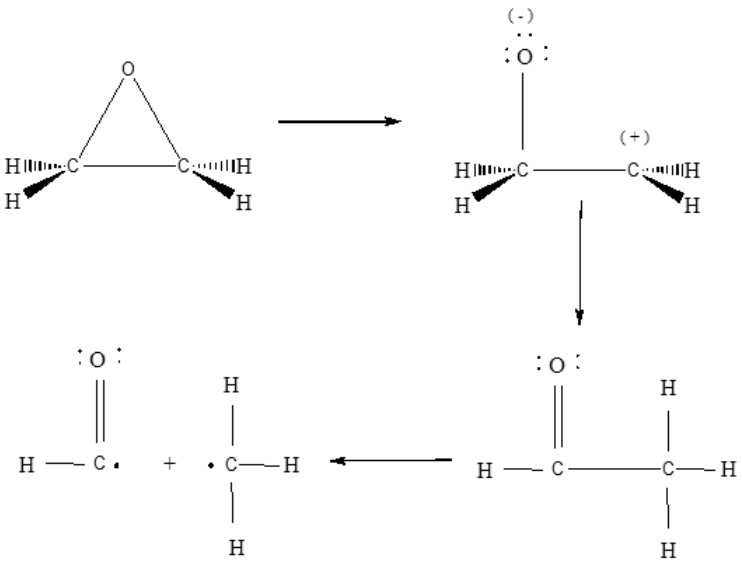

Figure 2.6: Gomer-Noyer mechanisms for the oxirane molecule (Scheme from Ref. [11].)

- 500 °C [12], as well as at much higher temperatures. In this work Benson [12] demonstrated that the pyrolisis of oxirane proceeded through an excited $(CH_3CHO)^*$ molecule which may be quenched to ground state CH_3CHO or decomposed into CH_3 + CHO. The Fig. 2.7 represents this mechanism. We again observe that the

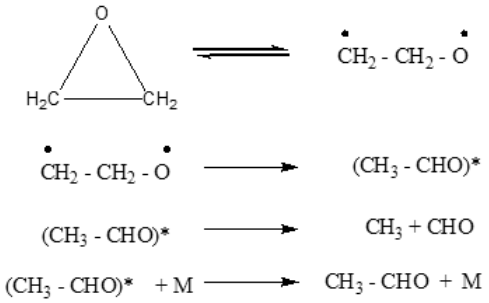

Figure 2.7: Pyrolisis of the oxirane molecule. Mechanism from Ref. [12].

formation of products depends first on the rupture of C - O bond and after by the hydrogen migration or C - C bond breaking.

In 1965 Linn, Webster and Benson [13, 14] synthesized a series of substituted oxiranes (tetracyanoethylene oxides TCNEO) which can be readily adds to olefin, acetylenes and certain aromatic systems to give tetracyanotetrahydro derivatives and dihydrofurans in good yield. For example, the reaction of TCNEO with ethylene and acetylene is represented in the Fig. 2.8. As can be seen this thermal reaction was

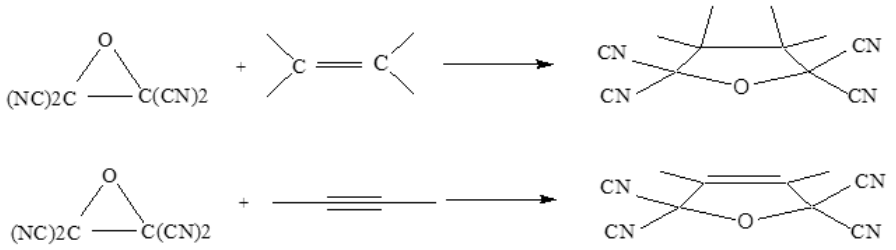

Figure 2.8: Reaction between TCNEO and ethylene (top) and acetylene (below).

marked by an unorthodox cleavage of the epoxide ring between C - C bond which is in contrast to the mechanism proposed in the photochemical reaction. Although in the reaction of TCNEO with benzene molecule (see Fig. 2.9) the yield is not higher than in the olefin case (approximatively 35 %) the experimental evidence, principally analytical and spectroscopy determinations, showed that it was possible. An interesting observation here is concerning to the reaction mechanism. Kinetic

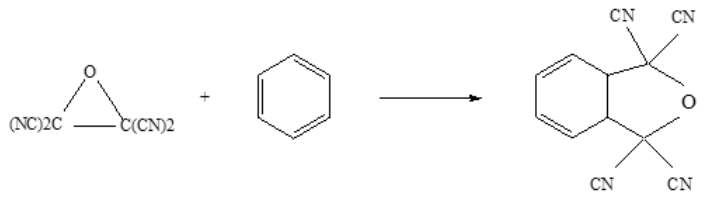

Figure 2.9: Thermal reaction of TCNEO and benzene.

studies [15] showed that the addition of TCNEO to olefins takes place in two steps, the first of which is a thermal promotion of the epoxide to an activated species followed by the C - C rupture giving rise to a hybrid biradical and zwitterionic species which adds to the olefin by a concerted or near-concerted cyclic process. Considering the TCNEO compound its hybrid structures are represented in the Fig. 2.10, and there is no doubt that this activated species are now the well-known carbonyl ylide compounds. Since TCNEO contains four identical substituents, no experimental conclusion about the stereochemistry of the ring opening can be drawn from this cycloadducts of (Fig. 2.8).

One interesting class of compounds is that utilized by Griffin et al., [16], the so-called aryl-oxiranes, which were utilized as new precursors for phenylcarbenes. Principally here, the nature of the final photoproducts of the phenyloxiranes (such as phenyloxirane, diphenyloxirane, triphenyloxirane and tetraphenyloxiranes with different substituent combinations i.e., cyano, methoxy and carbomethoxy) at ambient or higher temperatures conditions is such that they arise from splitting of bonds

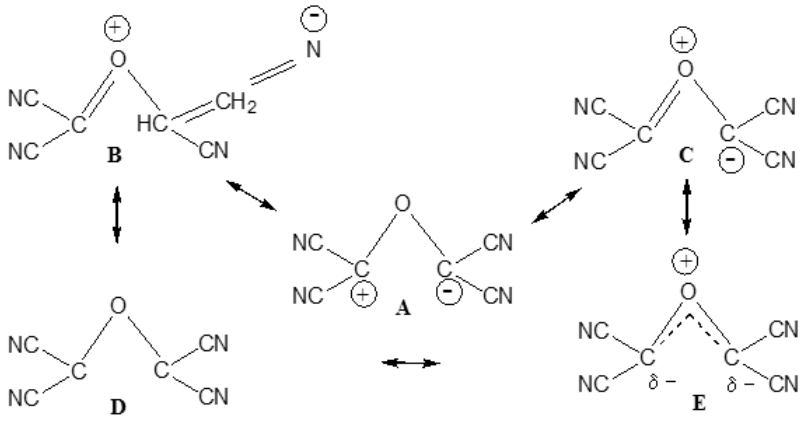

Figure 2.10: Hybrid structures for the TCNEO compound.

in pairs and where all pair combinations are possible; that is, a C - C bond and one of the other C - O bonds splits, as well as no C - C bonds but both C - O bonds can split [17]. Of course, the pathway reaction of this process involves the production of a carbene and a carbonyl species represented in the Fig. 2.11. These divalent carbon species were shown to have properties which are qualitatively and quantitatively similar to carbenes generated from diazo compounds in the reactions with alkanes, alkenes and alcohols. However, an interesting fact was observed when the photolysis

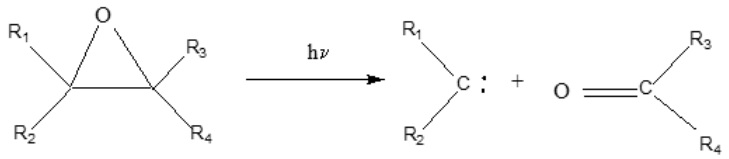

Figure 2.11: Photochemistry of phenyloxirane compounds. Here R_1, R_2, R_3 and R_4, can be represented by C_6H_5, CN, CH_3, OCH_3 or α-naphthyl groups. Scheme taken from Ref. [17].

of this phenyloxiranes was carried out at 77 °K (low-temperature photolysis). This photolysis also produced in small quantities aryl carbenes and carbonyl compounds but in addition, highly colored intermediates were formed, which were identified as the cabonyl ylides compounds. For example, if we consider the photolysis of *cis*- and *trans*-2,3-diphenyloxiranes (Fig. 2.12) the ring opening and recyclization is typical and for the *trans* isomer dissolved in ethanol glass produced an orange material along with small amounts of benzaldehyde, phenylmethylene and desoxybenzoin, while that irradiation of *cis* compound gave similar products, but the colored intermediate was a red compound, whose coloration disappeared when the system was

warm-up. Experimental evidence (where up to 90 % of the product was found)

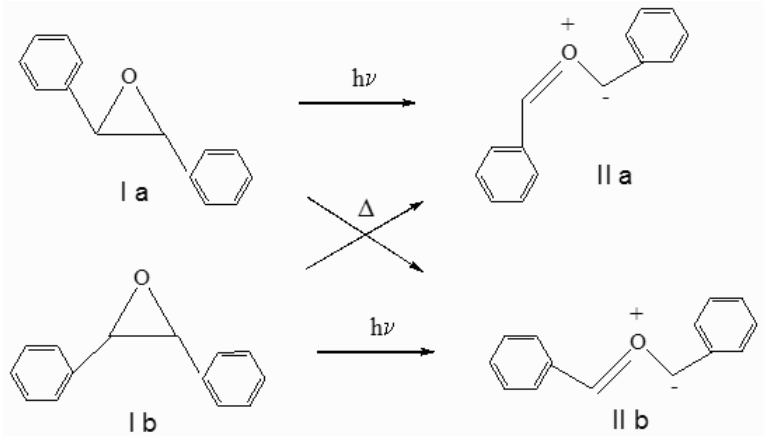

Figure 2.12: Photochemical and thermal reactions of diphenyloxiranes compounds. In the photochemical reaction a disrotatory process is allowed while a conrotatory process happens in the thermal reaction. Mechanism considered from Ref. [18].

confirmed that the opening and recyclization occurs via a concerted disrotatory process with conservation of orbital symmetry [19, 20]. Thermally, aryl-oxiranes open in a conrotatory fashion as predicted by the WH rules. However, the orbital symmetry restrictions are less stringent in the photochemical reaction, as compared to the thermal reaction, as indicated by chemical trapping of the photochemically generated carbonyl ylides. Thus, the photochemical ring opening of *cis*- and *trans*-2,3-diphenyloxiranes to isomeric intermediates and the stereospecific recyclization of the latter to oxiranes suggests general structures of the type 2a, rather than 2b, 1a or 1b which do not posses double bonds or double bond character (Fig. 2.13).

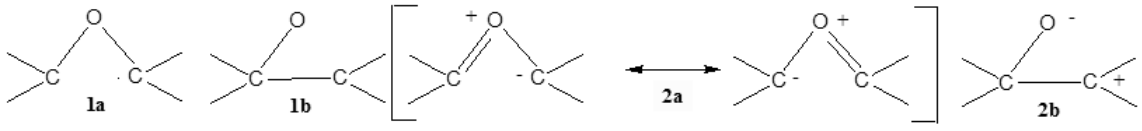

Figure 2.13: Zwitterions structures 2a or 2b formed directly or rapidly from short-lived diradical 1a or 1b.

Theoretically the first study reported in the literature about the ring opening reaction of oxirane compound was realized by F. Hayes [21]. In this study a non-empirical self-consistent field (SCF) molecular orbital (MO) theory in a contracted basis was used to calculate the potential energy surfaces for the carbon-carbon bond cleavage in oxirane. Two principal structures one which with the terminal methylene groups perpendicular to the C-O-C plane (structure 90, 90, form) and the other

one lying in the C-O-C plane (structure 0, 0 form) were determined being the later structure more stable. Huisgen and co-workers studied the thermal cycloadditions of oxiranes [22], and proved beyond doubt that carbonyl ylides are intermediates in these reactions. This work generated a great interest and many studies were dedicated to elucidate the chemistry of carbonyl ylides. Figure 2.14 shows the chemistry of substituted carbonyl ylides. In 1978 Bigot, Sevin and Devaquet [24], reported

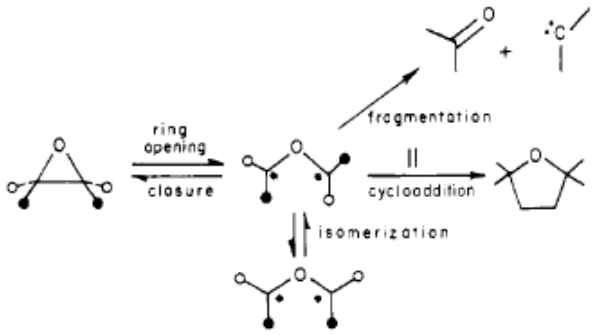

Figure 2.14: Chemistry of the carbonyl ylides. Mechanism taken from Ref. [23].

high-level *ab initio* calculations on the thermal and photochemical behavior of oxirane molecule. They showed different possible reaction paths for this molecule. The Fig. 2.15 shows the different intermediates and the final products obtained in the divers reaction paths. It is clear that different kind of intermediates and final products are possible depending on the form where the bond rupture happens. For

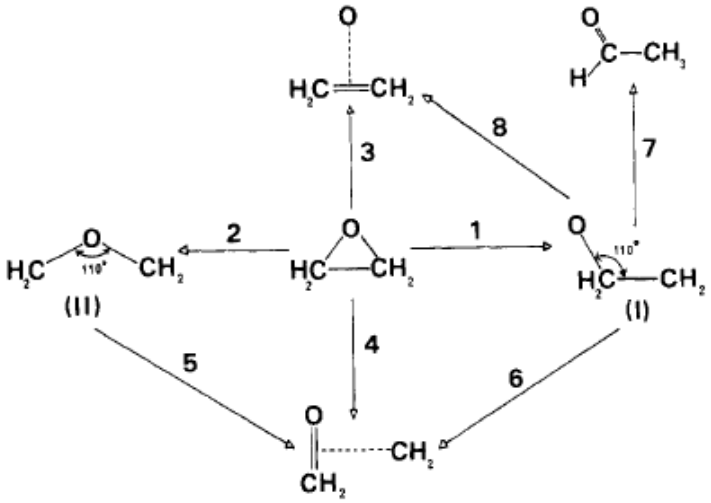

Figure 2.15: Possible reaction paths for the oxirane molecule. Mechanism taken from Ref. [24].

example the one-bond rupture (paths 1 and 2) produces the intermediates I and II (the intermediate II is often named the parent carbonyl ylide). We can obtain ethylene and atomic oxygen by doing a simultaneous two-bond rupture (path 3) or formaldehyde plus a carbenic methylene species (path 4) if the cycle breaking is done on the C-C and C-O bonds. The latter fragments can also proceed from evolution of the intermediates I, considering the C-C rupture (path 6) or II, by C-O cleavage (path 5), and the former from intermediate I by C-O rupture (path 8). In this scheme the hydrogen migration from a carbon to the other is also possible (path 7) giving acetaldehyde compound (path 7). However and due to the use of a minimal basis set (STO-3G) the theoretical values of singlet vertical excitations were not in good agreement with experimental values. In fact and as it is well-established now the electronic excitations in oxirane molecule involve the $O(n) \rightarrow 3s$ and $3p$ Ryberg transitions [25, 26], which require the use of a more extensive basis sets that include polarization and diffuse parts. This will be discussed in the chapter 6.

2.4 Conclusion

Suppose that we wish to investigate theoretically even as simple a photoreaction as that of oxirane. We have seen in Fig 2.1 the variety of possible photophysical and photochemical processes. At the very least we must consider seeking critical points such as minima, transitions states, and funnels involving PESs of one or more excited states, as well as pathways in-between them. Sometimes this appears sufficient for describing a given photochemical reaction. Often however, because photoreactions have excess energy due to the excitation process (unless the reactions can be run at the very low temperature) and because energy and forces alone do not control surface hopping, some type of dynamics calculations is also needed in photochemical modeling. This usually implies doing on-the-fly electronic structure calculations of the excited-state energies and forces. As such calculations can be quite costly in computational resources, a balance must be struck between accuracy and efficiency in the choice of electronic structure method. Today the most successful approaches are based upon the CASSCF method, however many workers hope that use can be made of efficient DFT-based methods. In this thesis we ask how TDDFT will have to be adopted for use in photochemical dynamics calculations. The next chapter provides a comparative review of different electronic structure methods.

Bibliography

[1] Nicolas J. Turro, *Modern Molecular Photochemistry*, University Science Books, Sausalito, **(1991)**.

[2] M. Born and J.R. Oppenheimer, *Ann. Phys.* **84**, 457 (1927).

[3] A. Szabo and N.S. Ostlund, *Modern quantum chemistry. Introduction to advanced electronic structure theory*, (McGraw-Hill Inc., New York, **1989**).

[4] Conical Intersections: Electronic Structure, Dynamics, and Spectroscopy, edited by W. Domcke, D.R. Yarkony, and H. Köppel, *Advanced Series in Physical Chemistry, Vol. 15* (World Scientific: Singapore, **2004**).

[5] L. Serrano-Andrés and M. Merchán, *Journal of Molecular Structure, Theochem*, **729**, 99 (2005).

[6] G. A. Jones, B. K. Carpenter, and M. N. Paddon-Row, *J. Am. Chem. Soc.*, **120**, 5499, (1998).

[7] M. Klessinger, J. Michl, *Excited states and Photochemistry or Organic Molecules*, VCH Publishers, New York, **1995**.

[8] R.B. Woodward and R. Hoffmann *J. Am. Chem. Soc.*, **87**, 395, (1965).

[9] W. R. Dolbier Jr., H. Koroniak, K. N. Houk, and C. Sheu, *Acc. Chem. Res.*, **29**, 471, (1996).

[10] M. K. Phibbs, B. de B. Darwent, and E. W. R. Steacie, *J. Chem. Phys.*, **16**, 39 (1948).

[11] E. Gomer and W.A. Noyes, Jr., *J. Am. Chem. Soc.*, **72**, 101 (1950).

[12] S. W. Benson, Jr., *J. Chem. Phys.*, **40**, 105 (1964).

[13] W. J. Linn, O. W. Webster and R. E. Benson, *J. Am. Chem. Soc.* **87**, 3651 (1965).

[14] W. J. Linn and R. E. Benson, *J. Am. Chem. Soc.* **87**, 3657 (1965).

[15] W. J. Linn, *J. Am. Chem. Soc.*, **87**, 3665, (1965).

[16] A. M. Trozzolo, W. A. Yager, G. W. Griffin, H. Kristinson and I. Sarkar, *J. Am. Chem. Soc.*, **89**, 3357, (1967).

[17] R. S. Becker, R. O. Bost, J. Kolv, N. R. Bertonier, R. L. Slith and G. W. Griffin, *J. Am. Chem. Soc.*, **92**, 1302, (1970).

[18] K. Peters, *Ann. Rev. Phys. Chem.*, **38**, 253, (1987).

[19] T. DoMinh, A. M. Trozzolo and G. W. Griffin, *J. Am. Chem. Soc.*, **92**, 1402, (1970).

[20] D. R. Arnold and L. A. Karnischky, *J. Am. Chem. Soc.*, **92**, 1404, (1970).

[21] E. F. Hayes, *J. Chem. Phys.*, **51**, 4787, (1969).

[22] R. Huisgen, *Angew. Chem., Int. Ed. Engl.*, **16**, 572, (1977).

[23] K. N. Houk, Nelson G. Rondan, Cielo Santiago, Catherine J. Gallo, Ruth Wells Gandour, and Gary W. Griffin, *J. Am. Chem. Soc.*, **102**, 1504, (1980).

[24] B. Bigot, A. Sevin, and A. Devaquet, *J. Am. Chem. Soc.*, **101**, 1095, (1978).

[25] H. Basch, M.B Robin, N.A. Kuebler, C. Baker, and D.W. Turner, *J. Chem. Phys.*, **51**, 52 (1969).

[26] T.-K. Liu and A.B.F. Duncan, *J. Chem. Phys.*, **17**, 241 (1949).

Chapter 3

Theoretical Methods

This chapter discusses the background and theory of electronic structure methods, beginning with the most basic approximate methods used to solve the Schrödinger equation and continuing on with advanced quantum chemical techniques, whose aim is to correct the deficiencies of Hartree-Fock theory by taking into account electron correlation.

3.1 Ground States

3.1.1 *Ab-Initio Methods*

In *ab-initio* (i.e. first principle wave function) methods, we seek to solve the Schrödinger equation,

$$\hat{H}\Psi(\vec{x}_1, \vec{x}_2, ..., \vec{x}_N) = E\Psi(\vec{x}_1, \vec{x}_2, ..., \vec{x}_N) \tag{3.1}$$

directly for N electrons in the field of M clamped nuclei. Here $\vec{x}_i = (\vec{r}_i, \sigma_i)$ includes both the space, $\vec{r}_i = (x_i, y_i, z_i)$, and spin, σ_i, coordinates of electron i and,

$$\hat{H} = -\frac{1}{2}\sum_{i=1,N}^{N}\nabla_i^2 - \sum_{i=1,N}\sum_{A=1,M}\frac{Z_A}{r_{iA}} + \sum_{i,j=1,N}^{j>i}\frac{1}{r_{ij}}. \tag{3.2}$$

is the Hamiltonian. The wave function must satisfy the Pauli principle that is, Ψ must be antisymmetric with respect to the exchange of pairs electrons.

$$\Psi(\vec{x}_1, ..., \vec{x}_i, ..., \vec{x}_j, ..., \vec{x}_N) = -\Psi(\vec{x}_1, ..., \vec{x}_j, ..., \vec{x}_i, ..., \vec{x}_N), \tag{3.3}$$

Since no exact solution of the Schrödinger equation is known for $N > 2$ (Hylleraas provided an essentially exact method for solving the helium atom), approximations must be made.

3.1.1.1 Variational Principle

One very successful way to make approximations is based upon the variational principle. We seek approximations for the exact solutions of

$$\hat{H}\Psi_I = E_I\Psi_I, \tag{3.4}$$

where $E_0 \leq E_1 \leq \cdots$.

Theorem (Variational principle)
Any trial wave function, Φ, which satisfies the same boundry conditions as the exact wave functions, Ψ_I and is orthonormal to the first M wave functions,

$$< \Psi_0|\Phi >=< \Psi_1|\Phi >= \cdots =< \Psi_{M-1}|\Phi >= 0, \tag{3.5}$$

satisfies

$$E_M \leq \frac{< \Phi|\hat{H}|\Phi >}{< \Phi|\Phi >} \tag{3.6}$$

with equality if and only if

$$\hat{H}\Phi = E_M\Phi. \tag{3.7}$$

In particular the variational principle applies to the lowest state of each symmetry as long as the trial wave function is chosen to have this same symmetry.

3.1.1.2 Hartree-Fock Approximation

In 1928, Hartree introduced his method for finding solutions to the Schrödinger equation [2]. In 1930, Fock recognized that Hartree's method violated the Pauli principle and so modified Hartree's method by using a trial wave function in the form of a Slater determinant [3],

$$\Phi(\vec{x}_1, \vec{x}_2, ..., \vec{x}_N) = \frac{1}{\sqrt{N!}} \begin{vmatrix} \psi_1(\vec{x}_1) & \psi_2(\vec{x}_1) & \cdots & \psi_N(\vec{x}_1) \\ \psi_1(\vec{x}_2) & \psi_2(\vec{x}_2) & \cdots & \psi_N(\vec{x}_2) \\ \vdots & \vdots & \ddots & \vdots \\ \psi_1(\vec{x}_N) & \psi_2(\vec{x}_N) & \cdots & \psi_N(\vec{x}_N) \end{vmatrix}, \tag{3.8}$$

constructed from N orthonormal spin orbitals, $\psi_1, \psi_2, ..., \psi_N$. A spin orbital is a product of a spatial orbital, $\phi_{i\sigma}$(r), and one of the two orthonormal functions α and β describing spin up and spin down, respectively, $\psi_i(\vec{x}) = \phi_{i\sigma}(\vec{r})\ \sigma$; $\sigma = \alpha$ or β.

The factor $1/\sqrt{N!}$ is a normalization constant. Often times the Slater determinant of Eq. (3.8) is abbreviated as

$$\Phi = |\psi_1 \psi_2 \cdots \psi_N|. \tag{3.9}$$

The optimal Hartree-Fock (HF) energy and the wave function are obtained by minimizing the variational energy,

$$\begin{aligned} E &= \min_{\Phi \to N} E[\Phi], \end{aligned} \tag{3.10}$$

subject to the constraint that the orbitals be orthonormal,

$$\langle \psi_i | \psi_j \rangle = \delta_{ij}. \tag{3.11}$$

The square bracket notation

$$E[\Phi] = \frac{< \Phi | \hat{H} | \Phi >}{< \Phi | \Phi >} \tag{3.12}$$

indicates that E is a functional - that is, a function of a function. The concept of a functional is especially important in density functional theory (DFT) which will be discussed later. The HF energy, E_{HF}, is given by

$$E_{HF} = \langle \Phi | H_{el} | \Phi \rangle = \sum_{i=1}^{N} \langle \psi_i | \hat{h} | \psi_i \rangle + \frac{1}{2} \sum_{i,j=1}^{N} [(ii|f_H|jj) - (ij|f_H|ji)], \tag{3.13}$$

where

$$(pq|f_H|rs) = \int \int \psi_p^*(x_1) \psi_q(x_1) \frac{1}{r_{12}} \psi_r^*(x_2) \psi_s(x_2) dx_1 dx_2 \tag{3.14}$$

is an electron repulsion integral in Mulliken (charge cloud) notation[1]. In the minimization of Eq. (3.13) the constraint that the spin orbitals remain orthonormal needs to be enforced. A convenient way to do this is using the method of Lagrange multipliers. The Lagrangian is [2],

$$\mathcal{L} = \langle \Psi | H_{el} | \Psi \rangle - \sum_{i,j} \epsilon_{i,j} (\langle \psi_i | \psi_j \rangle - \delta_{i,j}) \tag{3.15}$$

[1] $f_H(\vec{x}_1, \vec{x}_2) = 1/r_{12}$ is the Hartree kernel. Later we will introduce the exchange-correlation kernel, f_{xc}.

[2] We use the index convention $\underbrace{ab\ldots gh}_{virt}\underbrace{ij\ldots klmn}_{occ}\underbrace{pq\ldots xyz}_{free}$

where $\epsilon_{i,j}$ are the Lagrange multipliers. The minimization of Eq. (3.15) yields,

$$\hat{f}(i)\psi_i(\vec{x}) = \sum_{j=1}^{N} \epsilon_{i,j}\psi_j(\vec{x}) \tag{3.16}$$

where $\hat{f}(i)$ is the Fock operator, for electron i,

$$\hat{f}(i) = -\frac{1}{2}\nabla_i^2 - \sum_{A=1}^{M} \frac{Z_A}{r_{iA}} + \sum_{i=1}^{N}[\hat{\mathcal{J}}_i(i) - \hat{\mathcal{K}}_i(i)]. \tag{3.17}$$

This operator is identical for all electrons and so we may drop the label i. Here $\hat{\mathcal{J}}_i$ is the Coulomb operator describing the Coulomb interaction due to an electron in spin orbital ψ_i. The action of $\hat{\mathcal{J}}_i$ on an orbital ψ is given by

$$\hat{\mathcal{J}}_i\psi(\vec{x}_1) = \psi(\vec{x}_1)\int \frac{\psi_i^*(\vec{x}_2)\psi_i(\vec{x}_2)}{r_{12}}d\vec{x}_2. \tag{3.18}$$

The total Coulomb operator,

$$\hat{J} = \sum_{i=1,N} \hat{J}_i = \int \frac{\rho(\vec{x}_2)}{r_{12}}d\vec{x}_2, \tag{3.19}$$

may be expressed in terms of the density,

$$\rho(\vec{x}) = \sum_{i=1,N} |\psi_i(\vec{x})|^2. \tag{3.20}$$

The total Coulomb operator represents the classical Coulomb repulsion with the charge cloud of all the electrons. As such the Coulomb term contains a self-interaction error which must be removed somehow since an electron cannot interact with itself. The operator $\hat{\mathcal{K}}$ is called an exchanged operator. Its action on an orbital is given by

$$\hat{\mathcal{K}}_i\psi(\vec{x}_1) = \psi_i(\vec{x}_1)\int \frac{\psi_i^*(\vec{x}_2)\psi(\vec{x}_2)}{r_{12}}d\vec{x}_2. \tag{3.21}$$

The action of the total exchange operator,

$$\hat{\mathcal{K}}\psi(\vec{x}_1) = \sum_{i=1,N} \hat{\mathcal{K}}_i\psi(\vec{x}_1) = \int \frac{\gamma(\vec{x}_1,\vec{x}_2)\psi(\vec{x}_2)}{r_{12}}d\vec{x}_2, \tag{3.22}$$

may be expressed in terms of the density matrix,

$$\gamma(\vec{x}_1, \vec{x}_2) = \sum_{i=1,N} \psi_i(\vec{x}_1)\psi_i^*(\vec{x}_2). \tag{3.23}$$

The most important function of the exchange operator is to remove the self-interaction error in the Coulomb term because

$$(\hat{J}_i - \hat{K}_i)\psi_i(\vec{x}) = 0. \tag{3.24}$$

However the exchange operator also represents the fact that forbidding same-spin electrons to occupy the same orbital (Pauli exclusion principle) reduces the total electron repulsion energy by keeping electrons apart in space. The operator $\hat{f}$ is hermitian and invariant to a unitary transformation of the occupied orbitals. By choosing an unitary transformation Eq. (3.16) can be written in a diagonal form,

$$\hat{f}\psi_i = \epsilon_i\psi_i \tag{3.25}$$

This is known as the Hartree-Fock (molecular orbital) equation. The quantity ϵ_i is the orbital energy of ψ_i. Hence, the task is to find spin orbitals that are eigenfunctions of the Fock operator.

In 1951 Roothaan [6] made the Hartree-Fock approximation more practical for numerical solutions by introducing the concept of basis sets [linear combination of atomic orbitals (LCAO)]. The molecular orbitals are represented as a linear combination of carefully chosen three-dimensional one-electron functions, χ_μ, called atomic orbitals,

$$\phi_{i\sigma}(\vec{r}) = \sum_{\mu=1,K} \chi_\mu(\vec{r})c_{\mu i}^{\sigma} \tag{3.26}$$

where K is an integer (the size of the basis set) larger than the number of electrons in the system[3]. This results in a set of algebraic equations, [Eq. (3.29) below], where the coefficients $c_{\mu i}^{\sigma}$ are varied to minimize the energy. In the minimization of Eq. (3.13) the constraint that the spin orbitals remain orthonormal needs to be kept. Introduction of a basis set, i.e., Eq. (3.26), yields,

$$\hat{f}^{\sigma} \sum_{\mu=1}^{K} \chi_\mu(\vec{r})c_{\mu p}^{\sigma} = \epsilon_{a\sigma} \sum_{\mu=1}^{K} \chi_\mu(\vec{r})c_{\mu p}^{\sigma} \tag{3.27}$$

[3]In reality, the atomic orbitals are functions of $\vec{r}$ rather than $\vec{x}$– so $\chi_\mu(x) = \chi_\mu(\vec{r}\sigma) = \chi_\mu(\vec{r})\sigma$. However making the atomic orbitals functions of spins as well as of the spatial coordinates simplifies our notation whole still communicating the essential ideas.

and multiplication with χ_ν followed by integration result in

$$\sum_{\mu=1}^{K}\langle\chi_\nu|\hat{f}^\sigma|\chi_\mu\rangle c_{\mu p}^\sigma = \epsilon_{p\sigma}\sum_{\mu=1}^{K}\langle\chi_\nu|\chi_\mu\rangle c_{\mu p}^\sigma \tag{3.28}$$

where there are K such equations, $p = 1,2,\cdots, K$. Writing these in a matrix equation yields the Roothaan equation

$$\mathbf{FC} = \mathbf{SCE} \tag{3.29}$$

where,

$$F_{\mu\nu} = \langle\chi_\mu|\hat{f}|\chi_\nu\rangle \tag{3.30}$$

$$S_{\mu\nu} = \langle\chi_\mu|\chi_\nu\rangle \tag{3.31}$$

$$E_{pq} = \epsilon_p\delta_{pq} \tag{3.32}$$

By using a starting guess of the wave function, $\mathbf{C}$, Eq. (3.29) can be solved iteratively, in a so-called Self-Consistent Field (SCF) procedure [this procedure is shown in Fig. (3.1)]. For each iteration the norm of the new wave function is compared to the previous, and at a chosen accuracy the iteration is stopped.

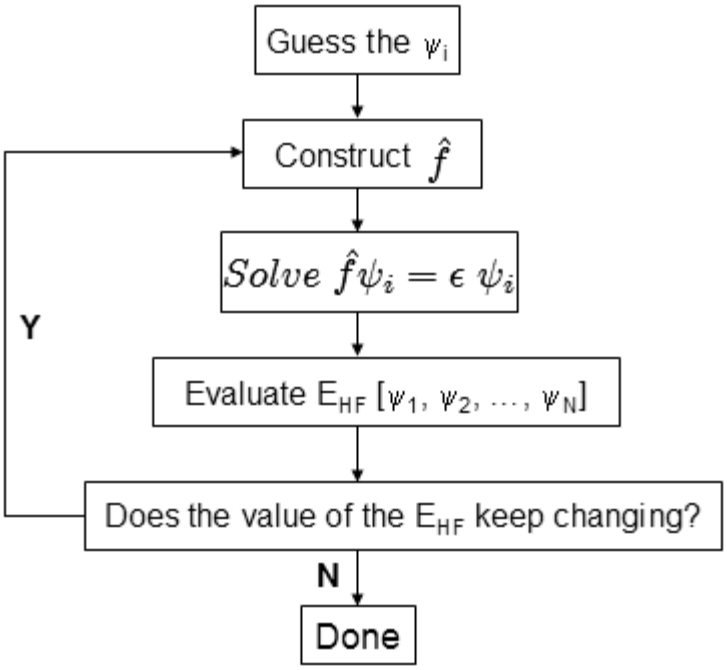

Figure 3.1: Flow diagram for solving HF equations

3.1.1.3 Configuration Interaction (CI)

In the Hartree-Fock approximation the HF wave function of a molecule has one determinant meaning that this theory is a single-particle approximation, and therefore cannot adequately treat the correlated motion of electrons that occurs due to electron-electron interactions. This neglecting of electron correlation has been blamed for systematic HF errors such as underestimated bond lengths and overestimated vibrational frequencies (we shall show this for the oxirane molecule). The methods that include the electron correlation energy, E_{corr},

$$E_{corr} = E - E_{HF}, \tag{3.33}$$

in its procedures are termed electron correlation, correlated or (if preceded by a HF calculation) post-HF methods. Many different approaches have been proposed, one being the Configuration Interaction (CI) method. The CI method is based on the

> ***Theorem.*** Let $\psi_1(\vec{x}), \psi_2(\vec{x}), \cdots$ form a complete basis for expanding an arbitrary one-electron function (such a basis can be obtained as eigenfunctions of a one-electron operator such as the Fock operator.) Then the set of Slater determinants
>
> $$\Phi_{i_1 i_2 \cdots i_N} = |\psi_{i_1}, \psi_{i_2}, \cdots, \psi_{i_N}| \tag{3.34}$$
>
> composed of all possible unique choices of $\{i_1, i_2, \cdots, i_N\}$ constitute a complete basis for expanding an arbitrary N-electron function
>
> $$\Psi = \sum_{i_1 i_2 \cdots i_N} \Phi_{i_1 i_2 \cdots i_N} \, C_{i_1, i_2, \cdots, i_N}. \tag{3.35}$$

Equation (3.35) is known as complete CI. It is referred to as full CI when the one-electron basis is incomplete and as truncated CI when, in addition, some choice of $\{i_1, i_2, \cdots, i_N\}$ have been omitted.

Minimizing the variational energy,

$$E(C_{i_1, i_2, \cdots, i_N}) = \frac{\langle \Psi | \hat{H} | \Psi \rangle}{\langle \Psi | \Psi \rangle}, \tag{3.36}$$

with respect to the linear variational parameters $C_{i_1, i_2, \cdots, i_N}$ results in the CI equation,

$$\sum_{j_1 j_2 \cdots j_N} \langle \phi_{i_1 i_2 \cdots i_N} | \hat{H} | \phi_{j_1 j_2 \cdots j_N} \rangle C_{j_1, j_2, \cdots, j_N} = E C_{i_1, i_2, \cdots, i_N}, \tag{3.37}$$

or in matrix form,

$$\mathbf{H}\vec{C} = E\vec{C}. \tag{3.38}$$

In this particular case there is a more powerful form of the variational principle, namely the

> **Theorem** (Hylleraas-Undheim-McDonald or Cauchy interlace).
> The Ith root of the linear variational problem is an upperbound for the true Ith energy.

For proofs and further discussion see Refs. [22, 23] and pp. 115 - 117 of the Ref. [24].

In practice truncated CI incorporates excited state configurations into the wave function by constructing new determinants from the original HF determinant. New determinants are created by replacing one or more occupied orbitals with unoccupied (virtual) orbitals of higher energy. The number of replacements within the determinants designates the level of CI. For instance, single substitution (CIS, for CI singles) replaces an occupied MO ψ_i with a virtual MO ψ_a,

$$\Psi = |\psi_1\psi_2\cdots\psi_{i-1}\psi_i\psi_{i+1}\cdots\psi_N| \rightarrow \Psi_i^a = |\psi_1\psi_2\cdots\psi_{i-1}\psi_a\psi_{i+1}\cdots\psi_N|, \tag{3.39}$$

and is equivalent to a one-electron excitation. Higher-order calculations include CID (double substitutions), which generates determinants where two occupied MOs are replaced by two virtual MOs; CISD, which adds single and double-substituted determinants; and CISDT, with single, double and triple excitations. The theoretical limit of this expansion - a full CI calculation - forms the molecular wave function as a linear combination of the HF determinant and all possible substituted determinants:

$$\Psi_{full-CI} = a_0\Psi_{HF} + \sum_{n>0} a_n\Psi_{S,D,T,\cdots} \tag{3.40}$$

where the coefficients a_n are determined by minimizing the energy of the total wave function. Full CI provides the most complete non-relativistic treatment possible for a molecular system with the exception of specialized methods such as Quantum Monte Carlo.

3.1.1.4 Complete Active Space SCF (CASSCF) Method

CASSCF [25] is a method that is especially well adapted to describe the making and breaking of chemical bonds (pages 598 - 647 of the Ref. [24] give a detailed technical explanation of the CASSCF method). In order to introduce the basic concepts involved consider the breaking of the σ bond in H_2 (note that this resembles the

breaking of the CC σ bond in oxirane.) The dissociation curve is shown in Fig. 3.2

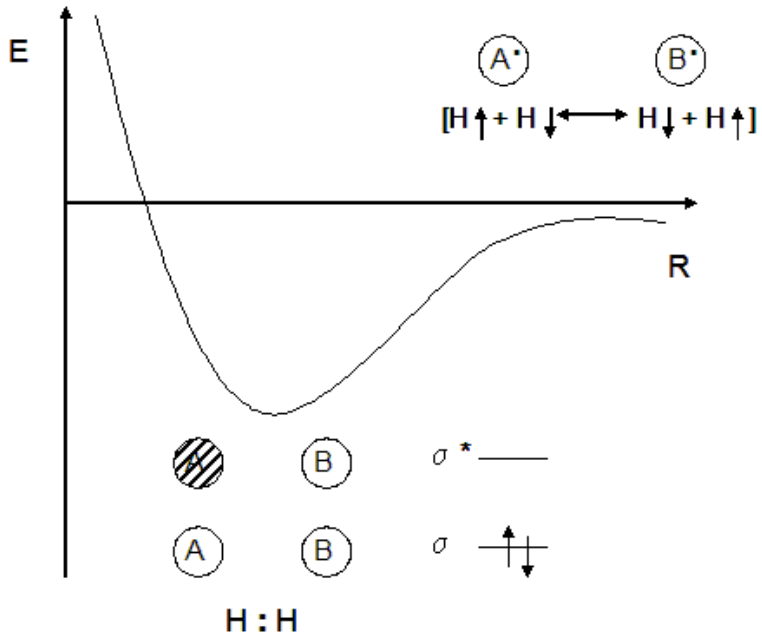

Figure 3.2: Dissociation curve for H_2

as are the molecular orbitals

$$\begin{aligned} \sigma &= \frac{1}{\sqrt{2(1+\langle s_A|s_B\rangle)}}\left(s_A + s_B\right) \\ \sigma^* &= \frac{1}{\sqrt{2(1-\langle s_A|s_B\rangle)}}\left(s_A - s_B\right). \end{aligned} \tag{3.41}$$

At the equilibrium geometry, the minimal description of the wave function is

$$\Psi_{react} = |\sigma\overline{\sigma}|. \tag{3.42}$$

At infinite internuclear distance, the appropriate wave function is

$$\begin{aligned} \Psi_{prod} &= \frac{1}{\sqrt{2}}\left(|s_A\overline{s}_B| + |s_B\overline{s}_A|\right) \\ &= \frac{1}{\sqrt{2}}\left(|\sigma\overline{\sigma}| - |\sigma^*\overline{\sigma}^*|\right). \end{aligned} \tag{3.43}$$

In order to describe the entire PES (curve), we must at least take a linear combination of the reactant and product forms of the wave function,

$$\Psi_{CAS} = c_1|\sigma\overline{\sigma}| + c_2|\sigma^*\overline{\sigma}^*| \tag{3.44}$$

This is a CASSCF [19] wave function. At each geometry, it is simultaneously necessary to optimize the CI coefficients, c_1 and c_2, and the molecular orbitals, σ and σ^*.

In general, a CAS(n,m) wave function is made by partitioning orbital space into three sets: inactive, active and virtual. The orbitals which constitute the inactive space remain doubly occupied in all configurations of the multiconfigurational wave function expansion. The orbitals in the secondary or virtual subspace remain unoccupied in all configurations. The active space contains a fixed number of electrons which are distributed over the active orbitals in all possible ways, restricted by the spin and spatial symmetry of the CASSCF wave function. More precisely, linear combinations of configurations are taken where each configuration is a spin-and spatial-symmetry adopted linear combination of Slater determinants.

The Restricted Active Space (RAS) SCF method [20, 21] has been viewed as an extension of the CASSCF method. The (spin-) orbital space contains again inactive and secondary spaces, defined as within CASSCF, but in addition, the active space is divided further into three subspaces RAS1, RAS2 and RAS3. In constructing the different RAS subspaces, one imposes restrictions on the maximum number of holes or electrons, allowed in the RAS1 and RAS3 sub-spaces, respectively. In the RAS2 space all possible configurations, arising from the distribution of the active electrons, that are not in RAS1 and RAS3, over the RAS2 orbitals are included. In the CASSCF approach one performs full CI within the active space, and thus, the redundant active-active orbital rotations need not to be considered. The additional subdivision of the active space within RASSCF introduces active-active orbital rotations between the three RAS spaces which are not redundant and thus, have to be considered. An advantage of the RASSCF approach is the possibility to use more active orbitals. The multi-reference (MR) singles and doubles (SD) wave function is a RASSCF wave function, which has the CAS space as a reference space and at most two holes and two electrons in RAS1 and RAS3, respectively. The RASSCF wave functions are suited to incorporate not only the non-dynamical correlation effects but also dynamical correlation effects. Efficient methods have been developed for performing the RASSCF, RASCI and CASSCF and CASCI calculations, based on SD-based CI algorithms [19].

The main problems with the CASSCF method are (i) that the method rapidly

becomes expensive as n and m increase and (ii) that the choice of active space can be a difficult trial and error learning process. Fortunately nowadays, TDDFT calculations can be very helpful in choosing an active space. The main advantage of CASSCF calculations is that they are able to capture so-called static correlation effects due to quasi degenerate configurations, often associated with chemical reactions processes. Dynamic correlation refers to the part of the correlation energy not captured in a CASSCF calculation.

3.1.1.5 Quantum Monte Carlo

Monte Carlo methods solve numerical difficult problems by running simulations using random numbers. Far from gambling, quantum Monte Carlo (QMC) provides us with some of the most accurate known solutions of the many electron Schrödinger equation. QMC calculations may proceed in two steps.

The first step is variational Monte Carlo (VMC). The trial wave function is written as the product of a CAS wave function (for static correlation) and a Jastrow factor (for dynamic correlation),

$$\Psi_{VMC} = J\Psi_{CAS}. \tag{3.45}$$

The parameters embedded in this wave function are optimized so as to minimize the energy,

$$E_{VMC} = \frac{\langle \Psi_{VMC}|\hat{H}|\Psi_{VMC}\rangle}{\langle \Psi_{VMC}|\Psi_{VMC}\rangle}. \tag{3.46}$$

Since the multidimensional integrals are too difficult to evaluate analytically, they are instead evaluated statistically using random numbers. This process can be illustrated by considering the one-dimensional integral,

$$\mathcal{I} = \int f(x)p(x)dx, \tag{3.47}$$

where

$$\begin{gathered} p(x) \geq 0 \\ \int p(x)dx = 1 \end{gathered} \tag{3.48}$$

can be interpreted as a probability distribution. (If $p(x) = |\psi(x)|^2$, then $\mathcal{I} = \langle\psi|f|\psi\rangle$.) By generating N_R random numbers, x_i, with distribution $p(x)$, then

$$\mathcal{I} = \frac{1}{N_R}\sum_{i=1,N_R} f(x_i). \tag{3.49}$$

The second step is diffusion Monte Carlo (DMC). The replacement, $t \rightarrow i\tau$, turns the Schrödinger equation

$$\hat{H}\Psi(t) = i\frac{\partial}{\partial t}\Psi(t), \tag{3.50}$$

into a diffusion equation,

$$\hat{H}\Psi(i\tau) = \frac{\partial}{\partial \tau}\Psi(i\tau). \tag{3.51}$$

It can be shown that any trial wave function Ψ with nonzero component on the exact wave function ψ_0, given enough time (τ), will diffuse into the exact ground state wave function, $\Psi \rightarrow \Psi_0$. Instead of random numbers, we now use walkers which diffuse to the correct distribution, Ψ_0.

It remains to point out a difficulty with QMC known as the "fixed node problem." A wave function is not a probability distribution and cannot be made to resemble a probability distribution by rescaling because the wave function has nodes where it changes sign. However these nodes separate electron configuration space into regions where the wave function has a single sign and so can be treated by QMC. The fixed node problem is that the nodes defining the regions in QMC are normally taken from approximate (such as CASSCF) wave functions. While very accurate, this prevents QMC results from becoming exact.

3.1.2 Density-Functional Theory

In 1964, Hohenberg and Kohn [9] established that knowing the electron density, determines the ground-state energy, E_0, and density, ρ, and hence the molecular properties for a given molecule. This is the fact that marked the formal beginning of Density Functional Theory (DFT). In practice DFT existed before 1964 in the form of Thomas-Fermi theory and Slater's $X\alpha$ theory. The Hohenberg-Kohn paper succeeded for the first time in providing a rigorous foundation for Thomas-Fermi theory. One year later, Kohn and Sham provided a rigorous foundation for Slater's $X\alpha$ method. At the beginning, except for a brief period in the 1970s when $X\alpha$ was popular among Quantum Chemists, DFT was primarily used by solid-state physicists principally for the prediction of properties of crystals. This changed in the late 1990s, when DFT became one of the most widely used quantum chemical methods. Thanks to Walter Kohn's seminal work within DFT, for which he won the Nobel Prize in chemistry in 1998 [7], this method can now be used to predict the chemical properties of molecules. All of the wave function-based techniques described earlier are dependent on the spin and the three spatial coordinates of every electron within the system (a total of 4N coordinates for an N-electron system).

DFT, on the other hand, reduces the complexity of the wave function methods by using the electron density to compute the energy, which is only dependent on x, y, and z. The mathematical expression for the energy in DFT [8] becomes a functional of the electron density (or probability density), and contains terms that correspond to those that are found in the electronic Hamiltonian.

3.1.2.1 Formal DFT

The basis of the DFT method is the

> **First Hohenberg-Kohn Theorem**
> For a system with a non-degenerate ground state the external potential is (to within a constant) a unique functional of the ground state charge $\rho(\vec{r})$. Since, in turn $v_{ext}(\vec{r})$ fixes $\hat{H}$ we see that the full many particle ground state is a unique functional of $\rho(\vec{r})$.

Although this theorem confirmed that there is a direct relationship between the $v_{ext}(\vec{r})$ and $\rho(\vec{r})$, the form of the functional representing the electron density remained unclear. That means that the first Hohenberg-Kohn theorem does not tell us how to calculate E_0 from $\rho(\vec{r})$. Fortunately, the second Hohenberg-Kohn theorem establishes a formal prescription for how this problem can be tackled.

> **Second Hohenberg-Kohn Theorem**
> The ground state charge density minimizes a variational expression for the ground state energy
>
> $$E[\rho] = F_{HK}[\rho] + \int v_{ext}(\vec{r})\rho(\vec{r})d\vec{r}, \tag{3.52}$$
>
> where v_{ext} is the external potential. The ground state energy is simply the minimum value of $E[\rho]$. The Hohenberg-Kohn functional $F_{HK}[\rho]$ is universal in the sense that it is independent of v_{ext}.

For a molecule in the absence of an applied field, we can write,

$$E_0 \leq E[\widetilde{\rho}] = T[\widetilde{\rho}] + E_{Ne}[\widetilde{\rho}] + E_{ee}[\widetilde{\rho}], \tag{3.53}$$

where $\widetilde{\rho}$ is a trial charge density –i.e.,

$$\widetilde{\rho}(\vec{r}) \geq 0, \int \widetilde{\rho}(\vec{r})d\vec{r} = N. \tag{3.54}$$

A year later, in 1965 Kohn and Sham [10], suggested an orbital-based procedure for how the hitherto unknown universal functional could be approached. Such a procedure was essential for developing an accurate treatment of the kinetic energy term.

In the Kohn-Sham formulation, the energy,

$$\begin{aligned} E[\rho] = E[\psi_1, \psi_2, \cdots, \psi_N] = & -\tfrac{1}{2}\sum_{i=1}^{N}\langle\psi_i|\nabla^2|\psi_i\rangle - \sum_\alpha \int \frac{Z_\alpha \rho(\vec{r}_1)}{r_{1\alpha}} d\vec{r}_1 \\ & + \tfrac{1}{2}\int\int \frac{\rho(\vec{r}_1)\rho(\vec{r}_2)}{r_{12}} d\vec{r}_1 d\vec{r}_2 + E_{xc}[\rho], \end{aligned} \tag{3.55}$$

and the Kohn-Sham orbitals $\psi_i, i = 1, 2, \cdots, N$ are found variationally by minimizing the energy, and the exchange-correlation energy $E_{xc}[\rho]$ is a functional of ρ. Kohn and Sham also showed that the exact ground-state ρ can be found from the ψ_i, according to

$$\rho(\vec{r}) = \sum_{i=1}^{N} |\psi_i(\vec{r})|^2. \tag{3.56}$$

Minimizing the total energy with respect to the orthonormal Kohn-Sham orbitals yields the Kohn-Sham (molecular orbital) equation,

$$\hat{F}_{KS}\psi_i(\vec{r}) = \epsilon_i \psi_i(\vec{r}). \tag{3.57}$$

The Kohn-Sham operator $\hat{F}_{KS}$ is

$$\hat{F}_{KS} \equiv -\frac{1}{2}\nabla^2 - \sum_\alpha \frac{Z_\alpha}{|\vec{r} - \vec{R}_\alpha|} + \hat{J} + v_{xc}, \tag{3.58}$$

where the Coulomb operator $\hat{J}$ is defined by

$$\hat{J}\psi(\vec{r}_1) = \psi(\vec{r}_1)\int \frac{\rho(\vec{r}_2)}{r_{12}} d\vec{r}_2 \tag{3.59}$$

and where the exchange-correlation potential v_{xc} is found as the functional derivative of E_{xc},

$$v_{xc}[\rho](\vec{r}) = \frac{\delta E_{xc}[\rho]}{\delta \rho(\vec{r})}. \tag{3.60}$$

If E_{xc} is known, its functional derivative can be found, and so v_{xc} is known. $\hat{F}_{KS}$ is like the Hartree-Fock operator Eq. (3.25), except that minus the exchange operators ($\hat{K}$) is replaced by v_{xc}, which handles the effects of both exchange (antisymmetry) and electron correlation. For a closed-shell ground-state, the electrons are paired in the Kohn-Sham orbitals, with two electrons of opposite spin having the same spatial

Kohn-Sham orbital. Substitution of Eq. (3.58) in Eq. (3.57) and use of Eq. (3.59) and Eq. (3.56) gives

$$\left(-\frac{1}{2}\nabla_1^2 - \sum_\alpha \frac{Z_\alpha}{r_{12}} + \int \frac{\rho(\vec{r}_2)}{r_{12}} d\vec{r}_2 + v_{xc}[\rho](\vec{r}_1)\right)\psi_i(\vec{r}_1) = \epsilon_i \psi_i(\vec{r}_1) \tag{3.61}$$

The Kohn-Sham orbitals ψ_i have no strict meaning other than in allowing the exact ρ to be calculated from Eq. (3.56). The determinant of the ψ_i is the Kohn-Sham wave function for the non-interacting system but not for the real system. Likewise, the Kohn-Sham orbital energies should not be confused with molecular orbital energies.

3.1.2.2 Applied DFT: LDA, GGA, Hybrids

No practical exact form is known for the exchange-correlation functional. So $E_{xc}[\rho]$ must be approximated in practice. In this part, we review the three main generations of approximations.

The first generation is the local density approximation (LDA) [10]. It assumes that the exchange-correlation (xc) energy density, $\epsilon_{xc}(\vec{r})$, depends only upon the density at $\vec{r}$,

$$E_{xc}^{LDA}[\rho] = \int \epsilon_{xc}(\rho(\vec{r}))\rho(\vec{r})d\vec{r}. \tag{3.62}$$

The xc energy density is obtained by fits to the calculated xc energy density of the homogeneous electron gas (HEG). A HEG is a hypothetical electrically neutral, infinite-volume system consisting of an infinite number of electrons moving in a space throughout which positive charge is continuously and uniformly distributed; the number of electrons per unit volume has a nonzero value ρ. In a molecule the positive charge is not uniformly distributed, but is located only at the nuclei. The LDA works remarkably well for many particles given that the density of a molecule is far from homogeneous. On the other hand, the LDA is known to drastically overestimates the energy of chemical bonds.

The second generation of functionals corrects the overbinding problem by inducing a dependence on the gradient, $\vec{\nabla}\rho(\vec{r})$, of the charge density at each point. These are the so-called generalized gradient approximations (GGAs) [11],

$$E_{xc}^{GGA} = \int \epsilon_{xc}(\rho(\vec{r}), x(\vec{r}))\rho(\vec{r})d(\vec{r}), \tag{3.63}$$

where

$$x(\vec{r}) = \frac{|\nabla\rho(\vec{r})|}{\rho^{4/3}(\vec{r})}, \tag{3.64}$$

is the reduced gradient. The GGAs introduced in the late 1980s by Perdew and Becke finally provided accurate enough functionals to study chemical reactions energies.

Sometime in the 1990s, Axel Becke introduced hybrid functionals as the third generation of density functionals. These functionals have the form

$$E_{xc} = E_{xc}^{GGA} + C_x(E_x^{HF} - E_x^{GGA}) \tag{3.65}$$

and often provide nearly thermodynamical accuracy (i.e. 1 kcal/mol). The fraction of HF exchange (C_x) is typically near 1/4 (25 %).

The calculations presented in this thesis are limited to the LDA and a particular hybrid functional known as B3LYP [12].

3.2 Excited States

3.2.1 *Ab Initio Methods*

In this part we describe the principal methods used to calculate the excitation energies needed to determine, among other quantities the electronic absorption spectra. We start our discussion with the *ab-initio*, wave-function-based methods, CIS, TDHF and CASSCF. Then we turn our attention to time-dependent DFT.

3.2.1.1 CASSCF and QMC for the Excited States

The CASSCF method, previously described for ground state calculations is section 3.1.1.4, requires little modification for excited states calculations.

This is particularly true when the excited states is the lowest state of a given symmetry. In particular, this excited state is by symmetry orthogonal to all energetically lower states, including the ground state. The variational principle (section 3.1.1.1) the guarantees that

$$E_0 \leq E_0^{CAS} = \langle \Psi_0^{CAS} | \hat{H} | \Psi_0^{CAS} \rangle, \tag{3.66}$$

where E_0 is the energy of the lowest state of the given symmetry and Ψ_0^{CAS} is a normalized CAS wave function of the same symmetry.

Problems do arise when we want to treat the lowest excited state with the same symmetry as the ground state. We are now dealing with the second state of a given

symmetry, Ψ_1^{CAS}, and variational collapse,

$$E_0 \leq E_1^{CAS} = \langle \Psi_1^{CAS} | \hat{H} | \Psi_1^{CAS} \rangle E_1, \tag{3.67}$$

may occur, since nothing guarantees that $\langle \Psi_0 | \Psi_1^{CAS} \rangle = 0$ or even that $\langle \Psi_0^{CAS} | \Psi_1^{CAS} \rangle = 0$. Nowadays the usual way to circumvent this problem is by minimizing the state-average (SA) energy [5],

$$E_{SA} = w_0 \langle \Psi_0^{SA} | \hat{H} | \Psi_0^{SA} \rangle + w_1 \langle \Psi_1^{SA} | \hat{H} | \Psi_1^{SA} \rangle, \tag{3.68}$$

where w_0 and w_1 are positive real weight factor whose sum is unity. The wave functions Ψ_0^{SA} and Ψ_1^{SA} are CASSCF wave functions obtained as the first and second roots of the Hamiltonian matrix expressed in an underlying basis consisting of the CASSCF configurations constructed from the same molecular orbitals.

By the Hylleraas-Undheim-McDonald or Cauchy interlace theorem (section 3.1.1.3), we then have that,

$$\begin{aligned} E_0 \leq E_0^{SA} &= \langle \Psi_0^{SA} | \hat{H} | \Psi_0^{SA} \rangle \\ E_1 \leq E_1^{SA} &= \langle \Psi_1^{SA} | \hat{H} | \Psi_1^{SA} \rangle. \end{aligned} \tag{3.69}$$

Most calculations use $w_0 = w_1 = 1/2$, however Werner and Meyer showed that even a very small value of $w_0 = 1 - w_1$, can eliminate the variational collapse of E_1^{SA}.

Since the SA calculations involves an additional state-averaging beyond a normal CASSCF calculation, then

$$E_0 \leq E_0^{CAS} \leq E_0^{SA}. \tag{3.70}$$

However the use of the same MOs to describe the two states introduces potentially useful error cancelation into the calculation of the excitation energy,

$$\omega_1^{SA} = E_1^{SA} - E_0^{SA}. \tag{3.71}$$

When calculating excited-state PESs with the SA procedure, we actually use,

$$E_1 = E_0^{CAS} + \omega_1^{SA}. \tag{3.72}$$

(However this was always found to be very close to E_1^{SA} in our calculations.)

The generalization of the QMC calculations (section 3.1.1.5) used in this thesis goes over the excited states in a relatively straight forward manner. This is because the QMC calculations are post CASSCF calculations and make use of similar energy expressions, including state averaging.

3.2.1.2 Time-Dependent Hartree-Fock (TDHF)

In 1930, Dirac [4] wrote the linear-response time-dependent Hartree-Fock (TDHF) equations following a density matrix and equation-of-motion formalism. In fact this method constitutes an approximation to the exact time-dependent Schrödinger equation, based on the assumption that the system can at all times be represented by a single Slater determinant composed of time-dependent single-particle wave functions. One of the most important application in quantum chemistry of TDHF is in the determination of electronic excitation spectra and frequency-dependent polarizabilities of molecular systems [13]. This method is also known as the random phase approximation (RPA), although this latter name appears to be used to mean a number of different things.

The derivation of the TDHF equations follow from the general time-dependent electronic Schrödinger equation for molecular systems

$$\hat{H}\Psi(r,t) = i\frac{\partial}{\partial t}\Psi(r,t) \tag{3.73}$$

where $\hat{H}$ is the time-dependent Hamiltonian

$$\hat{H}(r,t) = \hat{H}(r) + \hat{V}(r,t) \tag{3.74}$$

being $\hat{V}(r,t)$ an arbitrary single-particle time-dependent operator, for example, the time-dependent electric field

$$\hat{V}(r,t) = \sum_{i}^{N} \hat{v}_i(r,t) \tag{3.75}$$

and $\hat{H}(r)$ the Hamiltonian operator as in Eq. (2.6).

If the wave function $\Psi(\mathbf{x},t)$ is written as a single Slater determinant

$$\Phi(\mathbf{x},t) = |\phi_1(\vec{x}_1,t)\phi_2(\vec{x}_1,t)\cdots\phi_N(\vec{x}_1,t)| \tag{3.76}$$

a time-dependent variant of the Hartree-Fock equation is obtained

$$\hat{F}(\mathbf{x},t)\Phi(\mathbf{x},t) = i\frac{\partial}{\partial t}\Phi(\mathbf{x},t). \tag{3.77}$$

where the operator $\hat{F}(r,t)$ contains the time-dependent single-particle potential $\hat{V}(r,t)$ additionally to the definition of the time-independent Fock operator. It can be seen that the Coulomb and exchange operators [Eqs. (3.18 and 3.21)] respec-

tively now acquire a time dependence since the single-particle orbitals $\phi(r,t)$ are now time-dependent. It is clear that at $t = 0$ the system obeys the time-independent Hartree-Fock equation and if a small perturbation is applied the unperturbed orbitals of the Slater determinant will respond to this perturbation but change only slightly, since the perturbation is weak.

The linear-response TDHF (LR-TDHF) equations are obtained via time-dependent perturbation theory to first order, that is, the linear response of the orbitals and of the time-dependent Fock operator are taken into account. In this case the derivation of LR-TDHF equations is via a density matrix formulation. The results is that the excitations are obtained from a non-Hermitian eigenvalue equation which can be written in matrix notation as

$$\begin{bmatrix} \mathbf{A} & \mathbf{B} \\ \mathbf{B}^* & \mathbf{A}^* \end{bmatrix} \begin{bmatrix} \vec{X} \\ \vec{Y} \end{bmatrix} = \omega \begin{bmatrix} \mathbf{1} & \mathbf{0} \\ \mathbf{0} & -\mathbf{1} \end{bmatrix} \begin{bmatrix} \vec{X} \\ \vec{Y} \end{bmatrix} \tag{3.78}$$

where the matrix elements are defined as follows

$$\begin{aligned} A_{ia,jb} &= \delta_{ij}\delta_{ab}(\epsilon_a - \epsilon_i) + (ia|f_H|bj) - (ij|f_H|ba) \\ B_{ia,jb} &= (ia|f_H|jb) - (ib|f_H|ja) \end{aligned} \tag{3.79}$$

and the indices i,j, k, are for occupied orbitals, a,b, c, for virtual ones (or unoccupied) and p,q, r, for general orbitals. The difference of the energies of the orbitals i and a, is the leading term of the $\mathbf{A}$ matrix which are the ones from which and to which the electron is excited. The second term of the $\mathbf{A}$ matrix and the elements of the $\mathbf{B}$ matrix, stem from the linear response of the Coulomb and exchange operator to the first-order changes in the single particle orbitals. It is worth nothing that CIS scheme is obtained, when the $\mathbf{B}$ matrix of the TDHF equation is set to zero, it reduces to the CIS scheme. This approximation is well-known as the Tamm-Dancoff Approximation (TDA) [14].

The TDHF method and the CIS scheme share many similar properties. The TDHF is a size-consistent method, and one can obtain pure singlet and triplet states for closed-shell molecules. However, TDHF encounters problems with triplet states, and in general, triplet spectra are only very poorly predicted by TDHF calculations. This is because the HF ground state is used as the reference, which in many cases even leads to triplet instabilities (this subject will be analyzed in detail in chapter 6).

3.2.1.3 CIS

The LR-TDHF TDA, also know as CIS [15, 16], is the simplest acceptable model for describing electronic excitations.

The easiest formalism for understanding CIS is that of second quantization also known as the occupation-number formalism, which is an algebraic method that can be used as a symmetric alternative to Slater determinants which automatically and elegantly incorporates the antisymmetric nature of the wave function [15]. We will use the index convention adopted in THDF method,

$$\underbrace{abc\cdots gh}_{unoccupied}\underbrace{ijklmn}_{occupied}\underbrace{opq\cdots xyz}_{general}. \tag{3.80}$$

Creation operators are defined by the fact that they can add orbitals to the determinant and are expressed by

$$\hat{r}^\dagger|st\cdots\rangle = |rst\cdots\rangle = -|srt\cdots\rangle. \tag{3.81}$$

For,

$$\hat{r}^\dagger|rst\cdots\rangle = 0, \tag{3.82}$$

because of the Pauli Exclusion Principle. Annihilation operators, the adjoint of the creation operators, remove orbitals when acting to the right

$$\begin{aligned} \hat{r}|rst\cdots\rangle &= +|st\cdots\rangle \\ \hat{r}|srt\cdots\rangle &= -|st\cdots\rangle \\ \hat{r}|st\cdots\rangle &= 0 \text{ if } r\epsilon\{st\cdots\} \end{aligned} \tag{3.83}$$

The anticommutation relations,

$$\begin{aligned} \hat{p}\hat{q} + \hat{q}\hat{p} &= 0 \\ \hat{p}^\dagger\hat{q}^\dagger + \hat{q}^\dagger\hat{p}^\dagger &= 0 \\ \hat{p}^\dagger\hat{q} + \hat{q}\hat{p}^\dagger &= \delta_{pq}, \end{aligned} \tag{3.84}$$

follow from the foregoing definitions. However the most important consequence by far of second quantization is the ability to write the Hamiltonian without any explicit

reference to the number of electrons,

$$\hat{H} = \sum h_{pq}\hat{p}^\dagger\hat{q} + \frac{1}{2}\sum (pq|f_H|rs)\hat{p}^\dagger\hat{r}^\dagger\hat{s}\hat{q} \tag{3.85}$$

We are now in an excellent position to derive the CIS equations. The excited state wave function is a linear combination of the HF wave function

$$|\Psi_I\rangle = \sum \hat{b}^\dagger\hat{j}|HF\rangle C^I_{jb} \tag{3.86}$$

Minimizing

$$E_I = \frac{\langle\Psi_I|\hat{H}|\Psi_I\rangle}{\langle\Psi_I|\Psi_I\rangle} \tag{3.87}$$

gives

$$\sum \langle HF|\hat{i}^\dagger\hat{a}\hat{H}\hat{b}^\dagger\hat{j}|HF\rangle C^I_{jb} = E_I C^I_{ia} \tag{3.88}$$

The easiest way to evaluate

$$H_{ia,jb} = \langle HF|\hat{i}^\dagger\hat{a}\hat{H}\hat{b}^\dagger\hat{j}|HF\rangle \tag{3.89}$$

is via the commutator

$$\begin{aligned} H_{ia,jb} &= \langle HF|\hat{i}^\dagger\hat{a}[\hat{H},\hat{b}^\dagger\hat{j}]|HF\rangle + \langle HF|\hat{i}^\dagger\hat{a}\hat{b}^\dagger\hat{j}\hat{H}|HF\rangle \\ &= \langle HF|\hat{i}^\dagger\hat{a}[\hat{H},\hat{b}^\dagger\hat{j}]|HF\rangle + \delta_{ij}\delta_{ab}\langle HF|\hat{H}|HF\rangle. \end{aligned} \tag{3.90}$$

The first term works out to be $A_{ia,jb}$. The second term is zero unless $i = j$ and $a = b$. So

$$H_{ia,jb} = A_{ia,jb} + \delta_{ij}\delta_{ab}E_{HF}. \tag{3.91}$$

Hence the CIS equation may be rewritten as

$$\sum A_{ia,jb}C^I_{jb} = \underbrace{(E_I - E_{HF})}_{\omega_I} C^I_{ia} \tag{3.92}$$

i.e.,

$$\mathbf{A}\vec{C}_I = \omega_I\vec{C}_I. \tag{3.93}$$

The matrix elements of A are given by the expression

$$A_{ia,jb} = \delta_{ij}\delta_{ab}(\epsilon_a - \epsilon_i) + (jb|f_H|ai) - (ab|f_H|ji) \tag{3.94}$$

The TDA-TDDFT equation is identical except that

$$A_{ia,jb} = \delta_{ij}\delta_{ab}(\epsilon_a - \epsilon_i) + (jb|f_H + f_{xc}|ai) \tag{3.95}$$

where $f_{xc}(\vec{x}_1, \vec{x}_2) = \delta^2 E_{xc}/\delta\rho(x_1)\delta\rho(x_2)$ is the kernel. When CIS is applied to a molecule with a closed-shell ground state, the excited states generated are either of singlet spin or triplet spin. Taking explicit account of spin, we have

$$C^I_{ia_\uparrow} = +C^I_{ia_\downarrow} \tag{3.96}$$

for singlets and

$$C^I_{ia_\uparrow} = -C^I_{ia_\downarrow} \tag{3.97}$$

for triplets. Only the singlet excitations are spectroscopically allowed in the sense of having non zero oscillator strengths,

$$f_I = \frac{2}{3}\omega_I(|\langle\Psi_0|x|\Psi_I\rangle|^2 + |\langle\Psi_0|y|\Psi_I\rangle|^2 + |\langle\Psi_0|z|\Psi_I\rangle|^2). \tag{3.98}$$

In the case of a two orbital model (Fig. 3.3), there is one singlet-excited state

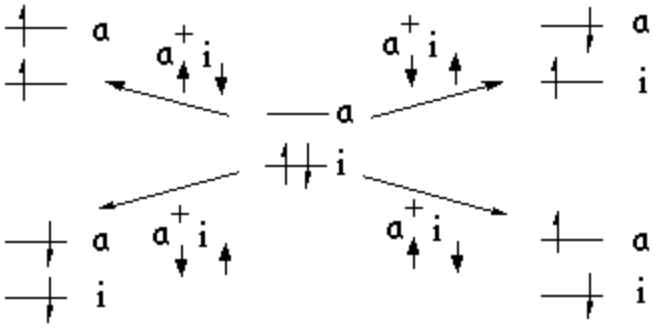

Figure 3.3: Two orbital model for spin-flip (left hand side) and non spin-flip (right hand side) excitations out of a closed-shell ground state.

$$
\begin{aligned}
\Psi_{00} &= \tfrac{1}{\sqrt{2}}\left(a_\uparrow^+ i_\uparrow + a_\downarrow^+ i_\downarrow\right)|i\bar{i}\rangle \\
&= \tfrac{1}{\sqrt{2}}\left(|a\bar{i}\rangle + |i\bar{a}\rangle\right) \\
&= \tfrac{1}{2}(a(1)\alpha(1)i(2)\beta(2) - i(1)\beta(1)a(2)\alpha(2) \\
&\quad + i(1)\alpha(1)a(2)\beta(2) - a(1)\beta(1)i(2)\alpha(2)) \\
&= \left[\tfrac{1}{\sqrt{2}}\left(a(1)i(2) + i(1)a(2)\right)\right]\left[\tfrac{1}{\sqrt{2}}\left(\alpha(1)\beta(2) - \beta(1)\alpha(2)\right)\right]
\end{aligned}
\tag{3.99}
$$

with excitation energy

$$
\begin{aligned}
\omega_s &= A_{ia\uparrow,ia\uparrow} + A_{ia\uparrow,ia\downarrow} \\
&= \epsilon_a - \epsilon_i + 2(ia|f_H|ai) - (aa|f_H|ii)
\end{aligned}
\tag{3.100}
$$

and three triplet excited states

$$
\begin{aligned}
\Psi_{11} &= a_\uparrow^+ i_\downarrow |i\bar{i}\rangle \\
&= |ia\rangle \\
&= \left[\tfrac{1}{\sqrt{2}}\left(i(1)a(2) - a(1)i(2)\right)\right][\alpha(1)\beta(2)] \\
\Psi_{10} &= \tfrac{1}{\sqrt{2}}\left(a_\uparrow^+ i_\downarrow - a_\downarrow^+ i_\downarrow\right)|i\bar{i}\rangle \\
&= \tfrac{1}{\sqrt{2}}\left(|a\bar{i}\rangle - |i\bar{a}\rangle\right) \\
&= \tfrac{1}{2}(a(1)\alpha(1)i(2)\beta(2) - i(1)\beta(1)a(2)\alpha(2) \\
&\quad - i(1)\alpha(1)a(2)\beta(2) + a(1)\beta(1)i(2)\alpha(2)) \\
&= \left[\tfrac{1}{\sqrt{2}}\left(a(1)i(2) - i(1)a(2)\right)\right]\left[\tfrac{1}{\sqrt{2}}\left(\alpha(1)\beta(2) + \beta(1)\alpha(2)\right)\right] \\
\Psi_{1,-1} &= a_\downarrow^+ i_\uparrow |i\bar{i}\rangle = |\bar{a}\bar{i}\rangle \\
&= \left[\tfrac{1}{\sqrt{2}}\left(i(1)a(2) - a(1)i(2)\right)\right][\beta(1)\beta(2)]
\end{aligned}
\tag{3.101}
$$

with excitation energy

$$\begin{aligned} \omega_T &= A_{ia\uparrow,ia\uparrow} - A_{ia\uparrow,ia\downarrow} \\ &= \epsilon_a - \epsilon_i - (aa|f_H|ii). \end{aligned} \tag{3.102}$$

Evidently $\omega_T < \omega_S$.

3.2.2 Time-Dependent Density-Functional Theory

It is well-known that the Hohenberg-Kohn-Sham formulation of DFT concerns only the time-independent case. For a time-dependent system, a generalization of the basic formalism of DFT is required. Time-dependent density functional theory (TDDFT) has been an answer to this need and it is now a popular method for calculating excitation energies of atoms, molecules, clusters, and solids. Its popularity increases every day because it often gives very reasonable excitation energies (error below 0.2 eV), and other properties of excited states are obtained with an accuracy comparable to (but somewhat less than) that of ground state. In this subsection we describe the fundamental equations used in TDDFT following the Runge-Gross [17] and Gross-Kohn [18] formalism, as well as the exchange-correlation (xc) functionals employed in this theory, finally obtaining the Casida equation implemented within the frame of the time-dependent density functional response theory (TD-DFRT) for calculating the excitation energies and oscillator strengths needed for the electronic spectra of molecular systems.

3.2.2.1 Runge-Gross Theorem

Considering that an N-electron system (be atoms or molecules) is described by the time-dependent Schrödinger equation

$$\hat{H}(t)\Psi(t) = i\frac{\partial}{\partial t}\Psi(t) \tag{3.103}$$

with Hamiltonian

$$\hat{H}(t) = \hat{T} + U + V(t) \tag{3.104}$$

where

$$\hat{T} = -\frac{1}{2}\sum_{i=1}^{N}\nabla_i^2 \tag{3.105}$$

$$U = \sum_{i<j} \frac{1}{|\vec{r}_i - \vec{r}_j|} \tag{3.106}$$

$$V(t) = \sum_{i=1}^{N} v(\vec{r}_i, t) \tag{3.107}$$

are the kinetic energy, the electron repulsion and the external potential, assumed constant for $t < t_0$. In this manner, the system is such as interacting with a time-dependent field switched on at time t_0.

The first formal problem is to show that the expectation values are functionals of the time-dependent charge density. This is the first Runge-Gross theorem [17]. This theorem states that

First Runge-Gross Theorem

The exact time-dependent electron density, $\rho(\vec{r}, t)$, determines the time-dependent external potential, $V(\vec{r}, t)$, up to a spatially constant, time-dependent function $C(t)$ and thus the time-dependent wave function, $\Psi(r, t)$, is determined up to a time-dependent phase factor.

This theorem would seem to imply that a functional of the density can be constructed, which has a stationary point at the true time-dependent density. As in the ground-state case, the system can be mapped onto a set of non-interacting electrons, moving in an effective potential. Thus the wave function is a functional of the electron density

$$\Psi(r, t) = \Psi[\rho](t) e^{-i\alpha(t)} \tag{3.108}$$

with $(d/dt)\alpha(t) = C(t)$. The electron density can be expressed as

$$\rho(\vec{r}_1, t) = \int |\Psi(\vec{x}_1, \vec{x}_2, \vec{x}_3, \cdots, \vec{x}_N, t)|^2 d\sigma_1 d\vec{x}_2 d\vec{x}_3 \cdots d\vec{x}_N \tag{3.109}$$

In the time-independent case the role of the second Hohenberg-Kohn theorem, is filled, in the time-dependent theory, by a variational principle involving the action,

$$A = \int_{t_0}^{t_1} \langle \Psi(t) | i\frac{\partial}{\partial t} - \hat{H}(t) | \Psi(t) \rangle dt. \tag{3.110}$$

The true time-dependent density is the one which makes the action stationary,

$$0 = \frac{\delta A}{\delta \rho(\vec{r}, t)} = \int_{t_0}^{t_1} \langle \frac{\delta \Psi(t')}{\delta \rho(\vec{r}, t)} | i\frac{\partial}{\partial t'} - \hat{H}(t') | \Psi(t') \rangle dt' + c.c. \quad . \tag{3.111}$$

In the last equation it is easy to see that in this case the effect of the phase factor

is simply to contribute and additive constant,

$$A = \int_{t_0}^{t_1} \langle \Psi[\rho](t) | i\frac{\partial}{\partial t} - \hat{H}(t) | \Psi[\rho](t) \rangle dt + \Phi(t_1) - \Phi(t_0) = A[\rho] + \text{const.} \quad (3.112)$$

Thus the time-dependent density determines the action, up to an additive constant. Applying the variational condition Eq.(3.111), the additive constant is immaterial, so this provides the analog of the second Hohenberg-Kohn theorem, for the time-dependent theory. Therefore the action functional can be written as

$$A[\rho] = B[\rho] - \int_{t_0}^{t_1} \int v(r,t)\rho(r,t) dr dt, \quad (3.113)$$

where the functional B is independent of the external potential v.

3.2.2.2 Time-Dependent Kohn-Sham Equation

Similar to the time-independent case, the Kohn-Sham equation can be derived for the time-dependent case by assuming the existence of a potential $v_{eff}(\vec{r},t)$, whose orbitals $\psi_i(\vec{r},t)$ yield the same charge density $\rho(\vec{r},t)$ as for the interacting system,

$$\rho(r,t) = \sum_i f_i |\psi_i(r,t)|^2, \quad (3.114)$$

where the f_i are orbitals occupation numbers. The question of whether such a potential exists is known as the "time-dependent v-representability problem". Assuming $v_{eff}(\vec{r},t)$ does exist, then the universal functional B can be expressed as

$$\begin{aligned} B[\rho] = \; & \textstyle\sum_i n_i \int_{t_0}^{t_1} \langle \psi_i(t) | i\frac{\partial}{\partial t} \\ & -\tfrac{1}{2}\nabla^2 |\psi_i(t)\rangle dt - \tfrac{1}{2}\int_{t_0}^{t_1} \int \int \tfrac{\rho(\vec{r}_1,t)\rho(\vec{r}_2,t)}{|\vec{r}_1-\vec{r}_2|} d\vec{r}_1 d\vec{r}_2 dt - A_{xc}[\rho] \end{aligned} \quad (3.115)$$

where A_{xc} is the exchange-correlation action functional, which play a role similar to the exchange-correlation energy functional in the time-dependent theory. Minimizing the action functional (3.113) subject to the condition of Eq. (3.114), provides the time-dependent Kohn-Sham equation

$$\left[-\frac{1}{2}\nabla^2 + v_{eff}(\vec{r},t) \right] \psi_i(\vec{r},t) = i\frac{\partial}{\partial t}\psi_i(\vec{r},t), \quad (3.116)$$

where

$$v_{eff}(\vec{r},t) = v(\vec{r},t) + \int \frac{\rho(\vec{r},t)}{|\vec{r}-\vec{r}'|} d\vec{r}' + v_{xc}(\vec{r},t) \quad (3.117)$$

and

$$v_{xc}(\vec{r},t) = \frac{\delta A_{xc}[\rho]}{\delta\rho(\vec{r},t)}. \tag{3.118}$$

3.2.2.3 Time-Dependent Density Functional Response Theory. Casida's Equations

In many cases, we are only interested in the response to a weak change in potential $\delta v_{ext}(rt)$, so the time-dependent generalization of the DFT formalism can offer a rigorous way to calculate the dynamic response of the charge density. In 1995 Casida [27] provided a procedure for how to get theses quantities, considering only the knowledge of the linear density response of the system, by developing time-dependent density functional response theory (TDDFRT) in the same form as LR-TDHF used in Quantum Chemistry. Since the dynamic polarizability, $\overline{\alpha}(\omega)$ describes the response of the dipole moment to a time-dependent electric field, it can be calculated from the response of the charge density obtained from TDDFT. This allows the determination of the electronic excitation spectrum in the usual dipole approximation, because according to the sum-over-states (SOS) relation,

$$\overline{\alpha}(\omega) = \sum_I \frac{f_I}{\omega_I^2 - \omega^2} \tag{3.119}$$

and considering that

$$f_I = \frac{2}{3}\omega_I(|\langle\Psi_0|\hat{x}|\Psi_I\rangle|^2 + |\langle\Psi_0|\hat{y}|\Psi_I\rangle|^2 + |\langle\Psi_0|\hat{z}|\Psi_I\rangle|^2) \tag{3.120}$$

and

$$\omega_I = E_I - E_0 \tag{3.121}$$

the poles of the dynamic polarizability determine the excitation energies, ω_I, while the residues, f_I, determine the corresponding oscillator strengths. By expressing the dynamic polarizability in the basis of unperturbed MOs, Casida was able to show that the TDDFT excitation energies are solutions of the equation

$$\begin{bmatrix} \mathbf{A}(\omega) & \mathbf{B}(\omega) \\ \mathbf{B}^*(\omega) & \mathbf{A}^*(\omega) \end{bmatrix} \begin{bmatrix} \vec{X}_I \\ \vec{Y}_I \end{bmatrix} = \omega_I \begin{bmatrix} \mathbf{1} & \mathbf{0} \\ \mathbf{0} & -\mathbf{1} \end{bmatrix} \begin{bmatrix} \vec{X}_I \\ \vec{Y}_I \end{bmatrix}. \tag{3.122}$$

Here

$$\begin{aligned} A_{ia\sigma,jb\tau}(\omega) &= \delta_{\sigma\tau}\delta_{ij}\delta_{ab}(\epsilon_{a\sigma} - \epsilon_{i\sigma}) + (ia|f_H + f_{xc}^{\sigma\tau}(\omega)|jb) \\ B_{ia\sigma,jb\tau}(\omega) &= (ia|f_H + f_{xc}^{\sigma\tau}(\omega)|jb), \end{aligned} \tag{3.123}$$

where

$$f_{xc}^{\sigma t}(\vec{r}_1,\vec{r}_2;\omega)=\int_{-\infty}^{+\infty}e^{i\omega(t_1-t_2)}\frac{\delta^2 A_{xc}[\rho_\uparrow,\rho_\downarrow]}{\delta_{\rho\sigma}(\vec{r}_1t_1)\delta\rho_2(\vec{r}_2t_2)}d(t_1-t_2). \tag{3.124}$$

In the two orbital model of Fig. 3.3 and the TDA (i.e., $\mathrm{B}(\omega)=0$),

$$\begin{aligned}\omega_S &= A_{ia\uparrow,ia\uparrow}(\omega_S)+A_{ia\uparrow,ia\downarrow}(\omega_S)\\ &= \epsilon_a-\epsilon_i+2(ia|f_H|ai)+(ia|f_{xc}^{\uparrow\uparrow}(\omega_S)+f_{xc}^{\uparrow\downarrow}(\omega_S)|ia)\end{aligned} \tag{3.125}$$

and

$$\begin{aligned}\omega_T &= A_{ia\uparrow,ia\uparrow}(\omega_T)-A_{ia\uparrow,ia\downarrow}(\omega_T)\\ &= \epsilon_a-\epsilon_i+(ia|f_{xc}^{\uparrow\uparrow}(\omega_T)-f_{xc}^{\uparrow\downarrow}(\omega_T)|ia)\end{aligned} \tag{3.126}$$

These are non-linear equations which may have multiple solutions. For example, a polarization propagator correction to adiabatic TDDFT is [28, 29, 30],

$$\begin{aligned}&(ia|f_{xc}^{\uparrow\uparrow}(\omega_S)+f_{xc}^{\uparrow\downarrow}(\omega_S)|ia)\\ =\;&(ia|f_{xc}^{\uparrow\uparrow}(0)+f_{xc}^{\uparrow\downarrow}(0)|ia)+\tfrac{|\langle\Psi_S|\hat{H}|\Psi_D\rangle|^2}{\omega_S-\omega_D},\end{aligned} \tag{3.127}$$

where Ψ_D and ω_D refor to an explicit doubly excited configuration. In this case, Eq. (3.125) becomes a quadratic equation with two real solutions corresponding to the splitting of one excitation into two satellites as in Fig. 3.4. This illustrates the generality of Casida's equations since it describes how explicit two-electrons excitations may be included.

3.2.2.4 Adiabatic Approximation in TDDFT

In analogy to the traditional time-independent Kohn-Sham scheme all exchange and correlation effects are collected in $(\delta A_{xc}[\rho]/\delta\rho(r,t))$. It is important to note that no approximation has been introduced and consequently the time-dependent Kohn-Sham theory is a formally exact many-body theory. However, the exact time-dependent "exchange-correlation" action functional (also called the xc kernel) is not known, and approximations to this functional have to be introduced. The first approximation generally made is the so-called *adiabatic approximation* (AA). The AA assumes that the TDDFT xc potential,

$$v_{xc}^{\sigma}[\rho_\uparrow,\rho_\downarrow](\vec{r}t)=\frac{\delta A_{xc}[\rho_\uparrow,\rho_\downarrow]}{\delta\rho_\sigma(\vec{r}t)}, \tag{3.128}$$

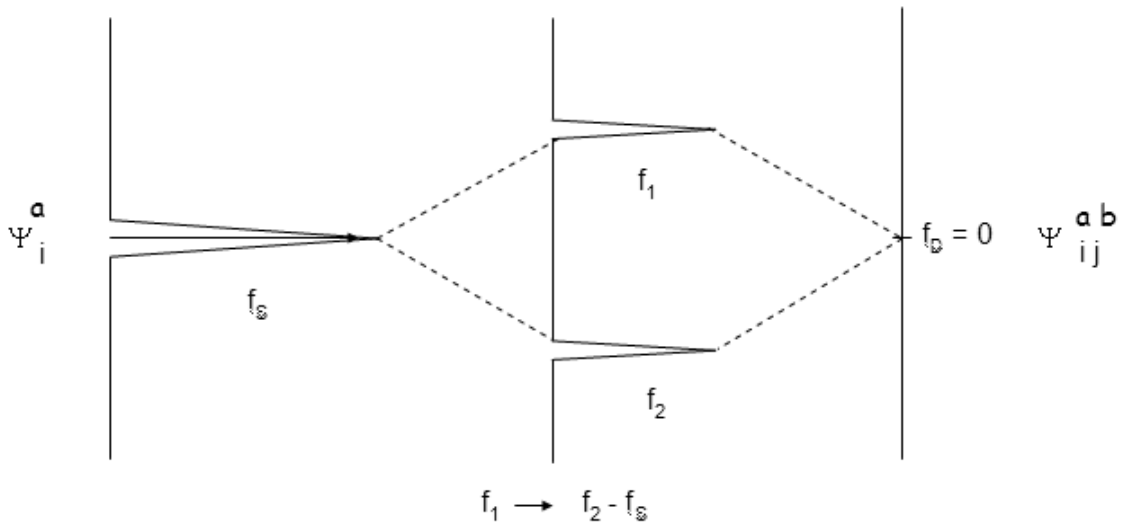

Figure 3.4: Splitting of a single electron excitation into two satelite peaks by interaction with a nearly double excitation.

responds instantaneously and without memory to any temporal change in the charge density. Then,

$$v_{xc}^{\sigma}[\rho_{\uparrow},\rho_{\downarrow}](\vec{r}t) = \frac{\delta E_{xc}[\rho_{\uparrow}^{t},\rho_{\downarrow}^{t}]}{\delta\rho_{\sigma}^{t}(\vec{r})} \tag{3.129}$$

where

$$\rho_{\sigma}^{t}(\vec{r}) = \rho_{\sigma}(\vec{r}t) \tag{3.130}$$

is a function of only x, y, and z because t is regarded as a fixed parameter. In this way, all the approximate functionals, E_{xc}, from time-independent DFT may be used in TDDFT. (With a few obvious modifications, this also includes hybrid functionals.) The xc in Casida's equations becomes

$$f_{xc}^{\sigma\tau}(\vec{r},\vec{r}\,') = \frac{\delta^2 E_{xc}[\rho_{\uparrow},\rho_{\downarrow}]}{\delta\rho_{\sigma}(\vec{r})\delta\rho_{\sigma}(\vec{r}\,')}. \tag{3.131}$$

Note that it is independent of time, so that the number of solutions to Casida's equations is just the dimensionality of Casida's equations. This is exactly the number of one-electron excitations. Hence we can conclude that, although the AA does include important correlations effects it is essentially a one-electron (CIS-like) theory.

LR-TDDFT with the AA has come to define conventional TDDFT. This theory is known to work well for low-lying excitations of primarily single electron character which do not involve too much charge density relation and which are at least somewhat localized in space.

3.3 Conclusion

This chapter has described both conventional *ab initio* and DFT electronic structure methods. We see DFT as extrapolating *ab initio* accuracy to systems too large to conveniently treat with conventional *ab initio* methods, rather than replacing *ab initio* for highly accurate calculations on small molecules. From this point of view approximate functionals must be validated not only against experiment but also against high quality *ab initio* calculations whose goal is to solve the same non relativistic Born-Oppenheimer separated N-electron problem as does DFT. This program has been extensively carried out for the ground state. Much less has been done for TDDFT and excited states, particularly in the context of photochemistry. In the following chapters we discuss a new implementation of LR-TDDFT and its application to molecules with open-shell ground states (not uncommon in photochemical applications). Then in chapter 6 TDDFT is carefully evaluated against QMC results for excited state curves of relevance for the photochemical ring-opening of oxirane.

Bibliography

[1] M. Born and J. Oppenheimer, *R. Ann. Phys.*, **84**, 457, (1927).

[2] D. R. Hartree, *Proc. Camb. Phil. Soc.*, **24**, 111, (1928).

[3] V. Fock, *Physik*, **61**, 126, (1930).

[4] P. A. M., Dirac, *Proc. Cambridge Philos. Soc.*, **26**, 376, (1930).

[5] H. J. Werner and W. Meyer, *J. Chem. Phys.*, **74**, 5494, (1981).

[6] C. C. J. Roothaan, *Phys. Rev.*, **23**, 69, (1951).

[7] Kohn, W. *Rev. Mod. Phys.*, **71**, 1253, (1999).

[8] W. Koch and M. Holthausen *A Chemist's Guide to Density Functional Theory*, New York, Wiley-VCH, **(2000)**.

[9] P. Hohenberg and W. Kohn, *Phys. Rev.*, **136**, B864, (1964).

[10] W. Kohn and L.J. Sham, *Phys. Rev.*, **140**, A1133, (1965).

[11] J. P. Perdew, K. Burke, *Int. J. Quantum Chem.*, **57**, 309, (1996).

[12] A. D. Becke, *J. Chem. Phys.*, **98**, 5648, (1993).

[13] H. Sekino, R. J. Bartlett, *J. Chem. Phys.*, **85**, 976, (1986).

[14] Andreas Dreuw and Martin Head-Gordon, *Chem. Rev.*, **105**, 4009, (2005).

[15] A. Szabo and N. S. Ostlund, *Modern Quantum Chemistry* (Dover, New York, 1996).

[16] C. E. Dykstra, *Ab initio Calculations of the Structure and Properties of Molecules* (Elsevier, Amsterdam, 1988).

[17] Erich Runge and E. K. U. Gross, *Physical Review Letters*, **52**, 997, (1984).

[18] E. K. U. Gross and W. Kohn, *Advances in Quantum Chemistry*, **21**, 255, (1990).

[19] B. O. Roos, P. Taylor and P. E. M. Siegbahn, *Chem. Phys.*, **48**, 157, (1980).

[20] J. Olsen, B. O. Roos, P. Jorgensen and H. J. A. Jensen, *J. Chem. Phys.*, **89**, 2185 (1988).

[21] P. A. Malmqvist, A. Rendell and B. O. Roos, *J. Phys. Chem.*, **94**, 5477, (1990).

[22] E. A. Hylleraas and B. Undheim, *Z. Phys.*, **65**, 759, (1930).

[23] J. K. L. McDonald, *Phys. Rev.*., **43**, 830, (1933).

[24] T. Helgater, P. Jörgensen and J. Olsen, *Molecular Electronic-Structure Theory* (John Wiley and Sons, Ltd.: New York, 2000).

[25] B. Roos, *Advances in Chemical Physics*; Ab Initio Methods in Quantum Chemistry - II, Lawley, K. P., Ed. John Wiley & Sons Ltd.: Chichester, England, p 399, (1987).

[26] B. O. Roos, *Acc. Chem. Res.*, **32**, 137, (1999).

[27] M. E. Casida, in *Recent Advances in Density Functional Methods, Part I*, edited by D.P. Chong (World Scientific: Singapore, 1995), p. 155.

[28] N. T. Maitra, F. Zhany, R. J. Cave and K. Burke, *J. Chem. Phys.*, **120**, 5932, (2004).

[29] R. J. Cave, F. Zhany, N. T. Maitra and K. Burke, *Chem. Phys. Lett.*, **389**, 39, (2004).

[30] M. Casida, *J. Chem. Phys.*, **122**, 54111, (2005).

Chapter 4

TDDFT in deMon2k

The first two implementations of Casida's equations for linear response TDDFT were the nearly simultaneous implementations in deMon-DynaRho and in Turbomol. Since then the deMon suite of programs has changed considerably and a new implementation of LR-TDDFT was needed which was more consistent with the auxiliary function approach used in deMon2k. In particular, we wanted a numerical method that would be fully consistent with future implementation of analytic derivatives for LR-TDDFT excited states. Two approaches are presented here, one with and one without the constraint that the fit density integrate to the total number of electrons. On the basis of this work, future versions of deMon2k will use unconstrained fitting for response theory calculations.

This work has been published as,

> Andrei Ipatov, Antony Fouqueau, Carlos Perez del Valle, Felipe Cordova, Mark E. Casida, Andreas M. Köster, Alberto Vela, and Christine Jödicke Jamorski, *J. Molec. Struct. (Theochem)*, **762**, 179 (2006).
> "Excitation Energies from an Auxiliary-Function Formulation of Time-Dependent Density-Functional Response Theory with Charge Conservation Constraint"

The list of authors is long (8 names) because this work was developed slowly over a long period of time. C. Jödicke Jamorski showed that the Davidson diagonalization routine in deMon-DynaRho failed to converge when applied to molecules beyond a certain size (converged answers were always correct.) C. Perez del Valle showed that the problem was not algorithmic. A. Fouqueau interfaced deMon2k with deMon-DynaRho, a critical step towards implementing LR-TDDFT directly into deMon2k. In the process, Fouqueau showed that the Davidson diagonalization problem was machine dependent, allowing us finally to trace the problem to a memory leak which was then fixed. M. E. Casida and A. Köster developed the new algorithm for LR-TDDFT in deMon2k which was the implemented by A. Vela, A.

Köster, and A. Ipatov. The algorithm was validated by M. E. Casida, A. Ipatov, and F. Cordova by comparing results from the new implementation of deMon2k (calculated by A. Ipatov) with those from Gaussian (calculated by F. Cordova).

In my case, this study provided me with the first chance to master the fine art of carrying out and interpreting LR-TDDFT calculations with Gaussian.

4.1 *Excitation Energies from an Auxiliary-Function Formulation of Time-Dependent Density-Functional Response Theory with Charge Conservation Constraint*

Excitation Energies from an Auxiliary-Function Formulation of Time-Dependent Density-Functional Response Theory with Charge Conservation Constraint

Andrei Ipatov, Antony Fouqueau, Carlos Perez del Valle, Felipe Cordova, and Mark E. Casida[1]
Équipe de Chimie Théorique,
Laboratoire d'Etudes Dynamiques et Structurales de la Sélectivité (LEDSS), UMR CNRS/UJF 5616,
Institut de Chimie Moléculaire de Grenoble (ICMG, FR-2607),
Université Joseph Fourier (Grenoble I),
301 rue de la Chimie, BP 53,
F-38041 Grenoble Cedex 9, FRANCE

Andreas M. Köster and Alberto Vela
Departamento de Química,
Cinvestav,
Avenida Instituto Politécnico Nacional 2508,
A.P. 14-740 Mexico D.F. 07000,
MEXICO

Christine Jödicke Jamorski
Laboratorium für Physikalische Chemie,
ETH Hoenggerberg,
CH-8093, Zürich,
SWITZERLAND

[1]Mark.Casida@ujf-grenoble.fr

Abstract

A key feature of the implementation of density-functional theory (DFT) in many quantum chemistry programs is the use of a charge density fitting (CDF) or resolution-of-the-identity (RI) auxiliary basis. One of these, namely the present-day **deMon2k** (21st century version of *densité de Montréal*) program, makes particulary heavy use of the CDF algorithm. We report the first fully consistent implementation of time-dependent density-functional theory (TDDFT) response theory into the present-day **deMon** code, by which we mean both (i) that the static limit yields analytic derivatives which are correct for the numerical method adapted by **deMon2k** in solving the Kohn-Sham orbital equations and (ii) that the eigenvalue equation appearing in the Casida formulation of TDDFT is properly symmetric. The new implementation is also entirely consistent with using the charge conservation constraint (CCC) in the CDF algorithm. Example calculations on the sodium dimer and tetramer and on *para*-aminobenzonitrile are given showing that the effect of the CCC on TDDFT excitation energies is minor compared to the importance of choosing an adequate auxiliary basis set.

I Introduction

Density-functional theory (DFT) provides a formalism for extrapolating to larger molecules the accuracy of highly elaborate correlated *ab initio* calculations which are presently only possible for smaller molecules. Limitations to the accuracy of DFT quantities come from the need to approximate the exchange-correlation (xc) functional for which no practical exact form is known. Many approximate xc functionals are known and hybrid functionals, which include Hartree-Fock exchange, allow calculations with *ab initio*-like accuracy to be carried out for molecules at a cost comparable to a Hartree-Fock calculation. Pure density functionals (i.e., those which depend only on the density and not on the orbitals) allow high accuracy for a cost considerably lower than that of a Hartree-Fock calculation, provided that the algorithm which is used can take advantage of the relatively simple multiplicative nature of the xc potential. This might be termed DFt (for "Density-Functional *t*echnology") [1]. One of the most successful of these technologies is that of using a set of charge density fitting (CDF) auxiliary functions. We will show how time-dependent density functional theory (TDDFT) response theory can be implemented in a fully consistent way into a code, namely **deMon2k** (for the 21st century version of *densité de Montréal*), which makes heavy use of the CDF approach. In this way

Table 4.1: Some index conventions used in this work. The arrows indicate how the functions are abbreviated when bra-ket notation is used.

Function	Index Type	Notation
Atomic Orbitals (AOs)	Greek letters	$\chi_\mu(\vec{r}) \rightarrow \mu$
Molecular Orbitals (MOs)	Latin lower case	$\psi_i^\sigma(\vec{r}) \rightarrow i_\sigma$
Auxiliary Functions (AFs)	Latin upper case	$f_K(\vec{r}) \rightarrow K$

we are completely able to avoid some small inconsistencies which have plagued our earlier work with the **deMon-DynaRho** (**deMon**-dynamic response of the density, ρ) program [2, 3].

As is well-known, Hartree-Fock calculations have a formal scaling of $\mathcal{O}(N^4)$ with the number of basis functions, N. This is the number of 4-center electron repulsion integrals (ERIs) over atomic orbitals (AOs),

$$\langle \mu\nu||\mu'\nu'\rangle = \int\int \chi_\mu(\mathbf{r})\chi_\nu(\mathbf{r})\frac{1}{|\mathbf{r}-\mathbf{r}'|}\chi_{\mu'}(\mathbf{r}')\chi_{\nu'}(\mathbf{r}')\,d\mathbf{r}d\mathbf{r}'\,, \tag{4.1}$$

in Mulliken ("charge cloud") notation. The problem remains even for pure DFT because of the classical Coulomb repulsion (Hartree) part of the electronic energy. However, pure DFT may be reduced to a formal scaling of $\mathcal{O}(N^3)$ by the introduction of an auxiliary basis and the use of the resolution-of-the-identity (RI) formula,

$$\hat{1} = \sum_{I,J} ||I\rangle\langle I||J\rangle^{-1}\langle J||\,, \tag{4.2}$$

where we are using the condensed notation summarized in Table 4.1 in an abstract bra-ket representation with double bars to indicate the integral metric defined in Eq. (4.1). The action of the right hand side in the position-space representation on an arbitrary auxiliary basis function, f_K, is,

$$\begin{aligned}\hat{1}f_K(\mathbf{r}) &= \sum_{I,J} f_I(\mathbf{r})\langle I||J\rangle^{-1}\langle J||K\rangle \\ &= \sum_I f_I(\mathbf{r})\delta_{I,K} \\ &= f_K(\mathbf{r})\,. \end{aligned} \tag{4.3}$$

These manipulations, so very simple in appearance, allow the $\mathcal{O}(N^4)$ 4-center ERIs

in terms of the $\mathcal{O}(N^3)$ 3-center ERIs,

$$\langle \mu\nu||\mu'\nu'\rangle = \sum_I \langle \mu\nu||I\rangle\langle I||J\rangle^{-1}\langle J||\mu'\nu'\rangle\,. \tag{4.4}$$

The RI strategy has been used as early as the late 1950's [4]. It was used in the early 1970s both in what was to become the modern-day **ADF** (Amsterdam Density Functional) program [5] and in the auxiliary function-based **LCAO-X**α (Linear Combination of Atomic Orbitals Xα) program of Sambe and Felton [6]. It continues to be used today to simplify Hartree-Fock and other quantum chemistry calculations. For example, Hamel *et al.* have used the method to help in the calculation of the exact exchange-only Kohn-Sham potential [7, 8, 9]. Of particular note in the present context is that the RI strategy is now used in the **Gaussian** [10] and **TurboMol** [11] programs to simplify the Coulomb integrals in DFT calculations. It was also used in the older **DGauss** DFT program [12] and in the **RESTDD** TDDFT program [13, 14]. Other uses have been reviewed by Kendall and Früchtl [15].

In reality, the RI approximation is less simple than it first appears. Practical auxiliary basis sets are always incomplete, making

$$\hat{P} = \sum_{I,J} ||I\rangle\langle I||J\rangle^{-1}\langle J||\,, \tag{4.5}$$

a projector, instead of the indentity operator, and making the RI method into an approximation. The quality of the approximation is closely related to the choice of metric. In fact, we could equally well write the resolution-of-the-identity using the simple overlap metric (denoted using a single bar),

$$\begin{aligned} \hat{1} &= \sum_{I,J} |I\rangle\langle I|J\rangle^{-1}\langle J| \\ \langle \mu\nu|\mu'\nu'\rangle &= \int \chi_\mu(\mathbf{r})\chi_\nu(\mathbf{r})\chi_{\mu'}(\mathbf{r})\chi_\nu(\mathbf{r})\,d\mathbf{r}\,, \end{aligned} \tag{4.6}$$

but the resultant RI approximation using a finite auxiliary basis set has been found, by explicit computation, to be distinctly inferior to that obtained using the Coulomb metric of Eq. (4.5) [16]. The basic reason was first given by Dunlap *et al.* [17, 18] who continued the earlier work of Sambe and Felton [6]. Dunlap introduced the notion of variational fitting of the charge density, ρ. A fit density,

$$\tilde{\rho}(\vec{r}) = \sum_I f_I(\vec{r})x_I\,, \tag{4.7}$$

was introduced and the CDF coefficients were obtained by minimizing the error,

$$\mathcal{E} = \langle \rho - \tilde{\rho} || \rho - \tilde{\rho} \rangle \,, \tag{4.8}$$

which is equivalent to maximizing the approximate Coulomb repulsion energy, [18, 19]

$$\begin{aligned} \tilde{J} &= \langle \tilde{\rho} || \rho \rangle - \frac{1}{2} \langle \tilde{\rho} || \tilde{\rho} \rangle \\ &\leq J = \frac{1}{2} \langle \rho || \rho \rangle \,. \end{aligned} \tag{4.9}$$

Minimizing Eq. (4.8) yields the RI approximation with the Coulomb metric,

$$\tilde{\rho}(\vec{r}) = \hat{P} \rho(\vec{r}) \,. \tag{4.10}$$

As Dunlap has emphasized [20], it is the variational nature of this particular RI approximation which accounts for its success.

Strictly speaking, the CDF approach of Dunlap is not the same as the RI approach except at convergence of the self-consistent field (SCF) calculations. This is because the Coulomb energy at the nth SCF iteration is calculated using the fit density obtained from the density of the previous iteration,

$$\begin{aligned} \tilde{J}^{(n)} &= \langle \rho^{(n)} || \tilde{\rho}^{(n-1)} \rangle - \frac{1}{2} \langle \tilde{\rho}^{(n-1)} || \tilde{\rho}^{(n-1)} \rangle \\ &\neq J^{(n)} = \frac{1}{2} \langle \rho^{(n)} || \rho^{(n)} \rangle \,. \end{aligned} \tag{4.11}$$

However the CDF and RI methods do become equivalent at SCF convergence and it is likely that most RI calculations use the CDF approach during the SCF steps.

Dunlap *et al.* also introduced the notion of a charge conservation constraint (CCC) during the variational fitting,

$$\langle \rho - \tilde{\rho} \rangle = 0 \,, \tag{4.12}$$

where we have introduced the notation (not to be confused with the expectation value of an operator),

$$\langle g \rangle = \int g(\mathbf{r}) \, d\mathbf{r} \,. \tag{4.13}$$

This makes sense to the extent that a small error in the number of electrons described by the fit charge density could lead to a chemically significant error in the total energy, and is why the CCC has always been included in the **deMon** programs.

This CCC had been introduced sometime before in what was latter to become the **ADF** program [21].

In the next section of the paper we will describe our auxiliary function implementation of TDDFT in **deMon2k**.

II Numerical Method

A molecular implementation of TDDFT response theory for the calculation of dynamic polarizabilities and excitation energies has been previously presented by one of us [22]. The fundamental quantities that we need to implement this theory in **deMon2k**, within the TDDFT adiabatic approximation, are analytic derivatives of the appropriate ground state energy within the CDF formalism.

A Elaboration of Charge Density Fitting

The CDF in **deMon2k** makes use of a particular matrix formulation [19] which is easily generalized to any number of constraints, not just the CCC. We first present the generalized version of the CDF here.

The problem to be solved is to minimize the error defined by Eq. (4.8) subject to the constraints,

$$\langle A_i|\tilde{\rho}\rangle = \int A_i(\mathbf{r})\tilde{\rho}(\mathbf{r})\,d\mathbf{r} = a_i\,, \tag{4.14}$$

where, once again, we have used the ordinary overlap metric indicated by a single bar. The CCC is just the case where there is a single $A_i(\mathbf{r})$ which is everywhere equal to unity and $a_i = N$, the total number of electrons. *Note that the a_i are taken to be independent of ρ.* It is interesting to note that this resembles the constrained self-consistent field (SCF) idea of Mukerji and Karplus [23] who noted that constraining an SCF calculation to give the experimental value for one property may improve the calculated value of a related property. One could, for example, imagine fixing the value taken by some property in an electronic excited state so as to guide the SCF calculation towards that state [24]. Probably the most recent application of constrained SCF theory is to the problem of extracting wave functions from X-ray diffraction data [25, 26, 27, 28, 29]. Note however that true constrained SCF calculations use a constraint on properties calculated from the exact (i.e., orbitally-derived) density, $\rho(\mathbf{r})$, while the present CDF method constrains the *fit* density, $\tilde{\rho}(\mathbf{r})$.

The constrained CDF minimization is carried out by the Lagrange multiplier

method by minimizing,

$$\begin{aligned} L &= \langle \rho - \tilde{\rho} || \rho - \tilde{\rho} \rangle - 2 \sum_i \lambda_i \left(a_i - \langle A_i | \tilde{\rho} \rangle \right) \\ 0 &= \frac{\partial L}{\partial x_I} \\ &= -2\langle I || \rho \rangle + 2 \sum_J \langle I || J \rangle x_J + 2 \sum_i \langle I | A_i \rangle \lambda_i \,, \end{aligned} \tag{4.15}$$

subject to the constraints in Eq. (4.14). This means that we have to solve the simultaneous equations,

$$\begin{aligned} \sum_J \langle I || J \rangle x_J + \sum_i \langle I | A_i \rangle \lambda_i &= \langle I || \rho \rangle \\ \sum_J \langle A_i | J \rangle x_J &= a_i \,. \end{aligned} \tag{4.16}$$

This can be expressed in matrix notation as,

$$\begin{bmatrix} \mathbf{A} & \mathbf{B} \\ \mathbf{C} & \mathbf{D} \end{bmatrix} \begin{pmatrix} \vec{x} \\ \vec{\lambda} \end{pmatrix} = \begin{pmatrix} \vec{\rho} \\ \vec{a} \end{pmatrix} , \tag{4.17}$$

where,

$$
\begin{aligned}
\mathbf{A} &= \begin{bmatrix} \langle 1||1\rangle & \langle 1||2\rangle & \cdots & \langle 1||M\rangle \\ \langle 2||1\rangle & \langle 2||2\rangle & \cdots & \langle 2||M\rangle \\ \vdots & \vdots & \ddots & \vdots \\ \langle M||1\rangle & \langle M||2\rangle & \cdots & \langle M||M\rangle \end{bmatrix} \\
\mathbf{B} &= \begin{bmatrix} \langle 1|A_1\rangle & \langle 1|A_2\rangle & \cdots & \langle 1|A_m\rangle \\ \langle 2|A_1\rangle & \langle 2|A_2\rangle & \cdots & \langle 2|A_m\rangle \\ \vdots & \vdots & \ddots & \vdots \\ \langle M|A_1\rangle & \langle M|A_2\rangle & \cdots & \langle M|A_m\rangle \end{bmatrix} \\
\mathbf{C} &= \begin{bmatrix} \langle A_1|1\rangle & \langle A_1|2\rangle & \cdots & \langle A_1|M\rangle \\ \langle A_2|1\rangle & \langle A_2|2\rangle & \cdots & \langle A_2|M\rangle \\ \vdots & \vdots & \ddots & \vdots \\ \langle A_m|1\rangle & \langle A_m|2\rangle & \cdots & \langle A_m|M\rangle \end{bmatrix} \\
\mathbf{D} &= \begin{bmatrix} 0 & 0 & \cdots & 0 \\ 0 & 0 & \cdots & 0 \\ \vdots & \vdots & \ddots & \vdots \\ 0 & 0 & \cdots & 0 \end{bmatrix},
\end{aligned}
\tag{4.18}
$$

and,

$$\begin{aligned}
\vec{x} &= \begin{pmatrix} x_1 \\ x_2 \\ \vdots \\ x_M \end{pmatrix} \\
\vec{\lambda} &= \begin{pmatrix} \lambda_1 \\ \lambda_2 \\ \vdots \\ \lambda_m \end{pmatrix} \\
\vec{\rho} &= \begin{pmatrix} \langle 1||\rho\rangle \\ \langle 2||\rho\rangle \\ \vdots \\ \langle M||\rho\rangle \end{pmatrix} \\
\vec{a} &= \begin{pmatrix} a_1 \\ a_2 \\ \vdots \\ a_m \end{pmatrix} .
\end{aligned} \tag{4.19}$$

By using the fact that, for $\mathbf{A}$ invertible,

$$\begin{aligned}
\begin{bmatrix} \mathbf{A} & \mathbf{B} \\ \mathbf{C} & \mathbf{D} \end{bmatrix}^{-1} &= \begin{bmatrix} \tilde{\mathbf{A}} & \tilde{\mathbf{B}} \\ \tilde{\mathbf{C}} & \tilde{\mathbf{D}} \end{bmatrix} \\
\tilde{\mathbf{A}} &= \mathbf{A}^{-1} + \mathbf{A}^{-1}\mathbf{B}\left(\mathbf{D} - \mathbf{C}\mathbf{A}^{-1}\mathbf{B}\right)^{-1}\mathbf{C}\mathbf{A}^{-1} \\
\tilde{\mathbf{B}} &= \mathbf{A}^{-1}\mathbf{B}\left(\mathbf{D} - \mathbf{C}\mathbf{A}^{-1}\mathbf{B}\right)^{-1} \\
\tilde{\mathbf{C}} &= -\left(\mathbf{D} - \mathbf{C}\mathbf{A}^{-1}\mathbf{B}\right)^{-1}\mathbf{C}\mathbf{A}^{-1} \\
\tilde{\mathbf{D}} &= \left(\mathbf{D} - \mathbf{C}\mathbf{A}^{-1}\mathbf{B}\right)^{-1} ,
\end{aligned} \tag{4.20}$$

that $\mathbf{D} = \mathbf{0}$ and that $\mathbf{C} = \mathbf{B}^\dagger$, we arrive at the following formulae for the interesting quantities:

$$\begin{aligned}
\vec{\lambda} &= \left(\mathbf{B}^\dagger\mathbf{A}^{-1}\mathbf{B}\right)^{-1}\mathbf{B}^\dagger\mathbf{A}^{-1}\vec{\rho} \\
&- \left(\mathbf{B}^\dagger\mathbf{A}^{-1}\mathbf{B}\right)^{-1}\vec{a} \\
\vec{x} &= \left[\mathbf{A}^{-1} - \mathbf{A}^{-1}\mathbf{B}\left(\mathbf{B}^\dagger\mathbf{A}^{-1}\mathbf{B}\right)^{-1}\mathbf{B}^\dagger\mathbf{A}^{-1}\right]\vec{\rho} \\
&- \mathbf{A}^{-1}\mathbf{B}\left(\mathbf{B}^\dagger\mathbf{A}^{-1}\mathbf{B}\right)^{-1}\vec{a} .
\end{aligned} \tag{4.21}$$

In principle, the problem of the constrained CDF is now solved. However it is interesting and informative to rederive the same answer within the abstract vector space spanned by the fitting functions with the Coulomb metric. We immediately face a problem, namely that the observables, $A_i(\mathbf{r})$, are more closely associated, via Eq. (4.14), with the overlap metric than with the Coulomb metric. This is a problem because it means that we are really obliged to work with objects in two distinct metric spaces. However we can transfer objects from one metric space to the other by a procedure that we shall call embedding. An embedded observable is defined by,

$$\tilde{A}_i(\mathbf{r}) = \sum_{I,J} f_I(\mathbf{r}) \langle I||J\rangle^{-1} \langle J|A_i\rangle \,. \tag{4.22}$$

This has the advantage that,

$$\langle \tilde{A}_i||\tilde{\rho}\rangle = \langle A_i|\tilde{\rho}\rangle = a_i \,. \tag{4.23}$$

Thus the constrained fit amounts to fixing the lengths of the components of $\tilde{\rho}$ along the various $\tilde{A}_i$ to have appropriate values. This is done with the aid of the projector of Eq. (4.5),

$$\tilde{\rho} = \hat{P}\rho - \sum_j \tilde{A}_j \lambda_j \,. \tag{4.24}$$

Then

$$\begin{aligned}
a_i &= \langle \tilde{A}_i||\tilde{\rho}\rangle \\
&= \langle \tilde{A}_i||\rho\rangle - \sum_i \langle \tilde{A}_i||\tilde{A}_j\rangle \lambda_j \\
\lambda_j &= \sum_i \langle \tilde{A}_j||\tilde{A}_i\rangle^{-1} \left(\langle \tilde{A}_i||\rho\rangle - a_i \right) \\
||\tilde{\rho}\rangle &= \hat{P}||\rho\rangle - \sum_{i,j} ||\tilde{A}_j\rangle \langle \tilde{A}_j||\tilde{A}_i\rangle^{-1} \left(\langle \tilde{A}_i||\rho\rangle - a_i \right) \\
&= \left(\hat{P} - \sum_{i,j} ||\tilde{A}_j\rangle \langle \tilde{A}_j||\tilde{A}_i\rangle^{-1} \langle \tilde{A}_i|| \right) ||\rho\rangle \\
&- \sum_{i,j} ||\tilde{A}_j\rangle \langle \tilde{A}_j||\tilde{A}_i\rangle^{-1} a_i \,.
\end{aligned} \tag{4.25}$$

This is the same answer given in Eq. (4.21), albeit in a different form. The quantity in the last parentheses is a new projector,

$$\hat{Q} = \hat{P} - \sum_{i,j} ||\tilde{A}_i\rangle \langle \tilde{A}_i||\tilde{A}_j\rangle^{-1} \langle \tilde{A}_j|| \,. \tag{4.26}$$

Finally, it is useful for future use to summarize a few relations involving this projector and the projector $\hat{P}$ of Eq. (4.5),

$$\begin{aligned} \hat{P}^2 &= \hat{P} \\ \hat{Q}\hat{P} &= \hat{P}\hat{Q} = \hat{Q} \\ \hat{Q}^2 &= \hat{Q} \\ \hat{Q}\left(\rho(\mathbf{r}) - \tilde{\rho}(\mathbf{r})\right) &= 0\,. \end{aligned} \tag{4.27}$$

B Energy Expression, Kohn-Sham Matrix, and Coupling Matrices

Having introduced the basic theory of the CDF method with constaints, we may now go on to present the basic DFT equations used in **deMon2k**. Only pure density functionals are used in **deMon2k**, so that the xc energy is only a functional of the spin-up and spin-down charge densities. There are, however, always two different sets of densities in **deMon2k**.

The usual linear combination of atomic orbitals (LCAO) approximation,

$$\psi_{r\sigma}(\mathbf{r}) = \sum_{\mu} \chi_{\mu}(\mathbf{r}) c^{\sigma}_{\mu,i}\,, \tag{4.28}$$

is assumed in **deMon2k** whereby the molecular orbitals (MOs), $\psi_{r\sigma}$, are expressed in terms of atomic orbitals (AOs), χ_{μ}. The spin-σ charge density is,

$$\begin{aligned} \rho_{\sigma}(\mathbf{r}) &= \sum_{i\sigma} \psi_{i\sigma}(\mathbf{r}) n_{i\sigma} \psi_{i\sigma}(\mathbf{r}) \\ &= \sum_{\mu,\nu} \chi_{\mu}(\mathbf{r}) P^{\sigma}_{\mu,\nu} \chi_{\nu}(\mathbf{r})\,. \end{aligned} \tag{4.29}$$

Here, $n_{i\sigma}$ is the occupation number of the MO $\psi_{i\sigma}$ and

$$P^{\sigma}_{\mu,\nu} = \sum_{i} c^{\sigma}_{\mu,i} n_{i\sigma} c_{\nu,i} \tag{4.30}$$

is the spin-σ density matrix. Of course, we can also talk about the total charge density and total density matrix,

$$\begin{aligned} \rho(\mathbf{r}) &= \rho_{\uparrow}(\mathbf{r}) + \rho_{\downarrow}(\mathbf{r}) \\ P_{\mu,\nu} &= P^{\uparrow}_{\mu,\nu} + P^{\downarrow}_{\mu,\nu}\,. \end{aligned} \tag{4.31}$$

All of these relations concern the *orbital density*.

There is also the *fit density*,

$$\tilde{\rho}_\sigma(\mathbf{r}) = \hat{Q}\rho_\sigma(\mathbf{r}) - \sum_{i,j} \tilde{A}_i(\mathbf{r})\langle \tilde{A}_i||\tilde{A}_j\rangle^{-1} a_j \,, \tag{4.32}$$

discussed at length in the previous subsection. Because the fit density is a functional of the orbital density, the fit density is also a function of the density matrix. Its derivative,

$$\frac{\partial \tilde{\rho}_\sigma(\mathbf{r})}{\partial P^{\sigma'}_{\nu,\mu}} = \delta_{\sigma,\sigma'}\hat{Q}\chi_\nu(\mathbf{r})\chi_\mu(\mathbf{r}) \,. \tag{4.33}$$

This is a key equation for what follows.

The usual Kohn-Sham energy expression for a pure density functional is,

$$E = \sum_{i\sigma} n_{i\sigma}\langle\psi_{i\sigma}|\hat{h}|\psi_{i\sigma}\rangle + \frac{1}{2}\langle\rho||\rho\rangle + E_{xc}[\rho_\uparrow,\rho_\downarrow] \,, \tag{4.34}$$

where $\hat{h}$ is the core hamiltonian, representing the noninteracting kinetic energy and the attraction energy between the electrons and nuclei. The standard approach to DFT in quantum chemistry consists of replacing this expression with,

$$E = \sum_{\mu,\nu} h_{\mu,\nu}P_{\nu,\mu} + \frac{1}{2}\langle\rho||\rho\rangle + E^{\text{num}}_{xc}[\rho_\uparrow,\rho_\downarrow] \,, \tag{4.35}$$

where $h_{\mu,\nu} = \langle\mu|\hat{h}|\nu\rangle$ and the superscript on E^{num}_{xc} indicates that matrix elements are to be evaluated by direct numerical integration over a grid in physical (x,y,z) space. This, for example, is the approach used in the program **Gaussian**[10]. The approach taken in **deMon2k** is different.

There are two options in **deMon2k**. The option "VXCTYPE BASIS" calculates the energy according to the formula,

$$E = \sum_{\mu,\nu} h_{\mu,\nu}P_{\nu,\mu} + \langle\rho||\tilde{\rho}\rangle - \frac{1}{2}\langle\tilde{\rho}||\tilde{\rho}\rangle + E^{\text{num}}_{xc}[\rho_\uparrow,\rho_\downarrow] \,. \tag{4.36}$$

This method has been around since at least early versions of the **deMon** programs and something very similar can be found as the Coulomb fitting option of **Gaussian**. However, the energy in **deMon2k** may also be calculated using the option "VXCTYPE AUXIS" according to the expression,

$$E = \sum_{\mu,\nu} h_{\mu,\nu}P_{\nu,\mu} + \langle\rho||\tilde{\rho}\rangle - \frac{1}{2}\langle\tilde{\rho}||\tilde{\rho}\rangle + E^{\text{num}}_{xc}[\tilde{\rho}_\uparrow,\tilde{\rho}_\downarrow] \,. \tag{4.37}$$

Calculations with the VXCTYPE AUXIS option make full use of the CDF strategy and so are considerably faster than the corresponding calculations with the VXCTYPE BASIS option. In particular, no more than 2-center integrals need to be evaluated numerically, instead of the usual numerical 4-center integrals. To see this more clearly, and for the sake of simplicity, consider the non spin density local density approximation where

$$E_{xc}[\rho] = \int \epsilon_{xc}\left(\rho(\mathbf{r})\right)\rho(\mathbf{r})\,d\mathbf{r}\,. \tag{4.38}$$

Here $\epsilon_{xc}(\rho)$ is the xc energy for the homogeneous electron gas with density ρ. When the VXCTYPE BASIS option is used, the density is a linear combination of products of atomic orbitals, $\chi_\mu(\mathbf{r})\chi_\nu(\mathbf{r})$, so that the numerical evaluation of the xc energy involves terms of the form,

$$\epsilon_{xc}\left(\sum_{\mu,\nu}\chi_\mu(\mathbf{r})P_{\mu,\nu}\chi_\nu(\mathbf{r})\right)\chi_{\mu'}(\mathbf{r})\chi_{\nu'}(\mathbf{r})\,, \tag{4.39}$$

where the four AOs, χ_μ, χ_ν, $\chi_{\mu'}$ and $\chi_{\nu'}$, may be on different centers. In contrast, when the VXCTYPE AUXIS option is used, the density is a linear combination of auxiliary functions, $f_I(\mathbf{r})$, so that the numerical evaluation of the xc energy only involves terms of the form,

$$\epsilon_{xc}\left(\sum_{I} f_I(\mathbf{r})x_I\right)f_J(\mathbf{r})\,, \tag{4.40}$$

which involves only two auxiliary functions, f_I and f_J, on at most two different centers. When spin and dependence on density gradients are taken into account, the reasoning is similar. *Only the* VXCTYPE AUXIS *option is considered in the present paper.*

The density matrix in Eq. (4.37) is obtained by minimizing the energy subject to the usual orbital orthonormality constraint [30]. This leads to the matrix form of the Kohn-Sham equation,

$$\mathbf{F}^\sigma\vec{c}_{i\sigma} = \epsilon_{i\sigma}\mathbf{S}\vec{c}_{i\sigma}\,. \tag{4.41}$$

The quantity,

$$S_{\mu,\nu} = \langle\mu|\nu\rangle\,, \tag{4.42}$$

is the usual AO overlap matrix. The quantity,

$$F^{\sigma}_{\mu,\nu} = \frac{\partial E}{\partial P^{\sigma}_{\nu,\mu}}\,, \tag{4.43}$$

is the Kohn-Sham matrix. The density-matrix derivative of the energy expression (4.37) is straightforward to carryout with the help of relation (4.33). It gives,

$$F^{\sigma}_{\mu,\nu} \;=\; h_{\mu,\nu} + \langle \mu\nu||\tilde{\rho}\rangle + \langle \hat{Q}\mu\nu||\rho-\tilde{\rho}\rangle + \langle \hat{Q}\mu\nu|v^{\sigma}_{xc}[\tilde{\rho}_{\uparrow},\tilde{\rho}_{\downarrow}]\rangle\,, \tag{4.44}$$

where the xc potential,

$$v^{\sigma}_{xc}[\tilde{\rho}_{\uparrow},\tilde{\rho}_{\downarrow}](\mathbf{r}) = \left[\frac{\delta E_{xc}[\rho_{\uparrow},\rho_{\downarrow}]}{\delta\rho_{\sigma}(\mathbf{r})}\right]_{\rho_{\sigma}=\tilde{\rho}_{\sigma}}\,. \tag{4.45}$$

However,

$$\begin{aligned}\langle \hat{Q}\mu\nu||\rho-\tilde{\rho}\rangle &= \langle \mu\nu||\hat{Q}\,(\rho-\tilde{\rho})\rangle \\ &= 0\,,\end{aligned} \tag{4.46}$$

because of the last of the relations (4.27). Thus,

$$F^{\sigma}_{\mu,\nu} \;=\; h_{\mu,\nu} + \langle \mu\nu||\tilde{\rho}\rangle + \langle \hat{Q}\mu\nu|v^{\sigma}_{xc}[\tilde{\rho}_{\uparrow},\tilde{\rho}_{\downarrow}]\rangle\,. \tag{4.47}$$

It is convenient to introduce the matrix representation of the projector, $\hat{Q}$, namely,

$$\hat{Q} = \sum_{I,J} ||I\rangle Q_{I,J}\langle J||\,, \tag{4.48}$$

where,

$$\begin{aligned}Q_{I,J} &= \langle I||J\rangle^{-1} \\ &- \sum_{i,j,K,L}\langle I||K\rangle^{-1}\langle K|A_i\rangle\langle\tilde{A}_i||\tilde{A}_j\rangle^{-1}\langle A_j|L\rangle\langle L||J\rangle^{-1}\,.\end{aligned} \tag{4.49}$$

Then

$$\langle v^{\sigma}_{xc}[\tilde{\rho}_{\uparrow},\tilde{\rho}_{\downarrow}]|\hat{Q}\mu\nu\rangle = \sum_{I,J}\langle v^{\sigma}_{xc}[\tilde{\rho}_{\uparrow},\tilde{\rho}_{\downarrow}]|I\rangle Q_{I,J}\langle I||\mu\nu\rangle\,. \tag{4.50}$$

Note that, in the absence of constraints, the fitting procedure just yields,

$$F^{\sigma}_{\mu,\nu} = h_{\mu,\nu} + \langle \mu\nu||\tilde{\rho}\rangle + \langle \mu\nu||\tilde{v}^{\sigma}_{xc}[\tilde{\rho}_{\uparrow},\tilde{\rho}_{\downarrow}]\rangle \,, \tag{4.51}$$

the expected equation for the Kohn-Sham matrix, but using an embedded (or fit) xc potential.

$$\tilde{v}^{\sigma}_{xc}[\tilde{\rho}_{\uparrow},\tilde{\rho}_{\downarrow}] = \sum_{I} f_I(\mathbf{r})\langle I||J\rangle^{-1}\langle I|v^{\sigma}_{xc}[\tilde{\rho}_{\uparrow},\tilde{\rho}_{\downarrow}]\rangle \,. \tag{4.52}$$

Casida [22] recast basic TDDFT linear response theory in terms of the linear response of the Kohn-Sham density matrix,

$$\delta P_{rs\sigma}(\omega) = \frac{n_{r\sigma} - n_{s\sigma}}{\omega - (\epsilon_{r\sigma} - \epsilon_{s\sigma})}\langle \psi_{r\sigma}|\delta v^{\sigma}_{\text{eff}}(\omega)|\psi_{s\sigma}\rangle \,, \tag{4.53}$$

and the coupling matrix,

$$K^{\sigma,\sigma'}_{\mu\nu,\mu'\nu'} = \frac{\partial^2 E}{\partial P^{\sigma}_{\nu,\mu}\partial P^{\sigma'}_{\nu'\mu'}} \,. \tag{4.54}$$

Here the coupling matrix has been expressed in the AO representation, but it is easy to transform to the representation of the unperturbed MOs, which is prefered, at least for formel work. Casida's final result looks very much like the so-called random phase approximation (RPA) used in quantum chemistry. This is usually expressed in terms of the **A** and **B** matrices,

$$\begin{aligned} A_{ia\sigma,jb\tau} &= \delta_{\sigma,\tau}\delta_{i,j}\delta_{a,b}\left(\epsilon_{a\sigma} - \epsilon_{i\sigma}\right) + K_{ia\sigma,jb\tau} \\ B_{ia\sigma,jb\tau} &= K_{ia\sigma,bj\tau} \,, \end{aligned} \tag{4.55}$$

where the "Fortran MO index convention,"

$$\underbrace{abc\cdots fgh}_{\text{unoccupied}} \,|\, \underbrace{ijklmn}_{\text{occupied}} \,|\, \underbrace{opq\cdots xyz}_{\text{free}} \tag{4.56}$$

has been introduced. Then

$$\left\{\omega\begin{bmatrix} -\mathbf{1} & \mathbf{0} \\ \mathbf{0} & \mathbf{1} \end{bmatrix} - \begin{bmatrix} \mathbf{A} & \mathbf{B} \\ \mathbf{B} & \mathbf{A} \end{bmatrix}\right\}\begin{pmatrix} \delta\vec{P}(\omega) \\ \delta\vec{P}^{*}(\omega) \end{pmatrix} = \begin{pmatrix} \Delta\vec{v}_{\text{ext}}(\omega) \\ \Delta\vec{v}^{*}_{\text{ext}}(\omega) \end{pmatrix} \,, \tag{4.57}$$

where the particle-hole ($ia\sigma$) parts of the applied perturbation and linear response of the Kohn-Sham density-matrix have been represented as column vectors. At an electronic excitation energy, even a small resonance will lead to a discontinuous (i.e.,

infinite) response of the density matrix. This means that the excitation energies may be determined as the eigenvalues of the pseudo-eigenvalue equation,

$$\left[\begin{array}{cc} \mathbf{A} & \mathbf{B} \\ \mathbf{B} & \mathbf{A} \end{array} \right] \left(\begin{array}{c} \vec{X}_I \\ \vec{Y}_I \end{array} \right) = \omega_I \left[\begin{array}{cc} \mathbf{1} & \mathbf{0} \\ \mathbf{0} & -\mathbf{0} \end{array} \right] \left(\begin{array}{c} \vec{X}_I \\ \vec{Y}_I \end{array} \right) , \tag{4.58}$$

which has the classic solution,

$$\begin{aligned} \mathbf{\Omega}\vec{F}_I &= \omega_I^2 \vec{F}_I \\ \mathbf{\Omega} &= (\mathbf{A}-\mathbf{B})^{1/2}(\mathbf{A}+\mathbf{B})(\mathbf{A}-\mathbf{B})^{1/2} \\ \vec{F}_I &= (\mathbf{A}-\mathbf{B})^{-1/2}(\vec{X}_I+\vec{Y}_I)\,. \end{aligned} \tag{4.59}$$

In the particular cases of the local and generalized gradient approximations (as opposed to hybrid approximations), the matrix,

$$A_{ia\sigma,jb\tau} - B_{ia\sigma,jb\tau} = \delta_{\sigma,\tau}\delta_{i,j}\delta_{a,b}\left(\epsilon_{a\sigma} - \epsilon_{i\sigma}\right) , \tag{4.60}$$

is particularly simple, making Eq. (4.57) a particularly appealing way to calculate excitation energies from TDDFT.

It remains to establish the form of the coupling matrix for the CDF method with constraints. The coupling matrix used in taking analytic derivatives and in TDDFT is,

$$\begin{aligned} K^{\sigma,\sigma'}_{\mu\nu,\mu'\nu'} &= \frac{\partial^2 E}{\partial P^{\sigma}_{\nu\mu} P^{\sigma'}_{\nu'\mu'}} \\ &= \langle \mu\nu || \hat{Q}\nu'\nu' \rangle + \langle \hat{Q}\mu\nu | f^{\sigma,\sigma'}_{xc}[\tilde{\rho}_\uparrow, \tilde{\rho}_\downarrow] | \hat{Q}\mu'\nu' \rangle \,, \\ &= \langle \hat{Q}\mu\nu || \hat{Q}\nu'\nu' \rangle + \langle \hat{Q}\mu\nu | f^{\sigma,\sigma'}_{xc}[\tilde{\rho}_\uparrow, \tilde{\rho}_\downarrow] | \hat{Q}\mu'\nu' \rangle \,, \end{aligned} \tag{4.61}$$

where,

$$f^{\sigma,\sigma'}_{xc}(\mathbf{r},\mathbf{r}') = \frac{\delta^2 E_{xc}}{\delta\rho_\sigma(\mathbf{r})\delta\rho_{\sigma'}(\mathbf{r})} \,, \tag{4.62}$$

is the xc kernel. Thus the coupling matrix divides into a spin-independent Coulomb (Hartree) part,

$$\langle \hat{Q}\mu\nu || \hat{Q}\mu'\nu' \rangle = \sum_{I,J} \langle \mu\nu || I \rangle Q_{I,J} \langle J || \mu'\nu' \rangle \,, \tag{4.63}$$

and into a spin-dependent xc part,

$$\begin{aligned}\langle\hat{Q}\mu\nu|f_{xc}^{\sigma,\sigma'}[\tilde{\rho}_\uparrow,\tilde{\rho}_\downarrow]|\hat{Q}\mu'\nu'\rangle &= \sum_{I,J,K,L}\langle\mu\nu||I\rangle Q_{I,J} \\ &\times \langle I|f_{xc}^{\sigma,\sigma'}[\tilde{\rho}_\uparrow,\tilde{\rho}_\downarrow]|J\rangle \\ &\times Q_{J,K}\langle K||\mu'\nu'\rangle\,. \end{aligned} \tag{4.64}$$

Note that the RI-2 approximation in the **RESTDD** program [14] is obtained from these last two equations by replacing $Q_{I,J}$ with $\langle I||J\rangle^{-1}$, that is by neglect of the fitting constraints. However what is particularly interesting is that this equation is introduced in **RESTDD** as an additional approximation to help in solving Casida's equation, without regard to consistence with approximations in the pre-**RESTDD** self-consistent field program used (**PARAGAUSS**). Here, of course, we have taken special care that the response equations are completely consistant with both the self-consistent field Kohn-Sham equations solved and with the initial DFT energy expression used. This has the important advantage that Casida's equation may eventually be used to calculate excited state analytic derivatives without any fear of inconsistencies.

This completes our explanation of the methodology used in this paper. The method is, of course, very general. Even without the inclusion of constraints, this numerical approach is a distinct improvement over what had been done previously in **deMon-DynaRho**. In the initial version of **deMon-DynaRho**[2], we were careful that the coupling matrix elements corresponded to the second derivatives of the energy expression used in **deMon-KS**[31]. That guaranteed that the static polarizability calculated as the static limit of the TDDFT polarizability was the correct analytic derivative quantity. However the coupling matrix was not exactly symmetric and this lead to difficulties in calculating nearly degenerate excitation energies [2]. That is why a later version of **deMon-DynaRho** used the numerical method proposed in Ref. [3] where the coupling matrix is symmetric but the static limit of TDDFT no longer gave the exact analytic derivatives. In the numerical method described here and now implemented, the coupling matrix is symmetric (and in fact resembles that described in Ref. [3]) *and* the static limit of TDDFT is the exact analytic derivative for the appropriate energy expression. Thus certain small but irritating inconveniences which plagued the TDDFT implementation in **deMon-DynaRho** have been overcome in a new elegant formalism.

In the remainder of the paper, we will illustrate how this new method compares with an auxiliary function-free method, in particular giving an idea of what quality of results can be expected from different auxiliary basis sets. But our real interest

is in the utility (or lack thereof) of the CCC for calculating TDDFT excitation energies. Thus we will confine our calculations to the case of the CCC — that is, the case of a single A_i which is equal to unity.

III Computational Details

The **deMon** series of programs dates back to code first developed at the University of Montreal in the mid-1980s, during the course of Alain St-Amant's Ph.D. thesis. Suffice it to say that the **deMon** programs share a common philosophy of using Gaussian-type orbital and auxiliary basis sets. Exchange-correlation integrals are evaluated by direct numerical integration over a Becke-type grid. Details of the original implementation may be found in Alain St-Amant's thesis (in French). In the mid-1990s, Casida described the molecular implementation of TDDFT [C95b] [22] , which has now been adapted in a most widely-used quantum chemistry programs. The initial **deMon** impementation of the Casida equations appeared as **deMon-DynaRho** [32], a post-**deMon-KS** [31] program. The first calculations with **deMon-DynaRho** were reported in Refs. [33] and [2]. Improved numerical methodology was described in Ref. [3] and subsequently implemented in **deMon-DynaRho**. The original **deMon-KS** of Alain St-Amant's Ph.D. thesis has undergone many evolutions. It was finally decided to rewrite the entire program making numerous algorithmic improvements. The result is **deMon2k**[34].

Only the most recent version of **deMon2k** includes TDDFT. It is to be emphasized here that our object is to make a new more efficient auxiliary function-based implementation of TDDFT whose finite orbital and auxiliary-function formalism are as trustworthy a reflection as possible of the formal properties of the formally exact Casida equations[22], in the sense of having symmetric matrices and reducing to true analytic derivatives for the appropriate underlying energy expressions. Our initial modifications of **deMon-DynaRho** to make it a post-SCF program for **deMon2k** gave reasonable answers but did not completely meet our objective. That is why the numerical method for TDDFT described in this paper has been incorporated directly into the heart of **deMon2k**. This implementation is so far only partial in so far as some of the desirable features of **deMon-DynaRho** have yet to be transfered to the new program and calculations are limited to the adiabatic local density approximation (also called the time-dependent local density approximation). These are, of course, temporary limitations which will disappear in the normal course of development of **deMon2k**.

Test calculations were carried out on Na_2, Na_4 and *para*-aminobenzonitrile (pABN).

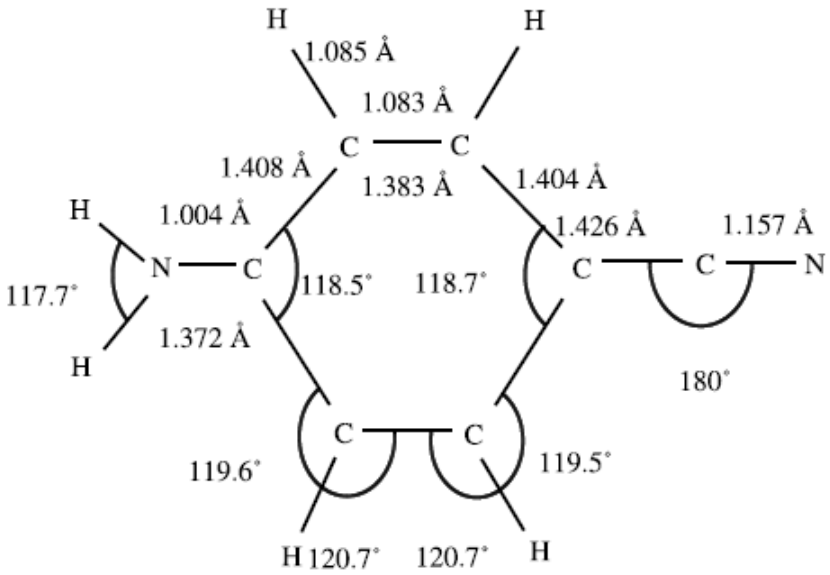

Figure 4.1: Planar C_{2v} geometry used in our pABN calculations.

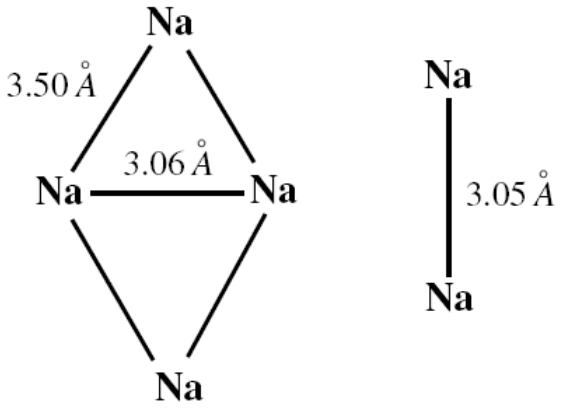

Figure 4.2: Na cluster geometries used in our calculations. Symmetries: Na_2 $D_{\infty h}$, Na_4 D_{4h}.

The geometry used for pABN is the symmetric planar geometry shown in Fig. 4.1, which is close to what is obtained from a DFT calculation with the B3LYP functional. The geometries used for the sodium clusters are shown in Fig. 4.2. They have been obtained with the program **Gaussian** [10] using the B3LYP functional and the Sadlej basis set [35]. The orbital basis sets used in all calculations reported here are the Sadlej basis sets[35] which were designed to describe polarizabilities (rather than excitation energies) but which are adequate for present purposes.

Most calculations were carried out with the MEDIUM grid, though some calculations were carried out with the FINE grid. The **deMon2k** program has the option to use an adaptive grid which adds grid points until a predetermined accuracy is obtained in the integration of the charge density. Tests showed that the CCC lead to the use of different adaptive grids and hence somewhat uncontrolled comparisons. We have therefore decided to avoid the use of adaptive grids in the calculations reported here.

Several different auxiliary basis sets were used. The GEN-An and GEN-An*, $n = 1, 2,$ or 3, auxiliary basis sets are generated automatically by the **deMon2k** program based upon the orbital basis set coefficients. Auxiliary functions are grouped into s, spd, and $spdfg$ sets with shared exponents. The GEN-An basis sets make use of the s and spd groups, while the GEN-An* also uses $spdfg$ groups. The exponents are determined by the smallest and largest primitive Gaussian exponents in the orbital basis set via an essentially even tempered progression [36, 37]. The larger the value of n the better the coverage of the auxiliary function space, so the quality of the auxiliary basis sets increase in going from A1 to A2 to A3. The exact procedure is described in **deMon2k** manual.

Comparisons were made against **Gaussian**[10] TDDFT calculations using the same geometry and orbital basis sets, but without the use of auxiliary basis functions. That is, the charge density fitting option in **Gaussian** was *not* used and no approximation took place for the 4-center integrals.

IV Results

We wanted to answer two related questions here. The first is to obtain an idea of the quality of auxiliary basis set necessary to get converged answers for TDDFT excitation energies and oscillator strengths. We also wanted to determine the importance (or lack thereof) of the CCC. The fit density is used in **deMon2k** in calculating the Coulomb (Hartree) and xc contributions to the orbital hamiltonian and total energy. It is logical to think that a small error in the charge density would lead

Table 4.2: Ionization potentials for molecules treated in this work.

Na_2 Excitation Energies (eV)[1]			
Molecule	$-\epsilon_{\mathrm{HOMO}}$[1]	ΔSCF[2]	Expt[3]
Na_2	3.56	5.25	4.93
Na_4	3.00	4.30	4.27
pABN	6.25	8.16	8.17

[1] The negative of the highest occupied molecular orbital energy, present work.
[2] The ΔSCF ionization potential, present work.
[3] Experimental values for sodium clusters from Ref. [38]. Experimental value for pABN from Ref. [39].

to small errors in the orbital hamiltonian and total energy, which would nevertheless be large on the scales of spectroscopic and chemical accuracy. Indeed it has been found that the inclusion of the CCC increases the accuracy of the electron number obtained by total numerical integration of the orbital density by at least an order of magnitude. It is reasonable to think that excitation energies and oscillator strengths would also benefit from the CCC by reducing the size of the auxiliary-basis set needed for a given level of convergence. We decided to test this hypothesis with calculations on *para*-aminobenzonitrile (pABN) and some small sodium clusters. This choice was partly governed by our own prior experience with these types of systems [40, 41, 42, 43, 44, 45, 46, 47, 48, 49, 50, 51, 52, 53, 54, 55, 56, 57, 58], but also makes sense in that the physics and chemistry of these two types of systems is very different. The excitation energies considered are all well below the TDLDA ionization threshold at minus the highest occupied molecular orbital energy (see Table 4.2.)

Even for most of these molecules, full diagonalization of the TDLDA method is not possible and the block Davidson Krylov space method is usually used to find the lowest 20 or so excitations. Thus this molecule is also a test of the **deMon2k** block Davidson procedure which showed no particular problems.

TDLDA calculations were performed both with and without the charge conservation constraint (CCC) in the SCF and/or TDDFT steps with 5 different auxiliary basis sets.

A Small Sodium Clusters

To a first approximation, the electronic structure of even very small sodium clusters is relatively well described by the shell model [59]. In this model, the cluster is

Table 4.3: Comparison of our TDLDA excitation energies with experimental and *ab initio* results from the literature.

Na_2 Excitation Energies (eV)[1]					
Excitation	Expt[1]	TDLDA[2]	FCI[3]	CI[4]	MBPT[5]
$^1\Sigma_u^+$	1.820	2.10	1.928	1.823	1.627
$^1\Pi_u$	2.519	2.64	2.576	2.517	2.572

[1] As cited in Ref. [60].
[2] Present work.
[3] Full configuration interaction [61].
[4] Configuration interaction [62].
[5] Many-body perturbation theory [63].

thought of as an elipsoidal jellium droplet, filled with the valence electrons in a harmonic oscillator-type potential. The shape of the cluster can be obtained by varying the major axes of the elipsoid so as to minimize the total energy. That the nuclei arrange themselves to minimize the energy of the electrons, instead of the electrons arranging themselves to minimize the nuclear repulsions, may be considered as evidence of metallic rather than covalent bonding. In any event, the harmonic oscillator aspect of the shell model implies that there should be three major electronic transitions corresponding to the harmonic modes along each of the three different axes. Should these axes be degenerate (as is the case for cylindrically symmetric diatomics), even fewer major transitions will be observed.

The shell model predicts two principle excitations for Na_2: a non degenerate $^1\Sigma_u^+(\sigma_g \rightarrow \sigma_u)$ excitation and a degenerate $^1\Pi_u(\sigma_g \rightarrow \pi_u)$ excitation. In practice the two Π_u excitations are not exactly degenerate in our calculations because of very slight symmetry breaking which occurs due to the use during the numerical integration steps of the calculation of a grid whose symmetry is not strictly identical to that of the molecule. This effect is however very small. Our TDLDA results are compared with experiment and *ab initio* results in Table 4.3. The TDLDA somewhat overestimates the excitation energies of the two singlet states.

Numerical errors in our calculated excitation energies and oscillator strengths are shown in Figs. 4.3 and 4.4. As expected, the errors in calculated excitation energies and oscillator strengths decreases, albeit nonmonotonically, as the quality of the auxiliary basis set increases. The most accurate work requires the inclusion of polarization functions in the auxiliary basis set. Maximal errors of less than 0.02 eV in the excitation energies are obtained with the Gen-A2* and Gen-A3* auxiliary basis sets. Perhaps most remarkable is that, apart from a few exceptions, it is the use

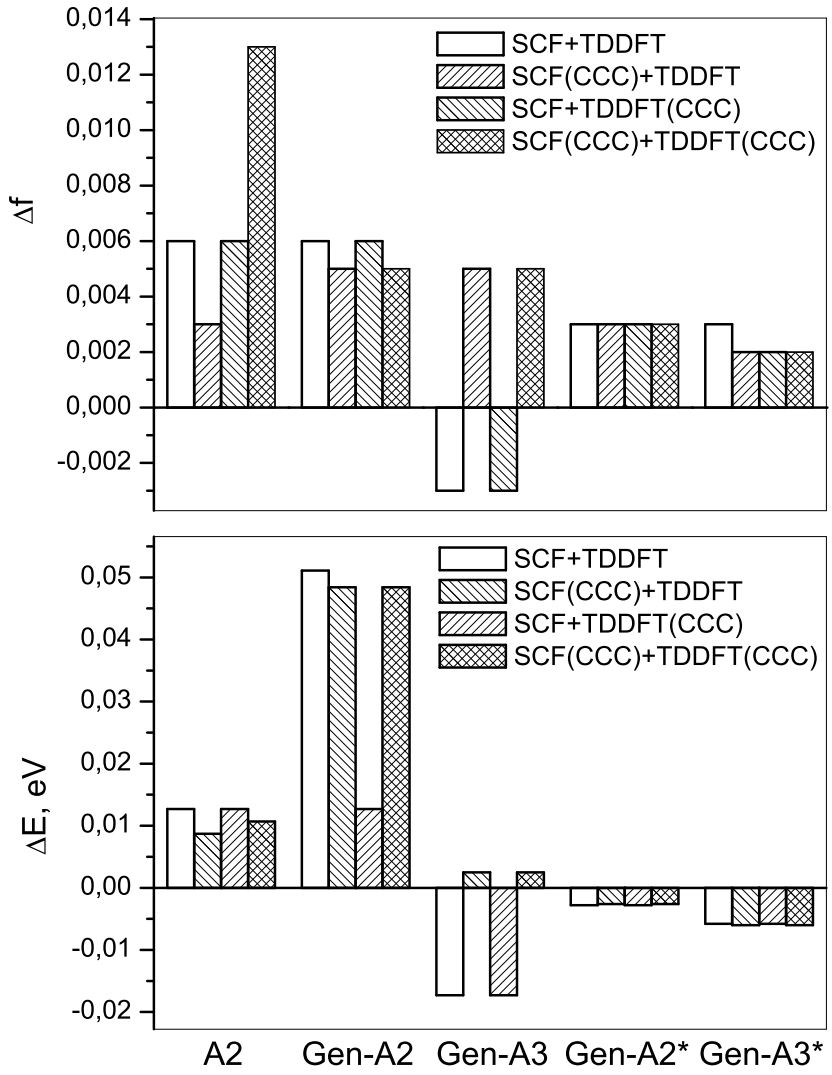

Figure 4.3: Errors in the Na_2 $^1\Sigma_u^+$ excitation (2.10 eV) as a function of algorithm and auxiliary basis set: bottom energy, top oscillator strength.

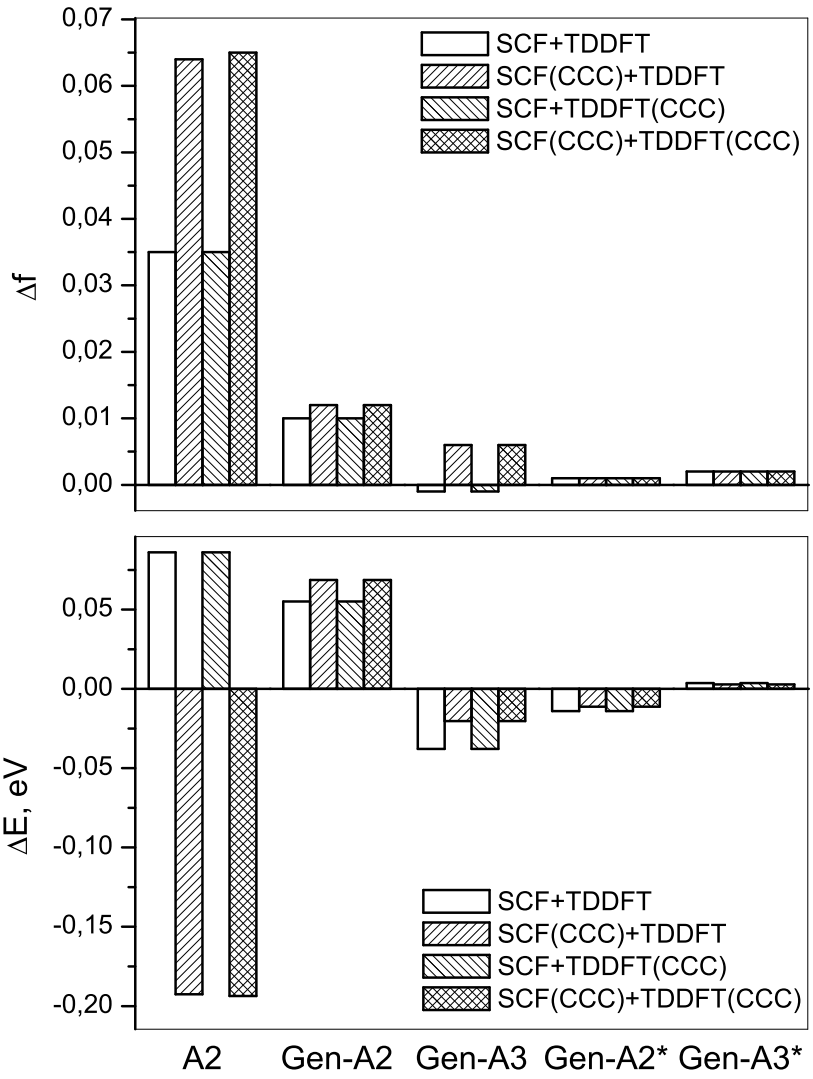

Figure 4.4: Errors in Na_2 $^1\Pi_u$ excitation (2.64 eV) as a function of algorithm and auxiliary basis set: bottom energy, top oscillator strength.

Table 4.4: Comparison of our TDLDA excitation energies with experimental and *ab initio* results from the literature.

Na_4 Excitation Energies (eV)[1]			
Excitation	Expt[1]	TDLDA[2]	MRD-CI[3]
1^1B_{2u}	1.63	1.49	1.51
1^1B_{3u}[4]	1.80	1.81	1.71
2^1B_{3u}	1.98	2.03	1.87
1^1B_{1u}	2.18	2.24	2.07
3^1B_{2u}[4]	2.51	2.57	2.45
2^1B_{1u}[4]	2.78	2.76	2.76

[1]From Ref. [64].
[2]Present work.
[3]Multireference doubles configuration interaction [65].
[4]Principle peaks corresponding expected from the shell model and found in the MRD-CI calculations of Ref. [65].

or non use of the CCC in the pre-TDDFT SCF calculation rather than in the post-SCF TDDFT which determines the size of the errors in the excitation energies and oscillator strengths. It is difficult to say if the CCC aids convergence with respect to the quality of the auxiliary basis set. However the CCC involves little computational overhead and does not markedly deteriorate the quality of the calculated excitation energies and oscillator strengths.

For Na_4, the shell model predicts three principle absorptions. As indicated in Table 4.4, this is indeed what is reported in the literature. Our tests concentrated on the four lowest singlet excitations, only one of which belongs to the 3 principle absorptions predicted by the shell model. Numerical errors for these four lowest singlet excitations are given in Figs. 4.5 and 4.6. Our conclusions are essentially identical to those already drawn for the dimer calculations. Increasing the quality of the auxiliary basis set decreases on average the size of the numerical error in the excitation energy. The Gen-A3* auxiliary basis set is able to give excitation energies to within 0.02 eV of those calculated using the **Gaussian** program without charge density fitting. Here, even more than in the case of the dimer, the size of the errors are determined almost exclusively by whether or not the CCC has been used in the SCF step.

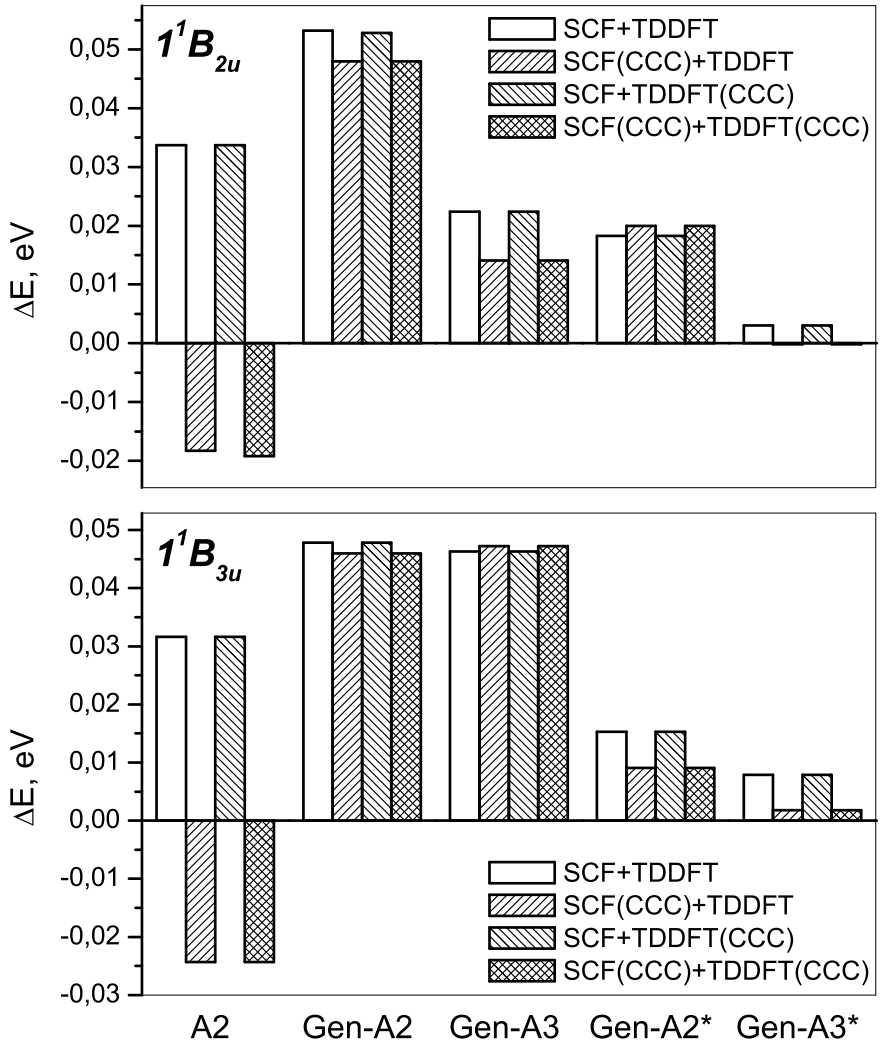

Figure 4.5: Errors in the Na_4 1^1B_{2u} (1.49 eV) and 1^1B_{3u} (1.81 eV) excitations as a function of algorithm and auxiliary basis set.

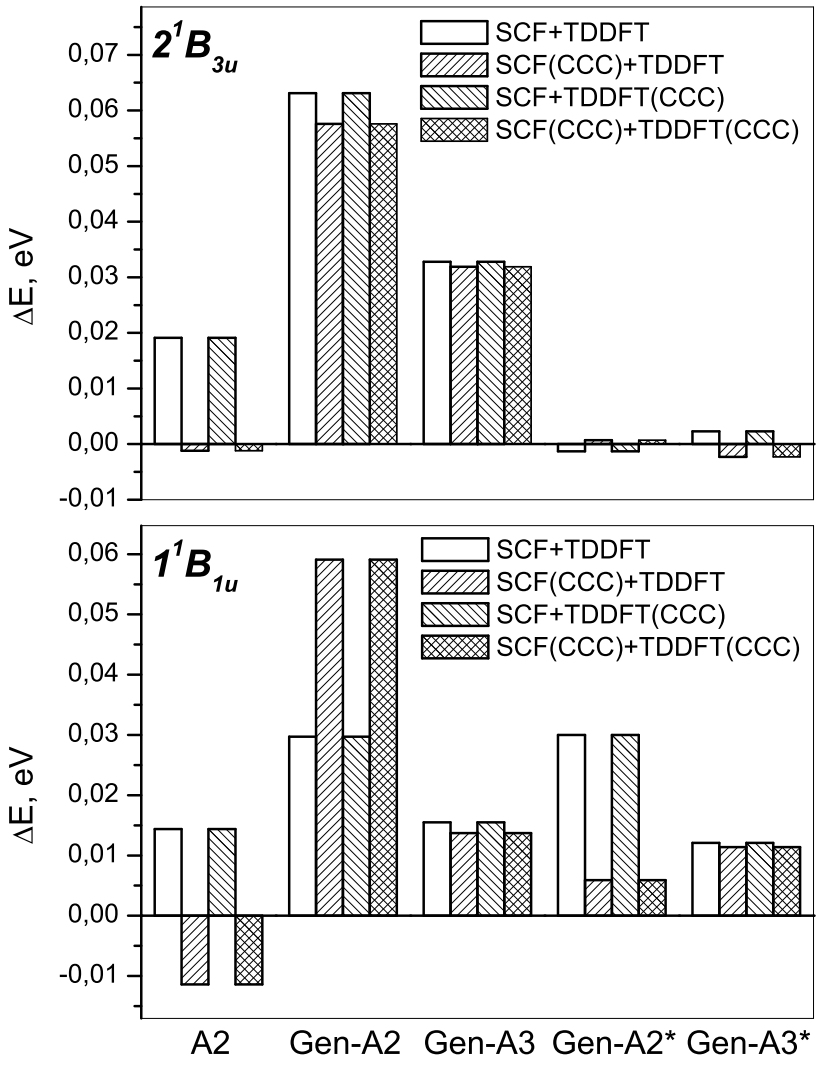

Figure 4.6: Errors in Na_4 2^1B_{3u} (2.03 eV) and 1^1B_{1u} (2.24 eV) excitations as a function of algorithm and auxiliary basis set.

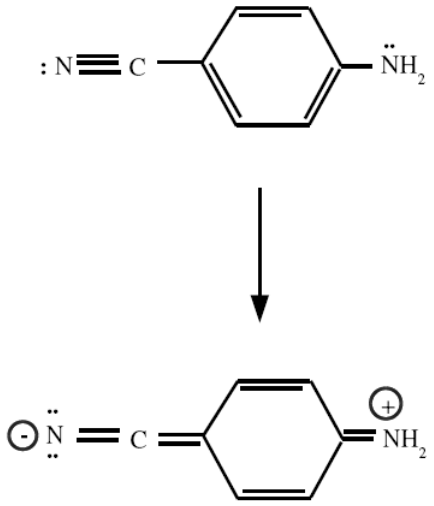

Figure 4.7: Traditional picture of the photoexcited charge transfer state in pABN.

B *Para*-Aminobenzonitrile

pABN is a classic example of a push-pull chromophore which has a strong charge transfer excitation (Fig.4.7). Such chromophores can be attached to polymer backbones and aligned in an electric field to obtain Langmuir-Blodget films with important nonlinear optical properties [66]. In particular, as a first approximation, the second hyperpolarizability is often described in terms of this one excitation,

$$\beta(\omega) \propto \frac{\mu\omega_{CT} f_{CT} \Delta\mu}{(\omega_{CT}^2 - \omega^2)\,(\omega_{CT}^2 - 4\omega^2)}\,, \tag{4.65}$$

where ω_{CT} is the charge transfer excitation energy, f_{CT} is the corresponding oscillator strength, μ is the groundstate dipole moment, and $\Delta\mu$ is the change in the dipole moment upon excitation (e.g., Ref. [66] p. 54). pABN and related molecules also show an interesting double florescence phenomenon which has been studied using TDDFT by Gutierrez [67] and especially by Jamorski and coworkers [52, 53, 54, 55, 56, 57, 58]. Results from previous work are shown in Table 4.5. Our calculated TDLDA spectrum for pABN is given in Fig. 4.8. The first excitation at about 4.15 eV is the so-called local excitation (LE) corresponding to the highest occupied molecular orbital (HOMO) to lowest unoccupied molecular orbital (LUMO) singlet excitation. The charge transfer (CT) excitation is at about 4.7 eV and corresponds

Table 4.5: Previous results for ABN vertical singlet excitations.

Vertical Excitations (eV)	
Method	Excitation Energy (Oscillator Strength)
^1B(LE,HOMO → LUMO)	
Expt.[1]	4.2
CASPT2[2]	4.01 (0.00)
CASPT2[3]	4.09
TD-LDA/6-31G*[3]	∼4.25
TD-LDA[4]	4.21 (0.02)
TD-B3LYP[3]	4.58
TD-B3LYP[4]	4.57 (0.02)
CS-INDO[5]	4.08
^1A(CT,HOMO → LUMO+1)	
Expt.[1]	4.7
CASPT2[2]	4.44 (0.36)
CASPT2[3]	4.45
TD-LDA/6-31G*[3]	∼4.70
TD-LDA[4]	4.61 (0.39)
TD-B3LYP/6-31G*[3]	4.89
TD-B3LYP[4]	5.06 (0.40)
CS-INDO[5]	4.67

[1]As given in Table II of Ref. [52].
[2]L. Serrano-Andres *et al.* [68]. Oscillator strengths are calculated at the CASSCF level.
[3]F. Gutierrez, PhD thesis [67].
[4]Calculations denoted (Sm/Bg) in Table II of Ref. [52].
[5]A. Germain, PhD thesis [69].

to the HOMO → LUMO+1.

Numerical errors in the singlet transition energies for different auxiliary basis sets are shown in Fig. 4.9 for the LE excitation and in Fig. 4.10 for the CT excitation. We have already seen in our sodium cluster calculations that the size of the error in our excitation energies is dominated by whether or not the CCC is used at the SCF step. For this reason only calculations consistantly using or neglecting the CCC at both the SCF and TDDFT steps have been shown. Excitation energy errors are below or about 0.02 eV with use of the GEN-A2* or GEN-A3* auxiliary basis sets.

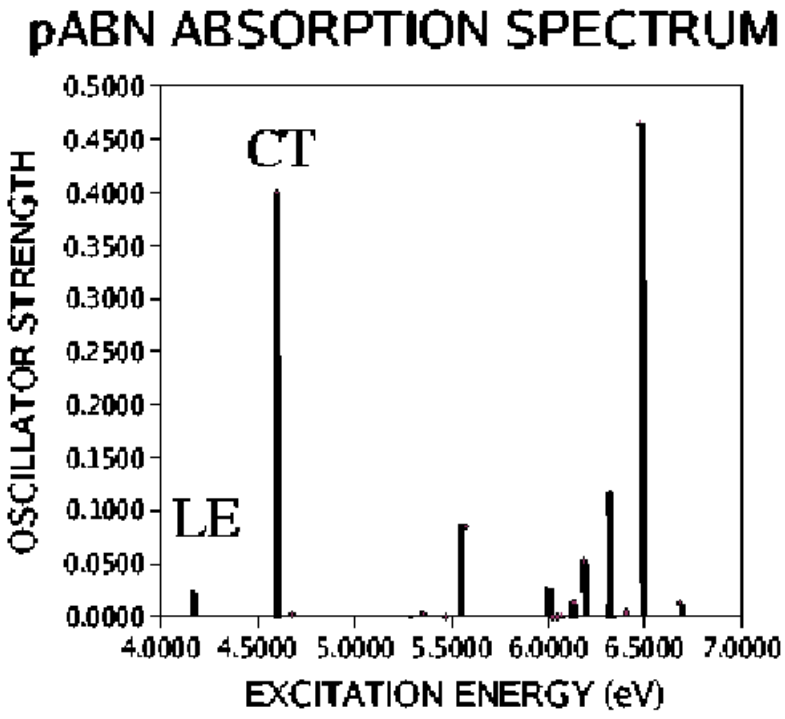

Figure 4.8: pABN TDLDA spectrum calculated using the Sadlej basis set and Fine grid.

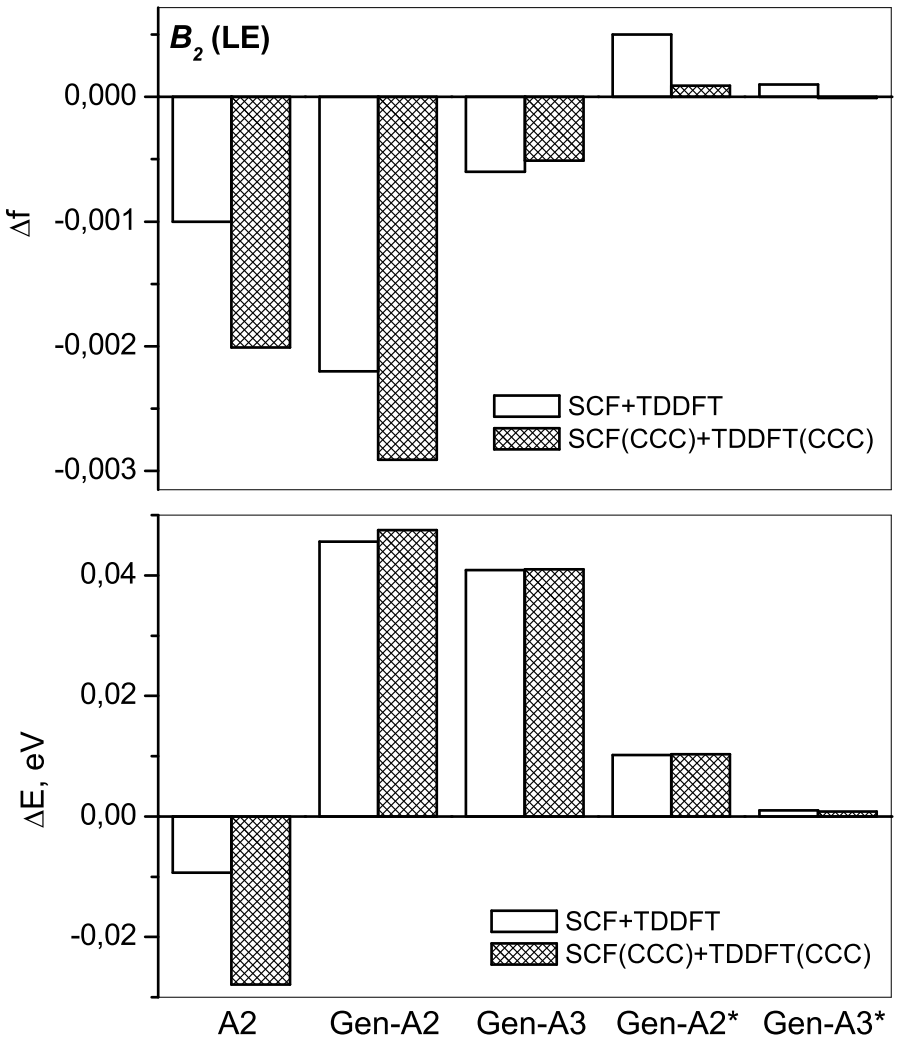

Figure 4.9: Errors in the pABN singlet local excitation (LE) energy (4.12 eV) as a function of algorithm and auxiliary basis set: bottom energy, top oscillator strength.

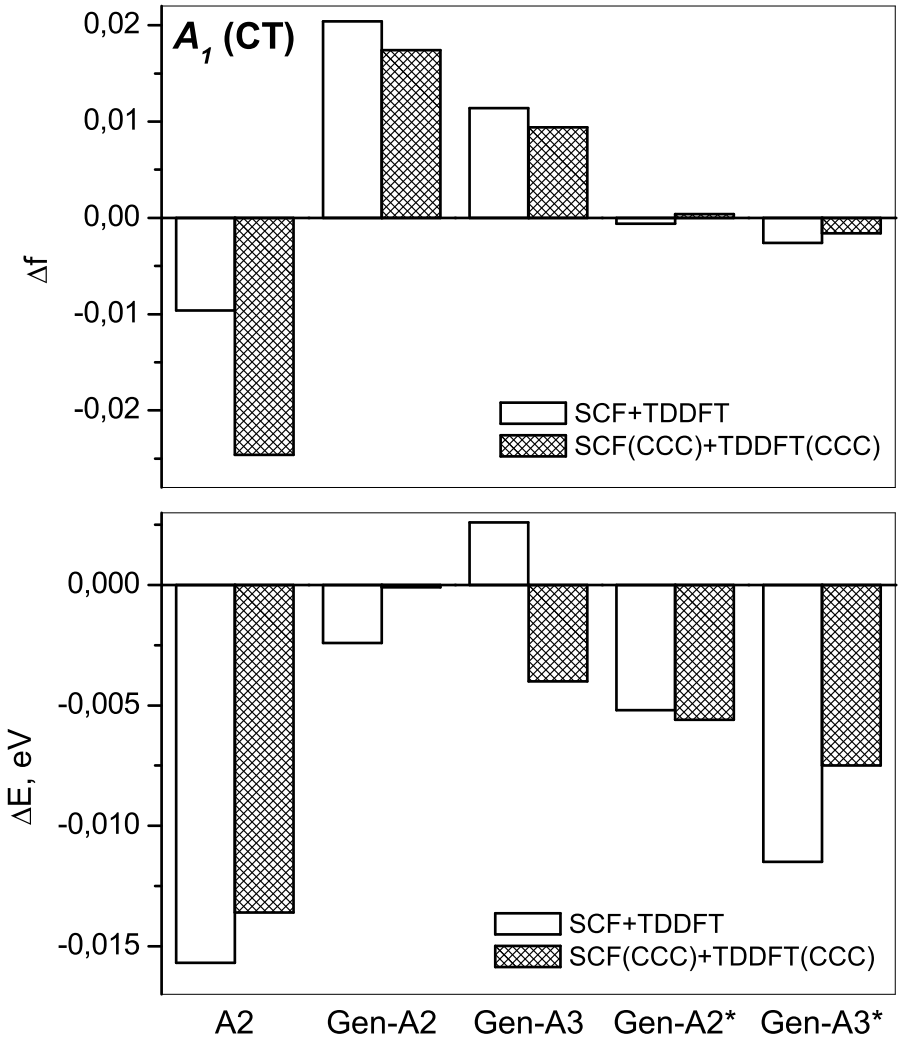

Figure 4.10: Errors in the pABN singlet local excitation (CT) energy (4.60 eV) as a function of algorithm and auxiliary basis set: bottom energy, top oscillator strength.

V Conclusion

Many quantum chemists think of density-functional theory (DFT) as a Hartree-Fock (HF) like theory which includes some electronic correlation through the use of an approximate exchange-correlation functional. If we restrict ourselves to this point of view, we should expect DFT to give better results than HF calculations for a similar amount of computational effort. Indeed, this is what is typically found since many quantum chemistry codes continue to evaluate 4-center integrals. However, pure DFT (as opposed to hybrid methods) is a Hartree-like, rather than a HF-like method, in so far as the self-consistent field is described by a purely multiplicative potential (v_{xc}). That means that a properly implemented DFT should give results comparable to correlated *ab initio* methods, but for *less* effort than a HF calculation. This is made possible in the **deMon2k** program by using auxiliary functions and the charge density fitting (CDF) method to completely eliminate 4-center integrals, replacing them with at most 3-center integrals. In the case of those integrals which have to be evaluated numerically, the VXCTYPE AUXIS option avoids the numerical evaluation of more than 2-center integrals, yielding a substantial reduction of computational effort. In this paper, we have extended the CDF strategy to include TDDFT and report results of our implementation in **deMon2k**.

The equations are general for a constrained CDF. Philosophically, this is similar to the constrained SCF idea of Mukherji and Karplus [23] who reported that calculated properties could be improved if SCF calculations were constrained to give the experimental values of related properties. This is a subtle idea which implicitly assumes that the properties of interest depend on regions of configuration space which have a relatively low energetic weighting and so are unlikely to be completely fixed by a variational minimization.

Only a charge conservation constraint (CCC) was imposed upon our fit density in our calculations. In lines with the ideas of Mukherji and Karplus, the CCC is found to increase by an order of magnitude the precision of the electron number obtained by direct numerical integration of the orbital density. Comparisons between our **deMon2k** TDDFT excitation energies and oscillator strengths, and those obtained from GAUSSIAN without the use of auxiliary basis function methodology, indicates that inclusion of the CCC may or may not have value for TDDFT calculations. What is clear cut is that the CCC affects the SCF part of the calculation more than the TDDFT part of the calculation and that the effect is small. Also clear is that the choice of a good auxiliary basis set is more important than the CCC. In terms of Mukherji and Karplus' idea, the total electron number is probably adequately

determined for subsequent TDDFT calculations by the initial SCF calculation, and so it is not an especially important property to constrain when considering excitation spectra. On the other hand, inclusion of the CCC involves only a small additional computational cost and leads to a fully consistent method which may also be applied to properties which are more sensitive to the the CCC.

Overall, the major advantage of the present method is that it is simultaneously efficient and yet satisfies key properties of the exact TDDFT equations. That is, the coupling matrix is manifestly symmetric, as it should be, and the static limit of TDDFT gives proper analytic derivatives of the appropriate energy expression. This means that we have a schema which allows TDDFT to be fully integrated within the **deMon2k** code without modification of the underlying **deMon2k** numerical approximations and which will allow the method to form an essential building block for the calculation of excited-state analytical derivatives at some point in the future.

Acknowledgments

It is a pleasure to dedicate this paper to Annick Goursot on the occasion of her sixtieth birthday. Annick was one of the first theoretical chemists in France to make broad use of DFT. MEC, CJJ, AV, and AK came to know Annick through her involvement in the development of the **deMon** suite of DFT programs. For this reason, it seems particularly meaningful to us to be able to dedicate a paper to her volume on a methodological subject concerning DFT and, in particular, **deMon**.

This study was carried out in the context of a Franco-Mexican collaboration financed through *ECOS-Nord* Action M02P03. It has also benefited from participation in the French *groupe de recherche en density functional theory* (DFT) and the European working group COST D26/0013/02. Those of us at the Université Joseph Fourier would like to thank Pierre Vatton, Denis Charapoff, Régis Gras, Sébastien Morin, and Marie-Louise Dheu-Andries for technical support of the LÉDSS and *Centre d'Expérimentation pour le Calcul Intensif en Chimie* (CECIC) computers used for the calculations reported here. AF would like to thank the French *Ministère d'Education* for a *Bourse de Mobilité*. CP and AI would like to acknowledge funding from LÉDSS during their postdoctoral work. (An early part of this work was performed by CP as a postdoc before he obtained a permanent position in the LÉDSS.) The LÉDSS funded a 1 month working visit for CJJ in 2002. FC acknowledges support from the Mexican Ministry of Education via a CONACYT (SFERE 2004) scholarship and from the Universidad de las Americas Puebla (UDLAP). We would also like to thank Jean-Pierre Daudey and Fabien Gutierrez for interesting

discussions concerning the spectrocopy of aminobenzonitrile. Roberto Flores is also thanked for many useful discussions.

Bibliography

[1] Term proposed by the late Jan Almlöf.

[2] C. Jamorski, M.E. Casida, and D.R. Salahub, J. Chem. Phys. **104**, 5134 (1996).

[3] M.E. Casida, in *Recent Developments and Applications of Modern Density Functional Theory*, edited by J.M. Seminario (Elsevier, Amsterdam, 1996), p. 391.

[4] S.F. Boys and I. Shavitt, University of Wisconsin, Report WIS-AF-13 (1959).

[5] E.J. Baerends, D.E. Ellis, and P. Ros, Chem. Phys. **2**, 41 (1973).

[6] H. Sambe and R.H. Felton, J. Chem. Phys. **62**, 1122 (1975).

[7] S. Hamel, M.E. Casida, and D.R. Salahub, J. Chem. Phys. **114**, 7342 (2001).

[8] S. Hamel, M.E. Casida, and D.R. Salahub, J. Chem. Phys. **116**, 8276 (2002).

[9] S. Hamel, P. Duffy, M.E. Casida, and D.R. Salahub, J. Electr. Spectr. **123**, 345 (2002).

[10] **Gaussian 03**, Revision C.02, M.J. Frisch, G. W. Trucks, H.B. Schlegel, G.E. Scuseria, M.A. Robb, J. R. Cheeseman, J. A. Montgomery, Jr., T. Vreven, K. N. Kudin, J. C. Burant, J. M. Millam, S. S. Iyengar, J. Tomasi, V. Barone, B. Mennucci, M. Cossi, G. Scalmani, N. Rega, G. A. Petersson, H. Nakatsuji, M. Hada, M. Ehara, K. Toyota, R. Fukuda, J. Hasegawa, M. Ishida, T. Nakajima, Y. Honda, O. Kitao, H. Nakai, M. Klene, X. Li, J. E. Knox, H. P. Hratchian, J. B. Cross, V. Bakken, C. Adamo, J. Jaramillo, R. Gomperts, R. E. Stratmann, O. Yazyev, A. J. Austin, R. Cammi, C. Pomelli, J. W. Ochterski, P. Y. Ayala, K. Morokuma, G. A. Voth, P. Salvador, J. J. Dannenberg, V. G. Zakrzewski, S. Dapprich, A. D. Daniels, M. C. Strain, O. Farkas, D. K. Malick, A. D. Rabuck, K. Raghavachari, J. B. Foresman, J. V. Ortiz, Q. Cui, A. G. Baboul, S. Clifford, J. Cioslowski, B. B. Stefanov, G. Liu, A. Liashenko, P. Piskorz, I. Komaromi, R. L. Martin, D. J. Fox, T. Keith, M. A. Al-Laham, C. Y. Peng, A. Nanayakkara, M. Challacombe, P. M. W. Gill, B. Johnson, W. Chen, M. W. Wong, C. Gonzalez, and J. A. Pople, Gaussian, Inc., Wallingford CT, 2004.

[11] R. Bauernschmitt, M. Häser, O. Treutler, and R. Ahlrichs, Chem. Phys. Lett. **264**, 573 (1997).

[12] J. Andzelm, in *Density Functional Methods in Chemistry*, edited by J. Labanowski and J. Andzelm (Springer: New York, 1991), p. 155.

[13] A. Görling, H.H. Heinze, S.Ph. Ruzankin, M. Staufer, and N. Rösch, J. Chem. Phys. **110**, 2785 (1999).

[14] H.H. Heinze, A. Görling, and N. Rösch, J. Chem. Phys. **113**, 2088 (2000).

[15] R.A. Kendall and H.A. Früchtl, Theor. Chem. Acc. **97**, 158 (1997).

[16] O. Vahtras, J. Almlöf, and M.W. Feyereisen, Chem. Phys. Lett. **312**, 514 (1993).

[17] B.I. Dunlap, J.W.D. Connolly, and J.R. Sabin, J. Chem. Phys. **71**, 3396 (1979).

[18] B.I. Dunlap, J.W.D. Connolly, and J.R. Sabin, J. Chem. Phys. **71**, 4993 (1979).

[19] A.M. Köster, P. Calaminici, Z. Gómez, U. Reveles, in *Reviews of Modern Quantum Chemistry*, edited by K.D. Sen (World Scientific, Singapore, 2002), pg. 1439.

[20] B.I. Dunlap, Phys. Chem. Chem. Phys. **2**, 2113 (2000); B.I. Dunlap, J. Molec. Struct.: THEOCHEM **501-502**, 221 (2000); B.I. Dunlap, *ibid.* **529**, 37 (2000).

[21] E.J. Baerends and P. Ros, Int. J. Quant. Chem. Symp. **12**, 169 (1978).

[22] M.E. Casida, in *Recent Advances in Density Functional Methods, Part I*, edited by D.P. Chong (Singapore, World Scientific, 1995), p. 155.

[23] A.Mukherji and M. Karplus, J. Chem. Phys. **38**, 44 (1963).

[24] P.H. Dederichs, S. Blügel, R. Zeller, and H. Akai, Phys. Rev. Lett. **53**, 2512 (1984).

[25] D. Jayatilaka and D. J. Grimwood, Acta Cryst. **A57**, 76 (2001).

[26] D.J. Grimwood and D. Jayatilaka, Acta Cryst. **A57**, 87 (2001).

[27] I. Bytheway, D. J. Grimwood and D. Jayatilaka, Acta Cryst. **A58** 232 (2002).

[28] I. Bytheway, D. J. Grimwood, B. N. Figgis, G. S. Chandler and D. Jayatilaka, Acta Cryst. **A58** 244 (2002).

[29] D.J. Grimwood, I. Bytheway, and D. Jayatilaka, J. Comput. Chem. **24**, 470 (2003).

[30] A.M. Köster, J.U. Reveles, and J.M. del Campo, J. Chem. Phys. **121**, 3417 (2004).

[31] A. St-Amant and D.R. Salahub, Chem. Phys. Lett **169**, 387 (1990); Alain St-Amant, Ph.D. Thesis, University of Montreal, 1992; M.E. Casida, C. Daul, A. Goursot, A. Köster, L.G.M. Pettersson, E. Proynov, A. St-Amant, and D.R. Salahub principal authors, S. Crétien, H. Duarte, N. Godbout, J. Guan, C. Jamorski, M. Leboeuf, V. Malkin, O. Malkina, M. Nyberg, L. Pedocchi, F. Sim, and A. Vela (contributing authors), computer code **deMon-KS**, version 3.5, deMon Software, 1988.

[32] **deMon-DynaRho** version 3.2, M.E. Casida, C. Jamorski, E. Fadda, J. Guan, S. Hamel, and D.R. Salahub, University of Montreal and Université Joseph-Fourier, copyright 2002.

[33] M.E. Casida, C. Jamorski, F. Bohr, J. Guan, and D.R. Salahub, in *Theoretical and Computational Modeling of NLO and Electronic Materials*, edited by S.P. Karna and A.T. Yeates (ACS Press: Washington, D.C., 1996), (Proceedings of ACS Symposium, Washington, D.C., 1994), p. 145.

[34] Andreas M. Koester, Patrizia Calaminici, Mark E. Casida, Roberto Flores, Gerald Geudtner, Annick Goursot, Thomas Heine, Andrei Ipatov, Florian Janetzko, Serguei Patchkovskii, J. Ulises Reveles, Alberto Vela and Dennis R. Salahub, **deMon2k**, Version 1.8, The deMon Developers (2005).

[35] A.J. Sadlej, Collec. Czech. Chem. Commun. **53**, 1995 (1988); A.J. Sadlej, Theor. Chim. Acta **79**, 123 (1992); A.J. Sadlej, Theor. Chim. Acta **81**, 45 (1992); A.J. Sadlej, Theor. Chim. Acta **81**, 339 (1992).

[36] J. Andzelm, E. Radzio, and D.R. Salahub, J. Comput. Chem. **6**, 520 (1985).

[37] J. Andzelm, N. Russo, and D.R. Salahub, J. Chem. Phys. **87**, 6562 (1987).

[38] A. Herrmann, E. Schumacher, and L. Wöste, J. Chem. Phys. **68**, 2327 (1978).

[39] A. Modelli and G. Distefano, Z. Naturforsch. A **36**, 1344 (1981).

[40] J. Guan, M.E. Casida, A.M. Köster, and D.R. Salahub, Phys. Rev. B **52**, 2184 (1995).

[41] P. Calaminci, K. Jug, and A.M. Köster, J. Chem. Phys. **111**, 4613 (1999).

[42] P. Calaminici, A.M. Köster, A. Vela, and K. Jug, J. Chem. Phys. **113**, 2199 (2000).

[43] L.G. Gerchikov, C. Guet, and A.N. Ipatov, Phys. Rev. A **65**, 13201, (2002).

[44] L.G. Gerchikov, C. Guet, and A.N. Ipatov, Phys. Rev. A **66**, 53202, (2003).

[45] L.G. Gerchikov and A.N.Ipatov, J. Phys. B **36**, 1193 (2003).

[46] A.N. Ipatov, P.-G. Reinhard, and E. Suraud, Int. J. Mol. Sci. **4**, 300 (2003).

[47] A.N.Ipatov, P.-G. Reinhard, and E. Suraud, Eur. Phys. J. D **30**, 65 (2004).

[48] B. Gervais, E. Giglio, E. Jacquet, A. Ipatov, P.-G. Reinhard, F. Fehrer, E. Suraud, Phys. Rev. A **71**, 015201 (2005).

[49] B. Gervais, E. Giglio, E. Jacquet, A. Ipatov, P.-G. Reinhard, and E. Suraud, J.Chem.Phys. **121**, 8466 (2004).

[50] A. Ipatov, L. Gerchikov, and C. Guet, J.Comp.Mat.Sci., *in press.*

[51] L.G. Gerchikov, C. Guet, and A.N. Ipatov, Israel Journal of Chemistry **44**, 205 (2004).

[52] C. Jamorski, J.B. Foresman, C. Thilgen, and H.-P. Lüthi, J. Chem. Phys. **116**, 8761 (2002).

[53] C. Jamorski Jödicke and H.P. Lüthi, J. Chem. Phys. **117**, 4146 (2002).

[54] C. Jamorski Jödicke and H.P. Lüthi, J. Chem. Phys. **117**, 4157 (2002).

[55] C. Jödicke Jamorski and H.-P. Lüthi, J. Chem. Phys. **119**, 12852 (2003).

[56] C. Jamorski Jödicke and H.-P. Lüthi, J. Am. Chem. Soc. **125**, 252 (2003).

[57] C. Jamorski Jödicke and H.-P. Lüthi, Chem. Phys. Lett. **368**, 561 (2003).

[58] C. Jödicke Jamorski and M.E. Casida, J. Phys. Chem. B **108**, 7132 (2004).

[59] W.A. de Heer, Rev. Mod. Phys. **65**, 611 (1993).

[60] U. Kaldor, Israel J. Chem. **31**, 345 (1991).

[61] M. Gross and F. Spiegelmann, J. Chem. Phys. **108**, 4148 (1998).

[62] A. Henriet and F. Masnou-Seeuws, J. Phys. B **20**, 671 (1987).

[63] D.W. Davies and G.J.R. Jones, Chem. Phys. Lett. **81**, 279 (1981).

[64] C.R.C. Wang, S. Pollack, D. Cameron, and M. Kappes, J. Chem. Phys. **93**, 3789 (1990).

[65] V. Bonačić-Koutecký, P. Fantucci, and J. Koutecký, J. Chem. Phys. **96**, 7938 (1990).

[66] P.P. Prasad and D.J. Williams, *Introduction to Nonlinear Optical Effects in Molecules and Polymers* (John Wiley and Sons: New York, 1991).

[67] F. Gutierrez, PhD Thesis, Université Paul Sabatier, Toulouse, France, 2002.

[68] L. Serrano-Andres, M. Merchán, B.O. Roos, and R. Lindh, J. Am. Chem. Soc. **117**, 3189 (1995).

[69] A. Germain, PhD Thesis, Univeristé de Paris Sud, Orsay, France, 1996.

Chapter 5

TDDFT for Open-Shell Molecules

It is well-known that TDDFT in its linear formulation was initially introduced to the quantum chemistry community for calculating the excitation spectra of molecules with closed-shell ground states. However Casida's formulation of LR-TDDFT allowed both different-orbitals-for-different-spin (DODS) and fractional occupations numbers, thus opening the way to applying the method to molecules with open-shell ground states. Some common quantum chemistry programs allow DODS LR-TDDFT calculations of excitation energies.

This is offered (perhaps inadvertently) in the spirit of caveat emptor (at the user's own risk) because these calculations can produce unphysical of on-going research. This chapter contains two contributions towards understanding the problem of TDDFT calculations on molecules with open-shell ground states.

The first contribution has appeared as

> M.E. Casida, A. Ipatov, and F. Cordova, in *Time-Dependent Density-Functional Theory*, edited by M.A.L. Marques, C. Ullrich, F. Nogueira, A. Rubio, and E.K.U. Gross, *Lecture Notes in Physics* (Springer: Berlin, 2006), pp. 243-257.
> "Linear-Response Time-Dependent Density-Functional Theory for Open-Shell Molecules"

This article shows how unphysical artifacts can arise in two different ways. The first is due to the absence of explicit two– and higher– excitations in LR-TDDFT when the TDDFT adiabatic approximations is used. This results in incorrect spin couplings, hence spin contamination. The second source of unphysical artifacts is due to the use of approximate exchange-correlation functionals which allow closed-shell ground states to lower their energies by adopting broken symmetry DODS configurations. This is especially typical of biradical species and results in imaginary triplet excitation energies, known as triplet instabilities. This review articles is largely based upon the 2^{nd} contribution in this chapter and of Chapter 6.

The second contribution is the article

> A. Ipatov, F. Cordova, and M.E. Casida, *in preparation.*
> "Excited-State Spin-Contamination in Time-Dependent Density-Functional Theory for Molecules with Open-Shell Ground States".

Formulas are presented for calculating spin-contamination (i.e., the expectation value of $\langle \hat{S}^2 \rangle$) in DODS LR-TDDFT excited states and the formulas are validated by appliaction to small open-shell species. The results show the method to be useful. Terms beyond the Tamm-Dancoff approximation (TDA) are small, but only given in a certain approximation (neglecting density-matrix relaxation). The formula for DODS LR-TDDFT spin contamination was developed by M. E. Casida and programmed in deMon2k by A. Ipatov. Validation required careful comparison by M. E. Casida of Ipatov's deMon2k results and Cordova's Gaussian results.

5-1 *Linear-Response Time-Dependent Density-Functional Theory for Open-Shell Molecules*

Linear-Response Time-Dependent Density Functional Theory for Open-Shell Molecules

Mark E. Casida[1], Andrei Ipatov and Felipe Cordova,
Équipe de Chimie Théorique,
Laboratoire d'Etudes Dynamiques et Structurales de la Sélectivité (LEDSS), UMR CNRS/UJF 5616,
Institut de Chimie Moléculaire de Grenoble (ICMG, FR-2607),
Université Joseph Fourier (Grenoble I),
301 rue de la Chimie, BP 53,
F-38041 Grenoble Cedex 9, FRANCE

[1]M.E. Casida et al.: Linear-Response Time-Dependent Density Functional Theory for Open-Shell Molecules, Lect. Notes Phys. 706, 243-257 (2006)

I Introduction

While typical stable organic and many stable inorganic molecules have closed shell ground states, interesting chemistry and molecular physics is by no means limited to these species. For example, O_2 is a common molecule with a triplet ground state and whose spectroscopic importance is dramatically illustrated by its role in the photochemical explanation of the aurora borealis, and the ultraviolet spectra of the high spin d^6 complex that ferrous cation forms in water, $[Fe(H_2O)_6]^{2+}$, is a source of information for fixing ligand field parameters. Excited states of molecules with open-shell ground states also appear as higher energy peaks in photoelectron (ionization) spectra. Moreover nearly all of photochemistry involves some nuclear configurations which may be qualified as having open-shell ground states. It is small wonder that Casida's equations [Casida 1995a] began to be applied to calculate the spectra of open-shell molecules just five years after their introduction [Spielfiedel 1999, Hirata 1999a, Hirata 1999c, Adamo 1999, Guan 2000, Radziszewski 2000, Anduniow 2000]. While it is safe to say that the initial developpers [Casida 1995a, Petersilka 1996a, Jamorski 1996, Bauernschmitt 1996a] of linear-response time-dependent density-functional theory (LR-TDDFT) for the calculation of excitation spectra were thinking about applications to molecules with closed-shell ground states having the same orbitals for different spin (SODS), the original formulation of Casida's equations foresaw their eventual application to molecules with an open-shell ground state by allowing both for different orbitals for different spin (DODS) and for fractional occupation number [Casida 1995a]. Application of the DODS formulation of Casida's equations has led to spectacularly good agreement with experimental spectra in some cases and significant errors in interpretation of calculated results in other cases. This chapter tries to point out where DODS LR-TDDFT is a reasonable approach to the excited states of open-shell molecules and where it is likely to fail. In the cases where it is likely to fail, we give an indication of how the theory may be fixed. Some of the results reported here come from our own unpublished work [Cordova 2006, Ipatov 2006]. Although we do not have the space here to go into the details normally expected for new work, we trust that fuller accounts will eventually be published elsewhere.

To our knowledge, the first application of Casida's equations to an open shell molecule was that of Spielfiedel and Handy who used CADPAC to investigate the excited states of PO [Spielfiedel 1999]. At about the same time, both the SODS and DODS version of Casida's equations were programmed in the very popular Gaussian quantum chemistry program [Stratmann 1998]. Users soon began to calculate

the spectra of open-shell molecules, though there was still almost no prior experience regarding even the correct interpretation of output in this case. It is to Hirata and Head-Gordon that credit should go for the first systematic study of Casida's equations for open-shell molecules [Hirata 1999a, Hirata 1999c]. This group, who was seeking an efficient but still relatively simple configuration-interaction singles (CIS)-like method for calculating excitation energies, used the QChem program to investigate the use of TDDFT for the calculation of the excitation energies of radicals. As Fig. (5.1) shows for two excitation energies of the cyanide radical, DODS CIS (UCIS in the figure) and CIS beginning with a SODS spin-restricted open-shell Hartree-Fock wave function (ROCIS in the figure) show large errors. Inclusion of "extended singles," which are double excitations obtained from single excitations by spin transpositions, helps remarkably (XCIS in the figure). Still, it is the simple TDLDA which is giving the most impressive results for a computational cost similar to the relatively simple CIS. Guan et al. went further and investigated entire spectra for small molecules with open-shell ground states [Guan 2000]. Such spectra are, as a general rule, much more complex than corresponding spectra for closed-shell molecules, showing a plethora of satellite peaks due to oscillator strength fragmentation. The results of that study confirmed that some excitations are remarkably well described. Other early applications of Casida's equations to molecules with open-shell ground states include [Radziszewski 2000, Anduniow 2000, Broclawik 2001, Andreu 200l, Weisman 200lb, Pou-Amérigo 2002, Rinkevicius 2003]. The remainder

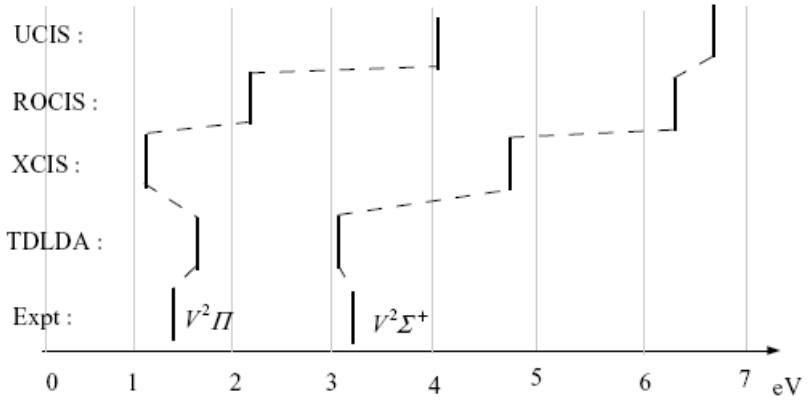

Figure 5.1: Comparison of CN radical excitation energies calculated with different simple theories. Numerical values taken from Table 1 of [Hirata 1999a].

of this chapter is organized as follows. Before discussing the excited-states of open-shell molecules, we first consider the performance of DFT for the ground state of open-shell molecules. Perhaps surprisingly one way to judge the quality of a SODS

description of the Kohn-Sham ground state is to examine the first excited triplet state from Casida's equations. This also provides a good place to introduce the idea of spin contamination and symmetry-broken DODS calculations. This is followed by a section on TDDFT excitation spectra for open-shell molecules in which it is pointed out that some excited states are simpler than others and that the difficulty that TDDFT has in describing all the excited states of molecules with open-shell ground states is closely related to a failure of the adiabatic approximation. As it turns out, one way to detect and guard against the problem is to calculate spin contamination in the excited states. In the penultimate section, ways to go beyond the adiabatic approximation are very briefly discussed. The final section sums up.

II Open-Shell Ground States

One of the first difficulties one runs into in discussing open-shell molecules is one of definition. While it may seem evident that an open-shell molecule is any molecule which is not closed-shell and that "closed-shell" means that the molecular wave function belongs to the completely symmetric representation of the appropriate symmetry group, the breaking of a bond typically yields a biradical whose wave function belongs to the completely symmetric representation. Nevertheless it has the chemical physics of two open-shell species! We begin first by discussing the problem of biradicals with a singlet ground state and then take a look at molecules with a non-singlet ground state. One way to generate a biradical ground state is molecular dissociation, the bond breaking of H_2 (H_A-H_B) being the classic textbook case. Our discussion is based upon that of [Casida 2000b]. At the equilibrium geometry the Kohn-Sham wave function has the form of a single determinant, $|\sigma_\uparrow\sigma_\downarrow|$. At large internuclear distance, this wave function takes the form of a linear combination of ionic and covalent parts,

$$\begin{aligned} |\sigma_\uparrow\sigma_\downarrow| &= |\frac{1}{\sqrt{2}}(s_{A\uparrow}+s_{B\uparrow}),\frac{1}{\sqrt{2}}(s_{A\downarrow}+s_{B\downarrow})| \\ &= \frac{1}{2}\underbrace{(|s_{A\uparrow}s_{A\downarrow}|+|s_{B\uparrow}s_{B\downarrow}|)}_{\left[\mathrm{H}:^-_A+\mathrm{H}^+_B\leftrightarrow\mathrm{H}^+_A+\mathrm{H}:^-_B\right]}+\frac{1}{2}\underbrace{(|s_{A\uparrow}s_{B\downarrow}|+|s_{B\uparrow}s_{A\downarrow}|)}_{[\mathrm{H}_A\uparrow+\mathrm{H}_B\downarrow\leftrightarrow\mathrm{H}_A\downarrow+\mathrm{H}_B\uparrow]}\ . \end{aligned} \tag{5.1}$$

As H_2 dissociates into neutral H atoms the covalent part should dominate asymptotically, otherwise the energy is too high. This can be simulated by a DODS wave function since it can break symmetry and become $|s_{B\uparrow}s_{A\downarrow}|$. The point where the

DODS wave function becomes lower in energy than the SODS wave function is often referred to as the Coulson-Fischer point. Were the exact exchange-correlation functional used in Kohn-Sham theory, the wave function should remain SODS for every bond distance. In practice the exchange-correlation functional is approximate and symmetry breaking does occur.

The Coulson-Fischer point is an example of a triplet instability. Stability conditions for DFT have been presented by Bauernschmitt and Ahlrichs [Bauernschmitt 1996b] but no explicit link was made with TDDFT excitation energies. That link was later put into print by Casida et al. [Casida 2000b]. Our goal here is not to give a complete analysis of the general case but rather to give a simple analysis showing the relation between symmetry breaking in the ground state and imaginary triplet excitation energies for the particular case of the Coulson-Fischer point. To this end, consider the single determinant Kohn-Sham wave function, $|\sqrt{1-\lambda^2}\sigma_\uparrow + \lambda\sigma_\uparrow^*, \sqrt{1-\lambda^2}\sigma_\downarrow - \lambda\sigma_\downarrow^*|$ where λ is a symmetry-breaking parameter. Expanding the energy expression in λ gives, in the notation of [Casida 2000b],

$$E_\lambda = E_0 + 2\lambda^2 \left[\Delta\epsilon + 2\left(K_{\uparrow,\uparrow} - K_{\uparrow,\downarrow}\right)\right] + \mathcal{O}(\lambda^3) \; . \tag{5.2}$$

This DODS energy becomes lower than the SODS energy when the coefficient of λ^2 becomes negative. Since the triplet excitation energy is,

$$\omega_T = \sqrt{\Delta\epsilon\left[\Delta\epsilon + 2\left(K_{\uparrow,\uparrow} - K_{\uparrow,\downarrow}\right)\right]} \; , \tag{5.3}$$

this is exactly the point where the TDDFT triplet excitation energy becomes imaginary, hence nonphysical. Explicit calculations on H_2 [Casida 2000b] confirm that the TDDFT triplet excitation energy becomes grossly underestimated at bond distances shorter than the Coulson-Fischer point and that the degradation of the quality of the excitation energy also shows up in singlet excitation energies. Although an elegant solution in some ways, symmetry breaking is also a problem in other ways. The Coulson-Fischer point is known to occur at larger intermolecular distance in DFT than in Hartree-Fock calculations, and must disappear entirely (i.e., move to infinity) in the limit that the exchange-correlation functional becomes exact. Nevertheless, *the occurace of imaginary excitation energies at some molecular configurations is unphysical and may be considered to be one danger of open-shell* TDDFT. The ring opening of oxirane (Fig. 5.2) provides a concrete example of how this analysis applies to something less trivial than H_2. The ground and triplet excited states are shown in

Fig. 5.3 for conrotatory and disrotatory ring opening [Cordova 2006]. As expected from the famous Woodward-Hoffmann rules, the conrotatory reaction is favored over the disrotatory reaction. More interesting for present purposes are the ridges which correspond to regions of configuration space where the ground state surface approaches an excited state potential energy surface. By convention, a triplet state

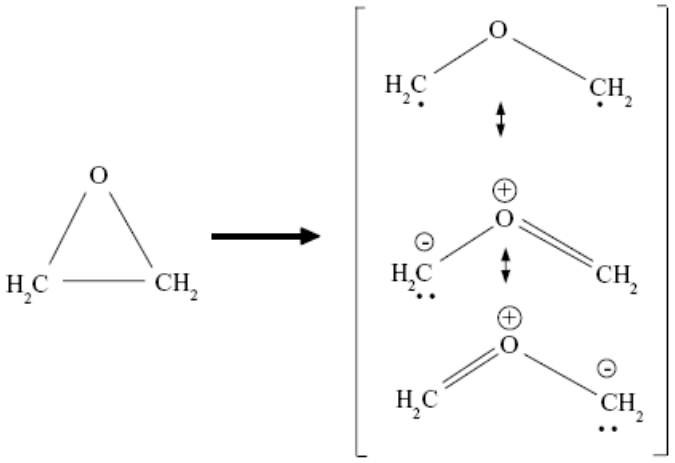

Figure 5.2: Lewis structures for the CC ring opening of oxirane. If the two methyl groups rotate in the same direction during the ring opening, preserving C_2 symmetry, then the ring opening is said to be conrotatory. If the two methyl groups rotate in the opposite direction during the ring opening, preserving C_s symmetry, then the ring opening is said to be disrotatory

lying below the ground state ("negative" excitation energy) indicates that the triplet excitation has become imaginary. Imaginary triplet excitation energies are occurring around the ridges. Quantum chemists normally describe these regions with a two-determinant wave function where one determinant corresponds to the reactant and the other to the product. Interestingly enough, while the TDLDA surfaces show triplet instabilities over 51 % of the configurational space studies, this percentage increases to 93 % when the LDA functional is replaced by the B3LYP functional, confirming that Hartree-Fock exchange increases the "symmetry-breaking problem." To be fair however this may be less of a problem and more of a reflection that the LDA tends to overly favor electron pairing (ionic structures in Fig. 5.2). Typical DFT procedures which do not involve symmetry breaking are multiplet sum theory [Ziegler 1977, Daul 1994] and multiconfigurational DFT. Both also provide limited access to excited states. Spin-flip noncollinear density functional theory is also another promising option for avoiding symmetry breaking by de-exciting to the singlet ground state from a suitable triplet excited state [Wang 2004]. The Tamm-Dancoff approximation (TDA) [Hirata 1999b] decouples the ground state stability problem

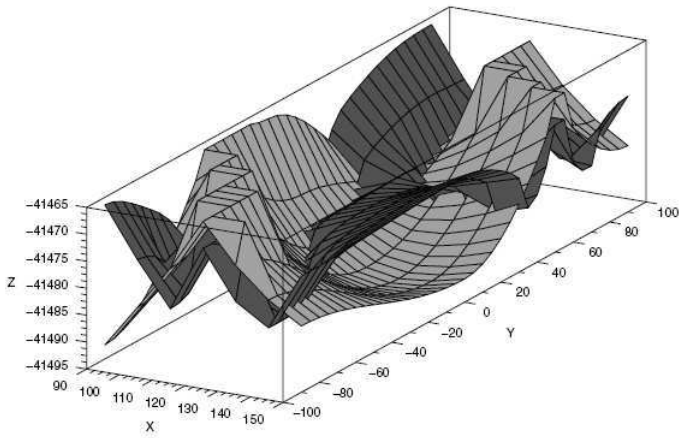

Figure 5.3: Ground (LDA, *light grey*) and triplet (TDLDA, *dark grey*) excited state potential energy surfaces for the conrotatory and disrotatory C-C ring opening of oxirane (CH_2-O-CH_2): X, C-O-C angle in degrees; Y, CH_2 twist angle in degrees (positive if conrotatory, negative if disrotatory); Z, total energy in units of 10 eV. (X,Y)=(90,± 90) corresponds to the closed ring while (X,Y)=(150,0) corresponds to the open ring

from the excited-state problem giving qualitatively correct results [Casida 2000b]. The TDA for LR-TDDFT may be understood as an approximation to Casida's equation written as,

$$\begin{bmatrix} \mathbf{A} & \mathbf{B} \\ \mathbf{B} & \mathbf{A} \end{bmatrix} \begin{pmatrix} X \\ Y \end{pmatrix} = \omega \begin{bmatrix} \mathbf{1} & \mathbf{0} \\ \mathbf{0} & \mathbf{-1} \end{bmatrix} \begin{pmatrix} X \\ Y \end{pmatrix} \tag{5.4}$$

Casida's equation is coupled to the DFT ground state stability problem because the stability of the Kohn-Sham wave function with respect to symmetry-breaking can be tested by considering an arbitrary unitary transformation of orbitals,

$$\varphi_r^{\lambda}(\boldsymbol{r}) = \mathrm{e}^{\mathrm{i}\lambda\left(\hat{R}+i\hat{I}\right)}\varphi_r(\boldsymbol{r}) \ , \tag{5.5}$$

where $\hat{R}$ and $\hat{I}$ are real operators [Casida 2002]. After a fair amount of algebra, one arrives at the energy expression,

$$E_\lambda = E_0 + \lambda^2 \left[\boldsymbol{R}^\dagger \left(\boldsymbol{A}-\boldsymbol{B}\right)\boldsymbol{R} + \boldsymbol{I}^\dagger \left(\boldsymbol{A}+\boldsymbol{B}\right)\boldsymbol{I}\right] + \mathcal{O}(\lambda^3) \ , \tag{5.6}$$

where matrix elements of the $\hat{R}$ and $\hat{I}$ operators have been arranged in column vectors and the $\mathcal{O}(\lambda)$ term disappears because the energy has already been minimized

before considering symmetry-breaking. The presence of the terms (A ± B) shows the connection with Casida's equation. In fact, Casida's equation can be rewritten as the eigenvalue equation,

$$(\boldsymbol{A}+\boldsymbol{B})\,(\boldsymbol{A}-\boldsymbol{B})\,\boldsymbol{Z}_I = \omega_I^2 \boldsymbol{Z}_I \ . \tag{5.7}$$

For pure DFT, assuming that the *aufbau* principle is obeyed, the matrix (**A** - **B**) is always positive definite. However (**A** + **B**) may have negative eigenvalues. In that case, the energy E_λ will fall below E_0 for some value of I. At the same time, this will correspond to a negative value of ω_I^2 I (i.e., an imaginary value of ω_I.) This curious mathematical relationship is exactly the famous triplet instability. The TDA consists of setting $\mathbf{B} = \mathbf{0}$. Not only does this decouple the LR-TDDFT excitation energy problem (which no longer involves **B**) from the ground state stability problem (which still involves **B**), but the resulting TDA equation,

$$\mathbf{AX} = \omega\mathbf{X} \tag{5.8}$$

is the exact TDDFT analogue of the configuration interaction singles (CIS) method (it is the CIS method if we accept that Hartree-Fock is a particular case of a hybrid density functional!) Since the CIS method is also a variational method, it is free of the "variational collapse" observed in time-dependent Hartree-Fock when the square of the excitation energy goes first to zero and then becomes imaginary. This is exactly why the Tamm-Dancoff "approximation" to Casida's equation is expected to behave *better* than Casida's equation for calculating excitation energies away from the ground state equilibrium geometry.

Let us now put biradicals aside and focus on open-shell molecules in the sense of spin symmetry. A general many-electron spin eigenfunction must be a simultaneous eigenfunction of the operators,

$$\begin{aligned} \hat{S}_z &= \tfrac{1}{2}(\hat{n}_\uparrow - \hat{n}_\downarrow) \\ \hat{S}^2 &= \sum \hat{\mathcal{P}}_{\uparrow,\downarrow} + \hat{n}_\uparrow + \hat{S}_z(\hat{S}_z - \hat{1}), \end{aligned} \tag{5.9}$$

where the spin number operators may be expressed in second-quantized notation as,

$$\hat{n}_\sigma = \sum r_\sigma^\dagger r_\sigma, \tag{5.10}$$

and,

$$\sum \hat{\mathcal{P}}_{\uparrow,\downarrow} = \sum r_{\downarrow}^{\dagger} s_{\uparrow}^{\dagger} s_{\downarrow} r_{\uparrow} \ , \tag{5.11}$$

is the spin-transposition operator. All SODS single determinantal wave functions are eigenfunctions of $\hat{S}_z$ but only closed-shell and half-closed-shell determinants are eigenfunctions of $\hat{S}^2$. However DODS determinants often become linear combinations of determinants when expressed in terms of SODS. This means that DODS wave functions may be or nearly may be simultaneous eigenfunctions of $\hat{S}_z$ and $\hat{S}^2$. Since most applications of DFT to open-shell systems are of the spin-unrestricted (DODS) type, it is important to be able to calculate the degree of spin-contamination in the DODS determinant. This is most easily done by realizing that spin-unrestricted calculations generate two molecular orbital basis sets - one for up spin and one for down spin. Denoting the latter by an overbar, the spin-transposition operator becomes,

$$\sum \hat{\mathcal{P}}_{\uparrow,\downarrow} = \sum \bar{p}_{\downarrow}^{\dagger} s_{\uparrow}^{\dagger} \bar{q}_{\downarrow} r_{\uparrow} \langle s|\bar{q}\rangle \langle \bar{p}|r\rangle \ . \tag{5.12}$$

Table 5.1: Spin-contamination in LDA calculations of some small molecules.

	$\hat{S}^2$	Multiplicity (2S + 1)
BeH	0.7503	2.0003
CN	0.7546	2.0046
CO^+	0.7620	2.0120
N_2^+	0.7514	2.0014
CH_2O^+	0.7512	2.0012

From this it is easy to deduce that, for the ground state, the spin contamination for a DODS determinant is,

$$\langle \hat{S}^2 \rangle = \left(\frac{n_{\uparrow} - n_{\downarrow}}{2} \right)^2 + \frac{n_{\uparrow} + n_{\downarrow}}{2} - \sum_{i,\bar{j}}^{\text{occ}} |\langle i|\bar{j}\rangle|^2 \ . \tag{5.13}$$

Table 5.1 shows some typical values of the ground state-spin contamination in spin-unrestricted LDA calculations for some small radicals. In this case, the spin contamination is small. Note that, strictly speaking, this gives the $\langle \hat{S}^2 \rangle$ value of the fictious Kohn-Sham system of noninteracting electrons and not necessarily that of

the physical system. It is however the best we have for practical purposes and few people, if any, would doubt its diagnostic value.

III Open-Shell Excitation Spectra from TDDFT

We want to understand why LR-TDDFT may fail for the excited states of open-shell molecules. To do so, we begin with a simple three orbital model and solve the spin problem assuming SODS. This provides some guide lines for when open-shell excitation energies should be trusted. Then we return to the DODS problem and show that spin-contamination may be used as a guide to which TDDFT excited states are nonsense.

Figure 5.4 shows which excitations are needed for a minimal description of our three orbital model. A spin-adapted basis set for this model consists of four doublet functions,

$$\begin{aligned} |D_1\rangle &= |i_\uparrow i_\downarrow a_\uparrow\rangle \\ |D_2\rangle &= |i_\uparrow v_\downarrow v_\uparrow\rangle \\ |D_3\rangle &= \tfrac{1}{\sqrt{2}}(|i_\downarrow v \uparrow a \uparrow - |i_\uparrow v_\uparrow a_\downarrow\rangle) \\ |D_4\rangle &= \tfrac{1}{\sqrt{6}}(|i_\downarrow v_\uparrow a_\uparrow + |i_\uparrow v \uparrow a \downarrow\rangle - 2|i_\uparrow v_\downarrow a_\uparrow\rangle) \end{aligned} \tag{5.14}$$

and one quartet,

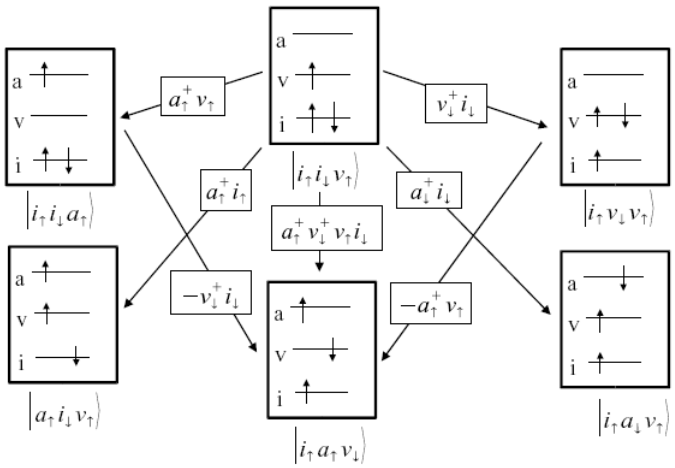

Figure 5.4: Possible M_S-conserving excitations in a SODS 3-orbital model of a radical

$$|Q\rangle = \frac{1}{\sqrt{3}}(|i_\downarrow v_\uparrow a_\uparrow\rangle + |i_\uparrow v_\uparrow a_\downarrow\rangle + |i_\uparrow v_\downarrow a_\uparrow\rangle). \tag{5.15}$$

Note the inclusion of the double (i.e., two-electron excited determinant) $|i_\uparrow v_\downarrow a_\uparrow$. Such a state has been called an "extended singles" since it differs from a true single (i.e., one-electron excited determinant) only by a permutation of spins among the spatial orbitals. Nevertheless it is a double and not a single and must be there. It is excluded from single excitation methods such as CIS and linear response time-dependent Hartree-Fock. Inspection of Casida's equations [Casida 1995a] shows that explicit double and higher excitations are also excluded from adiabatic LR-TDDFT. That is: Casida's equations are formulated within a finite basis set representation where counting arguments apply. When the adiabatic approximation is made, the number of solutions is exactly equal to the number of single excitations. *This is the second danger of open-shell TDDFT.* Of course adiabatic LR-TDDFT still includes electron correlation effects which Hartree-Fock-based methods describe using multiply-excited determinants. Thus Hartree-Fock-based methods may indicate that an excitation which is well-described by adiabatic LR-TDDFT has substantial double-excitation character even though this double-excitation character is not evident from the TDDFT calculation.

What adiabatic LR-TDDFT actually does is to treat excited states as either singlet-coupled excitations or triplet-coupled excitations. Returning to the three orbital model, one sees that this excludes the D_4 doublet function altogether and produces a triplet coupled excitation,

$$|TC\rangle = \frac{1}{\sqrt{2}}(|i_\downarrow v_\uparrow a_\uparrow\rangle + |i_\uparrow v_\uparrow a_\downarrow\rangle), \tag{5.16}$$

which is neither a doublet nor a quadruplet. The reduction of the dimensionality of the doublet solution space means that LR-TDDFT finds fewer peaks in the absorption spectrum than would otherwise be the case. From a physical point of view, LR-TDDFT is best adapted for describing excitations from one half-closed shell configuration to another half-closed shell configuration ($v_\uparrow \longrightarrow a_\uparrow$ and $i_\downarrow \longrightarrow v_\downarrow$) and for describing a singlet-coupled excitation which leaves untouched the open-shell orbitals of the ground state ($i \longrightarrow a$). Both types of excitations preserve spin quantum numbers. The fact that the triplet-coupled solution is neither a doublet nor a quadruplet shows that Casida's equations contain unphysical solutions when,

$$\Delta\langle\hat{S}^2\rangle_I = \langle\Phi_I|\hat{S}^2|\Phi_I\rangle - \langle\Phi_0|\hat{S}^2|\Phi_0\rangle, \tag{5.17}$$

is nonzero. An exception is the case of a molecule with a closed-shell ground state, in which case the triplet-coupled excitations are true triplets.

In practice, DFT calculations for open-shell molecules are of the DODS type. This

makes it difficult to select which LR-TDDFT excitations on the basis of physical arguments alone. However we can still try to eliminate unphysical states on the basis of spin contamination. In particular,

$$\Delta\langle\hat{S}^2\rangle_I = \sum \Delta\Gamma^I_{r_\uparrow\overline{q}_\downarrow,\overline{p}_\downarrow s_\uparrow}\langle s|\overline{q}\rangle\langle\overline{p}|r\rangle, \tag{5.18}$$

where,

$$\Gamma_{rq,ps} = \langle p^\dagger s^\dagger q r\rangle, \tag{5.19}$$

is the two-electron reduced density matrix (2-RDM) and $\Delta\Gamma^I$ is the difference between the 2-RDM for the Ith excited state and the 2-RDM for the ground state. We have derived the appropriate expression for linear response time-dependent Hartree-Fock theory using the unrelaxed 2-RDM obtained by taking the derivative,

$$\Delta\Gamma^I_{rq,ps} = \frac{\partial\omega_I}{\partial[pr|qs]/2}. \tag{5.20}$$

The result is,

$$\begin{aligned}
\Delta\langle\hat{S}^2\rangle_I &= \langle\hat{S}^2\rangle_I - \langle\hat{S}^2\rangle_0 \\
&= \sum X^{I*}_{\bar{a}\bar{j}\downarrow}X^I_{\bar{a}\bar{k}\downarrow}\langle\bar{k}|i\rangle\langle i|\bar{j}\rangle + \sum X^{I*}_{ai\uparrow}X^I_{al\uparrow}\langle l|\bar{j}\rangle\langle\bar{j}|i\rangle \\
&\quad + \sum Y^{I*}_{\bar{k}\bar{a}\downarrow}Y^I_{\bar{j}\bar{a}\downarrow}\langle\bar{k}|i\rangle\langle i|\bar{j}\rangle + \sum Y^{I*}_{la\uparrow}Y^I_{ia\uparrow}\langle l|\bar{j}\rangle\langle\bar{j}|i\rangle \\
&\quad - \sum X^{I*}_{bi\uparrow}X^I_{\bar{a}\bar{j}\downarrow}\langle b|\bar{a}\rangle\langle\bar{j}|i\rangle - \sum Y^{I*}_{\bar{j}\bar{a}\downarrow}Y^I_{ib\downarrow}\langle b|\bar{a}\rangle\langle\bar{j}|i\rangle \\
&\quad - \sum X^{I*}_{\bar{b}\bar{k}\downarrow}X^I_{\bar{a}\bar{k}\downarrow}\langle\bar{b}|i\rangle\langle i|\bar{a}\rangle - \sum Y^{I*}_{\bar{k}\bar{a}\downarrow}Y^I_{\bar{k}\bar{b}\downarrow}\langle\bar{b}|i\rangle\langle i|\bar{a}\rangle \\
&\quad - \sum X^{I*}_{bk\uparrow}X^I_{ak\uparrow}\langle b|\bar{i}\rangle\langle\bar{i}|a\rangle - \sum Y^{I*}_{ka\uparrow}Y^I_{kb\uparrow}\langle b|\bar{i}\rangle\langle\bar{i}|a\rangle \\
&\quad - \sum X^{I*}_{\bar{b}\bar{i}\downarrow}X^I_{aj\uparrow}\langle j|\bar{i}\rangle\langle\bar{b}|a\rangle - \sum Y^{I*}_{ja\uparrow}Y^I_{\bar{i}\bar{b}\downarrow}\langle j|\bar{i}\rangle\langle\bar{b}|a\rangle \\
&\quad + \sum X^{I*}_{bi\uparrow}Y^I_{\bar{j}\bar{a}\downarrow}\langle b|\bar{j}\rangle\langle\bar{a}|i\rangle + \sum X^{I*}_{\bar{a}\bar{j}\downarrow}Y^I_{ib\uparrow}\langle b|\bar{j}\rangle\langle\bar{a}|i\rangle \\
&\quad + \sum Y^{I*}_{\bar{i}\bar{b}\downarrow}X^I_{aj\uparrow}\langle j|\bar{b}\rangle\langle\bar{i}|a\rangle + \sum Y^{I*}_{ja\uparrow}X^I_{\bar{b}\bar{i}\downarrow}\langle j|\bar{b}\rangle\langle\bar{i}|a\rangle\ ,
\end{aligned} \tag{5.21}$$

where we have assumed the normalization,

$$|\mathbf{X}|^2 - |\mathbf{Y}|^2 = 1, \tag{5.22}$$

and i, j, $\bar{i}$, and $\bar{j}$ refer to occupied orbitals while a, b, $\bar{a}$, and $\bar{b}$ refer to unoccupied orbitals. This agrees with the CIS result of Maurice and Head-Gordon [Maurice 1995] when the $\mathbf{Y}$ –component is set equal to zero.

The formaldehyde cation, CH_2O^+, is a good example of the type of information provided by calculations of excited-state spin contamination in LR-TDDFT. Experimental data for the excited states of this species are available from ionization spectra of neutral formaldehyde [Bawagan 1988] and high quality multireference configuration interaction (MRCI) calculated excitation energies are also available [Bawagan 1988, Bruna 1998]. The ground state of the cation and excitations into its singly occupied molecular orbital (SOMO) correspond to principal ionization potentials [one-hole (1h) states], normally treated in DFT using the ΔSCF method or Slater's transition orbital approximation to ΔSCF ionization potentials. However LR-TDDFT also offers the attractive possibility to be able to treat more complex ionization satellites which involve correlation between 1h states and two-hole/one-particle (2h1p) states. Table 5.2 shows the results of our TDLDA calculations on the CH_2O^+ at the equilibrium geometry of neutral formaldehyde using the two programs GAUSSIAN03 [Gaussian 2003] and our own version of DEMON2K [deMon2k 2005]. Note that all of the lowest ten excited states are shown. The main numerical differences between results of the two programs come from the use of an auxiliary function-based method in deMon2k, not used in our GAUSSIAN03 calculations. More importantly, GAUSSIAN03 automatically assigns the symmetry representation of each molecular orbital which this version of DEMON2K does not do and DEMON2K calculates spin contamination which GAUSSIAN03 does not do. So, between the two programs, we have a powerful set of tools for assigning TDLDA excited states. Spin contamination is small in this example so that interpretation is straightforward. In particular, it is immediately seen from the table that $\Delta\langle\hat{S}^2\rangle$ is close to either zero or two. The former indicates a doublet excited state. The latter indicates an unphysical triplet-coupled (TC) excited state which is neither a doublet nor a quadruplet, but which will ultimately generate a doublet and a quadruplet when coupled with suitable extended singles (i.e., doubly excited determinants). In the case of a doublet excited state, we can go further and distinguish between 1h excited states and 2h1p excited states. Comparison with experimental data and the results of the MRCI calculations is straightforward, at least for some states. States 2 and 7 correspond to principal ionization potentials while state 1 is a shakeup satellite of state 7. There is an obvious disagreement between the TDLDA and MRCI assignments of these excitation energies which comes from an LDA ordering of the cationic molecular orbitals,

$$\underbrace{(1a_1)^2(2a_1)^2}_{core}\underbrace{(3a_1)^2(1b_2)^2(4a_1)^2(1b_1)^2(5a_1)^2(2b_2)^1}_{valence}, \tag{5.23}$$

Table 5.2: Spin contamination in CH_2O^+ excited states. All excited states are well below the TDLDA ionization threshold (-ϵ_{HOMO} = 15.1 eV, -ϵ_{HOMO} = 18.2 eV). SOMO refers to the singly occupied molecular orbital (spin up HOMO). TC refers to a triplet = coupled excitation. See the discussion in the text

	Excitation Energy (eV) ($\Delta\langle\hat{S}^2\rangle$)				
State	TDLDA[a]	TDLDA[b]	TDLDA TDA[b]	Assignment[c]	MRCI[d]
10	9.9685	9.9403	10.0286	$^2B_2$	
		(0.0127)	(0.0067)	($2b_2^{\mathrm{SOMO}} \rightarrow 3b_2$)	
9	9.7157	9.7036	9.7862	$^2B_2$	
		(0.0380)	(0.0367)	($2b_2^{\mathrm{SOMO}} \rightarrow 3b_2$,	
				$5a_1 \rightarrow 6a_1$)	
8	8.6708	8.3665	8.5006	$^{TC}B_2$	
		(2.0046)	(1.9834)	($5a_1 \rightarrow 6a_1$)	
7	7.9952	7.8765	7.8980	$^2B_1$	3.86[e], 3.84[f]
		(0.0058)	(0.0047)	($1b_1 \rightarrow 2b_2^{\mathrm{SOMO}}$)	
6	7.9510	7.6532	7.7987	$^{TC}B_2$	
		(1.9870)	(1.9619)	($5a_1 \rightarrow 6a_1$)	
5	7.5641	7.5623	7.7839	$^2A_2$	
		(0.0061)	(0.0050)	($5a_1 \rightarrow 2b_1$)	
4	5.4543	5.1002	5.2638	$^{TC}A_2$	
		(0.0064)	(1.9933)	($5a_1 \rightarrow 2b_1$)	
3	5.1707	5.0833	5.1678	$^2A_1$	
		(2.0502)	(0.0045)	($2b_2^{\mathrm{SOMO}} \rightarrow 6a_1$)	
2	4.7445	4.6046	4.6862	$^2A_1$	5.30[e], 5.46[f]
		(0.0019)	(0.0019)	($5a_1 \rightarrow 2b_2^{\mathrm{SOMO}}$)	
1	2.7014	2.6439	2.6669	$^2B_1$	5.78[e], 6.46[f]
		(0.0020)	(0.0012)	($2b_2^{\mathrm{SOMO}} \rightarrow 2b_1$)	

[a] GAUSSIAN03. [b] DEMON2K. [c] TDLDA TDA. [d] Multireference configuration interaction. [e] [Bruna 1998]. [f] [Bawagan 1988].

which differs from the expected ordering in the neutral [Bawagan 1988],

$$\underbrace{(1a_1)^2(2a_1)^2}_{core}\underbrace{(3a_1)^2(4a_1)^2(1b_2)^2(5a_1)^2(1b_1)^2(2b_2)^2}_{valence}.$$

On the other hand, it is an open question whether TDLDA and MRCI assignments should agree with each other since they refer to different one-particle reference systems. Perhaps only the total state symmetry should be taken into consideration since this is ultimately related to spectroscopic selection rules. In that case, we might try interchanging the MRCI energies for the TDLDA states 1 and 7 and numerical agreement between the two types of calculations, although still imperfect, looks a lot better. This example is one of the first where a very detailed comparison has been made between the results of LR-TDDFT and traditional Hartree-Fock-based

calculations for open-shell systems. More of this type of work will have to be done before we can be ultimately comfortable with using LR-TDDFT for calculating and assigning the spectra of such systems.

IV Beyond the Adiabatic Approximation

It should now be clear that multiple-electron excitations are important for the proper treatment of the excitations of molecules with open-shell ground states. However, as emphasized above, adiabatic LR-TDDFT only includes one-electron excitations (albeit "dressed" to include important electron correlation effects). There is thus a problem. It had been hoped that higher-order response theory might allow the extraction of two-electron excitations within the TDDFT adiabatic approximation [Gross 1996], but it is now clear that this is not the case. In particular, the poles of the dynamic second hyperpolarizability are identical to the poles of the dynamic polarizability, [Tretiak 2003] which is to say the one electron excitations of adiabatic LR-TDDFT. A more successful strategy has been the spin-flip TDDFT developed by Shao, Head-Gordon, and Krylov [Shao 2003, Slipchenko 2003] in which extended singles appear in TDDFT through consideration of perturbations which flip spins. Unfortunately the treatment is restricted to hybrid functionals and depends strongly on the coefficient of Hartree-Fock exchange. Wang and Ziegler have made a potentially major advance by showing that spin-flip TDDFT can be developed for nonhybrid functionals provided one begins with the noncollinear formulation of the exchange-correlation potential which arises naturally in the context of relativistic density-functional theory [Wang 2004]. A more general strategy is to add a non-DFT many-body polarization propagator correction [Casida 2005] and that is briefly described here.

The idea behind the propagator correction approach is the similarity of the relation,

$$\chi^{-1}(\boldsymbol{r}_1,\boldsymbol{r}_2;\omega) = \chi_{\rm KS}^{-1}(\boldsymbol{r}_1,\boldsymbol{r}_2;\omega) + f_{\rm Hxc}(\boldsymbol{r}_1,\boldsymbol{r}_2;\omega)\ , \tag{5.24}$$

which defines the Hartree (Coulomb) and exchange-correlation kernel of LRTDDFT and the Bethe-Salpeter equation,

$$\Pi^{-1}(\boldsymbol{r}_1,\boldsymbol{r}_2;\boldsymbol{r}_3,\boldsymbol{r}_4;\omega) = \Pi_{\rm KS}^{-1}(\boldsymbol{r}_1,\boldsymbol{r}_2;\boldsymbol{r}_3,\boldsymbol{r}_4;\omega) + K_{\rm Hxc}(\boldsymbol{r}_1,\boldsymbol{r}_2;\boldsymbol{r}_3,\boldsymbol{r}_4;\omega)\ , \tag{5.25}$$

which defines the kernel, K_{Hxc}, in terms of the polarization propagator, $\prod$. (See [Onida 2002].) Here we have deliberately chosen the Kohn-Sham orbital hamiltonian

as the zero-order hamiltonian. The main difference between the two equations is that the TDDFT equation is a two-point equation (involving only $\mathbf{r_1}$ and $\mathbf{r_2}$) while the Bethe-Salpeter equation is a four-point equation (involving $\mathbf{r_1}$, $\mathbf{r_2}$, $\mathbf{r_3}$, and $\mathbf{r_4}$). However,

$$\begin{aligned} \Pi(r_1, r_2; r_3, r_4; \omega) &= \chi(r_1, r_2; \omega) \\ \Pi_{\mathrm{KS}}(r_1, r_2; r_3, r_4; \omega) &= \chi_{\mathrm{KS}}(r_1, r_2; \omega) \ , \end{aligned} \tag{5.26}$$

so that we can write that,

$$\begin{aligned} f_{\mathrm{Hxc}}(r_1, r_2; \omega) = \int \mathrm{d}r_3 \cdots \int \mathrm{d}r_9 \, \chi_{\mathrm{KS}}^{-1}(r_1, r_3; \omega) \Pi_{\mathrm{KS}}(r_3, r_3; r_4, r_5; \omega) \\ \times K_{\mathrm{Hxc}}(r_4, r_5; r_6, r_7; \omega) \Pi(r_7, r_8; r_9, r_9; \omega) \chi^{-1}(r_9, r_2; \omega) \ . \end{aligned} \tag{5.27}$$

This provides a way to calculate the TDDFT kernel from many-body theory, though it of course does not provide a functional. More importantly it provides a way to determine a non-DFT many-body nonadiabatic correction to the adiabatic TDDFT kernel. Thus only,

$$\Delta f_{Hxc}(\omega) = f_{Hxc}(\omega) - f_{Hxc}(0), \tag{5.28}$$

need be obtained using the polarization propagator formalism, obtaining $f_{Hxc}(0)$ in the usual way from adiabatic TDDFT. The ultimate usefulness of this method is yet to be determined but will most likely depend upon the complexity of the nonadiabatic correction. Some simplifications already occur because Casida's equation is a four-point formulation of TDDFT. This means that it is reasonable to use,

$$\Delta K_{Hxc}(\omega) = K_{Hxc}(\omega) - K_{Hxc}(0), \tag{5.29}$$

directly in Casida's equation. That is what is proposed in [Casida 2005] where connections are also made with results from Gonze and Scheffler [Gonze 1999], the "dressed TDDFT" of Maitra, Zhang, Cave, and Burke [Maitra 2004, Cave 2004], and spin-flip TDDFT [Shao 2003, Slipchenko 2003]. It is pointed out that the grafting of TDDFT and propagator theory is not smooth in the open-shell case and spin-projectors are recommended to help join the two formalisms.

V Conclusion

With a few notable exceptions (atomic term symbols, dissociation of H_2, ...) quantum chemistry courses place a great deal of emphasis on closed-shell molecules, un-

doubtedly because the theory is simpler. However molecules with open-shell ground states and their spectra are hardly infrequent in nature. DFT and TDDFT offer a tempting toolbox for their study, provided they are used cautiously by informed users. In practice, this typically means the use of spin-unrestricted DODS formulations of (TD)DFT. We have tried to point out two dangers - namely (i) the existance of triplet instabilities for biradicals and (ii) the lack of explicit multiple excitations in adiabatic TDDFT. The first danger means that TDDFT excitation energies are often seriously in error in regions of space where ground and excited potential energy surfaces come close together. This is where traditional *ab initio* quantum chemistry prescribes the use of at least a two determinantal wave function. One can argue that the Kohn-Sham determinant should be able to handle even this situation, provided the exchange-correlation functional is exact, but it is not and the lowest energy solution is typically a symmetry-broken DODS solution in practice. On the bright side, the occurance of an imaginary triplet energy in a LR-TDDFT calculation is an indication that there is a problem with the treatment of the ground state. Less optimistically, LR-TDDFT fails for calculating excitation energies in these regions of configurational space. One easy way to reduce this problem is to decouple the excited state problem from the ground state stability problem by invoking the Tamm-Dancoff approximation, though only a few programs seem to have this option. The second danger means that adiabatic TDDFT produces triplet coupled states which, except in the case of molecules with closed-shell ground states, can be quite unphysical. Moreover too few singlet coupled states are produced. This means that the wise user of LR-TDDFT for the spectra of molecules with open-shell ground states should carefully examine the physical nature of each transition before concluding that it is well-produced by LR-TDDFT. One aid is to calculate ground and excited state spin contamination. While calculating ground state spin contamination is a common option in many programs, we know of no common program which allows spin contamination to be calculated for LR-TDDFT excited states. In addition to implementing the TDA and calculation of excited state spin contamination, we have pointed out another promising option for developers. This is the inclusion of some type of polarization propagator corrections to account for nonadiabatic effects. The success of this last approach will depend upon how easy it is to develop simple effective corrections. The work has only just begun.

5-2 *Excited-State Spin-Contamination in Time-Dependent Density-Functional Theory for Molecules with Open-Shell Ground States*

Excited-State Spin-Contamination in Time-Dependent Density-Functional Theory for Molecules with Open-Shell Ground States

Andrei Ipatov, Felipe Cordova, and Mark E. Casida[1]
Équipe de Chimie Théorique,
Laboratoire d'Etudes Dynamiques et Structurales de la Sélectivité (LEDSS), UMR CNRS/UJF 5616,
Institut de Chimie Moléculaire de Grenoble (ICMG, FR-2607),
Université Joseph Fourier (Grenoble I),
301 rue de la Chimie, BP 53,
F-38041 Grenoble Cedex 9, FRANCE

[1]Mark.Casida@ujf-grenoble.fr

Abstract

Time-dependent density-functional theory (TDDFT) in its linear response formulation was introduced a decade ago to the quantum chemistry community for calculating excitation spectra. Since that time, TDDFT has become a standard tool for examining the excited states of large molecules. Most calculations are for molecules with closed-shell ground states, however the Casida's original formulation allowed both different-orbitals-for-different-spin and fractional occupation numbers, thus opening the way to applying the method to molecules with open-shell ground states. A number of publications have now appeared applying TDDFT to molecules with open-shell ground states and give surprisingly good results for simple excitations. This paper addresses the problem of finding *a priori* criteria for when TDDFT will fail to give an adequate description of the excitations of open-shell molecules. In particular we show how to calculate spin contamination for TDDFT excited states.

I Introduction

The computational efficiency of time-dependent density-functional theory (TDDFT) has made it a state-of- the-art method for the theoretical description of the electronic absorption spectra of large molecules with closed-shell ground states. In contrast, molecules with open-shell ground states have absorption spectra which are more difficult to describe with any method. Nevertheless indications are that the TDDFT formulation of Casida [1] gives an excellent description of simple excitations in radicals [2, 3, 4, 5]. What is still missing are (1) a priori criteria indicating when TDDFT will fail to give an adequate description of the excitations of open-shell molecules and (2) some means to correct TDDFT when the a priori criteria indicate a likely failure. This paper addresses the former problem by showing how to calculate spin contamination for TDDFT excited states. The latter problem has been previously addressed by one of us in a formal paper [6]. Another approach to the second problem is spin-flip TDDFT [7, 8, 9].

Several density-functional theory (DFT) approaches to the problem of studying electronically states have been proposed (see Ref. [10] for a review). Among these, TDDFT appears to be one of the most rigorous and practical approaches. The first TDDFT calculations on atoms were already carried out by Zangwill and Soven in 1980 [11] before there was any formal basis for the method. Modern time-dependent version of density-functional theory (DFT) is based upon two Hohenberg-Kohn-like theorems first presented by Runge and Gross in their 1984 landmark paper [12].

This formalism has been extensively studied since that time and minor difficulties have since been detected and corrected, giving confidence that the basic formalism is fundamentally correct [13]. TDDFT was introduced into quantum chemistry in 1995 as Casida's formulation of linear-response TDDFT for calculating electronic excitation energies [1]. This cast TDDFT into the RPA (random phase approximation) form, already familiar to quantum chemists from time-dependent Hartree-Fock (TDHF) theory. Note however that TDDFT and TDHF behave rather differently even though they may be cast in a similar form. (Unfortunately RPA means a number of different things in the literature, including time-dependent Hartree linear response theory using Kohn-Sham orbitals and orbital energies, so we prefer the term "Casida's equations" in order to minimize confusion.) Since then Casida's equations have been programmed in most world-class quantum chemistry DFT programs. The method has been extensively tested for vertical excitation energies and has been found good at describing low-lying excitations which do not involve significant amounts of charge density relaxation. For more information about TDDFT, the reader is referred to several recent reviews [13, 14, 15, 16, 17, 18, 19]. Most work has been for excitations in molecules with closed-shell ground states. Nevertheless the spectroscopy of molecules with open-shell ground states is also very interesting and, in particular, one of our objectives is to adapt DFT to describe the ground and excited states of low-spin and high-spin iron(II) hexacoordinate complexes [20, 21, 22, 23]. This involves a number of challenges. So far we have addressed primarily the spin-pairing energy problem for the relative energies of ground states with different spin [20, 21, 22, 23]. However another problem which needs to be addressed is the question of the applicability of TDDFT for the calculation of excitation energies in open-shell systems. The original formulation of Casida's equations [1] foresaw applications to molecules with open-shell ground states in that the formulation included both symmetry-broken ground (i.e., different orbitals for different spins) and fractional occupation number ground states. The first applications to calculate excitations of molecules with open-shell ground states came four years later [2, 3, 4, 5, 24, 25, 26, 27, 28, 29, 30, 31]. Particularly significant was that TDDFT seemed to provide the best simple theory for describing simple excitations in radicals [2, 3, 4, 5]. One of us has pointed out that adiabatic TDDFT must necessarily fail for describing more complex excitations whose description requires the explicit description of polyelectronic excited states [6]. This is because adiabatic TDDFT only includes singlet and triplet spin coupling operators which is insufficient for a complete description of the excited states of open-shell molecules. In particular, adiabatic TDDFT can only describe one electron excitations and the general

description of $\hat{S}^2$ spin eigenfunctions for the excited states of molecules with open-shell ground states also requires the inclusion of spin permutations of one-electron excitations, which are not necessarily themselves one-electron excitations. An important consequence is that one should only trust those excited states which preserve the expectation value of $\hat{S}^2$, and even then it is likely that some peaks will be missing. We are working on polarization propagator corrections which are nonadiabatic nonTDDFT corrections to adiabatic TDDFT which will remedy this problem [6]. Other approaches to the same problem are approximate corrections given by Piet van Duijnen, Lasse Jensen, Marcel Swart and Shannon Greene in their study of the visible spectrum of [Fe(PyPepS)$_2$] [32] and noncollinear TDDFT [9]. In the meantime, we turn our attention to the problem of better characterizing the reliability of conventional TDDFT excited state calculations for open-shell molecules by showing how to calculate spin contamination for TDDFT excited states.

II Theoretical Method

In this section we are concerned with the problem of calculating the spin contamination for the ground state Kohn-Sham determinant and for the excited-state multideterminantal TDDFT wave functions arising from broken-symmetry calculations. The system contains $n_\uparrow$ spin up electrons and $n_\downarrow$ spin down electrons for a total electron count of,

$$n = n_\uparrow + n_\downarrow. \tag{5.30}$$

In our (and most other) calculations spin up is always the majority spin,

$$n_\uparrow \geq n_\downarrow. \tag{5.31}$$

Throughout the present paper we will adhere to the molecular orbital index convention,

$$\underbrace{abc\ldots fgh}_{unoccupied} \,|\, \underbrace{ijklmn}_{occupied} \,|\, \underbrace{opq\ldots xyz}_{free}, \tag{5.32}$$

where "free" indicates that the orbital is free to be either occupied or unoccupied.

A Spin Contamination and Reduced Density Matrices

The usual treatment of spin for multielectron wave functions is not based upon broken-symmetry calculations [i.e., different-orbitals-for-different-spin (DODS)], but rather upon same-orbitals-for-different-spin (SODS). There is thus just one underlying basis of molecular orbitals (MOs) which is the same for both spins. Let us adopt this basis for the moment and express the many-electron spin operators in terms of second-quantized creation and annihilation operators, for which we use the shorthand,

$$r_\sigma^\dagger \hat{a}_{r\sigma}^\dagger \tag{5.33}$$

$$r_\sigma \hat{a}_{r\sigma}. \tag{5.34}$$

The many-electron azimuthal spin operator may be expressed in terms of the spin-up and spin-down number operators,

$$\begin{aligned} \hat{S}_z &= \tfrac{1}{2}(\hat{n}_\uparrow - \hat{n}_\downarrow) \\ \hat{n}_\sigma &= \sum r_\sigma^\dagger r_\sigma, \end{aligned} \tag{5.35}$$

from which it is easily seen that every single determinant is an eigenfunction of $\hat{S}_z$ with eigenvalue $(n_\uparrow - n_\downarrow)/2$. In contrast, the square of the many-electron total spin angular momentum operator is [33],

$$\begin{aligned} \hat{S}^2 &= \hat{\mathcal{P}}_{\uparrow,\downarrow} + \hat{n}_\uparrow + \hat{S}_z(\hat{S}_z - \hat{1}) \\ \hat{\mathcal{P}}_{\uparrow,\downarrow} &= \sum r_\downarrow^\dagger s_\downarrow^\dagger s_\downarrow r_\uparrow. \end{aligned} \tag{5.36}$$

The operator $\hat{\mathcal{P}}_{\uparrow,\downarrow}$ permutes spin up and spin down electrons and is known as the spin-transposition operator. This means that only highest weight spin eigenfunctions (i.e., those with $S = M_S$) may be represented as single determinants. The other spin eigenfunctions involve linear combinations of determinants corresponding to different permutations of spin up and spin down electrons among the occupied orbitals. Spin contamination is the extent to which the calculated expectation value of $\hat{S}$ differs from the expected eigenvalue of the same operator. A large amount of spin contamination is an indication that there is a problem in the calculation and so provides an *a priori* criterion for discarding a potentially meaningless result. In this article, we are not so much concerned with the SODS representation but rather with

broken-symmetry calculations. These are the spin-unrestricted Kohn-Sham calculations which are the status quo for treating opens-hell molecules in DFT, since only in this way can full advantage be taken of the spin-dependence of the exchange-correlation functional and still have a consistent exchange-correlation potential for the calculation of properties such as forces. Spin-unrestricted Kohn-Sham calculations may in fact be equivalent to a reasonably good single or multideterminantal SODS calculation, and spin contamination provides one criterion in order to judge if this is indeed the case. (An explicit example is given in Appendix A of the equivalence between a single determinantal DODS wave function and its corresponding multideterminantal SODS wave function.)

Let us then seek explicit formulae for evaluating the expectation value of $\hat{S}^2$. A critical characteristic in DODS calculations is that there are two orthonormal sets of molecular orbitals, constituting two complementary basis sets - one for each spin. We will denote the spin down basis set by an overbar to distinguish it from the spin up basis set. (This is actually overkill since only the overbar basis set will be used for spin down functions, but it is intended as an explicit reminder that the spin down molecular orbitals often differ significantly from the spin up molecular orbitals.) The overlap matrix between the two sets, $\Delta_{r,\bar{s}} = \langle r|\bar{s}\rangle$ is known as the spin similarity matrix. It allows us to expand one basis set in terms of the other,

$$\begin{aligned} r_{\downarrow}^{\dagger} &= \sum_{\bar{p}} \bar{p}_{\downarrow}^{\dagger}\langle\bar{p}|r\rangle \\ s_{\downarrow} &= \sum \bar{q}_{\downarrow}\langle s|\bar{q}\rangle. \end{aligned} \tag{5.37}$$

Since DODS wave functions typically have a well-defined value of $M_S = (n_{\uparrow} - n_{\downarrow})/2$, the crucial quantities to calculate when evaluating spin contamination are the expectation values of the spin up number operator and the expectation value of the spin transposition operator. The spin similarity matrix only enters into the calculation of the later. After transformation into the DODS basis set, the spin transposition operator becomes,

$$\hat{\mathcal{P}}_{\uparrow,\downarrow} = \sum \bar{p}_{\downarrow}^{\dagger} s_{\downarrow}^{\dagger} \bar{q}_{\downarrow} r_{\uparrow} \langle s|\bar{q}\rangle\langle\bar{p}|r\rangle. \tag{5.38}$$

Its expectation value is just,

$$\begin{aligned} \langle\hat{\mathcal{P}}_{\uparrow,\downarrow}\rangle &= \sum \langle \bar{p}_{\downarrow}^{\dagger} s_{\downarrow}^{\dagger} \bar{q}_{\downarrow} r_{\uparrow}\rangle \langle s|\bar{q}\rangle\langle\bar{p}|r\rangle \\ &= \sum \Gamma_{r_{\uparrow}\bar{q}_{\downarrow},\bar{p}_{\downarrow}s_{\uparrow}} \langle s|\bar{q}\rangle\langle\bar{p}|r\rangle, \end{aligned} \tag{5.39}$$

where the two-electron reduced density matrix (2-RDM), Γ has been introduced. (With this definition, Γ is normalized to $n(n$ - $1)$ for an n-electron system.) This makes it clear how to evaluate spin contamination once we have the 2-RDM.

B Ground-State Spin Contamination

The need for a 2-RDM poses a certain conceptual problem in DFT, since it is usually assumed that a wave function is needed to calculate the 2-RDM. However this is not entirely true since the 1-RDM and 2-RDMs may be calculated as analytic derivatives,

$$\begin{aligned} \gamma_{\nu,\mu} &= \tfrac{\partial E}{\partial h_{\mu,\nu}} \\ \Gamma_{\nu\tau,\mu\rho} &= \tfrac{\partial E}{\partial [\mu\nu|\rho\tau]/2}, \end{aligned} \tag{5.40}$$

of the electronic energy, expressed here in a fixed atomic (spin) orbital basis set (designated by Greek letters),

$$E = \sum h_{\mu,\nu}\gamma_{\nu,\mu} + \frac{1}{2}\sum [\mu\nu|\rho\tau]\Gamma_{\nu\tau,\mu\rho}, \tag{5.41}$$

where $[\mu\nu|\rho\tau]$ is Mulliken (charge cloud) notation for an electron repulsion integral. In terms of a more concise molecular spin orbital notation where the spin index ($\uparrow$, $\downarrow$) has been absorbed into the Latin letter, the analytic derivative for the ground state energy is

$$E^{\eta} = \sum \left[h^{\eta}_{p,q} + (1-c_x)(v_{xc})^{\eta}_{p,q}\right]\gamma_{q,p} - \sum S^{\eta}_{p,q}W_{p,q} + \frac{1}{2}\sum [pq,rs]^{\eta}\Gamma_{qs,pr}, \tag{5.42}$$

where the 2-RDM is,

$$\Gamma_{qs,pr} = n_q n_p(\delta_{q,p}\delta_{s,r} - c_x\delta_{q,r}\delta_{s,p}). \tag{5.43}$$

(See for example Ref. [34].) Here n_q is one if the spin-orbital, q, is occupied and zero otherwise; the superscript, η, means to take the derivative with respect to a perturbation, keeping the molecular orbital coefficients fixed, while the superscript, (η), means to take the total derivative with respect to the same perturbation; c_x is the coefficient defining the amount of Hartree-Fock exchange in the possibly hybrid functional ($c_x = 0$ for a pure density functional);

$$S_{p,q} = \langle p|q\rangle, \tag{5.44}$$

is the usual overlap matrix; and the quantity,

$$W_{p,q} = \delta_{p,q} n_p \epsilon_p, \tag{5.45}$$

is the so-called energy-weighted density matrix. Given this 2-RDM, the formula for the 2-RDM may be applied directly to the calculation of ground-state spin-contamination,

$$\begin{aligned} \langle \hat{\mathcal{P}}_{\uparrow,\downarrow} \rangle &= \Gamma_{r_\uparrow \bar{q}_\downarrow, \bar{p}_\downarrow s_\uparrow} \langle s|\bar{q}\rangle \langle \bar{p}|r\rangle \\ &= -c_x \sum_{i,\bar{j}}^{occ} \langle i|\bar{j}\rangle \langle \bar{j}|i\rangle \\ &= -c_x \sum_{i,\bar{j}}^{occ} |\langle i|\bar{j}\rangle|^2. \end{aligned} \tag{5.46}$$

Then

$$\langle \hat{S}^2 \rangle = \left(\frac{n_\uparrow - n_\downarrow}{2} \right)^2 + \frac{n_\uparrow + n_\downarrow}{2} - c_x \sum_{i,\bar{j}}^{occ} |\langle i|\bar{j}\rangle|^2. \tag{5.47}$$

This result implies that there is never any spin contamination in pure DFT ($c_x = 0$), even when the exchange-correlation functional is approximate. It is, however, hardly a very satisfactory result given the intimate relation between spin and the Pauli principle. In fact, the pure DFT 2-RDM given by Eq. 5.43 is, unfortunately, just the Hartree 2-RDM. This is certainly incorrect from the point of view that DFT is a correlated method which refers to the Kohn-Sham reference system of non-interacting electrons (whose wave function is single determinantal in nature because it must satisfy the Pauli principle.) Programs which calculate spin contamination for DFT calculate it for the Kohn-Sham reference determinant and hence use Eq. (5.47) with $c_x = 1$,

$$\langle \hat{S}^2 \rangle = \left(\frac{n_\uparrow - n_\downarrow}{2} \right)^2 + \frac{n_\uparrow + n_\downarrow}{2} - \sum_{i,\bar{j}}^{occ} |\langle i|\bar{j}\rangle|^2. \tag{5.48}$$

It is very important to understand this point clearly. Spin is intimately related to exchange and so cannot be treated correctly except with formulae which have been explicitly developed including exact exchange, either directly as analytic derivatives of Hartree-Fock expressions or indirectly through the exchange present in the single determinant form of the density matrix. This is why our formulae for excited-state spin contamination in TDDFT will be derived as analytic derivatives of time-dependent Hartree-Fock (TDHF) excitation energies.

C Reduced Difference Density Matrices

The problem of spin contamination is similar but more complicated for excited states. In this case, one works with reduced difference density matrices (RDDMs),

$$\begin{aligned} \Delta\gamma_{p,q} &= \gamma^I_{p,q} - \gamma^0_{p,q} \\ \Delta\Gamma_{pq,rs} &= \Gamma^I_{pq,rs} - \Gamma^0_{pq,rs}. \end{aligned} \tag{5.49}$$

We will obtain the RDDMs needed for excited-state spin contamination in TDDFT by taking derivatives of the TDHF excitation energy expression,

$$\begin{aligned} \Delta\gamma_{\nu,\mu} &= \frac{\partial\omega}{\partial h_{\mu,\nu}} \\ \Delta\Gamma_{\nu\tau,\mu\rho} &= \frac{\partial\omega}{\partial[\mu\nu|\rho\tau]/2}. \end{aligned} \tag{5.50}$$

It is convenient for present purposes to use the equations-of-motion (EOM) superoperator formalism for Green's functions [35, 36]. The TDHF excitation energy expression can then be expressed in a compact fashion as,

$$\omega = \langle\phi|\left[\hat{\mathcal{O}}, \left[\hat{H}, \hat{\mathcal{O}}^\dagger\right]\right]|\phi\rangle, \tag{5.51}$$

where ϕ is the Hartree-Fock determinant,

$$\hat{H} = \sum h_{p,q} p^\dagger q + \frac{1}{2}\sum [pr|qs] p^\dagger q^\dagger sr, \tag{5.52}$$

is the electronic hamiltonian, and

$$\hat{\mathcal{O}}^\dagger = \sum_{ia} a^\dagger i X_{ia} + \sum_{ia} i^\dagger a Y_{ia}, \tag{5.53}$$

is the transition operator. The coefficients, X_{ia} and Y_{ia}, are obtained by solving the TDHF equation,

$$\begin{bmatrix} \mathbf{A}(\omega) & \mathbf{B}(\omega) \\ \mathbf{B}^*(\omega) & \mathbf{A}^*(\omega) \end{bmatrix} \begin{pmatrix} \vec{X} \\ \vec{Y} \end{pmatrix} = \omega \begin{bmatrix} \mathbf{1} & \mathbf{0} \\ \mathbf{0} & -\mathbf{1} \end{bmatrix} \begin{pmatrix} \vec{X} \\ \vec{Y} \end{pmatrix}. \tag{5.54}$$

using the normalization,

$$|\vec{X}|^2 - |\vec{Y}|^2 = 1. \tag{5.55}$$

It is perhaps worth remarking that Eq. (5.54) has paired excitation solutions,

$$\begin{pmatrix} \vec{X} \\ \vec{Y} \end{pmatrix} \longleftrightarrow \omega$$
$$|\vec{X}|^2 - |\vec{Y}|^2 = 1. \tag{5.56}$$

and de-excitation solutions,

$$\begin{pmatrix} \vec{X} \\ \vec{Y} \end{pmatrix} \longleftrightarrow \omega$$
$$|\vec{X}|^2 - |\vec{Y}|^2 = -1. \tag{5.57}$$

For the excitation energy solutions,

$$\begin{aligned} \omega &= \omega^{XX} + \omega^{XY} + \omega^{YX} + \omega^{YY} \\ \omega^{XX} &= \sum X^*_{ia} A_{ia,jb} X_{jb} \\ \omega^{XY} &= \sum X^*_{ia} B_{ia,jb} Y_{jb} \\ \omega^{YX} &= \sum Y^*_{ia} B^*_{ia,jb} X_{jb} \\ \omega^{YY} &= \sum Y^*_{ia} A^*_{ia,jb} Y_{jb} \,, \end{aligned} \tag{5.58}$$

which is just another form of Eq. (5.51). Straightforward differentiation of Eq. (5.51) gives

$$\begin{aligned} \Delta\gamma_{p,q} &= \langle\phi| \left[\hat{\mathcal{O}}, q^\dagger p \hat{\mathcal{O}}^\dagger\right] |\phi\rangle \\ \Delta\Gamma_{rq,ps} &= \langle\phi| \left[\hat{\mathcal{O}}, p^\dagger s^\dagger q r \hat{\mathcal{O}}^\dagger\right] |\phi\rangle. \end{aligned} \tag{5.59}$$

Note that the two RDDMs are properly normalized with respect to one another because,

$$\sum_q \Delta\Gamma_{rq,ps} = (n-1)\Delta\gamma_{r,p}, \tag{5.60}$$

follows from the

$$\hat{n} = \sum q^\dagger q \tag{5.61}$$

form of the number operator and the fact that $\hat{\mathcal{O}}^\dagger$ ($\hat{\mathcal{O}}$) is number conserving. This is essentially the solution to our problem. It remains only to make it more explicit

by evaluating the commutators. When this is done, the 1-RDDM is given by

$$\begin{aligned}\Delta\gamma_{p,q} = &-n_p n_q \left(\sum_a X^*_{qa} X_{pa} + \sum_a Y^*_{qa} Y_{pa} \right) \\ &+ \bar{n}_p \bar{n}_q \left(\sum_i X^*_{ip} X_{iq} + \sum_a Y^*_{ip} Y_{iq} \right) ,\end{aligned} \tag{5.62}$$

where,

$$\bar{n}_p = 1 - n_p \tag{5.63}$$

is the hole occupation number corresponding to the particle occupation number, n_p. [Notice the presence of a minus sign in Eq. (5.55) but of a plus sign in Eq. (5.62).] Appendix B gives explicit expressions for,

$$\begin{aligned}\Delta\Gamma^{XX}_{rq,ps} &= \sum_{ia} X^*_{ia} X_{ja} \langle \Phi | [i^\dagger a, p^\dagger s^\dagger q r b^\dagger j] | \Phi \rangle \\ \Delta\Gamma^{XY}_{rq,ps} &= \sum_{ia} X^*_{ia} Y_{jb} \langle \Delta\Phi | [i^\dagger a, p^\dagger s^\dagger q r j^\dagger b] | \Phi \rangle \\ \Delta\Gamma^{YX}_{rq,ps} &= \sum_{ia} Y^*_{ia} X_{jb} \langle \Phi | [a^\dagger i, p^\dagger s^\dagger q r b^\dagger j] | \Phi \rangle \\ \Delta\Gamma^{YY}_{rq,ps} &= \sum_{ia} Y^*_{ia} Y_{jb} \langle \Phi | [a^\dagger i, p^\dagger s^\dagger q r j^\dagger b] | \Phi \rangle .\end{aligned} \tag{5.64}$$

Of course,

$$\Gamma_{rq,ps} = \Gamma^{XX}_{rq,ps} + \Gamma^{XY}_{rq,ps} + \Gamma^{YX}_{rq,ps} + \Gamma^{YY}_{rq,ps} \tag{5.65}$$

In Ref. [37], Eq. (5.59) is attributed to Rowe and apparently goes back to the very beginning of the equation-of-motion superoperator approach to Green's functions in nuclear physics. Although our derivation of Rowe's formula is rigorous as far as it goes, it is important to realize that it is in fact an approximation. Lynch, Herman, and Yeager [37] have criticized Rowe's formula because it misses terms which should be present in a more general EOM expression for excited-state expectation values. However the more important criticism from the perspective of the present work is that we have completely neglected MO orbital relaxation and hence have only obtained the unrelaxed RDDMs. The fully relaxed RDDMs can be obtained by using analytic derivative techniques, as has been done by Furche and Ahlrichs [38] in the case of TDDFT. A new element then enters into the theory in terms of the

Z vector obtained by solving a second coupled equation of the form,

$$(\mathbf{A}+\mathbf{B})\tilde{\mathbf{Z}} = \tilde{\mathbf{R}}, \tag{5.66}$$

where the reader is referred to Ref. [38] for an exact definition of $\vec{R}$. The fully relaxed 1-RDDM then becomes,

$$\begin{aligned}\Delta\gamma_{p,q} = &-n_p n_q \left(\sum_a X^*_{qa}X_{pa} + \sum_a Y^*_{qa}Y_{pa}\right) \\ &+ \bar{n}_p\bar{n}_q \left(\sum_i X^*_{ip}X_{iq} + \sum_a Y^*_{ip}Y_{iq}\right) \\ &+ n_p\bar{n}_q Z_{pq} + \bar{n}_q n_p Z^*_{pq}\,,\end{aligned} \tag{5.67}$$

with corresponding corrections in the 2-RDDM. This is why Rowe's formula should be taken as approximate in the context of the present work. Nevertheless it will be seen to be accurate enough for present purposes and is certainly easier to compute since we avoid having to solve the second coupled equation for the $\mathbf{Z}$ vector.

D Excited-state spin contamination

Plugging the explicit expression for the 2-RDDM into the equation,

$$\begin{aligned}\Delta\langle\hat{S}^2\rangle_I &= \langle\hat{S}^2\rangle_I - \langle\hat{S}^2\rangle_0, \\ &= \sum \Delta\Gamma_{r_\uparrow\bar{q}_\downarrow,\bar{p}_\downarrow s_\uparrow}\langle s|\bar{q}\rangle\langle\bar{p}|r\rangle,\end{aligned} \tag{5.68}$$

gives our final result for the difference in h $\langle S^2 \rangle$ between the Ith excited state and the ground state. This is,

$$\begin{aligned}
\Delta\langle \hat{S}^2 \rangle_I = & \sum X^{I*}_{\bar{j}\bar{a}\downarrow} X^{I}_{\bar{k}\bar{a}\downarrow} \langle \bar{k}|i\rangle \langle i|\bar{j}\rangle \\
& + \sum X^{I*}_{ia\uparrow} X^{I}_{la\uparrow} \langle l|\bar{j}\rangle \langle \bar{j}|i\rangle \\
& + \sum Y^{I*}_{\bar{k}\bar{a}\downarrow} Y^{I}_{\bar{j}\bar{a}\downarrow} \langle \bar{k}|i\rangle \langle i|\bar{j}\rangle \\
& + \sum Y^{I*}_{la\uparrow} Y^{I}_{ia\uparrow} \langle l|\bar{j}\rangle \langle \bar{j}|i\rangle \,, \\
& - 2\Re \sum X^{I*}_{ib\uparrow} X^{I}_{\bar{j}\bar{a}\downarrow} \langle b|\bar{a}\rangle \langle \bar{j}|i\rangle \\
& - 2\Re \sum Y^{I*}_{\bar{j}\bar{a}\downarrow} Y^{I}_{ib\downarrow} \langle b|\bar{a}\rangle \langle \bar{j}|i\rangle \\
& - \sum X^{I*}_{\bar{k}\bar{b}\downarrow} X^{I}_{\bar{k}\bar{a}\downarrow} \langle \bar{b}|i\rangle \langle i|\bar{a}\rangle \\
& - \sum Y^{I*}_{\bar{k}\bar{a}\downarrow} Y^{I}_{\bar{k}\bar{b}\downarrow} \langle \bar{b}|i\rangle \langle i|\bar{a}\rangle \,, \\
& - \sum X^{I*}_{kb\uparrow} X^{I}_{ka\uparrow} \langle b|\bar{i}\rangle \langle \bar{i}|a\rangle \\
& - \sum Y^{I*}_{ka\uparrow} Y^{I}_{kb\uparrow} \langle b|\bar{i}\rangle \langle \bar{i}|a\rangle \,, \\
& + 2\Re \sum X^{I*}_{ib\uparrow} Y^{I}_{\bar{j}\bar{a}\downarrow} \langle b|\bar{j}\rangle \langle \bar{a}|i\rangle \\
& + 2\Re \sum X^{I*}_{\bar{j}\bar{a}\downarrow} Y^{I}_{ib\uparrow} \langle b|\bar{j}\rangle \langle \bar{a}|i\rangle \,,
\end{aligned} \tag{5.69}$$

where $\mathcal{R}$ means to take the real part of the following expression. The result obtained by setting the Y components to zero is the same as that obtained by Maurice and Head-Gordon for the TDHF Tamm-Dancoff approximation (also known as CIS) [39].

When the general formula (5.69) is applied to the case of a closed-shell molecule with SODS, the singlet coupled solutions give

$$\Delta\langle \hat{S}^2 \rangle = 0. \tag{5.70}$$

In contrast, the triplet coupled solutions give,

$$\Delta\langle \hat{S}^2 \rangle = \sum_{ia} |X^2_{ia}| + \sum_{ia} |Y^2_{ia}|. \tag{5.71}$$

which is larger than the expected value of unity because of the normalization condition [Eq. (5.55)] unless the Tamm-Dancoff approximation has been made (i.e., the Y_{ia} are zero), in which case,

$$\Delta\langle \hat{S}^2 \rangle = 1. \tag{5.72}$$

exactly. The somewhat surprising observation that $\Delta\langle\hat{S}^2\rangle$ may exceed unity for triplet excitations in closedshell molecules comes from the approximate nature of the *unrelaxed* 2-RDDM and will presumably go away once relaxation is properly taken into account. However, as we will see in the section after next, the differences between excited-state spin contamination for full TDDFT and for TDA TDDFT calculations appears to be relatively small, and is certainly small enough that our formulae have definite practical value.

III COMPUTATIONAL DETAILS

Calculations were carried out with two different computer programs, namely GAUSSIAN [40] and a modified version of DEMON2K [41]. Both programs carry out DFT calculations in a similar way and in general give very similar results when the same calculation is performed with the two programs. This allows us to use the two programs in a complementary way. For example, GAUSSIAN automatically assigns the symmetries of the molecular orbitals. The particular version of DEMON2K used in the present work does not have this feature so we rely on comparison with the output of Gaussian calculations for this aspect of our analysis. The particular version of GAUSSIAN used in the present work does not allow TDDFT calculations to be performed using the Tamm-Dancoff approximation (TDA) while DEMON2K does have this feature. The calculation of spin-contamination for TDDFT excited states has been implemented using the unrelaxed density matrix in the program deMon2k [41]. The implementation of TDDFT in GAUSSIAN has been described in Ref. [42]. Our implementation of TDDFT in DEMON2K has been previously described elsewhere [43]. It was found in that study that DEMON2K calculations using the GENA3* auxiliary basis set and FINE grid gave excitation energies within 0.02 eV of those given with Gaussian without the use of density fitting functions. Calculations were carried out on five small molecules previously used as a test set for TDDFT calculations by Hirata and Head-Gordon [2] and Guan et al. [24, 26], namely BeH, BeF, CN, CO^+, and N_2^+ , plus a sixth molecule, CH_2O^+, included in the test set of Guan et al. [26]. All of these molecules are radicals with a doublet ground state. The molecular geometries used were the same as those experimental geometries previously used by Guan et al. [26]. The orbital basis set used was that of Sadlej [44]. Extensive use was made of defaults in carrying out calculations with Gaussian. Our deMon2k calculations used the GenA3* auxiliary basis set and the FINE grid. Since both the present calculations and the previous calculations of Guan et al. [24, 26] used programs from the deMon suite of programs, it may be useful to

point out that the present version (deMon2k) differs from the previous implementation used by Guan et al. in several ways, including different convergence criteria, grids, auxiliary basis sets, and the inclusion of a charge conservation constraint in the auxiliary basis charge density fitting algorithm. Figure 5.5 gives a visual idea of how excitation energies from the three programs compare on average. There is improved agreement between deMon2k and Gaussian than with respect to the previous deMon-DynaRho [26] and Gaussian. On the other hand, the agreement between deMon2k and Gaussian is not nearly as good as that previously found for closed-shell molecules [43]. Little is known about the source of these differences except that (i) it does not come from the orbital energies since these agree to better than 0.05 eV and that (ii) differences between deMon2k and Gaussian TDLDA excitation energies tend to correlate with differences between deMon2k TDLDA excitation energies with and without the TDA (Fig. 5.6). Whatever their origin these differences between the results of our Gaussian and deMon2k calculations are nevertheless sufficiently small so as to permit us to go on with our study of excited-state spin contamination and will not be further investigated here.

IV RESULTS

Our goal in this section is to show how the calculation of spin contamination in spin unrestricted TDDFT calculations can help with assignments. The calculated order of spectroscopically active LDA orbitals is shown in Table 5.3 for the five small molecules studied here. Before examining our TDLDA results in detail, let us first consider in a very general manner what type of excitations are possible. In discussing our results, we will follow a common convention when discussing radicals that the HOMO is the highest doubly occupied molecular orbital, the SOMO is the singly occupied molecular orbital, and the LUMO is the lowest unoccupied molecular orbital. With this scheme in mind, excitations may be classified according to whether they involve the SOMO (Fig. 5.7) or whether the SOMO is more of a spectator to the excitation process (Fig. 5.8). The simplest excitations are those involving the SOMO. They are clearly doublets and are typically found among the lowest excitations in radicals. Experimental data for the excitations denoted as type 2 in Fig. 5.7 is readily available for cations since the excited state configuration is easily obtained as the principle ionization out of a doubly occupied orbital of the parent neutral molecule. No particular problem with spin-contamination is anticipated with excitations involving the SOMO and the transitions may have nonzero oscillator strength. The situation is more complicated for excitations where the SOMO is

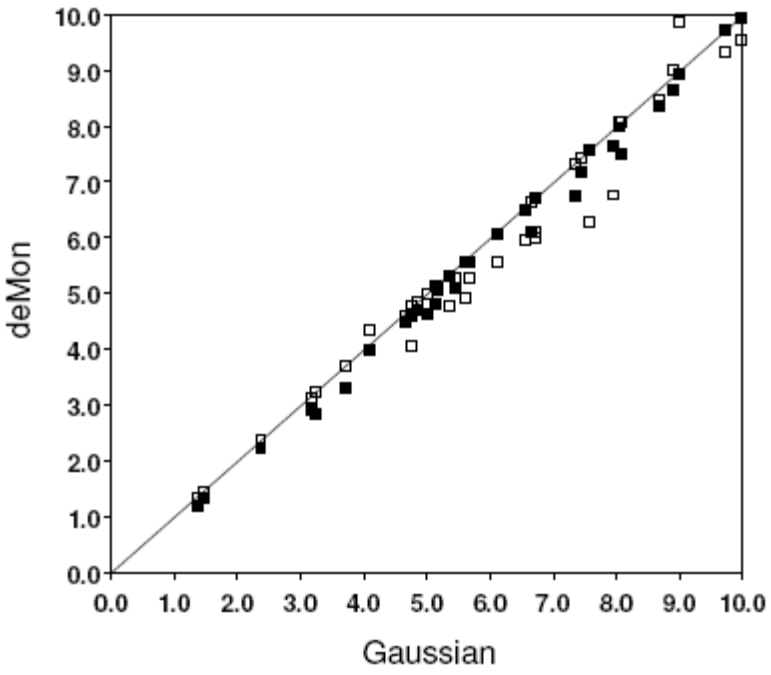

Figure 5.5: Correlation plot for excitation energies in eV calculated with GAUSSIAN and with DEMON2K (closed symbols) and with DEMON-DYNARHO (open symbols) [26].

nominally a spectator (Fig. 5.8). We now have the typical problem of three coupled spins. As summarized in Table 5.4, this gives rise to one quartet and two doublet states. Since ordinary TDDFT calculations cannot flip spins only singlet and triplet coupled excitations are allowed,

$$(1/\sqrt{2})(|\bar{i}sa| \pm |is\bar{a}|). \tag{5.73}$$

When the SOMO is a spectator to the excitation process and the singlet-coupled excitation has zero spin, the result is the $M_S = +1/2$ function of doublet 1. Thus the singlet-coupled excitation in TDDFT has a clear physical interpretation as a true eigenfunction of the spin operators. Moreover it may have nonzero oscillator strength. However the case of the triplet-coupled excitation in TDDFT is less straightforward. This triplet-coupled excitation carries a spin of 1 and so can couple with the SOMO spin of 1/2 to yield a quartet and a doublet. These are the quartet and second doublet $M_S = +1/2$ functions shown in the table. They have zero oscillator strength. However doublet 2 can mix with doublet 1 in order to produce two excited doublet states with nonzero oscillator strength. Unfortunately this can never happen in conventional TDDFT using the adiabatic approximation.

Table 5.3: Ordering and occupation of those LDA occupied and unoccupied ground state orbitals which are most likely to participate in low-lying excitations. The singly occupied molecular orbital (SOMO) has been emphasized by putting it is bold face.

molecule	configuration
BeH	$\ldots 2\sigma^2\mathbf{3\sigma^1}1\pi^0 4\sigma^0 5\sigma^0 \ldots$
BeF, CN, CO^+	$\ldots 4\sigma^2 1\pi^4 \mathbf{5\sigma^1} 2\pi^0 \ldots$
N_2^+	$\ldots 2\sigma_u^2 1\pi_u^4 \mathbf{3\sigma_g^1} 1\pi_g^0 \cdots$
CH_2O^+	$\ldots 1b_1^2 5a_1^2 \mathbf{2b_2^1} 2b_1^0 6a_1^0 3b_2^0 \ldots$

The problem is that the actual coupling involves the spin-flip configuration (5) of Fig. 5.8. This configuration is nominally a two electron excitation and as such is not accessible with the adiabatic approximation of TDDFT. In the absence of access to this configuration only the unphysical triplet excited state of Eq. (5.73) will be found and must either be discarded or the effects of the missing configuration must be included perturbatively via the introduction of integrals which do not arise naturally in TDDFT. This latter procedure has been used to advantage by Piet van Duijnen, Lasse Jensen, Marcel Swart, and Shannon Greene in their study of the visible spectrum of [Fe(PyPepS)$_2$] [32]. The ability to calculate $\langle S^2 \rangle$ for excited states is

Table 5.4: Coupling of three spins in three different orbitals, i, s, and a.

S	M_S	Wave Function
		Quartet
3/2	+3/2	$\lvert isa \rvert$
3/2	+1/2	$(1/\sqrt{3})(\lvert \bar{i}sa \rvert + \lvert is\bar{a} \rvert + \lvert i\bar{s}a \rvert)$
3/2	-1/2	$(1/\sqrt{3})(\lvert i\bar{s}\bar{a} \rvert - \lvert \bar{i}\bar{s}a \rvert + \lvert \bar{i}s\bar{a} \rvert)$
3/2	-3/2	$\lvert \bar{i}\bar{s}\bar{a} \rvert$
		Doublet 1
1/2	+1/2	$(1/\sqrt{2})(\lvert \bar{i}sa \rvert - \lvert is\bar{a} \rvert)$
1/2	-1/2	$(1/\sqrt{2})(\lvert i\bar{s}\bar{a} \rvert - \lvert \bar{i}\bar{s}a \rvert)$
		Doublet 2
1/2	+1/2	$(1/\sqrt{6})(\lvert \bar{i}sa \rvert + \lvert is\bar{a} \rvert - 2\lvert i\bar{s}a \rvert)$
1/2	-1/2	$(1/\sqrt{6})(\lvert i\bar{s}\bar{a} \rvert - \lvert \bar{i}\bar{s}a \rvert - 2\lvert \bar{i}s\bar{a} \rvert)$

an important help for distinguishing singlet- and triplet-coupled excited states, thus permitting intelligent decisions about how to treat them. It also permits the identification of TDDFT excited states which are neither singlet- nor triplet-coupled,

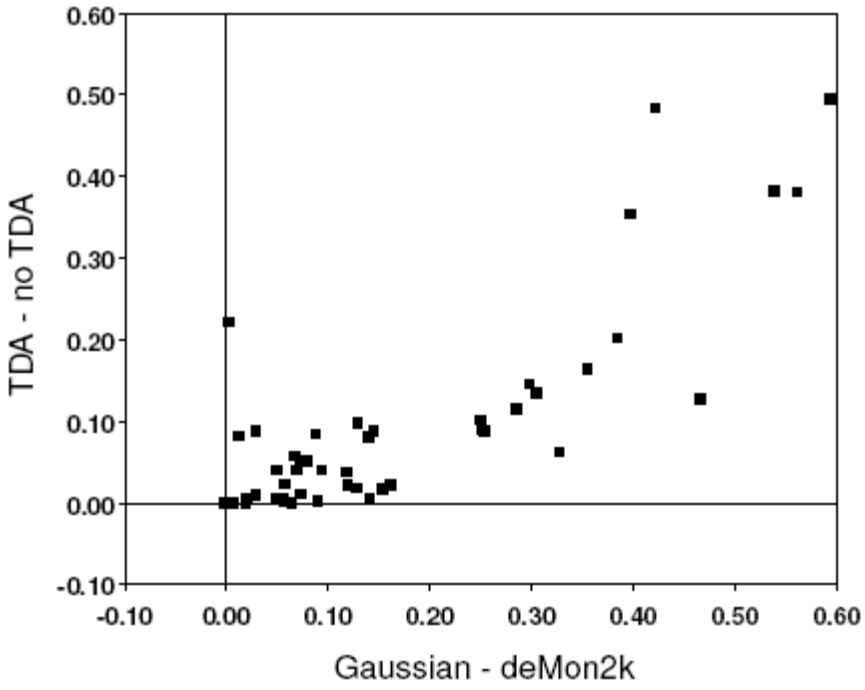

Figure 5.6: Correlation plot for the difference between the TDA TDLDA and full TDLDA excitation energies calculated with deMon2k (y-axis) and the difference between the TDLDA excitation energies calculated with deMon2k and with Gaussian 03 (x-axis). All energies are in eV.

but rather so spin contaminated as to be total nonsense. The ground state spin contamination of the molecules studied in this paper is given in Table 5.5. In the absence of spin contamination, $S(S+1) = 075$. The largest spin contamination is found for the carbon monoxide cation, with ($\hat{S}^2 = 0.7620$). If we assume that the quartet state (S(S +1) = 3.75) constitutes the primary source of contamination in the carbon monoxide cation,

$$|CO^+\rangle = C_D|\text{doublet}\rangle + C_Q|\text{quartet}\rangle, \tag{5.74}$$

then

$$0.7620 = 0.75 \times |C_D|^2 + 3.75|C_Q|^2, \tag{5.75}$$

and the Kohn-Sham wave function is 99.6 % doublet in character ($\times|C_D|^2 = 0.996$). This is an acceptably low level of spin contamination for most purposes and certainly allows the state to be classified as primarily doublet in character. The first several TDLDA excitation energies and spin contamination, $\Delta\langle\hat{S}^2\rangle$, in parentheses for our five test molecules are given in Tables 5.6, 5.7, 5.8, 5.9, 5.10, and 5.11. Also given

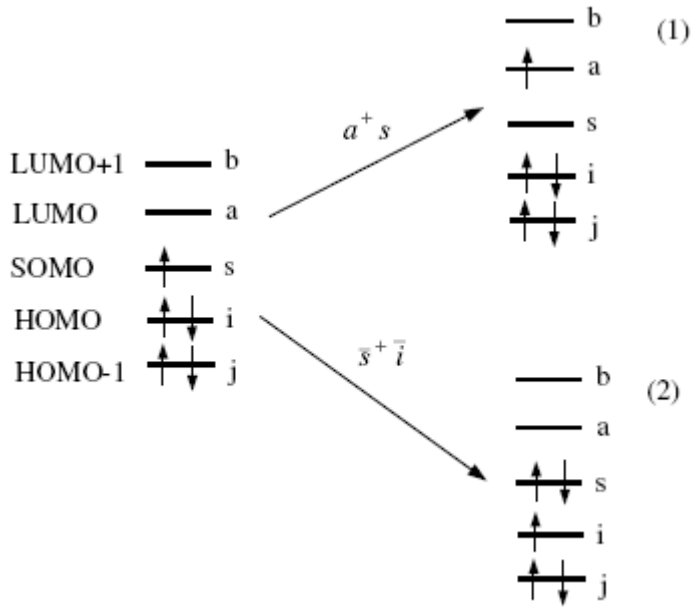

Figure 5.7: Excitations involving the SOMO.

are oscillator strengths in square brackets and results from our TDA calculations. Assignments have been made based upon analysis of the output of the deMon2k TDA calculations using the orbital symmetry assignments from Gaussian03. Some reference values are given in the last column. In this case we have preferred reference values obtained from theoretical calculations since these often contain more detailed information about assignments with which we may compare our own assignments. Inspection of the tables shows that there are mainly three values of $\Delta\langle\hat{S}^2\rangle$ found for the listed excited states of these molecules. These are $\Delta\langle\hat{S}^2\rangle \approx 0$, indicating singlet-coupling and hence excitation to a doublet excited state, $\Delta\langle\hat{S}^2\rangle \approx 2$, indicating triplet-coupling (TC) and hence excitation to a well-defined but unphysical state, and $\Delta\langle\hat{S}^2\rangle \approx 1$ which corresponds to states which are too spin contaminated to be considered any further. Not shown here are higher excitations which show values of $\Delta\langle\hat{S}^2\rangle$ significantly further from noninteger values. Figures 5.9 and 5.10 compare the values of $\Delta\langle\hat{S}^2\rangle$ for full and TDA TDLDA calculations. The comparison is of particular interest for the triplet excitation energies since we have seen that the value of $\Delta\langle\hat{S}^2\rangle$ may exceed 2 for full TDLDA calculations. Indeed triplet $\Delta\langle\hat{S}^2\rangle$ values in the full TDLDA calculations are always larger than the corresponding values from TDA TDLDA calculations. While the value of $\Delta\langle\hat{S}^2\rangle$ sometimes exceeds 2 for full TDLDA calculations, this never seems to be the case for TDA TDLDA calculations. On the whole, however, this seems to be at most a minor problem and in no way undermines the utility of the $\Delta\langle\hat{S}^2\rangle$ calculation. (It also suggests that we could just

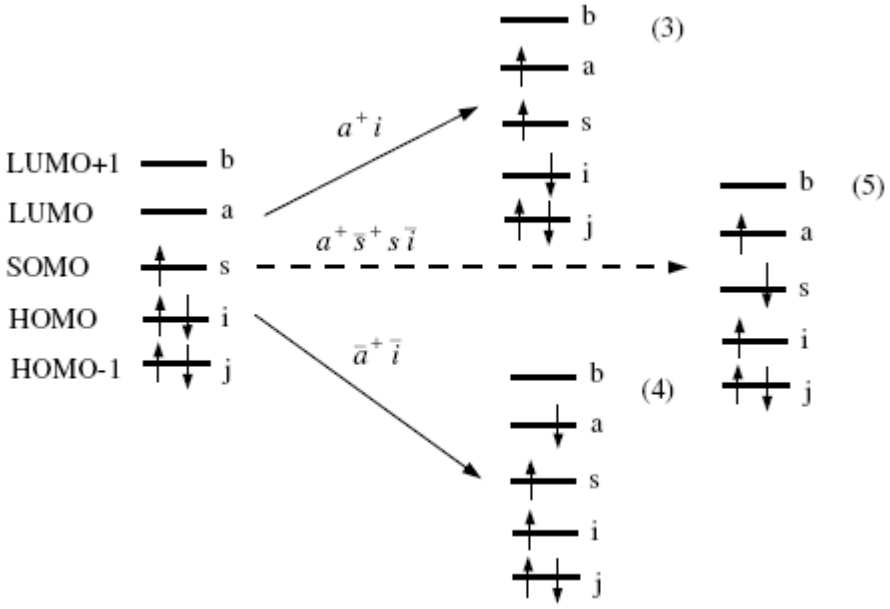

Figure 5.8: Excitation where the SOMO is a spectator.

as well use the TDA formula to calculate $\Delta\langle\hat{S}^2\rangle$ in full TDDFT calculations after first appropriately renormalizing the X components of the TDDFT vector, though we have not done this here.) The utility of calculating $\Delta\langle\hat{S}^2\rangle$ is immediately evident in the case of CN (Table 5.6). It is easily seen that only three out of first five states have physical meaning. The remaining four states are TC states which were misassigned in Ref. [26], for lack of the analytic tools presented in the present work. (Other examples of misassignments can be found in the same article for CO^+ and N_2^+.) Note that state 4 could not have been identified as a TC state on the basis of oscillator strength alone since it has nonzero oscillator strength. Once the TC states are eliminated, the remaining four states are in good agreement with reference values taken from the literature. A second criteria for eliminating TDDFT excitation energies is the position of the adiabatic TDDFT ionization continuum which occurs at minus the orbital energy of the highest orbital of occupied by an electron of a given spin [52]. Were the exchange-correlation functional exact this would be the exact ionization potential. However the LDA exchange-correlation potential goes too quickly to zero at large distances, leading to artifictual underbinding of the electrons and hence to a TDLDA ionization threshold which may be too low by several eV. A more accurate estimate of ionization energies may be obtained by ΔSCF calculations (not given here). The majority spin is up in all of our calculations. A priori this suggests that the spin up ionization potential should be smaller than the spin

Table 5.5: Ground state spin contamination in our deMon2k LDA calculations. The spin contamination obtained from Gaussian03 is identical to the number of significant figures shown.

Molecule	$\langle \hat{S}^2 \rangle$	multiplicity (2S + 1)[1]	% spin contamination [2]
BeH	0.7503	2.0003	0.010
BeF	0.7513	2.0013	0.043
CN	0.7546	2.0046	0.15
CO^+	0.7620	2.0120	0.40
N^+	2 0.7514	2.0014	0.047
CH_2O^+	0.7512	2.0012	0.040

[1] Calculated assuming that $\langle S^2 \rangle$ = S(S + 1).
[2] Coefficient of next highest allowed spin component squared times 100 %, calculated assuming that all spin contamination comes from the next highest allowed spin component.

down ionization potential. This is true for BeH, BeF, and CH_2O^+ where the spin up ionization potential is 3-5 eV lower than the spin down ionization potential. In CN, CO^+, and N_2^+ , the spin up and spin down ionization potentials are nearly identical because they refer to degenerate π orbitals. Interestingly the spin down ionization potential actually exceeds the spin up ionization potential for CO^+. This means that the spin down LUMO is actually lower in energy than the spin up HOMO. Such a violation of the *Aufbau* principal is frequently observed in spin unrestricted DFT calculations on open-shell ground states. It is sometimes interpreted as meaning that self-interaction errors are larger for occupied than for unoccupied orbitals. However it has also been shown that ground-state v-representability does not always hold for open-shell molecules, in which case it may be replaced by excited-state v-representability and unoccupied orbitals will then be found within the manifold of occupied orbitals [53]. For the states considered here, the energy of the TDDFT ionization continuum is only a problem for BeH (Table 5.6) and BeF (Table 5.7) and then only for excitations involving spin up electrons. This accounts for the very large error in the $^2\Pi(3\sigma^{SOMO} \rightarrow 2\pi)$ excitation energy of BeH with respect to the reference value from the literature. All things taken into consideration the remaining physically meaningful excitation energies are seen to be almost exclusively simple excitations involving the SOMO of the type illustrated in Fig. 5.7. Without doubt this is one of the main reasons that TDDFT has been found to work well for the

Table 5.6: Spin contamination in BeH excited states.

State	Excitation Energy (eV) $[f]$ $(\Delta\langle S^2\rangle)$ TDLDA[a]	TDLDA[b]	TDLDA TDA[b]	Assign.[c]	Ref. Values[d]
	TDLDA spin up ionization threshold = 8.0 eV				
7	5.6414	5.4803	5.5030	$^2\Sigma^+$	
	[0.1684]	(0.0034)	(0.0039)	$(3\sigma \rightarrow 6\sigma,$ $2\bar{\sigma} \rightarrow 3\sigma)$	
6	5.6338	5.1685	5.2953	$^{TC}\Pi$	
	[0.0010]	(2.0115)	(1.9784)	$(2\sigma \rightarrow 1\pi,$ $2\bar{\sigma} \rightarrow 1\bar{\pi})$	
5	5.1318	4.8049	4.8676	$^2\Sigma^+$	
	[0.0029]	(0.0297)	(0.0303)	$(2\bar{\sigma} \rightarrow 3\bar{\sigma}^{\mathrm{SOMO}})$	
4	4.8451	4.7047	4.7104	$^2\Pi$	6.31
	[0.0043]	(0.0200)	(0.0111)	$(3\sigma^{\mathrm{SOMO}} \rightarrow 2\pi)$	
3	4.7576	4.6300	4.6481	$^2\Sigma^+$	5.61
	[0.0022]	(0.0134)	(0.0091)	$(3\sigma^{\mathrm{SOMO}} \rightarrow 5\sigma)$	
	TDLDA spin up ionization threshold = 4.6 eV				
2	4.6633	4.5103	4.5278	$^2\Sigma^+$	5.51
	[0.0491]	(0.0083)	(0.0063)	$(3\sigma^{\mathrm{SOMO}} \rightarrow 4\sigma)$	
1	2.3657	2.2479	2.2860	$^2\Pi$	2.56
	[0.0427]	(0.0060)	(0.0011)	$(3\sigma^{\mathrm{SOMO}} \rightarrow 1\pi)$	

[a] GAUSSIAN03.
[b] DEMON2K.
[c] TDLDA TDA.
[d] From Table I of Ref. [45].

description of excitation energies in radicals. An exception is state 5 of CH_2O^+ (Table 5.11). However we have not found any comparison data for this state. The case of CH_2O^+ should also serve as a final word of warning. Thanks to the details of the *ab-initio* calculations given in the reference literature, we are able to give a detailed correspondence between our excitation energies and the *ab-initio* excitation energies, assuming that the orbitals have the same meaning in the two types of calculation. However we know of no theorem which says that this should be so. Had we simply relied on the total symmetry we would have exchanged the reference values for the first and seventh states and found much better agreement between TDDFT and the *ab-initio* theory. Even comparison of the TDDFT and *ab-initio* potential energy curves given in Ref. [26] is not able to clarify this point.

V CONCLUSION

Linear response TDDFT calculations of the electronic excitations of molecules with open-shell ground states began within about five years after the first implementations of Casida's equations in quantum chemistry programs [2, 4, 24, 25, 26, 27]. In many cases the results were very encouraging. However, *caveat emptor* [54].

Table 5.7: Spin contamination in BeF excited states.

State	Excitation Energy (eV) [f] ($\Delta\langle\hat{S}^2\rangle$) TDLDA[a]	TDLDA[b]	TDLDA TDA[b]	Assign.[c]	Ref. Values[d]
	TDLDA spin down ionization threshold = 10.41 eV				
7	6.7268	6.6988	6.7092	$^2\Pi$	
	[0.0027]	(0.0155)	(0.0114)	($5\sigma^{\mathrm{SOMO}} \rightarrow 4\pi$)	
6	6.5432	6.4884	6.4940	$^2\Delta$	
	[0.0000]	(0.0011)	(0.0009)	($5\sigma^{\mathrm{SOMO}} \rightarrow 1\delta$)	
5	6.1070	6.0584	6.0637	$^2\Sigma^+$	
	[0.0739]	(0.0031)	(0.0024)	($5\sigma^{\mathrm{SOMO}} \rightarrow 8\sigma$)	
4	5.6201	5.5811	5.5917	$^2\Sigma^+$	
	[0.0000]	(0.0003)	(0.0004)	($5\sigma^{\mathrm{SOMO}} \rightarrow 7\sigma$)	
3	5.6536	5.5639	5.5666	$^2\Pi$	
	[0.0000]	(0.0003)	(0.0003)	($5\sigma^{\mathrm{SOMO}} \rightarrow 3\pi$)	
	TDLDA spin up ionization threshold = 5.4 eV				
2	5.3462	5.3264	5.3314	$^2\Sigma^+$	6.345
	[0.0977]	(0.0017)	(0.0014)	($5\sigma^{\mathrm{SOMO}} \rightarrow 6\sigma$)	
1	4.0747	3.9816	4.0225	$^2\Pi$	4.2049
	[0.1693]	(0.0000)	(0.0005)	($5\sigma^{\mathrm{SOMO}} \rightarrow 2\pi$, $1\bar{\pi} \rightarrow 5\bar{\sigma}^{\mathrm{SOMO}}$)	

[a] GAUSSIAN03.
[b] DEMON2K.
[c] TDLDA TDA.
[d] Extended configuration interaction singles (XCIS) results from Ref. [46].

As pointed out by Casida in his seminal paper reformulating linear response TDDFT for the calculation of molecular electric excitation spectra [1], the TDDFT adiabatic approximation limits TDDFT to the description of single-electron excitations (albeit single-electron excitations dressed to include correlation effects). As shown here and elsewhere [6, 55], this means that TDDFT calculations of the electronic excitation spectra of molecules with open-shell ground states are fought with dangers. In particular the triplet-coupled excited states of radicals are clearly unphysical and so must either be discarded or corrected to make them physical and there may be too few states of doublet symmetry. This work presents equations for calculating the spin contamination of TDDFT excited states, thus presenting an analytic tool which can help the user to better interpret the results of his or her TDDFT calculations for open-shell molecules. Our formulae for the calculation of spin contamination have been used to analyze low-lying excitations in five small radicals. The occurrence of unphysical triplet-coupled states has been clearly demonstrated. Once these were eliminated from further consideration the remaining excitations were found to be of a particularly simple type involving either excitation into the singly occupied molecular orbital (SOMO) or excitation out of the SOMO, and the associated TDDFT excitation energies are completely reasonable.

Table 5.8: Spin contamination in CN excited states.

State	Excitation Energy (eV) $[f]$ $(\Delta\langle\hat{S}^2\rangle)$ TDLDA[a]	TDLDA[b]	TDLDA TDA[b]	Assign.[c]	Ref. Values[d]
	TDLDA spin up ionization threshold = 9.7 eV				
	TDLDA spin down ionization threshold = 9.5 eV				
7	8.3190	8.3210	8.3210		
	[0.0000]	(0.9967)	(0.9967)		
6	8.0324	8.0334	8.0334		
	[0.0000]	(0.9967)	(0.9967)		
5	8.0518	7.9829	8.0236	$^2\Pi$	8.619
	[0.0027]	(0.0948)	(0.0964)	$(5\sigma^{\mathrm{SOMO}} \rightarrow 2\pi)$	
4	7.4325	7.1807	7.2699	$^{\mathrm{TC}}\Delta$	
	[0.0000]	(2.0050)	(1.9838)	$(1\pi \rightarrow 2\pi,$ $1\bar{\pi} \rightarrow 2\bar{\pi})$	
3	6.6347	6.0967	6.4792	$^{\mathrm{TC}}\Sigma^+$	
	[0.0008]	(1.9928)	(1.9152)	$(1\pi \rightarrow 2\pi)$	
2	3.2333	2.8364	3.1908	$^2\Sigma^+$	3.661
	[0.0366]	(0.1566)	(0.0786)	$(4\bar{\sigma} \rightarrow 5\bar{\sigma}^{\mathrm{SOMO}})$	
1	1.3576	1.2131	1.3017	$^2\Pi$	1.235
	[0.0029]	(0.0160)	(0.0084)	$(1\bar{\pi} \rightarrow 5\bar{\sigma}^{\mathrm{SOMO}})$	

[a] GAUSSIAN03.
[b] DEMON2K.
[c] TDLDA TDA.
[d] Multireference configuration interaction vertical excitation energies calculated from the data in Table III of Ref. [47] at $R_e = 2.211$ bohr.

Some misassignments with regard to previous work [26] were corrected. We believe that the excited state spin contamination formula presented here is an important useful aid for conventional TDDFT. It is anticipated that it will be used as an aid to eliminate unphysical excited states. However in at least some cases these states may alternatively be corrected to yield physically meaningful states [32]. Recently Wang and Ziegler [9] have shown how TDDFT can be extended via a noncollinear reinterpretation of existent functionals to permit spin-flip excitations. (See also earlier work by Krylov and coworkers [7, 8].) This will certainly help in improving TDDFT calculations of the spectra of open-shell molecules. The spin contamination formula presented in the present work is easily adapted to this more general formulation of TDDFT where it is also expected to help in identifying unphysical spin-contaminated excited states.

ACKNOWLEDGMENTS

This study was carried out in the context of the Groupe de *Recherche en Commutateurs Optiques Moléculaires à l'État Solide* (COMES), the *Groupe de Recherche en Density Functional Theory* (DFT), the COST working group D26/0013/02, and a

Table 5.9: Spin contamination in CO^+ excited states.

State	Excitation Energy (eV) [f] ($\Delta\langle\hat{S}^2\rangle$) TDLDA[a]	TDLDA[b]	TDLDA TDA[b]	Assign.[c]	Ref. Values[d]
	TDLDA spin up ionization threshold = 21.8 eV				
	TDLDA spin down ionization threshold = 22.2 eV				
7	10.3165	10.3175	10.3175		
	[0.0000]	(0.9885)	(0.9885)		
6	9.4114	9.4107	9.4107		
	[0.0000]	(0.9884)	(0.9884)		
5	8.9870	8.9203	8.9782	$^2\Pi$	
	[0.0118]	(0.0950)	(0.1102)	($5\sigma^{\mathrm{SOMO}} \rightarrow 2\pi$)	
4	8.8850	8.6319	8.7202	$^{\mathrm{TC}}\Delta$	
	[0.0000]	(1.9189)	(1.8950)	($1\pi \rightarrow 2\pi$, $1\bar{\pi} \rightarrow 2\bar{\pi}$)	
3	8.0622	7.5015	7.8825	$^{\mathrm{TC}}\Sigma^+$	
	[0.0024]	(1.9106)	(1.8785)	($1\pi \rightarrow 2\pi$, $1\bar{\pi} \rightarrow 2\bar{\pi}$)	
2	5.0089	4.6249	4.8274	$^2\Sigma^+$	5.965
	[0.0176]	(0.1941)	(0.1081)	($4\bar{\sigma} \rightarrow 5\bar{\sigma}^{\mathrm{SOMO}}$)	
1	3.1623	2.9126	3.0144	$^2\Pi$	3.137
	[0.0038]	(0.0049)	(0.0074)	($1\bar{\pi} \rightarrow 5\bar{\sigma}^{\mathrm{SOMO}}$)	

[a] GAUSSIAN03.
[b] DEMON2K.
[c] TDLDA TDA.
[d] Full configuration interaction with the Huzinaga-Dunning [4s2p] basis set,calculated from the data in Table 2 of Ref. [48].

Franco-Mexican collaboration financed through ECOS-Nord Action M02P03. Some preliminary results of this study were reported in Ref. [55]. FC acknowledges support from the Mexican Ministry of Education via a CONACYT (SFERE 2004) scholarship and from the *Universidad de las Americas Puebla* (UDLAP). AI would like to acknowledge postdoctoral funding from the LÉDSS. We would like to thank Pierre Vatton, Denis Charapoff, Régis Gras, Sébastien Morin, and Marie-Louise Dheu-Andries for technical support of the LÉDSS and *Centre d'Expérimentation le Calcul Intensif en Chimie* (CECIC) computers used for the calculations reported here. MEC acknowledges useful discussions with Ed Brothers.

APPENDIX A: MULTIDETERMINANTAL NATURE OF DODS WAVEFUNCTIONS

Before examining spin contamination for DODS calculations in detail, it is useful to recall that a single determinant DODS wave function typically corresponds to a multideterminantal SODS wave function. In order to make this clear, consider the textbook problem of the minimal basis configuration interaction solution of the

Table 5.10: Spin contamination in N_2^+ excited states.

	Excitation Energy (eV) [f] ($\Delta\langle\hat{S}^2\rangle$)				
State	TDLDA[a]	TDLDA[b]	TDLDA TDA[b]	Assign.[c]	Ref. Values[d]
	TDLDA spin up ionization threshold = 22.7 eV				
	TDLDA spin down ionization threshold = 22.5 eV				
7	9.5045	9.5049	9.5049		
	[0.0000]	(0.9999)	(0.9999)		
6	9.2685	9.2617	9.2617		
	[0.0000]	(0.9999)	(0.9999)		
5	9.2685	9.1901	9.2415	$^2\Pi_g$	
	[0.0000]	(0.0016)	(0.0011)	$(3\sigma_g^{\mathrm{SOMO}} \rightarrow 1\pi_g)$	
4	8.3921	8.1080	8.2238	$^{\mathrm{TC}}\Delta_u$	
	[0.0000]	(2.0207)	(1.9965)	$(1\pi_u \rightarrow 1\pi_g,$ $1\bar{\pi}_u \rightarrow 1\bar{\pi}_g)$	
3	7.3319	6.7385	7.2329	$^{\mathrm{TC}}\Sigma_u^+$	
	[0.0007]	(1.9875)	(1.8996)	$(2\bar{\sigma}_u \rightarrow 3\bar{\sigma}_g^{\mathrm{SOMO}},$ $1\pi_u \rightarrow 1\pi_g,$ $1\bar{\pi}_u \rightarrow 1\bar{\pi}_g)$	
2	3.7195	3.2982	3.7822	$^2\Sigma_u^+$	3.57
	[0.0359]	(0.1954)	(0.0985)	$(2\bar{\sigma}_u \rightarrow 3\bar{\sigma}_g^{\mathrm{SOMO}})$	
1	1.4634	1.3345	1.4321	$^2\Pi_u$	
	[0.0021]	(0.0191)	(0.0081)	$(1\bar{\pi}_u \rightarrow 3\bar{\sigma}_g^{\mathrm{SOMO}})$	1.41

[a] GAUSSIAN03.
[b] DEMON2K.
[c] TDLDA TDA.
[d] Configuration interaction calculation from Ref. [49].

ground state separation of the molecule H_2. As is well known the most general form of the singlet CI wave function is,

$$\Psi = C_0|\sigma\bar{\sigma}| + C_1\frac{1}{\sqrt{2}}(|\sigma\bar{\sigma}^*| + |\sigma^*\bar{\sigma}|) + C_2|\sigma^*\bar{\sigma}^*|, \tag{5.76}$$

where

$$\begin{aligned} \sigma &= \tfrac{1}{\sqrt{2(1+\mathcal{S})}}(s_A + s_B) \\ \sigma^* &= \tfrac{1}{\sqrt{2(1-\mathcal{S})}}(s_A - s_B), \end{aligned} \tag{5.77}$$

and the overlap,

$$\mathcal{S} = \langle s_A|s_B\rangle. \tag{5.78}$$

So

$$\begin{aligned} s_A &= \sqrt{\tfrac{1+\mathcal{S}}{2}}\sigma + \sqrt{\tfrac{1-\mathcal{S}}{2}}\sigma^* \\ s_B &= \sqrt{\tfrac{1+\mathcal{S}}{2}}\sigma - \sqrt{\tfrac{1-\mathcal{S}}{2}}\sigma^* \end{aligned} \tag{5.79}$$

Table 5.11: Spin contamination in CH_2O^+ excited states.

State	Excitation Energy (eV) [f] ($\Delta\langle S^2\rangle$) TDLDA[a]	TDLDA[b]	TDLDA TDA[b]	Assign.[c]	Ref. Values[d]
	TDLDA spin up ionization threshold = 15.1 eV				
	TDLDA spin down ionization threshold = 18.2 eV				
10	9.9685	9.9403	10.0286	$^2B_2$	
	[0.0005]	(0.0127)	(0.0067)	($2b_2^{\rm SOMO} \rightarrow 3b_2$)	
9	9.7157	9.7036	9.7862	$^2B_2$	
	[0.0396]	(0.0380)	(0.0367)	($2b_2^{\rm SOMO} \rightarrow 3b_2$, $5a_1 \rightarrow 6a_1$)	
8	8.6708	8.3665	8.5006	$^{TC}B_2$	
	[0.0000]	(2.0046)	(1.9834)	($5a_1 \rightarrow 6a_1$, $5\bar{a}_1 \rightarrow 6\bar{a}_1$)	
7	7.9952	7.8765	7.8980	$^2B_1$	3.86[d], 3.84[e]
	[0.0006]	(0.0058)	(0.0047)	($1\bar{b}_1 \rightarrow 2\bar{b}_2^{\rm SOMO}$)	
6	7.9510	7.6532	7.7987	$^{TC}B_2$	
	[0.0000]	(1.9870)	(1.9619)	($5a_1 \rightarrow 6a_1$, $5\bar{a}_1 \rightarrow 6\bar{a}_1$)	
5	7.5641	7.5623	7.7839	$^2A_2$	
	[0.0391]	(0.0061)	(0.0050)	($5a_1 \rightarrow 2b_1$, $5\bar{a}_1 \rightarrow 2\bar{b}_1$)	
4	5.4543	5.1002	5.2638	$^{TC}A_2$	
	[0.0001]	(0.0064)	(1.9933)	($5a_1 \rightarrow 2b_1$, $5\bar{a}_1 \rightarrow 2\bar{b}_1$)	
3	5.1707	5.0833	5.1678	$^2A_1$	
	[0.0145]	(2.0502)	(0.0045)	($2b_2^{\rm SOMO} \rightarrow 6a_1$)	
2	4.7445	4.6046	4.6862	$^2A_1$	5.30[d], 5.46[e]
	[0.0083]	(0.0019)	(0.0019)	($5\bar{a}_1 \rightarrow 2\bar{b}_2^{\rm SOMO}$)	
1	2.7014	2.6439	2.6669	$^2B_1$	5.78[d], 6.46[e]
	[0.0000]	(0.0020)	(0.0012)	($2b_2^{\rm SOMO} \rightarrow 2b_1$)	

[a] GAUSSIAN03.
[b] DEMON2K.
[c] TDLDA TDA.
[d] Multireference configuration interaction calculation from Ref. [50].
[e] Multireference configuration interaction calculation from Ref. [51].

At the equilibrium geometry, the ground state is reasonably well represented by the first term,

$$\Psi(R_e) \approx |\sigma\bar{\sigma}|. \tag{5.80}$$

In contrast, the broken symmetry solution,

$$\begin{aligned} \Psi(\text{large } R) &\approx |s_A \bar{s}_B| \\ &= \tfrac{1+\mathcal{S}}{2}|\sigma\bar{\sigma}| - \sqrt{\tfrac{1-\mathcal{S}}{2}}\tfrac{1}{\sqrt{2}}(|\sigma\bar{\sigma}^*| - |\sigma^*\bar{\sigma}|) \\ &= \tfrac{1-\mathcal{S}}{2}|\sigma^*\bar{\sigma}^*|, \end{aligned} \tag{5.81}$$

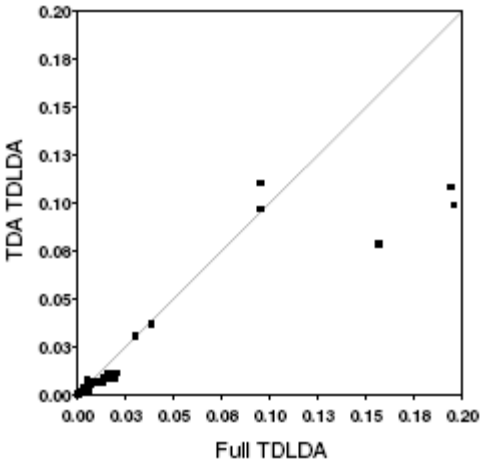

Figure 5.9: $\Delta\langle\hat{S}^2\rangle$ correlation graph for full and TDA TDLDA deMon2k singlet excitation energies.

provides a better description of the multideterminantal solution at large internuclear separation. It is not an eigenfunction of $\hat{S}^2$. In fact, although the first and third terms are pure singlet wave functions, the second term is a triplet wave function. There is thus spin contamination and the amount of spin contamination is related to the deviation from one of the overlap, S, between the spin-up and spin-down orbitals. Moreover, according to formula (5.48),

$$\langle\hat{S}^2\rangle = 1 - \mathcal{S}^2, \tag{5.82}$$

so $\langle\hat{S}^2\rangle$ differs from the expected singlet value of unity by the square of the overlap, $\mathcal{S}$. Energetically this small residual amount of spin contamination is not a big problem because,

$$\begin{aligned} \Psi(\text{large } R) &\approx \tfrac{1}{\sqrt{2(1+\mathcal{S}^2)}}(|s_A\bar{s}_B| + |s_B\bar{s}_A|) \\ &= \tfrac{1+\mathcal{S}}{\sqrt{2(1+\mathcal{S}^2)}}|\sigma\bar{\sigma}| \\ &= \tfrac{1-\mathcal{S}}{\sqrt{2(1+\mathcal{S}^2)}}|\sigma^*\bar{\sigma}^*|, \end{aligned} \tag{5.83}$$

is a pure singlet wave function which has the same energy as the spin contaminated wave function as long as the overlap,

$$\langle\det|s_A\bar{s}_B||\det|s_B\bar{s}_A|\rangle = \mathcal{S}^2, \tag{5.84}$$

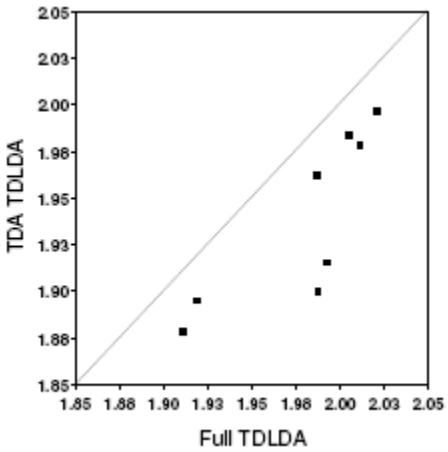

Figure 5.10: $\Delta\langle\hat{S}^2\rangle$ correlation graph for full and TDA TDLDA deMon2k triplet excitation energies.

is small. We can thus conclude that a broken-symmetry determinant represents a many-determinantal SODS solution, that the amount of spin contamination should depend (in part) on the overlap between the spin-up and spin-down orbitals, and that spin contamination may or may not have a significant impact on energy.

APPENDIX B: UNRELAXED TWO-ELECTRON REDUCED DIFFERENCE DENSITY MATRIX

In Hartree-Fock theory the ground state density matrix is given by,

$$\Gamma = \frac{1}{2}\gamma \wedge \gamma, \tag{5.85}$$

where the Grassman product is defined by the doubly antisymmetrized product,

$$(\mathbf{A} \wedge \mathbf{B})_{\mathbf{pq,rs}} = \mathbf{A_{p,r}B_{q,s}} - \mathbf{A_{p,s}B_{q,r}} - \mathbf{A_{q,r}B_{p,s}} + \mathbf{A_{q,s}B_{p,r}}. \tag{5.86}$$

If we assume that the excited state 2-RDM is also that of a single determinant, then

$$\begin{aligned} \Delta\Gamma &= \tfrac{1}{2}(\gamma + \Delta\gamma) \wedge (\gamma + \Delta\gamma) - \tfrac{1}{2}\gamma \wedge \gamma \\ &= \gamma \wedge \Delta\gamma + \tfrac{1}{2}\Delta\gamma \wedge \Delta\gamma. \end{aligned} \tag{5.87}$$

In fact the unrelaxed TDHF 2-RDDM is just given by $\gamma \wedge \Delta\gamma$ plus a few additional correction terms. Specifically the XX component is given by,

$$\begin{aligned}\Delta\Gamma^{XX}_{rs,pq} &= (\gamma \wedge \Delta\gamma)^{XX}_{rs,pq} \\ &\quad - n_r\bar{n}_s n_p \bar{n}_q X^*_{rq} X_{ps} - \bar{n}_r n_s \bar{n}_p n_q X^*_{sp} X_{qr} \\ &\quad + n_r\bar{n}_s \bar{n}_p n_q X^*_{rp} X_{qs} + \bar{n}_r n_s n_p \bar{n}_q X^*_{sq} X_{pr}\end{aligned} \tag{5.88}$$

where

$$\begin{aligned}(\gamma \wedge \Delta\gamma)^{XX}_{rs,pq} &= n_r n_s n_p n_q \\ &\quad \times \Bigg[\delta_{p,s} \sum_a X^*_{ra} X_{qa} - \delta_{p,r} \sum_a X^*_{sa} X_{qa} \\ &\quad - \delta_{q,s} \sum_a X^*_{ra} X_{pa} + \delta_{q,r} \sum_a X^*_{sa} X_{pa}\Bigg] \\ &\quad + n_r\bar{n}_s n_p \bar{n}_q \delta_{r,p} \sum_{\boldsymbol{i}} X^*_{iq} X_{is} \\ &\quad + \bar{n}_r n_s \bar{n}_p n_q \delta_{q,s} \sum_{\boldsymbol{i}} X^*_{ip} X_{ir} \\ &\quad - n_r\bar{n}_s \bar{n}_p n_q \delta_{q,r} \sum_{\boldsymbol{i}} X^*_{ip} X_{is} \\ &\quad - \bar{n}_r n_s n_p \bar{n}_q \delta_{p,s} \sum_{\boldsymbol{i}} X^*_{iq} X_{ir}\,.\end{aligned} \tag{5.89}$$

The YY component is given by,

$$\begin{aligned}\Delta\Gamma^{YY}_{rs,pq} &= (\gamma \wedge \Delta\gamma)^{YY}_{rs,pq} \\ &\quad - n_s\bar{n}_r n_q \bar{n}_p Y^*_{qr} Y_{sp} - \bar{n}_s n_r \bar{n}_q n_p Y^*_{ps} Y_{rq} \\ &\quad + n_s\bar{n}_r \bar{n}_q n_p Y^*_{pr} Y_{sq} + \bar{n}_s n_r n_q \bar{n}_p Y^*_{qs} Y_{rp}\,,\end{aligned} \tag{5.90}$$

where

$$
\begin{aligned}
(\gamma \wedge \Delta\gamma)^{YY}_{rs,pq} &= n_r n_s n_p n_q \\
&\times \left[\delta_{s,p} \sum_a Y^*_{qa} Y_{ra} - \delta_{p,r} \sum_a Y^*_{qa} Y_{sa} \right. \\
&\left. - \delta_{q,s} \sum_a Y^*_{pa} Y_{ra} + \delta_{q,r} \sum_a Y^*_{pa} X_{sa} \right] \\
&+ n_s \bar{n}_r n_q \bar{n}_p \delta_{q,s} \sum_i Y^*_{ir} Y_{ip} \\
&+ \bar{n}_s n_r \bar{n}_q n_p \delta_{p,r} \sum_i Y^*_{is} Y_{iq} \\
&- n_s \bar{n}_r \bar{n}_q n_p \delta_{p,s} \sum_i Y^*_{ir} Y_{iq} \\
&- \bar{n}_s n_r n_q \bar{n}_p \delta_{q,r} \sum_i Y^*_{is} X_{ip} \,.
\end{aligned}
\tag{5.91}
$$

The XY component is given by,

$$
\begin{aligned}
\Delta\Gamma^{XY}_{rs,pq} = n_r n_s \bar{n}_p \bar{n}_q \left(X^*_{rq} X_{sp} - X^*_{sq} X_{sp} \right. \\
\left. - X^*_{rp} X_{sq} + X^*_{sp} X_{rq} \right) \,,
\end{aligned}
\tag{5.92}
$$

and the YX component is given by,

$$
\begin{aligned}
\Delta\Gamma^{YX}_{rs,pq} = \bar{n}_r \bar{n}_s n_p n_q \left(Y^*_{ps} Y_{qr} - Y^*_{qs} Y_{pr} \right. \\
\left. - Y^*_{pr} Y_{qs} + Y^*_{qr} Y_{ps} \right) \,.
\end{aligned}
\tag{5.93}
$$

Bibliography

[1] M.E. Casida, in Recent Advances in Density Functional Methods, Part I, edited by D.P. Chong (World Scientific: Singapore, 1995), p. 155.

[2] S. Hirata and M. Head-Gordon, Chem. Phys. Lett. 302, 375 (1999).

[3] S. Hirata and M. Head-Gordon, Chem. Phys. Lett. 314, 291 (1999).

[4] S. Hirata, T.J. Lee, and M. Head-Gordon, J. Chem. Phys. 111, 8904 (1999).

[5] J.L. Weisman and M. Head-Gordon, J. Am. Chem. Soc. 123, 11686 (2001).

[6] M.E. Casida, J. Chem. Phys. 122, 054111 (2005).

[7] L.V. Slipchenko and A.I. Krylov, J. Chem. Phys. 118, 6874 (2003).

[8] Y. Shao, M. Head-Gordon, and A.I. Krylov, J. Chem. Phys. 118, 4807 (2003).

[9] F. Wang and T. Ziegler, J. Chem. Phys. 121, 12191 (2004).

[10] R. Singh and B.M. Deb, Phys. Reps. 311, 50 (1999).

[11] A. Zangwill and P. Soven, Phys. Rev. A 21, 1561 (1980).

[12] E. Runge and E.K.U. Gross, Phys. Rev. Lett. 52, 997 (1984).

[13] R. van Leeuwen, Int. J. Mod. Phys. B 15, 1969 (2001).

[14] N.T. Maitra, K. Burke, H. Appel, E.K.U. Gross, and R. van Leeuwen, in Reviews in Modern Quantum Chemistry, A Cellibration of the Contributions of R.G. Parr, edited by K.D. Sen (World Scientific: 2001).

[15] M.E. Casida, in Accurate Description of Low-Lying Molecular Excited States and Potential Energy Surfaces, ACS Symposium Series 828, edited by M.R. Hoffmann and K.G. Dyall (ACS Press: Washington, D.C., 2002), p. 199.

[16] G. Onida, L. Reining, and A. Rubio, Rev. Mod. Phys. 74, 601 (2002).

[17] C. Daniel, Coordination Chem. Rev. 238-239, 141 (2003).

[18] N.T. Maitra, A. Wasserman, and K. Burke, in Electron Correlations and Materials Properties 2, edited by A. Gonis, N. Kioussis, and M. Ciftan (Klewer/Plenum: 2003).

[19] J. Werschnik, E.K.U. Gross, and K. Burke, J. Chem. Phys. in press.

[20] M.E. Casida, A. Fouqueau, A. Hauser, L.M. Lawson Daku, S. Mer, T. Mineva, and F. Neese, J. Chem. Phys. 120, 9473 (2004).

[21] A. Fouqueau, M.E. Casida, L.M. Lawson Daku, A. Hauser, and F. Neese, J. Chem. Phys. 122, 044110 (2005).

[22] L.M. Lawson Daku, A. Vargas, A. Hauser, A. Fouqueau, and M.E. Casida, ChemPhysChem 6, 1 (2005).

[23] A. Fouqueau, PhD Thesis, Université Joseph Fourier, 3 March 2005.

[24] J. Guan, Ph.D. Thesis, University of Montreal, September 1999.

[25] A. Spielfiedel and N.C. Handy, Phys. Chem. Chem. Phys. 1, 2401 (1999).

[26] J. Guan, M.E. Casida, and D.R. Salahub, J. Mol. Struct. (Theochem) 524, 229 (2000).

[27] T. Anduniow, M. Pawlikowski, and M.Z. Zgierski, J. Phys. Chem. A 104, 845 (2000).

[28] J.G. Radziszewski, M. Gil, A. Gorski, J. Spanget-Larsen, J. Waluk,and B. Mroz, J. Chem. Phys. 115, 9733 (2001).

[29] E. Broclawik and T. Borowski, Chem. Phys. Lett. 339, 433 (2001).

[30] R. Pou-Amérigo, P.M. Viruela, R. Viruela, M. Rubio, and E. Orti, Chem. Phys. Lett. 352, 491 (2002).

[31] Z. Rinkevicius, I. Tunell, P. Salek, O. Vahtras, and H. Ågren, J. Chem. Phys. 119, 34 (2003).

[32] P. van Duijnen, personal communication.

[33] F.L. Pilar, Elementary Quantum Chemistry, (McGraw-Hill Book Company: New York, 1968), p. 290.

[34] R. Fournier, J. Andzelm, and D.R. Salahub, J. Chem. Phys. 90, 6371 (1989).

[35] P. Jørgensen and J. Simons, Second Quantization- Based Methods in Quantum Chemistry (Academic Press: New York, 1981).

[36] J. Linderberg and Y. Öhrn, Propagators in Quantum Chemistry (Academic Press: New York, 1973).

[37] D. Lynch, M.F. Herman, and D.L. Yeager, Chem. Phys. 64, 69 (1982).

[38] F. Furche and R. Ahlrichs, J. Chem. Phys. 117, 7433 (2002).

[39] D. Maurice and M. Head-Gordon, Int. J. Quant. Chem. Symp. 29, 361 (1995).

[40] Gaussian 03, Revision C.02, M.J. Frisch, G. W. Trucks, H.B. Schlegel, G.E. Scuseria, M.A. Robb, J. R. Cheeseman, J. A. Montgomery, Jr., T. Vreven, K. N. Kudin, J. C. Burant, J. M. Millam, S. S. Iyengar, J. Tomasi, V. Barone, B.

Mennucci, M. Cossi, G. Scalmani, N. Rega, G. A. Petersson, H. Nakatsuji, M. Hada, M. Ehara, K. Toyota, R. Fukuda, J. Hasegawa, M. Ishida, T. Nakajima, Y. Honda, O. Kitao, H. Nakai, M. Klene, X. Li, J. E. Knox, H. P. Hratchian, J. B. Cross, V. Bakken, C. Adamo, J. Jaramillo, R. Gomperts, R. E. Stratmann, O. Yazyev, A. J. Austin, R. Cammi, C. Pomelli, J. W. Ochterski, P. Y. Ayala, K. Morokuma, G. A. Voth, P. Salvador, J. J. Dannenberg, V. G. Zakrzewski, S. Dapprich, A. D. Daniels, M. C. Strain, O. Farkas, D. K. Malick, A. D. Rabuck, K. Raghavachari, J. B. Foresman, J. V. Ortiz, Q. Cui, A. G. Baboul, S. Clifford, J. Cioslowski, B. B. Stefanov, G. Liu, A. Liashenko, P. Piskorz, I. Komaromi, R. L. Martin, D. J. Fox, T. Keith, M. A. Al-Laham, C. Y. Peng, A. Nanayakkara, M. Challacombe, P. M. W. Gill, B. Johnson, W. Chen, M. W. Wong, C. Gonzalez, and 15 J. A. Pople, Gaussian, Inc., Wallingford CT, 2004.

[41] Andreas M. Köster, Patrizia Calaminici, Mark E. Casida, Roberto Flores, Gerald Geudtner, Annick Goursot, Thomas Heine, Andrei Ipatov, Florian Janetzko, Serguei Patchkovskii, J. Ulises Reveles, Alberto Vela and Dennis R. Salahub, deMon2k, Version 1.8, The deMon Developers (2005).

[42] R.E. Stratmann, G.E. Scuseria, and M. Frisch, J. Chem. Phys. 109, 8218 (1998).

[43] A. Ipatov, A. Fouqueau, C. Perez del Valle, F. Cordova, M.E. Casida, A.M. Köster, and A. Vela, J. Mol. Struct. (Theochem) 762, 179 (2006).

[44] A.J. Sadlej, Collec. Czech. Chem. Commun. 53, 1995 (1988); A.J. Sadlej, Theor. Chim. Acta 79, 123 (1992); A.J. Sadlej, Theor. Chim. Acta 81, 45 (1992); A.J. Sadlej, Theor. Chim. Acta 81, 339 (1992).

[45] I.D. Petsalakis, G. Theodorakopoulos, and C.A. Nicolaides, J. Chem. Phys. 97, 7623 (1992).

[46] D. Maurice and M. Head-Gordon, J. Phys. Chem. 100, 6131 (1996).

[47] G. Das, T. Janis, and A.C. Wahl, J. Chem. Phys. 61, 1274 (1974).

[48] H. Nakatsuji, Chem. Phys. Lett. 177, 331 (1991).

[49] N. Kosugi, H. Kuroda, and S. Iwata, Chem. Phys. 39, 337 (1979).

[50] P.J. Bruna, M.R.J. Hachey, and F. Grein, Mol. Phys. 94, 917 (1998).

[51] A.O. Bawagan, C.E. Brion, E.R. Davidson, C. Boyle, and R.F. Frey, Chem. Phys. 128, 439 (1988).

[52] M.E. Casida, C. Jamorski, K.C. Casida, and D.R. Salahub, J. Chem. Phys. 108, 4439 (1998).

[53] M. Levy, personal communication.

[54] A legal term, meaning "Let the buyer beware."

[55] M.E. Casida, A. Ipatov, and F. Cordova, in Time-Dependent Density-Functional Theory, edited by M.A.L. Marques, C. Ullrich, F. Nogueira, A. Rubio, and E.K.U. Gross, Lecture Notes in Physics (Springer: Berlin, 2006).

Chapter 6

TDDFT and Photochemistry

This chapter may be considered to be the heart of my thesis. It consists of the assessment of TDDFT for the ultimate application of TDDFT to modelling the photodynamics of oxirane. Nevertheless no photodynamics calculations are presented in this thesis. Instead TDDFT potential energy surfaces (PESs) are compared against the high quality quantum Monte Carlo (QMC) calculations of Claudia Filippi of the Instituut-Lorentz for Theoretical Physics, Universiteit Leiden in the Netherlands.

We wanted to go further and indeed carried out a number of calculations in this direction which are not reported here aimed at investigating Woodward-Hoffmann type conrotatory and disrotatory ring-opening of oxirane. Photochemistry is "spectroscopy plus plus" and we soon discovered that recent developments in photodynamics modelling had rendered our initial photochemical study largely obsolete. In particular it is now appreciated that the asymmetric reaction paths are most likely the role rather than the exception for photochemical reactions. Happily our work has formed the basis for oxirane photodynamics calculations carried out by our collaborators in Lausanne, Switzerland (not reported here) which are directly comparable with available experimental results.

This chapter contains our manuscript [1],

> F. Cordova, L. Joubert Doriol, A. Ipatov, M.E. Casida, C. Filippi and A. Vela, *accepted* 2007, in *J. Chem. Phys.*
> "Troubleshooting Time-Dependent Density-Functional Theory for Photochemical Applications: Oxirane"

Aside from my own DFT, TDDFT and CASSCF (using the Molcas program) calculations as well as the HF, CIS and TDHF results from an undergraduate project (L. Joubert Doriol) I directed, this work relies heavily on the QMC calculations of Claudia Filippi. Far from being a more approximation on LR-TDDFT, we show that the Tamm-Dancoff approximation (TDA) programmed by A. Ipatov in deMon2k is actually essential for overcoming the triplet instability problem in photodynamics

calculations. Also A. Vela has made important periodic contributions to this work through his insightful suggestions during semi-annual visits to Grenoble under the ECOS-Nord Franco-Mexican collaboration program. To begin this chapter I describe some interesting properties of oxirane molecule founded in the literature. After that the manuscript will be presented.

I Properties of Oxirane Molecule

Since that oxirane molecule will be the principal actor in this chapter we consider important emphasize some physico-chemical properties of this substance. As it has been established the geometrical structure is shown in the Fig. 2.5, where R_1=R_2=R_3=R_4 are H atoms. This molecule can be named in different manners i.e., ethylene oxide, anprolene, dihydrooxirene, dimethylene oxide, Epoxyethane, oxidoethane, etc.

Oxirane is very reactive, because its highly strained ring can be opened easily, and it is one of the most versatile chemical intermediates. Oxirane was first prepared in 1859 by Wurtz [2] using potassium hydroxide solution to eliminate hydrochloric acid from ethylene chlorohydrin. The chlorohydrin process developed from Wurtz's discovery and industrial production began in 1914. The importance and commercial production of oxirane have steadily grown since then. The direct catalytic oxidation of ethylene, discovered in 1931 by Lefort [3], has gradually superseded the chlorohydrin process. Currently, oxirane is produced by direct oxidation of ethylene with air or oxygen. Annual worldwide production capacity exceeds 11 million tons, making it an important industrial chemical. Virtually all oxirane produced is further reacted. Its most important derivative is ethylene glycol, which is used for the manufacture of polyester and in automotive antifreeze. Other oxirane derivatives include surfactants, solvents, amines, and poly(ethylene) glycols.

Theoretically oxirane molecule has also been studied. This will be presented in the article exposed here.

Bibliography

[1] F. Cordova, L. Joubert Doriol, A. Ipatov, M.E. Casida, C. Filippi and A. Vela, *accepted* 2007, in *J. Chem. Phys.*
"Troubleshooting Time-Dependent Density-Functional Theory for Photochemical Applications: Oxirane"

[2] A. Wurtz, Justus Liebigs, *Ann. Chem.*, **110**, 125 (1859).

[3] T. E. Lefort, *Societé Française de Catalyse Généralisée*, FR 729 952, 1931 ; 739 562, (1931).

II *Troubleshooting Time-Dependent Density-Functional Theory for Photochemical Applications: Oxirane*

Troubleshooting Time-Dependent Density-Functional Theory for Photochemical Applications: Oxirane

Felipe Cordova, L. Joubert Doriol, Andrei Ipatov, and Mark E. Casida[1]
Équipe de Chimie Théorique,
Laboratoire d'Etudes Dynamiques et Structurales de la Sélectivité (LEDSS), UMR CNRS/UJF 5616,
Institut de Chimie Moléculaire de Grenoble (ICMG, FR-2607),
Université Joseph Fourier (Grenoble I),
301 rue de la Chimie, BP 53,
F-38041 Grenoble Cedex 9,
FRANCE

Claudia Filippi[2]
Instituut-Lorentz for Theoretical Physics,
Universiteit Leiden, Niels Bohrweb 2, Leiden, NL-2333 CA,
THE NETHERLANDS

Alberto Vela
Departamento de Química,
Cinvestav,
Avenida Instituto Politécnico Nacional 2508,
A.P. 14-740 Mexico D.F. 07000,
MEXICO

[1]Mark.Casida@UJF-Grenoble.Fr
[2]filippi@lorentz.leidenuniv.nl

Abstract

The success of Car-Parrinello (CP) density-functional theory (DFT) molecular dynamics calculations for thermochemical reactions has generated interest in the extension of CP-like calculations to photochemical reactions through the use of time-dependent DFT (TDDFT). Although TDDFT is a formally rigorous way to obtain excitation energies, practical calculations involve the use of approximate functionals. In particular conventional TDDFT makes use of the adiabatic approximation which assumes that the exchange-correlation potential reacts instantaneously and without memory to any temporal change in the charge density, thus allowing TDDFT to make use of the same approximate exchange-correlation functionals as in regular time-independent ground state DFT. The development of analytic gradient methodology for excited states within conventional TDDFT, either with or without the Tammm-Dancoff approximation (TDA) is making possible TDDFT modeling of photochemical reactions. We demonstrate in the rather idealized case of the symmetric (Woodward-Hoffmann) CC ring opening of oxirane that, far from being an approximation, the TDA is a practical necessity for avoiding triplet instabilities and singlet near instabilities, thus helping maintain energetically reasonable excited-state potential energy surfaces (PESs) during bond breaking. Other more minor difficulties are pointed out with modeling oxirane photochemistry via CP-like TDDFT TDA photodynamics modeling. However none of these difficulties seem likely to prevent a qualitatively correct TDDFT TDA description of photochemistry in this molecule.

I Introduction

A complete understanding of photochemistry often requires photodynamics calculations. Although also true for thermal reactions, this statement is even more so for photochemical reactions since (i) such reactions often have excess energy and so need not follow the lowest energy pathway and since (ii) it is often dynamical, as much as energetic, considerations which govern how a photochemical reaction jumps from one electronic potential energy surface (PES) to another. Unfortunately full photodynamics calculations are prohibatively expensive for all but the smallest molecules unless simplifying approximations are made. One such approximation is that of mixed quantum/classical calculations which treat the electronic degrees of freedom quantum mechanically and the nuclear degrees of freedom classically. Except for the smallest molecules where calculations can make use of potential energy surfaces fit to a mixture of quantum mechanical calculations and experimental data,

the quantum part of mixed quantum/classical photochemical dynamics calculations is usually done on-the-fly at each point of the classical trajectory yet nevertheless remains a computational bottleneck of this type of approach. The success of density-functional theory (DFT) for extrapolating *ab initio* accuracy to molecular systems too large to treat with conventional *ab initio* theory and its time-dependent extension (TDDFT) which provides a way to calculate excitation energies seems to offer an accurate but relatively inexpensive alternative to more costly quantum chemical approaches for on-the-fly electronic structure calculations. However mixed TDDFT/classical dynamics methods are not yet a standard part of the computational chemistry repertory. This is because basic methodology is only just beginning to come on line, problems are being identified, and undoubtedly modifications in the basic mixed TDDFT/classical dynamics methods will be necessary in order to enlarge the class of problems to which this method can eventually be applied. It is the objective of this article to identify the most critical points where improvement needs to be made, at least for one molecule and one type of reaction path, in order to help move mixed TDDFT/classical dynamics from a dream to an off-the-shelf reality.

It is not our purpose here to review DFT-based mixed quantum/classical dynamics since Doltsinis and Marx did this so well in their recent review [1]. We will also not be reporting the results of mixed TDDFT/classical dynamics in this paper. But we would like to say a little bit about this approach since it is a primary motivation for the present work. Suffice it to say that what we have in mind by mixed TDDFT/classical dynamics is *not* the already well-established and widely applied Ehrenfest dynamics (also called eikonal or mean-field dynamics) [2, 3, 4, 5, 6, 7]. Rather we have in mind some variation on Tully's surface hopping (SH) method [8, 9] because of its potential for giving a more detailed state-by-state description of photochemical dynamics and because of its potential ultimately also to say something about branching yields. In order to implement the SH method, analytic derivatives are needed for excited-state PESs as are hopping integrals for moving between the surfaces. Progress has been made on these two approaches. Analytic derivatives are now available for TDDFT excited states both for conventional TDDFT [10, 11, 12, 13] and within the Tamm-Dancoff approximation (TDA) [14, 13]. The calculation off hopping integrals within TDDFT is a more challenging problem but here also important practical progress is being made [15, 16, 17, 18, 19, 20]. Indeed first applications of mixed TDDFT/classical SH dynamics are being reported [17, 19, 20]

Although most applications of TDDFT have been primarily to the calculation

of absorption spectra, there were a few applications of TDDFT to photochemical problems without the use of dynamics. Three particularly interesting studies from the applications point of view include a study of the femtochemistry of Norrish type-I reactions [21, 22, 23, 24], a theoretical study of firefly bioluminescence [25], and a study of the photoinduced keto-enol tautomerization of 9-methyl guanine [26]. A few attempts were made to assess the value of TDDFT for photochemical applications, some reporting encouraging results [27, 28, 29], and others discouraging results [30, 31, 32, 33, 34].

The fundemental reasons for these descrepencies stem from the fact that conventional TDDFT has several problems which may or may not be fatal for modeling a given photochemical reaction. The main difficulties encountered in conventional TDDFT include: (i) underestimation of the ionization threshold [27], (ii) underestimation of charge transfer excitations [35, 36, 37], and (iii) lack of explicit two- and higher-electron excitations [38, 39, 40, 41]. Still other difficulties are discussed in pertinant reviews [42, 43, 44, 45, 46, 47, 48].

It is clear that TDDFT must continue to evolve before it becomes a reliable "black-box" tool for modeling photochemical reactions. At the same time, we would like to concenntrate on solving the most severe problems first and for this we must first obtain a clear idea of what is the most severe problem or are the most severe problems of TDDFT for modeling photochemistry in specific photochemical reactions or classes of photochemical reactions.

The reaction chosen for our study is the photochemical ring opening of oxirane. In this paper we will study symmetric ring opening of this molecule. This is not because the photochemical ring opening follows a symmetric pathway. [It does *not* (Appendix VII).] Rather our reason is the usual reason [49], namely that the use of symmetry greatly facilitates analysis and hence the construction of and comparison with highly accurate quantum Monte Carlo results. A mixed quantum/classical dynamics study of asymmetric ring opening will be reported elsewhere [50].

In the next section, we give a brief review of DFT and of TDDFT. In sec. III, we review the formalism behind the more exact theory against which we will be comparing our TDDFT results. Computational details are given in Sec. IV. Section V reports our results and discussion and Sec. VI summarizes.

II (Time-Dependent) Density-Functional Theory

It is the purpose of this section to give a brief review of the most essential ideas needed to understand our construction of (TD)DFT PESs. In principle, calculating a PES means first solving the N-electron problem in the Born-Oppenheimer approximation to obtain the Ith electronic excitation energy, $E_I(\mathbf{R}_1, \mathbf{R}_2, \ldots, \mathbf{R}_N)$, at the nuclear configuration, $(\mathbf{R}_1, \mathbf{R}_2, \ldots, \mathbf{R}_N)$. Adding the nuclear repulsion energy gives the associated PES,

$$\begin{aligned} V_I(\mathbf{R}_1, \mathbf{R}_2, \cdots, \mathbf{R}_N) &= E_I(\mathbf{R}_1, \mathbf{R}_2, \cdots, \mathbf{R}_N) \\ &+ \sum_{I \leq J} \frac{Z_I Z_J}{|\mathbf{R}_I - \mathbf{R}_J|}, \end{aligned} \tag{6.1}$$

given here in hartree atomic units ($\hbar = m = e = 1$). By (TD)DFT, we mean the calculation of the ground state PES from the DFT electronic energy, $E_0(\mathbf{R}_1, \mathbf{R}_2, \ldots, \mathbf{R}_N)$, and excited-state PESs from the TDDFT excitation energies, $\omega_I(\mathbf{R}_1, \mathbf{R}_2, \ldots, \mathbf{R}_N)$. Thus the (TD)DFT PES for the Ith electronic excited state corresponds to the electronic energy,

$$\begin{aligned} E_I(\mathbf{R}_1, \mathbf{R}_2, \ldots, \mathbf{R}_N) &= E_0(\mathbf{R}_1, \mathbf{R}_2, \ldots, \mathbf{R}_N) \\ &+ \omega_I(\mathbf{R}_1, \mathbf{R}_2, \ldots, \mathbf{R}_N). \end{aligned} \tag{6.2}$$

It is already clear from this formula that problems with the ground state PES can easily become problems for the excited-state PESs. Let us briefly review the calculation of E_0 and ω_I, dropping the explicit dependence on the nuclear configuration.

The simplest methods for treating the ground-state electronic structure problem are the Hartree-Fock method and the Kohn-Sham formulation of DFT. In recent years, the use of hybrid functionals has permitted the two energy expressions to be written in the same well-known form,

$$\begin{aligned} E &= \sum_{i\sigma} n_{i\sigma} \langle \psi_{i\sigma} | \hat{h}_c | \psi_{i\sigma} \rangle \\ &+ \frac{1}{2} \int\int \frac{\rho(\mathbf{r}_1)\rho(\mathbf{r}_2)}{r_{12}} d\mathbf{r}_1 d\mathbf{r}_2 + E_{xc}[\rho_\uparrow, \rho_\downarrow] \\ &- c_x \left(E_x[\rho_\uparrow, \rho_\downarrow] + \sum_\sigma \int\int \frac{|\gamma_\sigma(\mathbf{r}_1, \mathbf{r}_2)|^2}{r_{12}} d\mathbf{r}_1 d\mathbf{r}_2 \right). \end{aligned} \tag{6.3}$$

where $\hat{h}_c$ is the usual core hamiltonian comprised of the kinetic energy term and external potential interaction energy. The coefficient c_x controls the amount of Hartree-Fock exchange, being unity for Hartree-Fock, zero for pure DFT, and fractional (typically around 0.25 [51]) for hybrid functionals. The spin-σ density matrix,

$$\gamma_\sigma(\mathbf{r}_1, \mathbf{r}_2) = \sum_{i\sigma} n_{i\sigma} \psi^*_{i\sigma}(\mathbf{r}_1) \psi_{i\sigma}(\mathbf{r}_2)\,, \tag{6.4}$$

spin-σ density,

$$\rho_\sigma(\mathbf{r}) = \gamma_\sigma(\mathbf{r}, \mathbf{r})\,, \tag{6.5}$$

and charge density,

$$\rho(\mathbf{r}) = \sum_\sigma \rho_\sigma(\mathbf{r})\,, \tag{6.6}$$

are all functions of N orthonormal spin-orbitals, $\psi_{i\sigma}$, with occupations, $n_{i\sigma}$. Minimizing the energy expression (6.3) gives the well-known Kohn-Sham (Hartree-Fock) orbital Schrödinger equation,

$$\begin{aligned} & \left[-\frac{1}{2}\nabla_1^2 + v_{ext}(\mathbf{r}_2) + \int \frac{\rho(\mathbf{r}_2)}{r_{12}}\, d\mathbf{r}_2 + v^\sigma_{xc}[\rho_\uparrow, \rho_\downarrow](\mathbf{r}_1)\right] \psi_{i\sigma}(\mathbf{r}_1) \\ - \;& c_x \left(v^\sigma_x[\rho_\uparrow, \rho_\downarrow](\mathbf{r}_1) \psi_{i\sigma}(\mathbf{r}_1) + \int \frac{\gamma_\sigma(\mathbf{r}_1, \mathbf{r}_2)}{r_{12}} \psi_{i\sigma}(\mathbf{r}_2)\, d\mathbf{r}_2 \right) \\ = \;& \epsilon_{i\sigma} \psi_{i\sigma}(\mathbf{r}_1)\,. \end{aligned} \tag{6.7}$$

A variety of approximate density functionals are available. The reader seeking additional information about DFT is refered to any one of a number of useful reviews [52, 53, 54].

Time-dependent density-functional theory offers a rigorous density-functional approach to calculating excition energies. The reader should keep two things in mind when reading what follows. The first is that, unlike time-dependent Hartree-Fock (TDHF), TDDFT is formally exact. This formal exactness means that, although approximate exchange-correlation functionals must be used in practice, we can hope that good approximations will lead to better results than those obtained from TDHF which lacks correlation effects present in TDDFT. Indeed this often seems to be the case. Secondly the reader is asked to bear in mind that the prevalent use of hybrid functionals means that in practice TDDFT contains TDHF as a particular choice of functional (i.e., the exchange-only hybrid functional with $c_x = 1$).

Since TDDFT is still relatively new compared to some of the other methods described above, we give a brief formal introduction. The Runge-Gross theorems [55] are to TDDFT what the Hohenberg-Kohn theorems are to conventional (static,

ground-state) DFT. Although some modification of the original theorems has proven necessary, the basic theorems have held up remarkably well. Imagine a molecule, initially in its ground stationary state, subjected to a time-dependent electric field. Then the first Runge-Gross theorem tells us that the (time-dependent) external potential is determined up to an additive function of time by the (time-dependent) ground-state charge density. The second theorem tells us that the charge density may be determined via a density-dependent action which is now recognized to be of the Keldysh type rather than of the originally proposed Frenkel type [56]. The most common implementation of TDDFT is via a Kohn-Sham formalism using the so-called adiabatic approximation which assumes that the self-consistent field responds instantaneously and without memory to any temporal change in the charge density. This allows the time-dependent exchange-correlation action quantity in TDDFT to be replaced with the more familiar exchange-correlation energy from conventional TDDFT. Excitations may be obtained from the linear response formulation of TDDFT (LR-TDDFT). A key quantity in LR-TDDFT is the exchange-correlation kernel,

$$f_{xc}^{\sigma,\tau}(\mathbf{r},\mathbf{r}') = \frac{\delta^2 E_{xc}[\rho_\uparrow,\rho_\downarrow]}{\delta\rho_\sigma(\mathbf{r})\delta\rho_\tau(\mathbf{r}')}\,, \tag{6.8}$$

which, along with the Hartree kernel,

$$f_{H}^{\sigma,\tau}(\mathbf{r},\mathbf{r}') = \frac{1}{|\mathbf{r}-\mathbf{r}'|}\,, \tag{6.9}$$

and the Hartree-Fock exchange kernel (whose integrals can be written in terms of the Hartree kernel) determines the linear response of the Kohn-Sham self-consistent field in the adiabatic approximation. In Casida's formulation [38], the excitation energies are obtained by solving a random phase approximation (RPA)-like pseudo-eigenvalue equation,

$$\begin{bmatrix} \mathbf{A} & \mathbf{B} \\ \mathbf{B} & \mathbf{A} \end{bmatrix} \begin{pmatrix} \vec{X}_I \\ \vec{Y}_I \end{pmatrix} = \omega_I \begin{bmatrix} +\mathbf{1} & \mathbf{0} \\ \mathbf{0} & -\mathbf{1} \end{bmatrix} \begin{pmatrix} \vec{X}_I \\ \vec{Y}_I \end{pmatrix}\,, \tag{6.10}$$

where the matrices $\mathbf{A}$ and $\mathbf{B}$ are defined by,

$$\begin{aligned} A_{ia\sigma,jb\tau} &= \delta_{i,j}\delta_{a,b}\delta_{\sigma,\tau}\left(\epsilon_{a\sigma}-\epsilon_{i\sigma}\right) + (ia|f_H|bj) + (ia|f_{xc}^{\sigma,\tau}|bj) \\ &- c_x\delta_{\sigma,\tau}\left[(ij|f_H|ba) + (ia|f_x^{\sigma,\sigma}|bj)\right] \\ B_{ia\sigma,bj\tau} &= (ia|f_H|jb) + (ia|f_{xc}^{\sigma,\tau}|jb) \\ &- c_x\delta_{\sigma,\tau}\left[(ib|f_H|ja) + (ia|f_x^{\sigma,\sigma}|jb)\right]\,, \end{aligned} \tag{6.11}$$

and the integrals are in Mullikan charge cloud notation,

$$(pq|f|rs) = \int\int \psi_p^*(\mathbf{r})\psi_q(\mathbf{r})f(\mathbf{r},\mathbf{r}')\psi_r^*(\mathbf{r}')\psi_s(\mathbf{r}')\,d\mathbf{r}d\mathbf{r}'\,. \tag{6.12}$$

It is to be emphasized that the TDDFT adiabatic approximation includes only dressed one-electron excitations [38, 41]. This is particularly easy to see in the context of the Tamm-Dancoff approximation (TDA) to Eq. (6.10) whose TDDFT variant is usually attributed to Hirata and Head-Gordon [57]. The TDA simply consists of neglecting the **B** matrices to obtain,

$$\mathbf{A}\vec{X}_I = \omega_I\vec{X}_I\,. \tag{6.13}$$

The number of possible solutions to this equation is the dimensionality of **A** which is just the number of single excitations. In fact, the LR-TDHF TDA (exchange-only hybrid functional with $c_x = 1$) is simply the well-known configuration interaction singles (CIS) method.

An issue of great importance in the context of the present work is triplet instabilities. These have been first analyzed by Bauernschmitt and Ahlrichs [58] in the context of DFT, but the explicit association with LR-TDDFT excitation energies was made later [36, 42]. Following Ref. [42], we suppose that the ground-state DFT calculation has been performed using a same-orbitals-for-different-spin (SODS) ansatz and we now wish to test to see if releasing the SODS restriction to give a different-orbitals-for-different-spin (DODS) solution will lower the energy. To do so we consider an arbitary unitary tranformation of the orbitals,

$$\psi_{r\sigma}^{\lambda}(\mathbf{r}) = e^{i\lambda\left(\hat{R}+i\hat{I}\right)}\psi_{r\sigma}(\mathbf{r})\,, \tag{6.14}$$

where $\hat{R}$ and $\hat{I}$ are real operators. The corresponding energy expression is,

$$E_\lambda = E_0 + \lambda^2\left[\vec{R}^\dagger\left(\mathbf{A}-\mathbf{B}\right)\vec{R} + \vec{I}^\dagger\left(\mathbf{A}+\mathbf{B}\right)\vec{I}\right] + \mathcal{O}(\lambda^3)\,, \tag{6.15}$$

where matrix elements of the $\hat{R}$ and $\hat{I}$ operators have been arranged in column vectors and the $\mathcal{O}(\lambda)$ term disappears because the energy has already been minimized before considering symmetry-breaking. The presence of the terms $(\mathbf{A}\pm\mathbf{B})$ shows the connection with the pseudoeigenvalue problem (6.10) which can be rewritten as the eigenvalue problem,

$$\left(\mathbf{A}+\mathbf{B}\right)\left(\mathbf{A}-\mathbf{B}\right)\vec{Z}_I = \omega_I^2\vec{Z}_I\,. \tag{6.16}$$

Since excitation energies are real, one would expect that, within the realm of validity of the adiabatic approximation, $\omega_I^2 \geq 0$. However imaginary excitation energies are sometimes found for approximate exchange-correlation functionals. Equation (6.16) makes it clear that such imaginary excitation energies correspond to negative eigenvalues of one of the two $(\mathbf{A} \pm \mathbf{B})$ matrices and hence to the energy lowering by symmetry breaking. In pure DFT, the matrix $(\mathbf{A} + \mathbf{B})$ is always positive definite and symmetry breaking is associated with imaginary triplet excitation energies – hence the name triplet instabilities. In principle, when hybrid functionals are used, singlet instabilities are also possible.

Thus imaginary excitation energies in LR-TDDFT should be taken as an indication that something is wrong in the description of the ground state whose time-dependent response is being used to obtain those excitation energies. As pointed out in Ref. [36] and in Ref. [59], the TDA actually acts to *decouple* the excited-state problem from the ground-state problem so that TDA excited state energies may actually be *better* than full LR-TDDFT excited-state energies. Typically full and TDA LR-TDDFT excitation energies are close near a molecule's equilibrium geometry, where a single-determinantal wave function is a reasonable first approximation and begin to differ as single-determinantal approximation breaks down.

Interestingly, there is a very simple argument against symmetry breaking in exact DFT for molecules with a nondegenerate ground state. It is based on the fact that the exact ground-state wave function of these molecules is a singlet belonging to the totally symmetric representation and so has the same symmetry as the molecule. Since the exact ground-state wave function is a singlet, the spin-up and spin-down charge densities will be equal,

$$\rho_\uparrow(\mathbf{r}) = \rho_\downarrow(\mathbf{r}) = \rho(\mathbf{r})/2\,, \tag{6.17}$$

and also have the same symmetry as the molecule. It follows that the spin-up and spin-down components of the exact exchange-correlation potential,

$$v_{xc}^{\uparrow}[\rho_\uparrow, \rho_\downarrow](\mathbf{r}) = v_{xc}^{\downarrow}[\rho_\uparrow, \rho_\downarrow](\mathbf{r}) = v_{xc}^{(\uparrow,\downarrow)}[\rho/2, \rho/2](\mathbf{r})\,, \tag{6.18}$$

must be equal and have the same symmetry as the molecule. Since the potentials are the same for different spins, then the molecular orbitals must also be the same for different spins. Thus no symmetry breaking is expected in exact DFT for molecules with a nondegenerate ground state.

Note however that the functional is still dependent on spin so that the parallel

and antiparallel spin kernels are different,

$$\begin{aligned} f_{xc}^{\uparrow,\uparrow}(\mathbf{r},\mathbf{r}') &= \frac{\delta^2 E_{xc}}{\delta\rho_\uparrow(\mathbf{r})\delta\rho_\uparrow(\mathbf{r}')} \\ \neq \quad f_{xc}^{\uparrow,\downarrow}(\mathbf{r},\mathbf{r}') &= \frac{\delta^2 E_{xc}}{\delta\rho_\uparrow(\mathbf{r})\delta\rho_\downarrow(\mathbf{r}')}\,. \end{aligned} \tag{6.19}$$

The interested reader will find additional information about TDDFT in a recent book based upon two summer schools on the subject [48].

III Quantum Monte Carlo

We will be judging the quality of our (TD)DFT calculations against high-quality quantum Monte Carlo (QMC) results. These results were obtained by a three step procedure for each state of interest. The first step towards calculating the Ith excited state consists of a conventional complete active space (CAS) self-consistent field (SCF) calculation. The resultant CASSCF wave function, $\Psi_I^{\rm CAS}$, is then used in a a variational Monte Carlo (VMC) calculation to include dynamic correlation via the inclusion of Jastrow factors. Finally the VMC wave function is further improved via diffusion Monte Carlo (DMC).

Even though the Hartree-Fock determinant is often (but not always) a reasonable first approximation to the true wave function at the equilibrium geometry of a molecule, this is not true everywhere on the ground state potential energy surface. For example, the wave function for the transition state of a chemical reaction is often best described as a linear combination of two wave functions, one describing the reactant and the other describing the product. In the CASSCF method, the orbital space is divided into an active space of orbitals whose occupancy is allowed to vary, with the occupancy of all other orbitals fixed as either doubly occupied or unoccupied. In a CASSCF(n,m) calculation, n electrons are distributed among an active space of m orbitals to make all possible space- and symmetry-adapted configuration state functions (CSFs). The final CASSCF(n,m) wave function consists of a linear combination of these CSFs.

In the present article we will be considering 4 electrons in an active space of 6 orbitals. Thus, the CASSCF wave function contains up to quadruple excitations, This is like a full configuration interaction (CI) calculation for n electrons in m orbitals, except that the orbitals themselves are also simultaniously optimized so as to minimize the total energy. In our case, unlike the Hartree-Fock method, which frequently lacks sufficient flexibility to give an adequate minimal description

of excited-state electron correlation, the CASSCF method is adequate for describing the lowest state of each symmetry.

When several states are requested which have the same symmetry, there is a danger that the variational procedure will favor the description of the ground state over that of the excited states, thus giving an unbalanced description of excitation energies. This is often handled by using a state averaged (SA) CASSCF which uses the same orbitals for all N-electron states [60]. According to the Hylleraas-Undheim theorem (also known as Cauchy's interlace theorem, see Ref. [61], p. 115-117), the energy of the Ith state obtained from SA-CASSCF will be an upperbond for the true energy of the Ith state. However the lowest SA-CASSCF energy will still be higher than the CASSCF energy obtained without SA. The only time we needed to apply the SA procedure in the present work was for the 2^1A_1 state in the C_{2v} ring opening. Although we found that the CASSCF and SA-CASSCF 1^1A_1 energies were really very close, we have prefered to take maximum advantage of possible error cancellations occuring in the SA approach due to the use of the same orbitals for the ground and excited state. Thus we calculated the 2^1A_1 energy as,

$$\begin{aligned} E(2^1A_1) &= E_{\mathrm{CAS}}(1^1A_1) \\ &+ \left[E_{\text{SA-CAS}}(2^1A_1) - E_{\text{SA-CAS}}(1^1A_1)\right] . \end{aligned} \tag{6.20}$$

(A similar procedure was used in the case of the corresponding QMC calculations to be described below.) A detailed technical description of multiconfigurational self-consistent field theory may be found in Chapter 12 of Ref. [61].

Compared to conventional highly-correlated *ab initio* methods, quantum Monte Carlo (QMC) [62] has a more favorable scaling with the number of electrons and can therefore provide an accurate description of both dynamical and static electronic correlation for relatively large systems. Although oxirane is a relatively small molecule, it must be kept in mind that we will use QMC to calculate 9 states at 9 geometries, for a total of 81 highly-correlated calculations, and hence that efficiency is important. The key ingredient which determines the quality of a QMC calculation is the many-body trial wave function which, in the present work, is chosen of the Jastrow-Slater type with the particular form,

$$\Psi_I^{\mathrm{VMC}} = \Psi_I^{\mathrm{CAS}} \prod_{A,i,j} \mathcal{J}(r_{ij}, r_{iA}, r_{jA}) , \tag{6.21}$$

where r_{ij} denotes the distance between electrons i and j, and r_{iA} the distance of

electron i from nucleus A. We use here a Jastrow factor $\mathcal{J}$ which correlates pairs of electrons and each electron separately with a nucleus, and employ different Jastrow factors to describe the correlation with different atom types. The determinantal components consists of a CAS expansion and includes all possible CSFs which are obtained by considering 4 electrons in the active space of 6 orbitals and are compatible with the spacial symmetry of the state of interest I.

All parameters in both the Jastrow and the determinantal component of the wave function are optimized by minimizing the energy, that is, the expectation value of the Hamiltonian on the trial wave function. Since the optimal orbitals and expansion coefficients in Ψ_I^{CAS} may differ from the CASSCF values obtained in the absence of the Jastrow factor $\mathcal{J}$, it is important to reoptimize them in the presence of the Jastrow component.

For a wave function corresponding to the lowest state of a given symmetry, we follow the energy-minimization approach of Ref. [63]. If the excited state is not the lowest in its symmetry, we obtain the Jastrow and orbitals parameters which minimize the average energy over the state of interest and the lower states, while the linear coefficients in the CSF expansion ensure that orthogonality is preserved among the states [64]. Therefore, the wave functions resulting from the state-average optimization will share the same Jastrow parameters and the same set of orbitals but have different linear coefficients. This scheme represents a generalization of the approach of Ref. [65] where only the orbitals were optimized and orthogonality was only approximately preserved. The present approach is therefore superior to the one of Ref. [65], which was however already giving excellent results when tested on several singlet states of ethylene and a series of prototypical photosensitive molecules [65, 66]. We note that, when a CAS expansion is used in the absence of the Jastrow component, the method is analogous to the CASSCF technique for the lowest state of a given symmetry, and to a SA-CASSF approach if the excited state is not the lowest in its symmetry.

The trial wave function is then used in diffusion Monte Carlo (DMC), which produces the best energy within the fixed-node approximation [i.e., the lowest-energy state with the same zeros (nodes) as the trial wave function]. All QMC results presented are from DMC calculations.

Reference [62] provides a nice review of QMC, even if oriented towards applications in solids.

IV Computational Details

A SCF and TD Details

Calculations were carried out with two different computer programs, namely GAUSSIAN [67] and deMon2k [68]. Both programs carry out DFT calculations in a similar way. Expansion of the molecular orbitals in a gaussian-type basis set allows most of the necessary integrals to be evaluated analytically. The exception to this rule are the exchange-correlation integrals which make DFT different from Hartree-Fock theory. These are evaluated by direct numerical integration over a grid in real space.

The two programs do differ in some ways which are important for this work. GAUSSIAN can carry out Hartree-Fock calculations while deMon2k, which has no Hartree-Fock exchange, cannot. Similarly GAUSSIAN can carry out time-dependent Hartree-Fock (TDHF) and Configuration Interaction Singles (CIS) calculations which are not implemented in deMon2k. In contrast, the Tamm-Dancoff approximation (TDA) for TDDFT may only be performed with deMon2k and not with Gaussian. The present version of deMon2k is limited to the local density approximation for the exchange-correlation kernel used in TDDFT calculations, while the kernel is more general in GAUSSIAN. Another important difference is that a charge-density fitting technique is used routinely in deMon2k to avoid evaluating more than three-center integrals. This is also an option in GAUSSIAN, though we have chosen not to use this option in the present study. However even when used, the use of charge-density fitting is more extensive in deMon2k where the density is expanded in an auxiliary basis set not only to evaluate Coulomb-type integrals but also as an aid in evaluating exchange-correlation integrals. GAUSSIAN makes automatic use of symmetry and prints out the irreducible representation for each molecular orbital. The particular version of deMon2k used in the present work does not have this feature so we rely on comparison with the output of GAUSSIAN calculations for this aspect of our analysis. Thus the deMon2k and GAUSSIAN programs are used in a complementary fashion in the present study.

GAUSSIAN calculations were carried out with version 03 of that program. All the results reported here were calculated with the extensive 6-311++G**(2d,2p) orbital basis set [69, 70] which is part of the standard GAUSSIAN library. All calculations used default convergence criteria. The DFT calculations used the default grid.

deMon2k calculations were carried out with version 1.7 of that program. The same orbital basis set was used as in the Gaussian calculations. The GEN-A3* density-fitting basis set was used and density-fitting was carried out without impos-

ing the charge conservation constraint. The SCF convergence cutoff was set at 10^{-7}. We always use the FIXED FINE option for the grid. Extensive use was made of a variant of Eric Cancès optimal damping algorithm (ODA) [71], called the optimal mixing algorithm (OMA) in deMon2k, without which many of our DFT calculations would have been much more difficult to converge (see the deMon2k user guide for the basic OMA equations). Our implementation of TDDFT in deMon2k is described in Ref. [72].

Two different density functionals were used. The first is the local density approximation (LDA) using the parameterization of Vosko, Wilk, and Nusair [73] (referred to as SVWN5 in the Gaussian input). The second is the popular B3LYP hybrid functional [74]. The corresponding TDDFT calculations are referred to as TDLDA and TDB3LYP respectively.

B CAS Details

Most of the CASSCF calculations are performed with the program GAMESS(US) [75]. In all SA-CASSCF calculations, equal weights are employed for the two states.

We use scalar-relativistic energy-consistent Hartree-Fock pseudopotentials [76] where the carbon and oxigen $1s$ electrons are replaced by a non-singular s-non-local pseudopotential and the hydrogen potential is softened by removing the Coulombic divergence. We employ the Gaussian basis sets [76] constructed for these pseudopotentials and augment them with diffuse functions. All calculations are performed with the cc-TZV contracted $(11s11p1d)/[3s3p1d]$ basis for carbon and oxygen, augmented with two additional diffuse s and p functions with exponents 0.04402 and 0.03569 for carbon, and 0.07376 and 0.05974 for oxygen. The d polarization functions for carbon and oxygen are taken from the cc-DZV set. For hydrogen, the cc-DZV contracted $(10s9p)/[2s1p]$ basis is augmented with one s diffuse function with exponent 0.02974.

C QMC Details

The program package CHAMP [77] is used for the QMC calculations. We employ the same pseudopotentials and basis sets as in the CASSCF calculations (see Sec. B).

Different Jastrow factors are used to describe the correlation with a hydrogen, an oxygen and a carbon atom. For each atom type, the Jastrow factor consists of an exponential of the sum of two fifth-order polynomials of the electron-nuclear and the electron-electron distances, respectively [78]. The parameters in the Jastrow

factor and in the determinantal component of the wave function are simultaneously optimized by energy minimization following the scheme of Ref. [63], where we employ the simple choice $\xi = 1$. For the excited states with the same symmetry as the ground state, the ground- and excited-state wave functions are optimized in a state-average manner with equal weights for both states [64]. An imaginary time step of 0.075 H^{-1} is used in the DMC calculations.

D Geometries

Three types of calculations were carried out. The purpose of the first type of calculation was the investigation of vertical excitation spectra. To this end, the equilibrium geometry was optimized at the HF, LDA, and B3LYP levels, and vertical excitation spectra were calculated using the TDHF, CIS, TDB3LYP, TDLDA, and TDLDA TDA methods. The initial (unopened ring) oxirane has a C_{2v} symmetry. Labels of the irreducible representations depend upon the labels of the x, y, and z coordinates. In this article, the COC ring lies in the (y, z)-plane and the z-axis coincides with the C_2 axis, in agreement with the IUPAC convention [79]

The purpose of the second type of calculation was an investigation of orbital and state energy levels as the O-C-O angle is opened, keeping C_{2v} geometry, and relaxing all other parameters in the ground electronic state. This is where we make the most detailed comparison between different levels of computation, aided in our assignments by the high symmetry of the reaction pathway.

The purpose of the third and final group of calculations is to investigate the conrotatory and disrotatory pathways for CC ring opening. The geometries are heavily constrained in that (i) the OCH_2 groups are constrained to be planar and (ii) the pathway for ring opening has either C_2 or C_s symmetry. Within these constraints the O-C-O angle and the H-C-O-C dihedral angle are varied while the CO and CH bond lengths are relaxed in the ground electronic state.

V Results

The Woodward-Hoffmann (WH) model for orbital control of symmetry in electrocyclic reactions is described in many advanced organic chemistry courses. These rules were an important motivation in the 1970s and 1980s to seek stereospecific photochemical ring-opening reactions of oxiranes [80, 81, 82, 83, 84, 85]. Seen from the point of view that the WH rules should already be familiar to many readers and that some oxiranes (notably diphenyl oxirane) do appear to follow the WH rules for

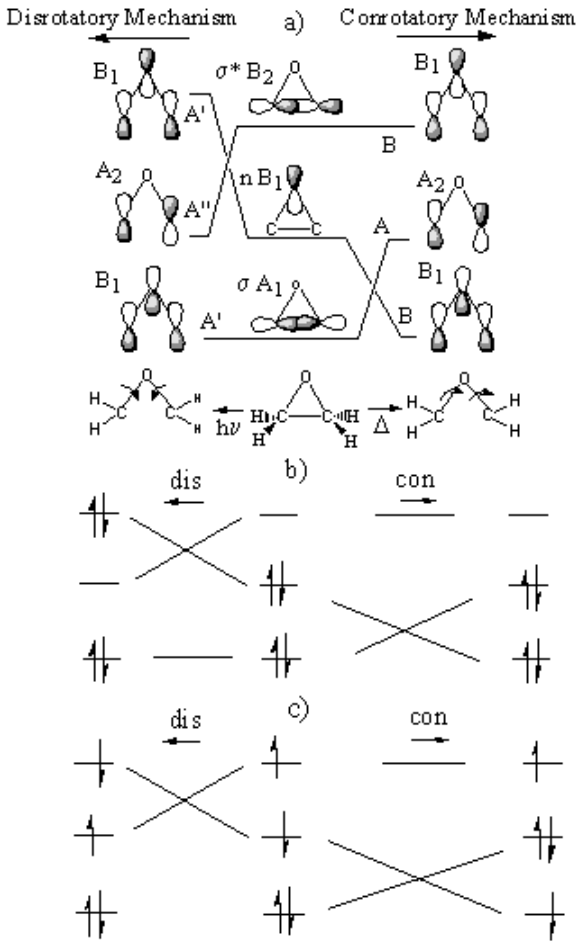

Figure 6.1: a) Woodward-Hoffmann orbital correlation scheme. Symmetry labels are for the C_{2v} point group in the case of reactants and products, for the C_s point group along the disrotatory pathway, and for the C_2 point group along the conrotatory pathway. b) Thermal ring opening. c) Photochemical ring opening.

thermal and photochemical ring opening, the WH rules might seem like the obvious place to begin our study of symmetric ring opening pathways in oxirane. This is somewhat counterbalanced by the fact that oxirane itself is an exception to the WH rules for photochemical ring opening and by the fact that it is now clear that the WH rules do not apply nearly as well to photochemical reactions as to thermal reactions (Appendix VII). Nevertheless we will take the WH model as a first approximation for understanding and begin by describing the model for the particular case of oxirane.

Many models at the time that Woodward and Hoffmann developed their theory [86, 88, 87] were based upon simple Hückel-like π-electron models, so it is not surprising that the historical WH model for oxirane uses a three-orbital model consisting of one p-orbital on each of the oxygen and two carbon atoms. (See Fig. 6.1.) Elementary chemical reasoning predicts that the closed cycle should form three molecular orbitals, σ, n, σ^*, in increasing order of energy. Similarly the open structure has the "particle-in-a-box" orbitals familiar from simple Hückel theory. Woodward and Hoffmann observed that a reflection plane (σ) of symmetry is preserved along the disrotatory reaction pathway while a C_2 rotatation symmetry element is preserved along the conrotatory reaction pathway. This observation allows the reactant-product molecular orbital correlation diagram to be completed by using the fact that the symmetry representation of each orbital is preserved within the relevant symmetry group of the molecule along each reaction path (WH principle of conservation of orbital symmetry) and connecting lowest orbitals with lowest orbitals. Figure 6.1 shows that a conrotatory (*con*) thermal reaction connects ground-state configurations in the reactant and product while a disrotatory (*dis*) thermal reaction connects the reactant ground-state configuration with an electronically excited-state configuration. Thus the *con* thermal reaction is expected to be prefered over the *dis* reaction. Also shown in Fig. 6.1 is the photochemical reaction beginning with the $n \rightarrow \sigma^*$ excited state. In this case, the *dis* mechanism is expected to be prefered since the *con* mechanism leads to a still higher level of excitation in the product than in the reactant molecule while the level of excitation is preserved along the *dis* pathway.

Let us now see how this orbital model is or is not reflected first in the vertical absorption spectrum of oxirane, then in the C_{2v} ring opening pathway, and finally in the *con* and *dis* ring-opening pathways. At each step the performance of (TD)DFT will be assessed against experiment and against other levels of theory.

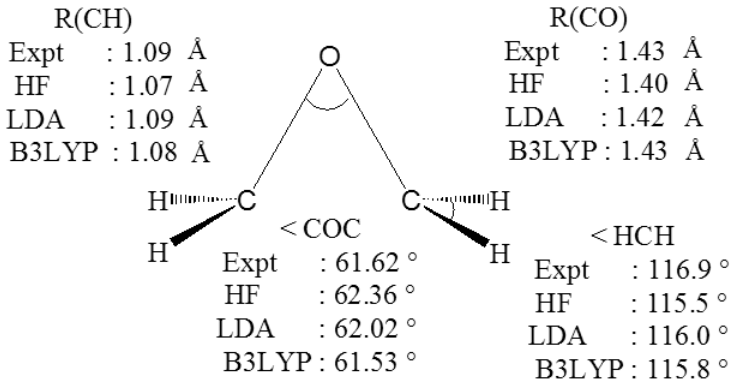

Figure 6.2: Comparison of HF/6-311G**(2d,2p), B3LYP/6-311G**(2d,2p), and LDA/6-311G**(2d,2p) optimized geometries with the experimental gas phase geometry from Ref. [89]. Note that the structure has C_{2v} symmetry.

A Absorption Spectrum

The first step towards calculating the electronic absorption spectrum of oxirane is the optimization of the geometry of the gas phase molecule. This was carried out using the HF method and DFT using the LDA and B3LYP functionals. The calculated results are compared in Fig. 6.2 with the known experimental values. The DFT calculations include electronic correlation effects not present in the HF approximation. It is seen that electron correlation shortens bond lengths, bringing the DFT optimized geometries into considerably better agreement with the experimental geometries than are the HF optimized geometries. This better agreement between DFT and experiment also holds for bond angles. Perhaps surprisingly there is not much difference between the LDA and B3LYP optimized geometries. The exception is the COC bond angle which is somewhat better described with the B3LYP functional than with the LDA functional.

Early studies of the experimental absorption spectrum of oxirane were made by Liu and Duncan[90], Lowrey and Watanabe[91], and by Fleming, Anderson, Harrison, and Pickett[92]. The most definitive study of the absorption spectrum of oxirane is probably that made by Basch *et al.* in 1969 [93] who combined information from vacuum ultraviolet spectra, photoelectron spectra, and quantum chemical computations. One of the most recent studies of the electronic excitation spectra is the 1992 study of Ben-Tzur *et al.* [94]. The positions of the principle electronic excitations were identified early on. Vibrational structure was found to be superimposed upon the electronic absorptions. Once this was removed Liu and Duncan were able to identify two strong electronic absorbtions. Lowry and Watabe confirmed these two

Table 6.1: Principle oxirane singlet excitation energies and oscillator strengths.

Principle Singlet Excitation Energies (eV) and Oscillator Strengths			
TDHF	TDLDA	TDB3LYP	Expt.
9.14 (0.0007)	6.01 (0.0309)	6.69 (0.0266)	7.24(s) [1] [2] [3]
9.26 (0.0050)	6.73 (0.0048)	7.14 (0.0060)	7.45(w)[2]
9.36 (0.0635)	6.78 (0.0252)	7.36 (0.0218)	7.88(s)[1], 7.89(s) [2]
9.56 (0.0635)	7.61 (0.0035)	7.85 (0.0052)	
9.90 (0.0478)	7.78 (0.0304)	8.37 (0.0505)	
9.93 (0.0935)	8.13 (0.0014)	8.39 (0.0168)	
8.15 (0.0405)	8.40 (0.0419)		

[1] Gas phase UV absorption spectrum [90].
[2] Obtained by a photoelectic technique [91].
[3] Gas phase UV absorption spectrum [92].

absorbtions and report another (unidentified) band at 7.45 eV. Fleming, Anderson, Harrison, and Pickett confirmed the position of the first electronic absorption. The assignment of these electronic transitions took a bit longer. The accepted interpretation is that given by Basch *et al.* that the observed transitions correspond to O(n) $\rightarrow$ 3s and 3p Rydberg transitions. Let us see how this is reflected in our calculations.

While theoretical absorption spectra are often shifted with respect to experimental absorption spectra, we expect to find two strong absorptions in the low energy spectrum, separated from each other by about 0.65 eV. Vertical absorption spectra were calculated using TDHF, TDLDA, and the TDB3LYP method, all at the B3LYP-optimized geometry. The results are shown in Table 6.1. Of the three methods, the one in best agreement with the experimental results is the TDB3LYP method which shows two strong absorptions red-shifted from experiment by about 0.5 eV and separated by 0.67 eV. The TDLDA method is qualitatively similar, apart from a stronger red shift. In particular, the TDLDA method shows two strong absorptions red-shifted from experiment by about 1.1 eV and separated by 0.78 eV. In contrast, the TDHF spectrum is blue-shifted by about 2 eV and is otherwise of questionable value for interpretting the experimental spectrum. In what follows we have decided to assign the lowest three absorptions using the results of our TDB3LYP calculations.

This first involves an examination of the B3LYP molecular orbitals (MOs). These

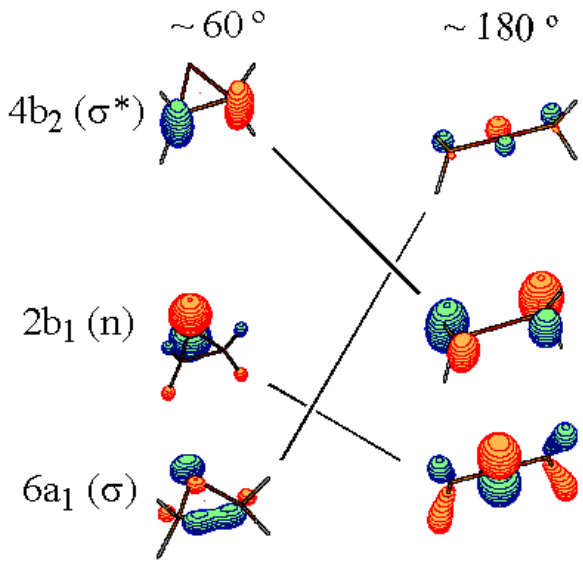

Figure 6.3: B3LYP MOs. Left: ring structure. Right: open structure.

orbitals are shown in Fig. 6.3. The electronic configuration of the ring structure is,

$$\cdots [6a_1(\sigma)]^2 [2b_1(n)]^2 [7a_1(3s)]^0 [4b_2(\sigma^*)]^0 \cdots . \tag{6.22}$$

The group theoretic MO labels (a_1, a_2, b_1, and b_2) correspond to representations of the C_{2v} symmetry group. The additional labels, σ, n, and σ^*, show our chemical interpretation of the B3LYP orbitals and their correspondance with the MOs in the WH three-orbital model.

Confirmation of the chemical nature of our B3LYP MOs was obtained by constructing a Walsh diagram for C_{2v} ring opening. This graph of MO energies as a function of ring-opening angle (α) is shown in Fig. 6.4. As the ring opens, the C($2p$) $6a_1(\sigma)$ bond breaks and so increases in energy. At the same time, the C($2p$) $4b_2(\sigma^*)$ antibond becomes less antibonding and so decreases in energy. The O($2p$) lone pair $2b_1(n)$ is not involved in bonding and so maintains a roughly constant energy throughout the ring-opening process. Experimental information about occupied MOs is available from electron momentum spectroscopy (EMS) via the target Kohn-Sham approximation [95]. The ordering of the B3LYP occupied orbitals is consistant with the results of a recent EMS study of oxirane [96]. In particular the two highest energy occupied orbitals are seen to have a dominant p-type character. The interpretation of the unoccupied orbitals is more problematic in that the B3LYP unoccupied orbitals in our calculations are not bound (i.e., have positive orbital energies). We are thus attempting to describe a continuum with a finite basis set. It is

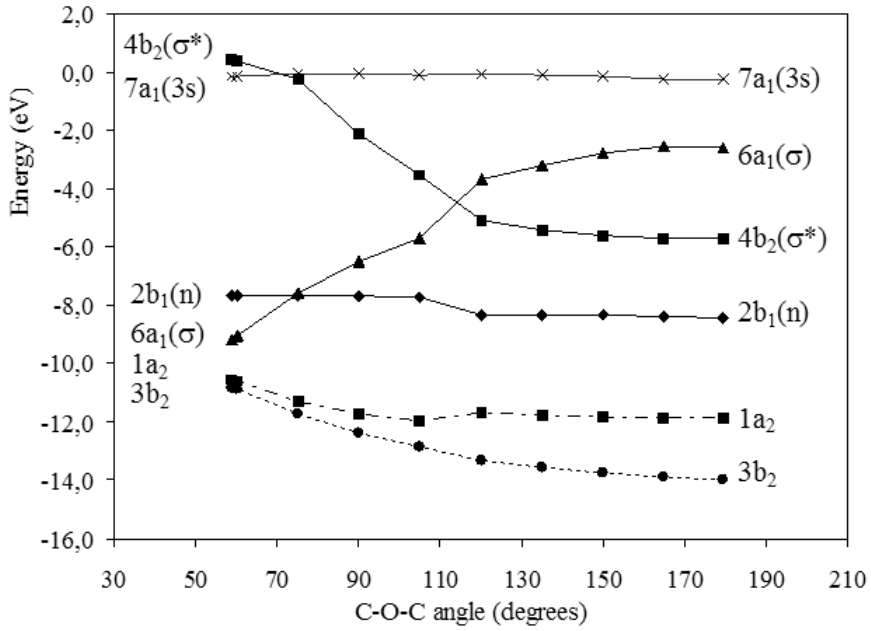

Figure 6.4: Walsh diagram for C_{2v} ring opening calculated at the B3LYP level. To construct this diagram, the COC bond angle was varied and all other geometric parameters were relaxed within the constraint of C_{2v} symmetry. The HOMO is the $2b_1$ orbital on the left hand side and the $4b_2$ orbital on the right hand side.

thus far from obvious that the unoccupied orbital energies will converge to anything meaningful as the finite basis set becomes increasingly complete. A notable exception to this rule are resonance states. These "bound states in the continuum" are long-lived fairly localized resonance states of predominantly valence-type character. The Walsh diagram shows that the $4b_2(\sigma^*)$ unoccupied orbital becomes bound for ring opening angles beyond about 80°. It is also rather localized and hence it makes sense to assign it some physical meaning. This is certainly consistant with previous HF studies using the STO-3G minimal basis set [97] and the more extensive 6-31G** basis sets [98]. Since our 6-311++G**(2d,2p) basis set is even larger, it is not too surprising that we find an additional unoccupied orbital, namely the $7a_1(3s)$ orbital shown in Fig. 6.5. Although apparently at least partially localized, this orbital remains unbound at all bond angles in the Walsh diagram and care should be taken not to over interpret its physical nature. Nevertheless this $7a_1(3s)$ orbital intervenes in an important way in the interpretation of our calculated electronic absorption spectra and it is upon analysis of the spectra that we will be able to associate this orbital with the $3s$ Rydberg state.

One should also be conscious in using the calculated TDB3LYP absorption spectrum to assign the experimental gas phase UV spectrum that the TDDFT ionization

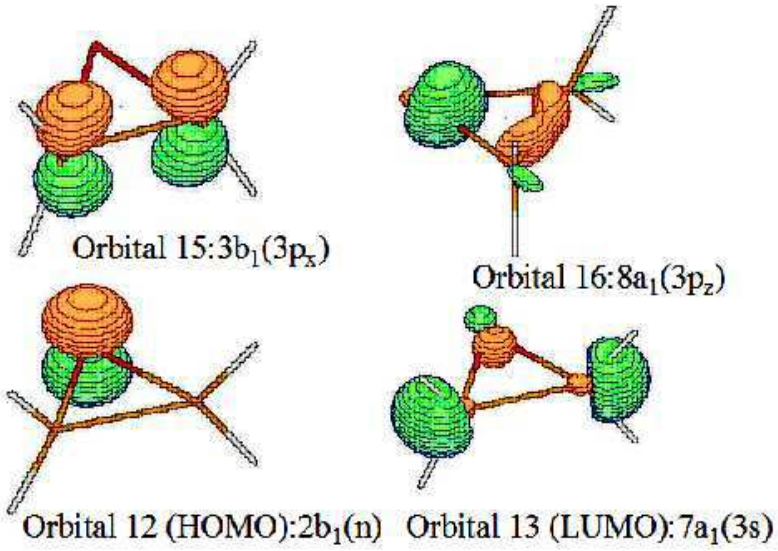

Figure 6.5: B3LYP MOs implicated in the principle UV absorptions.

continuum begins at minus the value of the HOMO orbital energy [99]. The value of $-\epsilon_{\mathrm{HOMO}}$ obtained in the different calculations is 6.40 eV with the LDA, 7.68 eV with the B3LYP hybrid functional, and 12.27 eV with HF. As expected from Koopmans' theorem, the HF value of $-\epsilon_{\mathrm{HOMO}}$ is in reasonable agreement with the experimental ionization potential of 10.57 eV [100]. The presence of a fraction of HF exchange in the B3LYP hybrid functional helps to explain why its value of $-\epsilon_{\mathrm{HOMO}}$ lies between that of the pure DFT LDA and that of HF. As far as our TDB3LYP calculations are concerned, the value of $-\epsilon_{\mathrm{HOMO}}$ means that assignment of experimental excitation energies higher than 7.7 eV should be avoided. Fortunately this still allows us to assign the first singlet excitation energies. Examination of the TDB3LYP coefficients yields the following assignments for the three principle UV absorption peaks:

$$6.69 \text{ eV} \quad : \quad 1^1B_1[2b_1(n) \rightarrow 7a_1(3s)] \tag{6.23}$$

$$7.14 \text{ eV} \quad : \quad 2^1B_1[2b_1(n) \rightarrow 8a_1(3p_z)] \tag{6.24}$$

$$7.36 \text{ eV} \quad : \quad 2^1A_1[2b_1(n) \rightarrow 3b_1(3p_x)]\,. \tag{6.25}$$

Comparison with the experimental assignment of Basch *et al.* justifies the identification of these orbitals with the Rydberg orbitals $3s$, $3p_z$, and $3p_x$.

It is worth pointing out that the expected $^1[2b_1(n), 4b_2(\sigma^*)]$ excitation is of $^1A_2$ symmetry and as such corresponds to a spectroscopically forbidden transition. It

is in any event fairly high in energy (9.77 eV with TDHF). The $^1[6a_1(\sigma), 4b_2(\sigma^*)]$ transition has $^1B_2$ symmetry and so is spectroscopically allowed, but is still found at fairly high energy in our calculations (8.15 eV with TDLDA, 8.37 with TDB3LYP, and 9.93 with TDHF).

B C_{2v} Ring-Opening

We now consider how DFT performs for describing the ground state and how well TDDDFT performs for describing the lowest excited state of each symmetry for C_{2v} ring-opening of oxirane. Comparisons are made against CASSCF and against high-quality DMC energies calculated at the same geometries. All geometries along the C_{2sv} pathway have been fully optimized at each O - C - O ring-opening angle (α) using the B3LYP functional. The orbital energies as a function of ring opening angle have already been given in the Walsh diagram (Fig. 6.4).

Figure 6.6 gives an overview of the (TD)B3LYP and (TD)LDA curves for the ground (1^1A_1) state and the lowest excited-states of each symmetry (2^1A_1, 1^3A_1, 1^1B_1, 1^3B_1, 1^1A_2, 1^3A_2, 1^1B_2, and 1^3B_2). Several things are worth noting here. The *first* point is that, some of the differences between the the (TD)B3LYP and (TD)LDA curves are apparent, not real, since the lines are only intended as a guide for the eye and points for the two graphs were not calculated at exactly the same angles. This is particularly true for (TD)LDA calculations around 120° where we encountered serious convergence difficulties due to a quasidegeneracy of σ and σ^* orbitals (Fig. 6.4). Under these circumstances the HOMO, which suffers from self-interaction errors, can lie higher than the LUMO, which is self-interaction-free. As the program tries to fill the orbitals according to the usual *aufbau* principle, electron density sloshes on each iteration between the two orbitals making convergence impossible without special algorithms. The (TD)B3LYP calculations were found to be easier to converge, presumably because they have less self-interaction error.

The *second* point to note is that only deMon2k (TD)LDA calculations are reported here, although we have also calculated (TD)LDA curves using Gaussian and found the results to be similar when both programs printed out the same information. Unfortunately, for the purposes of the present study, Gaussian did not always print out the lowest triplet excitation energy. So we prefer to report our more complete deMon2k results.

We presume that this difficulty with the Gaussian output is related to a *third* point, namely the presence of a triplet instability. This means that the *square* of the first triplet excitation energy decreases, going away from the equilibrium geometry,

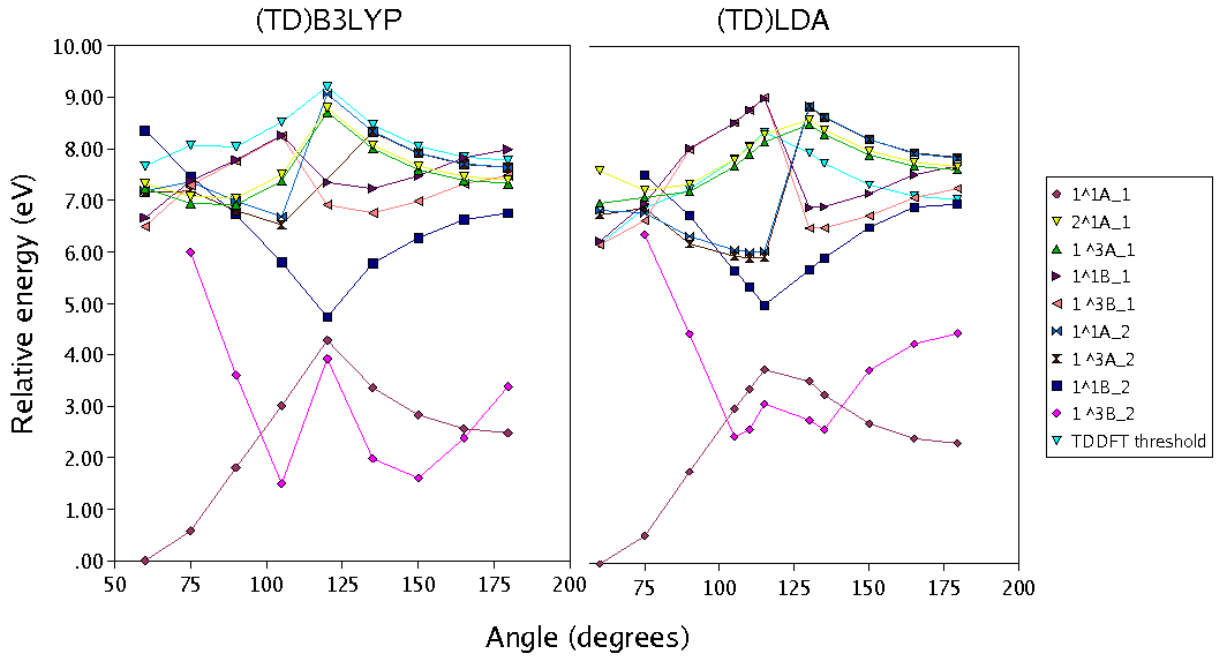

Figure 6.6: C_{2v} ring opening curves: ground state (1^1A_1) curve calculated using the B3LYP (GAUSSIAN) or the LDA (DEMON2K) functional, lowest excited state curve of each symmetry (2^1A_1, 1^3A_1, 1^1B_1, 1^3B_1, 1^1A_2, 1^3A_2, 1^1B_2, and 1^3B_2) calculated using the TDB3LYP excitation energies added to the B3LYP ground state energy (GAUSSIAN) or using the TDLDA excitation energies added to the LDA ground state energy (DEMON2K). Note that the energy zero has been chosen to be the ground state energy for the 60° structure. Note also that the "negative excitation energies" for the 1^3B_2 state relative to the ground state are really imaginary excitation energies (see text). Also shown is the TDDFT ionization threshold at $-\epsilon_{\text{HOMO}}$.

becomes zero, and then becomes imaginary. The exact meaning of triplet instabilities will be discussed further below. For now, note that the associated coefficients also become more complicated and we presume that GAUSSIAN had difficulty analyzing them. At other times, GAUSSIAN gave no indication of a problem. *We follow the usual practice for response calculations by indicating an imaginary excitation energy as a negative excitation energy.* However it is important to keep in mind that a negative excitation energy in this context is only a common convention and not a physical reality.

A *fourth* and final point worth making at this point is that the TDDFT ionization threshold occurs at minus the value of the HOMO energy which is significantly underestimated with ordinary functionals such as the LDA and B3LYP [99]. This artificially low ionization threshold is indicated in the two graphs in Fig. 6.6. In the (TD)B3LYP case, the TDDFT ionization threshold is high enough that it is not a particular worry. In the (TD)LDA case, the TDDFT ionization threshold is lower by about one eV. This may explain some of the quantitative differences between the high-lying (TD)B3LYP and (TD)LDA curves, although by and large the two calculations give results in reasonable qualitative, and even semi-quantitative, agreement.

We now wish to interpret the TDDFT curves. Excitations in TDDFT may be characterized in terms of single electron excitations from occupied to unoccupied MOs [38]. Unlike in Hartree-Fock, unoccupied and occupied orbitals in pure DFT (e.g., the LDA) see very similar potentials and hence the same number of electrons. This means that the orbitals are preprepared for describing electron excitations and that simple orbital energy differences are often a good first approximation to describing excitation energies. In the two-orbital model and pure DFT, the singlet, ω_S, and triplet, ω_T, TDDFT excitation energies for the transition from orbital i to orbital a are,

$$\begin{aligned} \omega_S &= \sqrt{(\epsilon_a - \epsilon_i)\left[(\epsilon_a - \epsilon_i) + 2(ia|2f_H + f_{xc}^{\uparrow,\uparrow} + f_{xc}^{\uparrow,\downarrow}|ai)\right]} \\ \omega_T &= \sqrt{(\epsilon_a - \epsilon_i)\left[(\epsilon_a - \epsilon_i) + 2(ia|f_{xc}^{\uparrow,\uparrow} - f_{xc}^{\uparrow,\downarrow}|ai)\right]}\,. \end{aligned} \tag{6.26}$$

In the TDA, this becomes

$$\begin{aligned} (\omega_S)_{\rm TDA} &= (\epsilon_a - \epsilon_i) + (ia|2f_H + f_{xc}^{\uparrow,\uparrow} + f_{xc}^{\uparrow,\downarrow}|ai) \\ (\omega_T)_{\rm TDA} &= (\epsilon_a - \epsilon_i) + (ia|f_{xc}^{\uparrow,\uparrow} - f_{xc}^{\uparrow,\downarrow}|ai)\,, \end{aligned} \tag{6.27}$$

from which it is clear that,

$$(\omega_S)_{\mathrm{TDA}} \leq \epsilon_a - \epsilon_i \leq (\omega_T)_{\mathrm{TDA}} \ . \tag{6.28}$$

For Rydberg states the inequalities become near equalities because the overlap of orbitals i and a goes to zero. While no longer strictly valid, these general ideas are still good starting points for understanding results obtained with the hybrid functional B3LYP.

The frontier MOs shown in the Walsh diagram (Fig. 6.4) supplemented with the addition of the two additional Rydberg orbitals, $3b_1(3p_x)$ and $5b_2(3p_y)$, provides a useful model not only for interpretting the results of our (TD)DFT calculations, but also for constructing the active space necessary for the CASSCF calculations used to construct the QMC wavefunctions. Table 6.2 gives an indication of which orbital excitations are most likely to be important for different electronic excited states. Figure 6.7 shows the results of our best QMC calculation and of the results of the CAS(4,6) calculation on which it is based. For the most part, the CAS and DMC curves differ quantitatively but not qualitatively. The exceptions are the 1^3A_1 and 1^1B_2 curves where the DMC results, which are significantly lower than the corresponding CAS(4,6) results at some geometries, contain important amounts of dynamic correlation not present at the CAS(4,6) level of calculation. In the remaining graphs (except for Fig. 6.9) we will suppress CAS(4,6) curves in favor of presenting the only the higher quality DMC curves since these offer the better comparison with TDDFT.

We now wish to give a detailed state-by-state comparison of our (TD)DFT results with DMC methods. Actually it is enough to divide the states into three sets. The first set consists of states where double excitations (lacking in the TDDFT adiabatic approximation) are likely to be important. The second set consists of states which show the effects of triplet instabilities. And the third set consists of Rydberg excitations.

The states of A_1 symmetry are those most likely to be affected by the absence of double excitations. Both single determinant states have $^1A_1$ symmetry. Although not shown here, we have constructed the two Hartree-Fock (HF) curves obtained by keeping on the one hand the $6a_1(\sigma)$ orbital doubly occupied and on the other hand the $4b_2(\sigma^*)$ orbital occupied. Both single determinant states have $^1A_1$ symmetry. The two curves thus generated simply cross at about 120°. In the absence of configuration mixing, the ground state curve follows whichever is the lower state and shows an important cusp at 120°. Introducing configuration mixing via a CASSCF calculation leads to an avoided crossing whose details. Depending upon the choice

Table 6.2: Electronic states and possible single excitations within the CASSCF(4,6) active space before and after the breaking of the CC σ bond. The $\sigma^2 \rightarrow (\sigma^*)^2$ double excitation has been added for completeness.

State	Possible Configurations
	$\alpha < 120°$
1^1A_1	$[b_1(n)]^2[a_1(\sigma)]^2$
2^1A_1	$[b_1(n)]^1[a_1(\sigma)]^2[b_1(3p_x)]^1$
	$[b_1(n)]^2[a_1(\sigma)]^1[a_1(3s)]^1$
	$[b_1(n)]^2[b_2(\sigma^*)]^2$
1^3A_1	$[b_1(n)]^1[a_1(\sigma)]^2[b_1(3p_x)]^1$
	$[b_1(n)]^2[a_1(\sigma)]^1[a_1(3s)]^1$
1^1B_1, 1^3B_1	$[b_1(n)]^1[a_1(\sigma)]^2[a_1(3s)]^1$
	$[b_1(n)]^2[a_1(\sigma)]^1[b_1(3p_x)]^1$
1^1A_2, 1^3A_2	$[b_1(n)]^1[a_1(\sigma)]^2[b_2(\sigma^*)]^1$
	$[b_1(n)]^1[a_1(\sigma)]^2[b_2(3p_z)]^1$
1^1B_2, 1^3B_2	$[b_1(n)]^2[a_1(\sigma)]^1[b_2(\sigma^*)]^1$
	$[b_1(n)]^2[a_1(\sigma)]^1[b_2(3p_y)]^1$
	$\alpha < 120°$
1^1A_1	$[b_1(n)]^2[b_2(\sigma^*)]^2$
2^1A_1	$[b_1(n)]^1[b_2(\sigma^*)]^2[b_1(3p_x)]^1$
	$[b_1(1)]^2[b_2(\sigma^*)]^1[b_2(3p_y)]^1$
	$[b_1(n)]^2[a_1(\sigma)]^2$
1^3A_1	$[b_1(n)]^1[b_2(\sigma^*)]^2[b_1(3p_x)]^1$
	$[b_1(n)]^2[b_2(\sigma^*)]^1[b_2(3p_y)]^1$
1^1B_1, 1^3B_1	$[b_1(n)]^1[b_2(\sigma^*)]^2[a_1(\sigma)]^1$
	$[b_1(n)]^1[b_2(\sigma^*)]^2[a_1(3s)]^1$
1^1A_2, 1^3A_2	$[b_1(n)]^1[b_2(\sigma^*)]^2[b_2(3p_z)]^1$
	$[b_1(n)]^2[b_2(\sigma^*)]^1[b_1(3p_x)]^1$
1^1B_2, 1^3B_2	$[b_1(n)]^2[b_2(\sigma^*)]^1[a_1(\sigma)]^1$
	$[b_1(n)]^2[b_2(\sigma^*)]^1[a_1(3s)]^1$

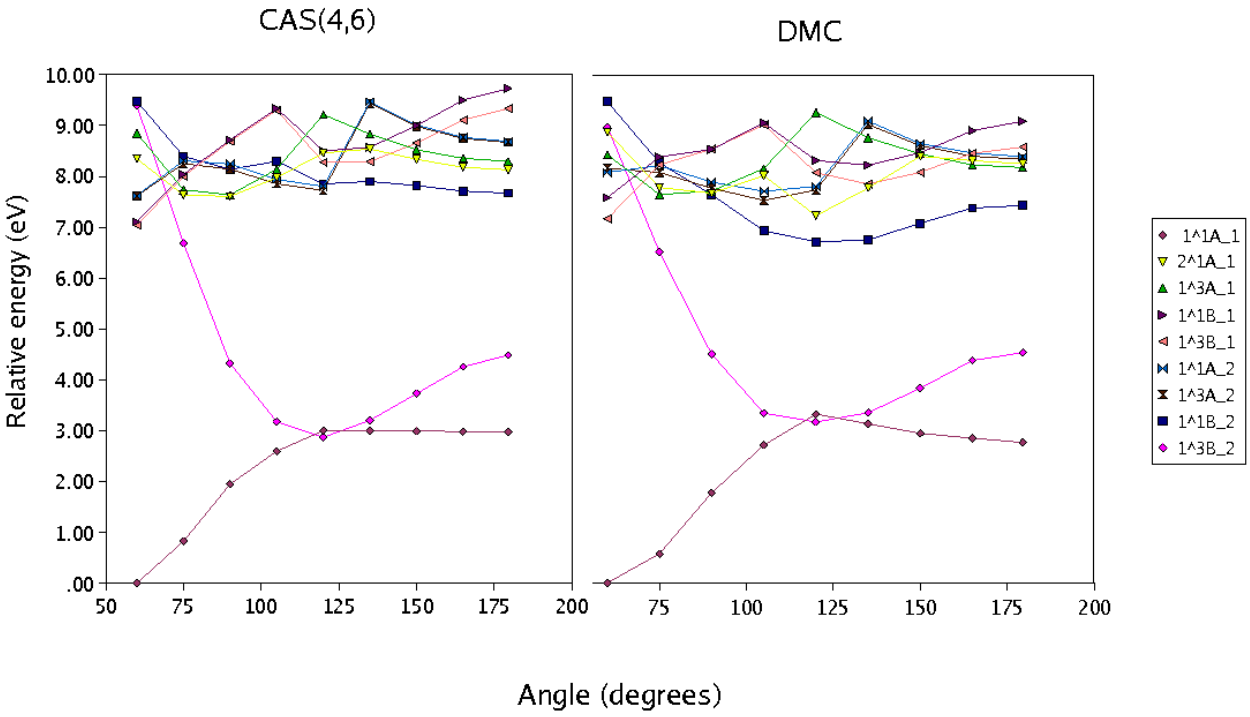

Figure 6.7: C_{2v} ring opening curves calculated with DMC: curves for the lowest state of each symmetry (1^1A_1, 1^3A_1, 1^1B_1, 1^3B_1, 1^1A_2, 1^3A_2, 1^1B_2, and 1^3B_2) are calculated using CAS(4,6) without state averaging, while the 2^1A_1 is the result of adding the excitation energy from a state averaged calculation to the ground state 1^1A_1 curve calculated without state averaging. Note that the energy zero has been chosen to be the ground state energy for the 60° structure. Note also that the negative excitation energies for the 1^3B_2 state relative to the ground state are really negative excitation energies. Numerical DMC energies are listed in the Supplementary Material associated with this article (Appendix VIII).

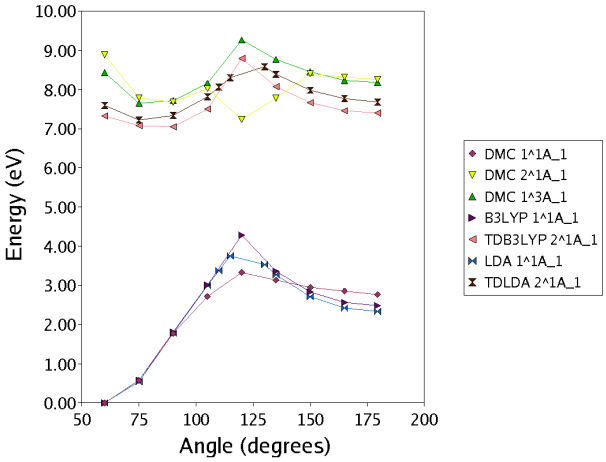

Figure 6.8: C_{2v} ring opening curves: 1^1A_1 and 2^1A_1 states. Note that the 1^3A_1 state has also been included at the DMC level of calculation.

of active space, this simple picture is complicated by the presence of one or more low-lying singly-excited configurations.

Now DFT is different from HF because DFT is exact when the functional E_{xc} is exact while HF always remains an approximation. On the otherhand, the Kohn-Sham equations of modern DFT resemble the HF equations and tend to inherit some of their faults when approximate functionals are used. Figure 6.8 shows the comparable curves at the (TD)DFT and DMC levels. As expected the unphysical cusp is absent in the 1^1A_1 ground state curve at the DMC level of calculation. The unphysical cusp is present at both the B3LYP and LDA levels where significant divergences between the DFT and DMC calculations occur between about 100° and 150°. However this region is very much reduced compared to what we have observed to happen for the HF curve where significant divergences beginning at about 75°. This is consistent with the idea that even DFT with approximate functionals still include a large degree of electron correlation.

As to the 2^1A_1 excited state curve, only the DMC calculation shows an indication of an avoided crossing. The inclusion of the 1^3A_1 excited state curve calculated at the DMC level helps to give a more complete understanding of the curve for this state. Below about 100° and above about 150°, the 2^1A_1 and 1^3A_1 states have nearly the same energy, consistant with the idea that these correspond to the $^1[a_1(\sigma), a_1(3s)]$ Rydberg transition below 110° and to the $^1[b_2(\sigma^*), b_2(3p_z)]$ Rydberg transition above 150°. In between the $^1[a_1(\sigma)^2, b_2(\sigma^*)^2]$ two-electron valence excitation cuts across the $^1A_1$ manifold. The TDDFT calculations are qualitatively capable of describing the one-electron Rydberg excitations but not of describing the two-electron excitation

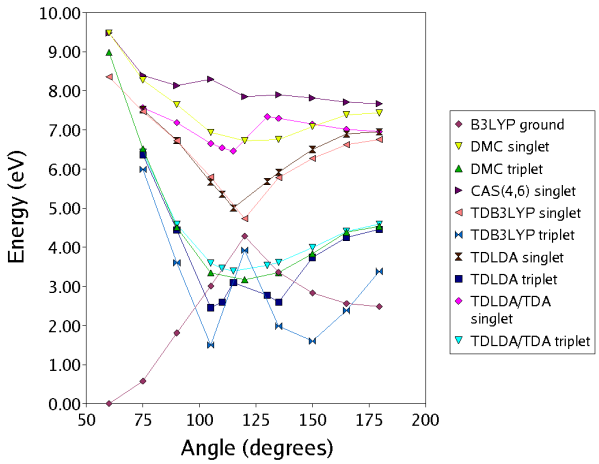

Figure 6.9: C_{2v} ring opening curves: 1^3B_2 and 1^1B_2 states. Note that the ground state (1^1A_1) curve has only been shown for the B3LYP calculation since the LDA curve is nearly identical.

in the bond-breaking region. As expected, the cusp in the DFT 1^1A_1 ground state curve is simply reflected as cusps in the (TD)DFT 2^1A_1 excited-state curve.

The only state which shows triplet instabilities is the 1^3B_2 state. The TDLDA 1^3B_2 energies are *imaginary* (even if designated as negative on the graph) between about about 100° and about 140° while the TDB3LYP 1^3B_2 energies are *imaginary* over a larger range, between about 90° and 160°. Certainly one way to understand how this can happen is through the formulae Eq. (6.26), but a better way to understand triplet instabilities is in terms of the fact that the quality of response theory energies depends upon having a high quality ground state. Problems occur in TDDFT excitation energies because the functional E_{xc} is only approximate.

Let us examine this question a little more deeply. Stability analysis and triplet instabilities have already been discussed in a general way in Sec. II where it was seen that no symmetry breaking is expected for a closed-shell singlet ground state when E_{xc} is exact. However symmetry breaking can occur when E_{xc} is approximate. Let us try to deepen our understanding of triplet instabilities by looking at a two orbital model for the the dissociation of the σ bond in H_2. This is strictly similar to the dissociation of the CC σ bond in oxirane. Here we follow the argument in Ref. [36] and consider the wave function,

$$\Psi_\lambda = |\sqrt{1-\lambda^2}\sigma + \lambda\sigma^*, \sqrt{1-\lambda^2}\bar{\sigma} - \lambda\bar{\sigma}^*| \rightarrow |s_A, \bar{s}_B|\,, \tag{6.29}$$

as $\lambda \rightarrow 1$. The corresponding energy expression is,

$$E_\lambda = E_0 + 2\lambda^2 \frac{\omega_T^2}{\epsilon_{\sigma^*} - \epsilon_\sigma} + \mathcal{O}(\lambda^3)\,. \tag{6.30}$$

This result suggests the more general result [42] that symmetry breaking will occur if and only if there is an imaginary triplet excitation energy ($\omega_T^2 < 0$). Certainly one way to try to overcome the problem of triplet excitation energies is to improve the quality of the exchange-correlation functional, thus reducing the region where triplet instabilities are a problem. However another way is to use the TDA. The reason is clear in HF theory. There TDHF TDA is the same as CIS, which is a true linear-variational-principle-based wave-function theory. By the Hylleraas-Undheim-McDonald/Cauchy interlace theorem, the Ith CIS excited state will be a rigorous upperbound to the true Ith excitation energy. Not only will the excitations remain real but variational collapse will not occur. To our knowledge, there is no way to extend these ideas to justify the use of the TDA in the context of TDDFT calculations except by carrying out explicit calculations to show that the TDA yields improved PESs for TDDFT calculations. This was previously shown for H_2 [36] and is evidently also true for oxirane judging from Fig. 6.9 where the TDLDA/TDA curve is remarkably similar to the DMC curve.

As shown in Fig. 6.9, triplet instabilities are often also associated with singlet near instabilities. In this case, the TDDFT 1^1B_2 singlet excitation energies are much too low. The TDA brings the TDLDA curve into the same energetic region of space as the corresponding DMC curve, but still compared with the DMC curve the TDLDA TDA curve appears to be qualitatively incorrect after 120° where it is seen to be decreasing, rather than increasing, in energy as the angle opens. This, in fact, is the behavior observed in the CAS(4,6) singlet calculation but is opposite to what happens in the more accurate DMC calculation.

The remaining $1^{1,3}B_1$ and $1^{1,3}A_2$ states are primarily Rydberg in nature with the corresponding singlets and triplets being energetically nearly degenerate. The graph for a single one of these states suffices to illustrate the general trend observed in the case of all four states. Figure 6.10 shows what happens for the 1^1B_1 states. All the curves have qualitatively the same form. This is particularly true for the TDB3LYP curve which closely resembles the DMC curve but shifted down by a little over one eV in energy. Notice also that the TDLDA and TDLDA/TDA curves are essentially

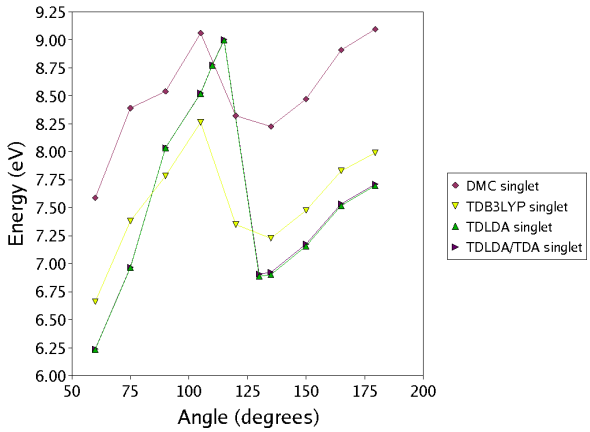

Figure 6.10: C_{2v} ring opening curves: 1^1B_1 state. The TDLDA and TDLDA/TDA curves are practically superimposed.

superimposed. This is because,

$$\begin{aligned}(\omega_S)^2_{TDA} - \omega_S^2 &= (ia|2f_H + f_{xc}^{\uparrow,\uparrow} + f_{xc}^{\uparrow,\downarrow}|ai)^2 \\ (\omega_T)^2_{TDA} - \omega_T^2 &= (ia|f_{xc}^{\uparrow,\uparrow} - f_{xc}^{\uparrow,\downarrow}|ai)^2 \,. \end{aligned} \tag{6.31}$$

For Rydberg states the overlap between orbitals i and a is very small and so the difference between full and TDA TDLDA calculations can be neglected. From Eq. (6.25) this also means that the Rydberg excitation energies also reduce to simple orbital energy differences.

Many problems with TDDFT have been reviewed in this subsection on the C_{2v} ring-opening pathway. We have pointed out that important difficulties arise at the point where the CC σ bond breaks because of the lack of explicit double excitations in TDDFT. However a more serious problem comes from the presence of triplet instabilities and singlet near instabilities. In the world of HF-based theories the solution of choice would probably not be the TDA because CIS (i.e., TDHF/TDA) is today not considered accurate enough to be accurate enough (TDDFT is better) [47]. The normal recommendation within HF-based theories would then be either to go on to response theory based upon a much improved ground state wave function or to carry out sophisticated multiconfigurational calculations. Still there is the hope [47] that problems encountered in present-day TDDFT will be overcome. It is the contention of the present paper that, although there is no formal justification for using the TDA in the framework of TDDFT, the use of the TDA is nevertheless a necessity. Figure 6.11 shows that the TDLDA/TDA yields, at least in this case, a

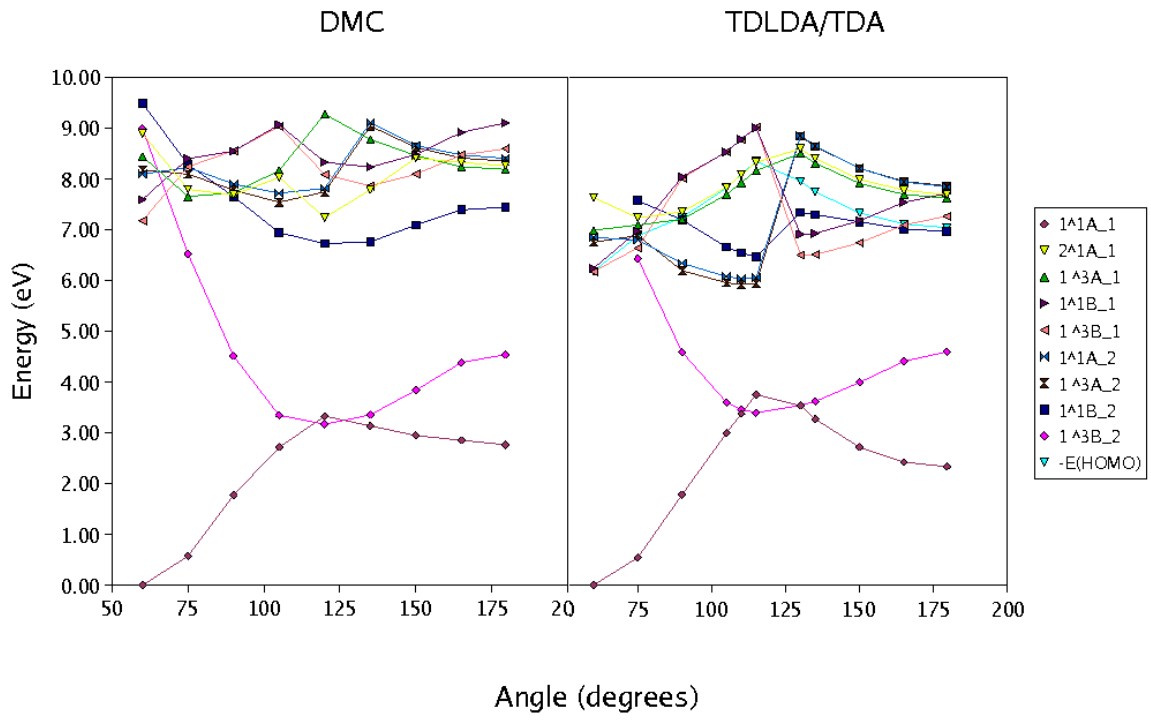

Figure 6.11: Comparison of TDLDA/TDA and DMCC C_{2v} ring opening curves.

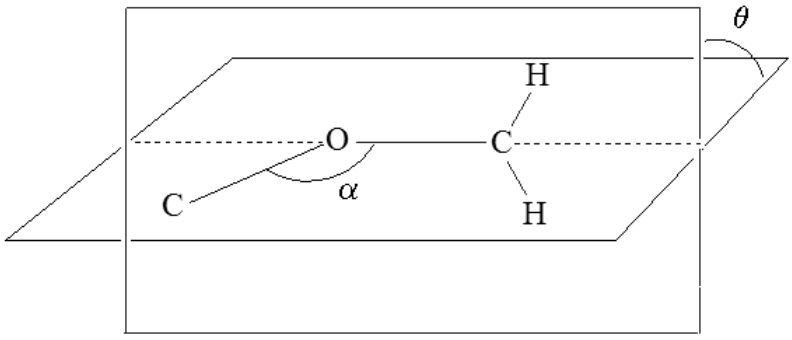

Figure 6.12: (α, θ) coordinate system used in this paper.

mostly qualitatively reasonable description of photochemically important PESs as compared with high-quality QMC PESs.

C *Con-* and *Dis*rotatory Ring Opening

Having started this section with the WH model for *con* and *dis* ring opening, it seems appropriate to say a few words about these ring-opening pathways before finishing discussing our results. Conrotatory and disrotatory potential energy surfaces were calculated using the simplifying assumption that each set of 4 atoms OCH_2 is constrained to lie in a plane. Our coordinate system is defined in Fig. 6.12. All other geometrical parameters were relaxed for the thermal reaction within the *con* and *dis* symmetries.

1 Thermal Reaction

Figure 6.13 shows the ground state (S_0) PES. In accordance with the WH model there appears to be a much lower energy barrier for *con* ring opening than for *dis* ring opening. Also shown is the lowest triplet state (T_1). It is clear that triplet instabilities occur along the disrotatory pathway as the CC σ bond breaks. Remarkably they do not occur along the conrotatory pathway in the LDA. (They should, of course, be everywhere absent when the exchange-correlation functional is exact.) Although triplet instabilities account for about 50% of the LDA surface, this fraction actually increases to 93% for the B3LYP functional where triplet instabilities occur along both the conrotatory and disrotatory reaction pathways. Finally, when the HF method is used triplet instabilities account for 100% of the PES. Perhaps because we forced the OCH_2 to lie in a single plane, triplet instabilities appear to be nearly everywhere in these last methods, potentially spelling trouble for mixed TDDFT/classical pho-

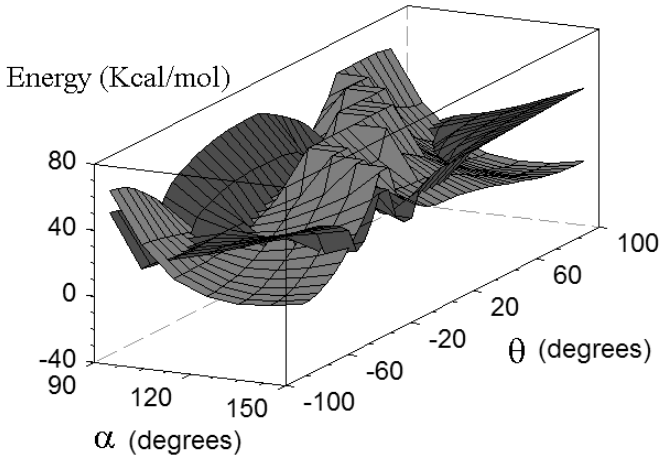

Figure 6.13: TDLDA S_0 (light grey) and T_1 (dark grey) PESs. Note that a "negative excitation energy" is just a convenient graphical trick for representing an imaginary excitation energy. Negative excitation energies correspond to triplet instabilities.

todynamics calculations. We would thus like to caution against the use of hybrid functionals for this type of application. At the same time, we reiterate our recommendation to use the TDA because, of course, the TDLDA/TDA excited state PESs (Fig. 6.14) show no triplet instabilities.

2 Photochemical Reaction

In considering whether the WH model has any validity for describing con- versus disrotatory rotation for photochemical ring opening in oxirane, we are immediately faced with the problem that there are a large number of excited states with similar energies which cross each other (Fig. 6.7). Which are important in this context? Provisionally we have decided to assume that state symmetry is conserved and so to look only at one PES, namely the "S_1" surface which begins as the $^1[2b_1(n) \rightarrow 7a_1(3s)]$ excitation for the closed cycle and then evolves as the molecular geometry changes. Turning back to the simple WH theory (Fig. 6.1) and thinking of excitation to a Rydberg state as analogous to electron removal, it suffices to remove an electron from the n orbital of the *thermal* WH diagram to have an idea of what might be the relative importace of the *con* and *dis* mechanisms for the S_1 surface. Since, in this case, both the *con* and *dis* mechanisms lead to a singly-excited state, no particular preference is expected for one mechaism over the other. The ground (S_0) and excited state singlet (S_1) surfaces calculated with the TDLDA TDA are shown in Fig. 6.15. Indeed the simple WH theory appears to be confirmed in that the S_1 surface is remarkably flat.

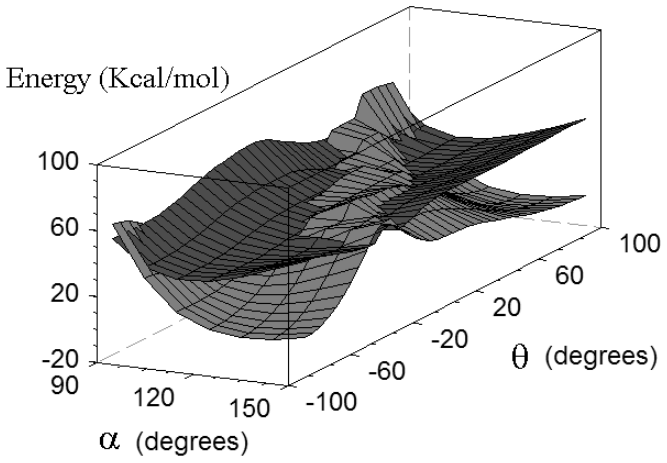

Figure 6.14: TDLDA TDA S_0 (light grey) and T_1 (dark grey) PESs. In this case negative excitation energies are real, not imaginary, quantities.

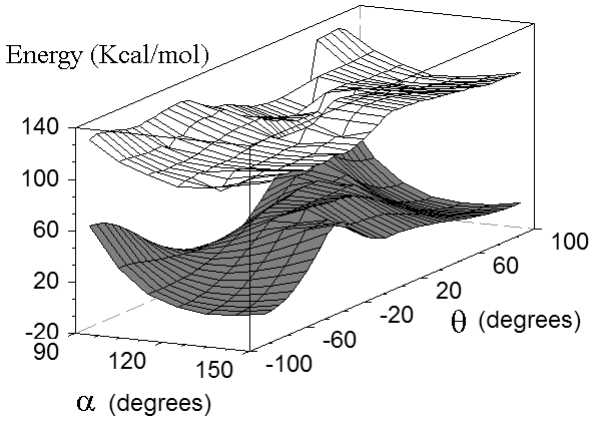

Figure 6.15: TDLDA TDA S_0 (light grey) and S_1 (white) potential energy surfaces.

Unfortunately this analysis is far too simplistic. In particular, Kasha's rule [101] tells us that the first excited triplet (T_1) or singlet (S_1) states are the most likely candidates for the initiation of a photochemical reaction. This is based upon the idea that relaxation of higher excited states is rapid. Such relaxation is due to environmental effects or vibronic coupling which need not preserve the symmetry of the electronic state. Hence S_1 at one geometry is not necessarily S_1 at another geometry. Indeed looking again at the DMC curves in Fig. 6.7, it is easy to believe that the molecule will easily arrive in the $1^1B_2(\sigma,\sigma^*)$ state during ring opening and that, because the σ orbital is higher in energy than the σ^* orbital at this geometry (Fig. 6.4), that the usual WH argument will still predict a preference for the *dis* mechanism.

Again we are falling into a trap imposed by the use of symmetry. Excitation, for example, from the $2b_1(n)$ orbital (Fig. 6.3) into the $8a_1(3p_z)$ Rydberg orbital (Fig. 6.5) might lead to preferential CO, rather than CC, bond breaking to the extent that ring opening augments the valence CO($\sigma*$) character of the target orbital [50]. The difficulty of predicting *a priori* such behavior is part of what motivates us to move towards dynamics as a better tool for photochemical modeling.

VI Conclusion

In this paper, we have examined the potential energy curves and surfaces for the symmetric ring opening of oxirane in view of assessing possible difficulties which might be encountered in mixed TDDFT/classical photodynamics simulations of its photochemistry. Our TDDFT calculations provided useful insight helpful in constructing the active space needed for more accurate CASSCF and still more accurate DMC calculations. Although in some sense trivial, it is probably worth noting that identifying active spaces is probably one of the more common uses of TDDFT in photochemical studies. Here we summarize our main conclusions obtained by comparing our TDDFT and DMC results.

Oxirane does not seem to be a molecule where charge transfer excitations are important. The artificially low ionization threshold typical in TDDFT for most functionals is still high enough for the B3LYP functional so as not to pose a serious problem. Even for the LDA functional, where the TDDFT ionization threshold is lower, the shapes of the excited-state Rydberg curves seem to be qualitatively correct even if they should not be considered quantitative.

Problems do show up as the CC σ bond breaks. By far, the most severe problem encountered is the presence of triplet instabilities and singlet near instabilities,

where the excited-state PES takes an unphysical dive in energy towards the ground state. In the case of the triplet, the excitation energy may even become imaginary, indicating that the ground state energy could be further lowered by allowing the Kohn-Sham orbitals to break symmetry. Although this problem is very much diminished compared to that seen in the HF ground state, it is still very much a problem as seen for example in the 2D surfaces.

It is difficult to overstate the gravity of the triplet instability problem for mixed TDDFT/classical photodynamics simulations. Allowing symmetry breaking is unlikely to be a viable solution here. Not only is there the difficulty that there may be more than one way to lower the molecular energy by breaking symmetry, and that searching for the lowest energy symmetry broken solution can be time consuming, but symmetry breaking should not occur at all when the exchange-correlation functional is exact. Thus not only would one have to design an algorithm to find the lowest of several possible broken symmetry solutions but one would also have to explain why one is looking for an artifact which should not exist in an exact calculation. Furthermore the assignment of excited states using broken symmetry orbitals is far from evident. On the whole, it thus seems better to avoid the problem by using the TDA to decouple (at least partially) the quality of the excited-state PES from that of the ground state PES. Our calculations show that this works remarkably well for the 1^3B_2 curve along the C_{2v} pathway, in comparison with good DMC results. The 1^1B_2 state, which appeared to collapse in energy without the TDA in the region of bond breaking, is also restored to a more reasonable range of energies. For this reason, we cannot even imagine carrying out photochemical simulations with TDDFT without the use of the TDA. Or, to put it more bluntly, the TDA, which is often regarded as an approximation on conventional TDDFT calculations, gives *better* results than does conventional TDDFT when it comes to excited-states PESs in situations where bond breaking occurs.

The TDA is unable to solve another problem which occurs as the CC σ bond breaks, namely the presence of an unphysical cusp on the ground state curve (or surface). This cusp is there because of the difficulty of approximate density functionals to describe a biradical structure with a single determinantal wave function. The cusp is also translated up onto the excited-state curves because of the way that PESs are constructed in (TD)DFT. However the problem is very much diminished compared to that seen in HF because of the presence of some correlation in DFT even when the exchange-correlation functional is approximate. The ultimate solution to the cusp problem is most likely some sort of explicit incorporation into (TD)DFT of two- and higher-electron excitations. Among the methods proposed for doing

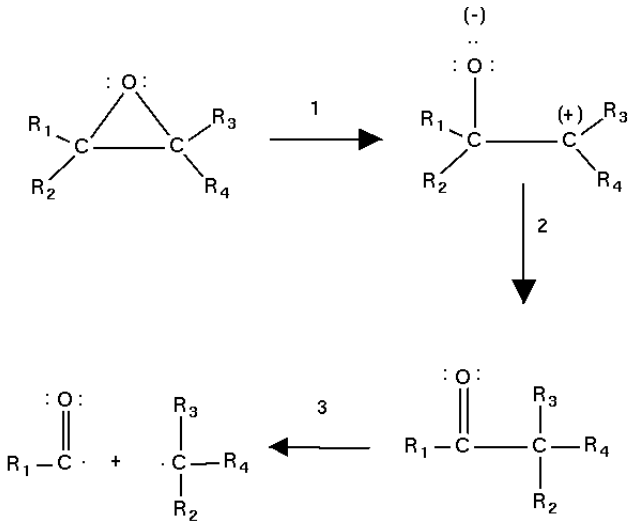

Figure 6.16: Typical reactions of alkyl oxiranes.

just this are dressed TDDFT or polarization propagator corrections [40, 39, 41] and spin-flip TDDFT [102, 103, 104].

Our examination of the con- and disrotatory ring-opening pathways revealed another important point which has nothing to do with TDDFT. This is that the manifold of excited state PESs is too complicated to visualize easily. The best way around this is to move from a PES interpretation of photochemistry to a pathway interpretation of photochemistry, and the best way to find the pathways moving along and between adiabatic PESs seems to us to be to carry out dynamics. For now it looks as though mixed TDDFT TDA/classical photodynamics simulations may suffice to describe the principle photochemical processes in oxirane. On-going calculations [50] do indeed seem to confirm this assertion in so far as trajectories have been found in good agreement with the accepted Gomer-Noyes mechanism[105, 106].

VII Photochemistry of Oxiranes

The generic structure of oxiranes is shown as the starting point in the chemical reactions in Figs. 6.16 and 6.17. When R_1, R_2, R_3, and R_4 are hydrogens or alkyl groups, then the prefered reaction is CO cleavage both photochemically and thermally (Step 1, Fig. 6.16). In particular it is estimated that the CO rupture energy is about 52 kcal/mol while the CC rupture energy is 5-7 kcal/mol higher [97]. Since the molecule is not symmetric along the CO ring-opening pathway, the WH model does not apply. Photochemical CO ring opening may be followed by alkyl migration [107] (Step 2,

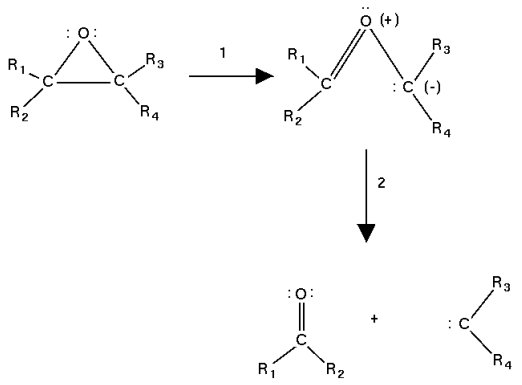

Figure 6.17: Typical reactions of aryl oxiranes.

Fig. 6.16). In the particular case of oxirane itself (R_1=R_2=R_3=R_4=H), hydrogen migration is followed by breaking of the CC single bond (Step 3, Fig. 6.16). This is the Gomer-Noyes mechanism [105] which was confirmed experimentally by Ibuki, Inasaki, and Takesaki [106].

In contrast, cyano and aryl substitutions favor CC bond breaking (Step 1, Fig. 6.17) to form what is often refered to as a 1,3-dipolar species or a carbonyl ylide. This is the case where there may be sufficient symmetry that the WH model applies. The photochemistry of phenyl and phenyl substituted oxiranes has been reviewed in Refs. [83, 84, 85] and on pages 565-566 of Ref. [108]. Evidence for carbonyl ylides goes back to at least the 1960s when Ullman and Milks investigated the tautomerization of 2,3-diphenylindenone oxide [109, 110] and Linn and Benson investigated the ring-opening reaction of tetracyanoethylene oxide [111, 112]. Finding cases where the WH model applies and where its predictions can be verified turns out to be less straightforward than might at first be believed, particularly in the photochemical case. There are several reasons for this. First of all, too much asymmetry should be avoided in order to assure the applicability of the WH orbital symmetry conservation rule and so avoid passing directly onto carbene formation (Step 2, Fig. 6.17). Secondly, the substituted oxirane should include groups which are bulky enough to confer the structural rigidity needed to avoid premature radiationless relaxation, but not bulky enough to favor carbene formation. The predictions of the WH model have been found to hold for *cis*- and *trans*-1,2-diphenyloxirane [113] while carbene formation dominates for tetraphenyl oxirane [114].

Table 6.3: A_1 DMC energies as a function of COC ring-opening angle along the C_{2v} ring-opening pathway.

A_1 DMC Energies (Variance) in Hartree		
$\angle$ COC (°)	1^1A_1	1^3A_1
60.	-29.7739004 (0.0009032)	-29.4639672 (0.0009953)
75.	-29.7526968 (0.0009446)	-29.4928219 (0.0009842)
90.	-29.7087620 (0.0009710)	-29.4902917 (0.0009437)
105.	-29.6740978 (0.0009763)	-29.4740573 (0.0009826)
120.	-29.6516759 (0.0009485)	-29.4333288 (0.0010583)
135.	-29.6586246 (0.0009361)	-29.4516324 (0.0009461)
150.	-29.6656198 (0.0009195)	-29.4632823 (0.0009725)
165.	-29.6691005 (0.0009842)	-29.4713557 (0.0009729)
179.5	-29.6722051 (0.0009631)	-29.4732433 (0.0009642)

VIII Supplementary Material

Benchmark quality diffusion Monte Carlo (DMC) energies calculated at the geometries given in Table 6.8 are reported here for the ground state (1^1A_1, Tables 6.3 and 6.4) and the lowest excited state of each symmetry (2^1A_1, Table 6.4; 1^3A_1, Table 6.3; 1^1B_1, 1^3B_1, Table 6.5; 1^1A_2, 2^3A_2, Table 6.6; and 1^1B_2, 1^3B_2, Table 6.7). We hope that these DMC data will encourage further developing and testing of improved (TD)DFT algorithms suitable for addressing the problems mentionned in this article.

Acknowledgements

This study was carried out in the context of a Franco-Mexican collaboration financed through *ECOS-Nord* Action M02P03. Some preliminary results of this study have been reported in Ref. [59].

Financing by *ECOS-Nord* made possible working visits of AV to the *Université Joseph Fourier* and of MEC to *Cinvestav*. FC acknowledges support from the Mexican Ministry of Education via a CONACYT (SFERE 2004) scholarship and from the *Universidad de las Americas Puebla* (UDLAP).

Over the course of this work, we have had so many useful discussions with so many different people that we can only acknowledge the most important here. MEC

Table 6.4: $^1A_1$ SA-DMC energies as a function of COC ring-opening angle along the C_{2v} ring-opening pathway.

$^1A_1$ SA-DMC Energies (Variance) in Hartree		
$\angle$ COC (°)	1^1A_1	2^1A_1
60.	-29.7757278 (0.0009334)	-29.4492821 (0.0009332)
75.	-29.7485069 (0.0009944)	-29.4835300 (0.0008956)
90.	-29.7044682 (0.0009595)	-29.4874122 (0.0010052)
105.	-29.6727632 (0.0009693)	-29.4776729 (0.0009476)
120.	-29.6475545 (0.0009388)	-29.5040407 (0.0010061)
135.	-29.6543193 (0.0009643)	-29.4837275 (0.0009683)
150.	-29.6635511 (0.0009947)	-29.4629627 (0.0011182)
165.	-29.6684986 (0.0010400)	-29.4676296 (0.0009659)
179.5	-29.6702180 (0.0009912)	-29.4685504 (0.0010219)

Table 6.5: B_1 DMC energies as a function of COC ring-opening angle along the C_{2v} ring-opening pathway.

B_1 DMC Energies (Variance) in Hartree		
$\angle$ COC (°)	1^1B_1	1^3B_1
60.	-29.4950664 (0.0009652)	-29.5102990 (0.0009690)
75.	-29.4655550 (0.0009215)	-29.4713018 (0.0009958)
90.	-29.4600803 (0.0009998)	-29.4598592 (0.0009164)
105.	-29.4409726 (0.0009558)	-29.4423196 (0.0009643)
120.	-29.4680768 (0.0009822)	-29.4769479 (0.0009958)
135.	-29.4716018 (0.0010480)*	-29.4852056 (0.0009786)
150.	-29.4625804 (0.0009950)	-29.4766687 (0.0010300)
165.	-29.4465277 (0.0009873)	-29.4628284 (0.0011035)
179.5	-29.4396495 (0.0009623)	-29.4583581 (0.0009661)

Table 6.6: A_2 DMC energies as a function of COC ring-opening angle along the C_{2v} ring-opening pathway.

A_2 DMC Energies (Variance) in Hartree

$\angle$ COC (°)	1^1A_2	1^3A_2
60.	-29.4766846 (0.0009661)	-29.4737798 (0.0009328)
75.	-29.4718098 (0.0009615)	-29.4767517 (0.0009109)
90.	-29.4837693 (0.0009730)	-29.4882303 (0.0010088)
105.	-29.4904399 (0.0009815)	-29.4970058 (0.0009891)
120.	-29.4869098 (0.0009569)	-29.4895892 (0.0009725)
135.	-29.4395258 (0.0009916)	-29.4420141 (0.0010677)
150.	-29.4559711 (0.0010337)	-29.4574126 (0.0010002)
165.	-29.4628003 (0.0009808)	-29.4651267 (0.0010395)
179.5	-29.4653049 (0.0010289)	-29.4672809 (0.0009573)

Table 6.7: B_2 DMC energies as a function of COC ring-opening angle along the C_{2v} ring-opening pathway.

B_2 DMC Energies (Variance) in Hartree

$\angle$ COC (°)	1^1B_2	1^3B_2
60.	-29.4254957 (0.0009295)	-29.4437656 (0.0009758)
75.	-29.4698509 (0.0010216)	-29.5343819 (0.0009873)
90.	-29.4928597 (0.0009523)	-29.6081805 (0.0010481)
105.	-29.5189668 (0.0010506)	-29.6510361 (0.0009440)
120.	-29.5268522 (0.0011071)	-29.6573927 (0.0009508)
135.	-29.5257722 (0.0010432)	-29.6507126 (0.0009200)
150.	-29.5134556 (0.0010089)	-29.6329311 (0.0009586)
165.	-29.5025238 (0.0010412)	-29.6128134 (0.0009405)
179.5	-29.5006345 (0.0009729)	-29.6071944 (0.0009653)

Table 6.8: Oxirane C_{2v} geometries obtained at different COC ring opening angles with all other parameters optimized at the B3LYP level.

C_{2v} geometries				
$\angle$ COC (°)	$\angle$ HCH (°)	$\angle$ HCOC (°)	R(CH) (Å)	R(CO) (Å)
60.	115.52	111.317	1.08375	1.44558
75.	118.69	105.214	1.08311	1.36333
90.	122.04	97.339	1.08131	1.34639
105.	122.28	84.096	1.08311	1.35811
120.	118.06	109.402	1.08576	1.38032
135.	119.88	105.829	1.08353	1.33439
150.	121.78	101.409	1.08154	1.30455
165.	123.27	96.054	1.08009	1.28694
179.5	123.86	90.207	1.07954	1.28114

and FC would like to acknowledge useful discussions with Mathieu Maurin and with Enrico Tapavicza. MEC would like to acknowledge useful discussions with Neepa Maitra, with Ivano Tavernelli, and with Todd Martínez. FC would like to acknowledge useful discussions with Massimo Olivucci.

MEC and FC would like to thank Pierre Vatton, Denis Charapoff, Régis Gras, Sébastien Morin, and Marie-Louise Dheu-Andries for technical support of the *Département de Chimie Moléculaire* and *Centre d'Expérimentation le Calcul Intensif en Chimie* (CECIC) computers used for calculations reported here. CF acknowledges the support by the *Stichting Nationale Computerfaciliteiten* (NCF-NWO) for the use of the SARA supercomputer facilities.

Bibliography

[1] N.L. Doltsinis and D. Marx, J. Theo. Comput. Chem. **1**, 319 (2002).

[2] A.N. Ipatov, P.-G. Reinhard, and E. Suraud, Int. J. Mol. Sci. **4**, 300 (2003)

[3] A.N. Ipatov, P.-G. Reinhard, and E. Suraud, Eur. Phys. J. D **65**, 2004.

[4] B. Gervais, E. Giglio, E. Jacquet, A. Ipatov, P.-G. Reinhard, F. Fehrer, and E.Suraud, Phys.Rev.A **71**, 015201 (2005).

[5] B. Gervais, E. Giglio, E. Jacquet, A. Ipatov, P.-G. Reinhard, and E.Suraud, J. Chem. Phys. **121**, 8466 (2004).

[6] F. Fehrer, P.-G. Reinhard, E. Suraud, E. Giglio, B. Gervais, A. Ipatov Applied Phys. A **82**, 151 (2006).

[7] T. Burnus, M.A.L. Marques, and E.K.U. Gross, Phys. Rev. A **71**, 01050(R) (2005).

[8] J.C. Tully and R.K. Preston, J. Chem. Phys. **55**, 562 (1971).

[9] J.C. Tully, J. Chem. Phys. **93**, 1061 (1990).

[10] C. Van Caillie and R.D. Amos, Chem. Phys. Lett. **308**, 249 (1999).

[11] C. Van Caillie and R.D. Amos, Chem. Phys. Lett. **317**, 159 (2000).

[12] F. Furche and R. Ahlrichs, J. Chem. Phys. **117**, 7433 (2002).

[13] D. Rappoport and F. Furche, J. Chem. Phys. **122**, 064105 (2005).

[14] J. Hutter, J. Chem. Phys. **118**, 3928 (2003).

[15] V. Chernyak and S. Mukamel, J. Chem. Phys. **112**, 3572 (2000).

[16] R. Baer, Chem. Phys. Lett. **364**, 75 (2002).

[17] C.F. Craig, W.R. Duncan, and O.V. Prezhdo, Phys. Rev. Lett. **95**, 163001 (2005).

[18] N.T. Maitra, J. Chem. Phys. **125**, 014110 (2006).

[19] B.F. Habenicht, C.F. Craig, and O.V. Prezhdo, Phys. Rev. Lett. **96**, 187401 (2006).

[20] E. Tapavicza, I. Tavernelli, and U. Röthlisberger, Phys. Rev. Lett. **98**, 023001 (2007).

[21] E. W.-G. Diau, C. Kötting, and A.H. Zewail, ChemPhysChem **2**, 273 (2001).

[22] E. W.-G. Diau, C. Kötting, and A.H. Zewail, ChemPhysChem **2**, 294 (2001).

[23] E. W.-G. Diau, C. Kötting, T.I. Søolling, and A.H. Zewail, ChemPhysChem **3**, 57 (2002).

[24] T.I. Søolling, E. W.-G. Diau, C. Kötting, S. De Feyter, and A.H. Zewail, ChemPhysChem **3**, 79 (2002).

[25] G. Orlova, J.D. Goddard, and L.Y. Brovko, J. Am. Chem. Soc. **125**, 6962 (2002).

[26] J. Černý, V. Špirko, M. Mons, P. Hobza, and D. Nachtigallová, Phys. Chem. Chem. Phys. **8**, 3059 (2006).

[27] M.E. Casida, K.C. Casida, and D.R. Salahub, Int. J. Quant. Chem. **70**, 933 (1998).

[28] S. Fantacci, A. Migani, and M. Olivucci, J. Phys. Chem. A **108**, 1208 (2004).

[29] L. Bertini, C. Greco, L. De Gioia, and P. Fantucci, J. Phys. A **110**, 12900 (2006).

[30] M. Ben-Nun and T.J. Martinez, Chem. Phys. **259**, 237 (2000).

[31] Z.-L. Cai, D.J. Tozer, and J.R. Reimers, J. Chem. Phys. **113**, 7084 (2000).

[32] N.J. Russ, T.D. Crawford, and G.S. Tschumper, J. Chem. Phys. **120**, 7298 (2004).

[33] M. Wanko, M. Garavelli, F. Bernardi, T.A. Niehaus, T. Frauenheim, and M. Elstner, J. Chem. Phys. **120**, 1674 (2004).

[34] B.G. Levine, C. Ko, J. Quenneville, and T.J. Martinez, Mol. Phys. **104**, 1039 (2006).

[35] D.J. Tozer, R.D. Amos, N.C. Handy, B.O. Roos, and L. Serrano-Andrés, Mol. Phys. **97**, 859 (1999).

[36] M.E. Casida, F. Gutierrez, J. Guan, F.-X. Gadea, D.R. Salahub, and J.-P. Daudey, J. Chem. Phys. **113**, 7062 (2000).

[37] A. Dreuw, J.L. Weisman, and M. Head-Gordon, J. Chem. Phys. **119**, 2943 (2003).

[38] M.E. Casida, in *Recent Advances in Density Functional Methods, Part I*, edited by D.P. Chong (World Scientific: Singapore, 1995), p. 155.

[39] N.T. Maitra, F. Zhang, F.J. Cave, and K. Burke, J. Chem. Phys. **120**, 5932 (2004).

[40] R.J. Cave, F. Zhang, N.T. Maitra, and K. Burke, Chem. Phys. Lett. **389**, 39 (2004).

[41] M.E. Casida, J. Chem. Phys. **122**, 054111 (2005).

[42] M.E. Casida, in *Accurate Description of Low-Lying Molecular States and Potential Energy Surfaces*, ACS Symposium Series 828, edited by M.R. Hoffmann and K.G. Dyall (ACS Press: Washington, D.C., 2002) pp. 199.

[43] N.T. Maitra, K. Burke, H. Appel, E.K.U. Gross, and R. van Leeuwen, in *Reviews in Modern Quantum Chemistry, A Cellibration of the Contributions of R.G. Parr*, edited by K.D. Sen (World Scientific: 2001).

[44] G. Onida, L. Reining, and A. Rubio, Rev. Mod. Phys. **74**, 601 (2002).

[45] C. Daniel, Coordination Chem. Rev. **238-239**, 141 (2003).

[46] N.T. Maitra, A. Wasserman, and K. Burke, in *Electron Correlations and Materials Properties 2*, edited by A. Gonis, N. Kioussis, and M. Ciftan (Klewer/Plenum: 2003).

[47] L. Serrano-Andrés and M. Merchán, J. Molec. Struct. (THEOCHEM) **729**, 99 (2005).

[48] *Time-Dependent Density-Functional Theory*, edited by M.A.L. Marques, C. Ullrich, F. Nogueira, A. Rubio, and E.K.U. Gross, *Lecture Notes in Physics* (Springer: Berlin, 2006).

[49] "... it is probably fair to say that in photochemical reactions, the unsymmetrical reaction paths are the ones most normally followed. In spite of this, most illustrations of potential energy curves in the literature and in this book are for symmetrical paths, since these are much easier to calculate or guess. It is up to the reader of any of the theoretical photochemistry literature to keep this in mind and to correct for it the best he or she can ..." (Ref. [115], p. 218.)

[50] E. Tapavicza, *personal communication.*

[51] J.P. Perdew, M. Ernzerhof, and K. Burke, J. Chem. Phys. **105**, 9982 (1996).

[52] R.G. Parr and W. Yang, *Density-Functional Theory of Atoms and Molecules* (New York, Oxford University Press, 1989)

[53] R.M. Dreizler and E.K.U. Gross, *Density Functional Theory, An Approach to the Quantum Many-Body Problem* (New York, Springer-Verlag, 1990).

[54] W. Koch and M.C. Holthausen, *A Chemist's Guide to Density Functional Theory* (New York, Wiley-VCH, 2000).

[55] Erich Runge and E. K. U. Gross, Phys. Rev. Lett., **52**, 997 (1984).

[56] R. van Leeuwen, Int. J. Mod. Phys. B **15**, 1969 (2001).

[57] S. Hirata and M. Head-Gordon, Chem. Phys. Lett. **314**, 291 (1999).

[58] R. Bauernschmitt and R. Ahlrichs, J. Chem. Phys. **104**, 9047 (1996).

[59] M.E. Casida, A. Ipatov, and F. Cordova, in Ref. [48], p. 243.

[60] H.-J. Werner and W. Meyer, J. Chem. Phys. **74**, 5794 (1981).

[61] T. Helgaker, P. Jørgensen, and J. Olsen, *Molecular Electronic-Structure Theory* (John-Wiley and Sons: New York, 2000).

[62] W.M.C. Foulkes, L. Mitas, R.J. Needs, and G. Rajagopal, Rev. Mod. Phys. **73**, 33 (2001).

[63] C. J. Umrigar, J. Toulouse, C. Filippi, S. Sorella and R. Henning, Phys. Rev. Lett. **98**, 110201 (2007).

[64] C. Filippi (unpublished).

[65] F. Schautz and C. Filippi, J. Chem. Phys. **120**, 10931 (2004).

[66] F. Schautz, F. Buda, and C. Filippi, J. Chem. Phys. **121**, 5836 (2004).

[67] GAUSSIAN 03, Revision C.02, M.J. Frisch, G. W. Trucks, H.B. Schlegel, G.E. Scuseria, M.A. Robb, J. R. Cheeseman, J. A. Montgomery, Jr., T. Vreven, K. N. Kudin, J. C. Burant, J. M. Millam, S. S. Iyengar, J. Tomasi, V. Barone, B. Mennucci, M. Cossi, G. Scalmani, N. Rega, G. A. Petersson, H. Nakatsuji, M. Hada, M. Ehara, K. Toyota, R. Fukuda, J. Hasegawa, M. Ishida, T. Nakajima, Y. Honda, O. Kitao, H. Nakai, M. Klene, X. Li, J. E. Knox, H. P. Hratchian, J. B. Cross, V. Bakken, C. Adamo, J. Jaramillo, R. Gomperts, R. E. Stratmann, O. Yazyev, A. J. Austin, R. Cammi, C. Pomelli, J. W. Ochterski, P. Y. Ayala, K. Morokuma, G. A. Voth, P. Salvador, J. J. Dannenberg, V. G. Zakrzewski, S. Dapprich, A. D. Daniels, M. C. Strain, O. Farkas, D. K. Malick, A. D. Rabuck, K. Raghavachari, J. B. Foresman, J. V. Ortiz, Q. Cui, A. G. Baboul, S. Clifford, J. Cioslowski, B. B. Stefanov, G. Liu, A. Liashenko, P. Piskorz, I. Komaromi, R. L. Martin, D. J. Fox, T. Keith, M. A. Al-Laham, C. Y. Peng, A. Nanayakkara, M. Challacombe, P. M. W. Gill, B. Johnson, W. Chen, M. W. Wong, C. Gonzalez, and J. A. Pople, Gaussian, Inc., Wallingford CT, 2004.

[68] Andreas M. Koester, Patrizia Calaminici, Mark E. Casida, Roberto Flores, Gerald Geudtner, Annick Goursot, Thomas Heine, Andrei Ipatov, Florian Janetzko, Serguei Patchkovskii, J. Ulises Reveles, Alberto Vela and Dennis R. Salahub, DEMON2K, Version 1.8, The deMon Developers (2005).

[69] R. Krishnan, J.S. Binkley, R. Seeger and J.A. Pople, J. Chem. Phys. **72**, 650 (1980).

[70] T. Clark, J. Chandrasekhar, and P.v.R. Schleyer, J. Comp. Chem. **4**, 294 (1983).

[71] E. Cancès, J. Chem. Phys. **114**, 10616 (2001).

[72] A. Ipatov, A. Fouqueau, C. Perez del Valle, F. Cordova, M.E. Casida, A.M. Köster, A. Vela, and C. Jödicke Jamorski , J. Mol. Struct. (Theochem), **762**, 179 (2006).

[73] S.H. Vosko, L. Wilk, and M. Nusair, Can. J. Phys. **58**, 1200 (1980).

[74] Gaussian NEWS, v. 5, no. 2, summer 1994, p. 2. "Becke3LYP Method References and General Citation Guidelines."

[75] M. W. Schmidt, K. K. Baldridge, J. A. Boatz, S. T. Elbert, M. S. Gordon, J. H. Jensen, S. Koseki, N. Matsunaga, K. A. Nguyen, S. Su, T. L. Windus, M. Dupuis, J. A. Montgomery, J. Comput. Chem. **14**, 1347 (1993).

[76] M. Burkatzki, C. Filippi, and M. Dolg, J. Chem. Phys. **126** XXXXX (2007).

[77] CHAMP is a quantum Monte Carlo program package written by C. J. Umrigar and C. Filippi; `http://www.ilorentz.org/~filippi/champ.html`.

[78] C. Filippi and C. J. Umrigar, J. Chem. Phys. **105**, 213 (1996). The Jastrow factor is adapted to deal with pseudo-atoms and the scaling factor κ is set to 0.5 for all atoms.

[79] R.S. Mulliken, J. Chem. Phys. **23**, 1997 (1955); *Erratum*, **24**, 1118 (1956).

[80] Huisgen, R., XXIIIrd Int. Congr. Pure Appl. Chem. **1**, 175 (1971).
"Ring Opening Reactions of Aziridines and Oxiranes"

[81] G.W. Griffin and A. Padwa, in *Photochemistry of Heterocyclic Compounds*, O. Buchardt, Ed. (Wiley: New York, 1976).

[82] G.A. Lee, J. Org. Chem., **41**, 2656 (1976).

[83] R. Huisgen, Angew. Chem., Int. Ed. Engl. **16**, 572 (1977).

[84] K.N. Houk, N.G. Rondan, C. Santiago, C.J. Gallo, R.W. Gandour, G.W. Griffin, J. Am. Chem. Soc. **102**, 1504 (1980).

[85] K. Peters, Ann. Rev. Phys. Chem. **38**, 253 (1987).

[86] R.B. Woodward and R. Hoffmann, J. Am. Chem. Soc. **87**, 395 (1965).

[87] R.B. Woodward and R. Hoffmann R., Angew. Chem., Int. Ed. Engl. **8**, 781 (1969).

[88] R.B. Woodward and R. Hoffmann, J. Am. Chem. Soc. **87**, 2046 (1965).

[89] C. Hirose, Bull. Chem. Soc. Jpn. **47**, 1311 (1947).

[90] T.-K. Liu and A.B.F. Duncan, J. Chem. Phys. **17**, 241 (1949).

[91] A. Lowrey III and K. Watanabe, J. Chem. Phys. **28**, 208 (1958).

[92] G. Fleming, M.M. Anderson, A.J. Harrison, and L.W. Pickett, J. Chem. Phys. **30**, 351, (1959).

[93] H. Basch, M.B Robin, N.A. Kuebler, C. Baker, and D.W. Turner, J. Chem. Phys. **51**, 52 (1969).

[94] S. Ben-Tzur, A. Basil, A. Gedanken, J.A. Moore, and J.M. Schwab, J. Am. Chem. Soc. **114**, 5751 (1992).

[95] P. Duffy, D. Chong, M.E. Casida, and D.R. Salahub, Phys. Rev. A **50**, 4707 (1994).

[96] D.A. Winkler, M.T. Michalewicz, F. Wang, and M.J. Brunger, J. Phys. B: At. Mol. Opt. Phys. **32**, 3239 (1999).

[97] B. Bigot, A. Sevin, and A. Devaquet, J. Am. Chem. Soc. **101**, 1095 (1979).

[98] M. Hô, W.A. Szarek, and V.H. Smith Jr., J. Mol. Struct. (Theochem), **537**, 253 (2001).

[99] M.E. Casida, C. Jamorski, K.C. Casida, and D.R. Salahub, J. Chem. Phys. **108**, 4439 (1998).

[100] W. von Niessen, L.S. Cederbaum, and W.P. Kraemer, Theor. Chim. Acta **44**, 85 (1977).

[101] M. Kasha, Disc. Faraday Soc. **9**, 14 (1950).

[102] Y. Shao, M. Head-Gordon, and A.I. Krylov, J. Chem. Phys. **118**, 4807 (2003).

[103] L.V. Slipchenko and A.I. Krylov, J. Chem. Phys. **118**, 6874 (2003).

[104] F. Wang and T. Ziegler, J. Chem. Phys. **121**, 12191 (2004).

[105] E. Gomer and W.A. Noyes, Jr., J. Am. Chem. Soc. **72**, 101 (1950).

[106] T. Ibuki, M. Inasaki, and Y. Takesaki, J. Chem. Phys. **59**, 2076 (1973).

[107] B.E. Arney Jr., R.C. White, A. Ramanathan, L. Barham, S. Sherrod, P. McCall, P. Livanec, K. Mangus, and K. White, Photochemical and Photobiological Sciences **3**, 851 (2004).

[108] N.J. Turro, *Modern Molecular Photochemistry* (Benjamin/Cummings: Menlo Park, California, 1991).

[109] E.F. Ullman and J.E. Milka, J. Am. Chem. Soc. **84**, 1315 (1962).

[110] E.F. Ullman and J.E. Milka, J. Am. Chem. Soc. **86**, 3814 (1964).

[111] W.J. Linn and R.E. Benson, J. Am. Chem. Soc. **87**, 3657 (1965).

[112] W.J. Linn, J. Am. Chem. Soc. **87**, 3665 (1965).

[113] L.E. Manring and K.S. Peters, J. Am. Chem. Soc. **106**, 8077 (1984).

[114] N.J. Turro, M. Aikawa, J.A. Butcher, Jr., and G.W. Griffin, J. Am. Chem. Soc. **102**, 5128 (1980).

[115] M. Klessinger and J. Michl, *Excited States and Photochemistry of Organic Molecules* (VCH : New York, 1995).

Conclusion

Sometime in the 1970s, Theoretical/Quantum/Computational Chemistry emerged as a legitimate subdiscipline of chemistry, along side such traditional subdisciplines as Organic, Inorganic, Physical and Analytical chemistry. Theory has made tremendous progress in the accurate modelling of the gas phase thermal chemistry of large molecules. The need to treat the practical chemistry of larger molecules in solution (in vitro) or in living systems (in vivo) has fueled the development and integration of new methods into the computational chemists repertory. One of these "new" methods for carrying out theoretical chemical modelling (in silico) is density-functional theory (DFT). The formal objectives of DFT were boldly declared in the unimpeachable theorems of Hohenberg and Kohn. More importantly practical approximations to the mysterious and imprecisely known exchange-correlation functional have made DFT an efficient method of choice for calculating ground state properties of large molecules, including for the study of thermal chemical reactions. But chemistry is not limited to the ground state. Can DFT help in understanding photochemical reactions?

The answer in principle is, "yes." Runge and Gross presented two Hohenberg-Kohn-like theorems which justify the extension of DFT to treat time-dependent (TD) perturbations. According to linear response (LR) theory, excitation energies and oscillator strengths may be obtained by examining the poles and residues of the dynamic polarizability, hence from the behavior of the TDDFT charge density. Casida's formulation of LR-TDDFT, which resembles the more familiar random phase approximation (RPA) of Quantum Chemistry, showed Quantum Chemists how to obtain electronic absorption spectra from TDDFT. More recently analytic derivatives of excited-state energies have been developed with the framework of LR-TDDFT. This opens the way for automatic searches for minima and transition states on excited-state potential energy surfaces (PESs) and even for dynamics on these surfaces.

Our optimism in reviewing these impressive advances in the DFT treatment of excited states must be tempered by the large number of problems left to be solved before TDDFT can be widely and safety applied as a black box method by naïve users to interesting practical problems. Some of these problems are primarily computational in nature.

What is the best implementations in TDDFT? Can the calculations be made faster? Can the numerical method chosen for implementing TDDFT be made fully compatible with the numerical method already present in a given program package? What quality of grid or auxiliary basis set is needed for reliable results? This is the type of problem addressed in Chapter 4 and which has led to the abandoning of

constrained charge density fitting in response theory calculations in deMon2k.

In Chapter 5, it was shown how LR-TDDFT calculations on molecules with open-shell ground states can lead to unphysical solutions. Some of these are triplet instabilities which can be eliminated by use of the Tamm-Dancoff approximations (TDA). Other problems stem from the TDDFT adiabatic approximations which limits LR-TDDFT to ("dressed") single-electron excitations. This leads to errors in spin-coupling for some states. Also presented in this chapter is a method for calculating excited-state spin contamination, hence allowing to identify and so eliminate (or otherwise deal with) the undesirable unphysical incorrectly spin-coupled excited states.

Chapter 6 assesses what conventional LR-TDDFT can do for a photochemically interesting small molecule, namely oxirane, where calculations against high-quality quantum Monte Carlo (QMC) calculations are possible. Conventional LR-TDDFT, which makes the TDDFT adiabatic approximations and uses the same approximate exchange-correlation functionals as in regular time-independent ground state DFT, is known to suffer from a number of problems, including

i) underestimation of the ionization threshold
ii) underestimation of charge transfer excitations
iii) lack of explicit 2– and higher– electron excitations

A pessimistic attitude says that these problems should render conventional LR-TDDFT useless for photochemical applications since these problems will necessarily occur somewhere on the surfaces sampled by photochemical dynamics. Our attitude is that the ability of LR-TDDFT to describe photochemistry will depend on the molecule and on the (perhaps) relatively small part of configuration space sampled during a given photochemical reaction. Our study on oxirane indicated that the major problem in this molecule is due to triplet instabilities which can be largely corrected with TDA. LR-TDDFT TDA photodynamics calculations on oxirane being carried out at Lausanne seem to confirm that present-day DFT can already provide results which compare favorably with experiment.

The dream of black box DFT-based photochemical simulations is still far off, but this thesis has brought us a little closer to making the dream a reality. Much remains to be done. Fortunately there is no shortage of good ideas. Future work should take into account progress in noncollinear spin-flip TDDFT and in polarization propagator corrections. Applications should also be extended to substituted oxiranes.

List of Tables

List of Figures